POLITECNICO DI MILANO
Dipartimento di Matematica "F. Brioschi"
Ph.D. Course in Mathematical Models and Methods in Engineering
XXV cycle

On the mathematical modeling of a metal foam expansion process.

Ph.D. Candidate: **Elisabetta REPOSSI**

Advisor: **Dr. Marco VERANI**
Co-advisor: **Prof. Riccardo ROSSO**

Tutor: Prof. Paolo Biscari
Ph.D. Coordinator: Prof. Roberto Lucchetti

Milan, 20th March, 2015

A papà Fiorenzo

Tieni sempre presente che la pelle fa le rughe,
i capelli diventano bianchi,
i giorni si trasformano in anni.

Però ciò che è importante non cambia;
la tua forza e la tua convinzione non hanno età.
Il tuo spirito è la colla di qualsiasi tela di ragno.
Dietro ogni linea di arrivo c'è una linea di partenza.
Dietro ogni successo c'è un'altra delusione.

Fino a quando sei vivo, sentiti vivo.
Se ti manca ciò che facevi, torna a farlo.
Non vivere di foto ingiallite...
insisti anche se tutti si aspettano che abbandoni.

Non lasciare che si arrugginisca il ferro che c'è in te.
Fai in modo che invece che compassione, ti portino rispetto.

Quando a causa degli anni
non potrai correre, cammina veloce.
Quando non potrai camminare veloce, cammina.
Quando non potrai camminare, usa il bastone.
Però non trattenerti mai!

Madre Teresa di Calcutta

Contents

Introduction. **7**

1 Metal Foams. **9**
1.1 What are Metal Foams? . . . 12
1.2 Local equilibrium rules. . . . 14
1.2.1 The law of Laplace. . . . 15
1.2.2 The laws of Plateau. . . . 15
1.2.3 Osmotic pressure. . . . 17
1.2.4 Topological changes. . . . 17
1.3 Essential properties of a foam. . . . 19
1.3.1 Rheology. . . . 19
1.3.2 Drainage. . . . 21
1.3.3 Coalescence. . . . 21
1.3.4 Coarsening. . . . 22
1.3.5 Collapse. . . . 22
1.4 Making foams. . . . 23
1.4.1 Alporas line. . . . 24
1.4.2 Alcan line. . . . 27
1.4.3 Powder line. . . . 28
1.4.4 Formgrip line. . . . 29
1.4.5 Gasar line. . . . 30
1.4.6 Other foaming processes. . . . 31
1.4.7 Final overview. . . . 31
1.5 Specific properties of solid metal foams. . . . 32
1.5.1 Density and porous structure. . . . 32
1.5.2 Mechanical properties. . . . 32
1.5.3 Acoustic properties. . . . 33
1.5.4 Thermal properties. . . . 33
1.5.5 Cell sizes and cell morphology. . . . 33
1.5.6 Dependence on the production methods. . . . 34
1.5.7 The quality of a foam. . . . 34
1.6 Methods for characterising a foam. . . . 34
1.6.1 Destructive testing. . . . 35
1.6.2 Non-destructive testing. . . . 37
1.6.3 Reproducibility tests. . . . 39
1.7 Applications of metal foams. . . . 39

2 Powder route: towards a mathematical modeling. 44
2.1 Powder metallurgical route. . . . 46
2.1.1 Main steps of the powder route process. . . . 46
2.1.2 Powders. . . . 47
2.1.3 Foam evolution. . . . 49
2.2 Factors influencing foam expansion behavior. . . . 55
2.2.1 Compaction of the powder mixture. . . . 55
2.2.2 Furnace temperature. . . . 56
2.2.3 Heating rate. . . . 58
2.3 Foam stabilisation. . . . 59
2.4 The expansion step in powder route process: experimental results at MUSP. . . . 60
2.4.1 Experimental set up 61
2.4.2 Outcome of the experiments 62
2.5 The expansion step in powder route process: hypotheses for a mathematical modeling. . . . 63

3 Phase-field modeling of metal foaming process. 65
3.1 Tensor and vector notation. . . . 68
3.2 Mixtures in a continuum model. . . . 69
3.2.1 Basic definitions. . . . 69
3.2.2 Balance of mass. . . . 70
3.2.3 Some useful identities. . . . 71
3.2.4 Balance of linear momentum. . . . 71
3.2.5 Balance of energy. . . . 72
3.3 Thermodynamically consistent phase-field models. . . . 72
3.4 Phase-field model of two-phase incompressible-compressible fluids. . . . 75
3.4.1 Gibbs free-energy. . . . 75
3.4.2 Metal-foam system of equations. . . . 77
3.4.3 Geometry and boundary-initial conditions. . . . 78
3.4.4 Dimensionless equations. . . . 79

4 Numerical methods for the LT system of equations. 81
4.1 Sobolev spaces. . . . 83
4.2 Quasi-incompressible Lowengrub-Truskinovsky model equations. . . . 84
4.2.1 A quasi-incompressible model for binary fluids. . . . 84
4.2.2 Mass conservation. . . . 85
4.2.3 Transformations on the momentum equation. . . . 85
4.2.4 Continuous mixed formulation. . . . 87
4.2.5 Momentum balance. . . . 88
4.2.6 Continuous energy dissipation law. . . . 90
4.3 Spatial DG discretisation. . . . 93
4.3.1 DG definitions, spaces and notation. . . . 93
4.3.2 Spatially discrete mixed formulation. . . . 95
4.3.3 Spatially discrete mass conservation. . . . 96
4.3.4 Spatially discrete energy dissipation law. . . . 97
4.3.5 Choice of the numerical fluxes. . . . 100
4.4 Temporal discretisation. . . . 103
4.4.1 Temporally discrete mixed formulation. . . . 103
4.4.2 Temporally discrete mass conservation. . . . 104
4.4.3 Temporally discrete energy dissipation law. . . . 104
4.5 Fully discrete energy consistent DG numerical method. . . . 108
4.5.1 Fully discrete mixed formulation. . . . 108
4.5.2 Fully discrete mass conservation and energy law. . . . 109

4.6 Numerical experiments. 110

5 Numerical methods for the MF system of equations. 114
5.1 Metal foam system of equations. 115
5.1.1 Metal foam system of equations. 115
5.1.2 Continuous mixed formulation. 116
5.1.3 Continuous mass conservation. 116
5.1.4 Continuous energy dissipation law. 117
5.2 Spatial DG discretisation. 120
5.2.1 Elementwise formulation. 120
5.2.2 Spatially discrete mixed formulation. 121
5.2.3 Spatially discrete mass conservation. 122
5.2.4 Spatially discrete energy dissipation law. 122
5.2.5 Choice of the numerical fluxes. 128
5.3 Temporal discretisation. 130
5.3.1 Temporally discrete mixed formulation. 131
5.3.2 Temporally discrete mass conservation. 132
5.3.3 Temporally discrete energy dissipation law. 132
5.4 Fully discrete energy consistent DG numerical method. 137
5.4.1 Fully discrete mixed formulation. 137
5.4.2 Fully discrete mass conservation and energy law. 139

Conclusions and Perspectives. 141

Acknowledgements. 142

Bibliography 143

Ringraziamenti. 147

Introduction.

Metal foams are special cases of cellular metals with closed cells. These materials attract the attention of researchers and engineers, thanks to properties like damping, high capability of energy absorption, high stiffness and low weight, that make them suitable for a wide range of applications, in particular in the automotive industry.

Many different processes have been developed for producing this kind of materials [6,8,37]. Precursor foaming is suggested in the literature as useful for filling processes and it is the method used in our research activities. It involves the heating of a solid material (called precursor) containing an embedded gas source (a blowing agent) that, upon temperature increasing, releases gas and drives the foaming process. Two processing methods can be distinguished depending on whether the precursor is prepared by a metallurgical or a melt route, which are respectively identified as "Powder line" or "Formgrip line". In this thesis we will consider the powder line. Precursor foaming is characterized by a pronounced foam expansion stage in the liquid state, as it will be highlighted in Chapter 2 by the experimental work performed at M.U.S.P. laboratory in Piacenza: the metal matrix is in the melted state upon heat treatment of the foaming precursor(s). In fact, during the heat treatment, at temperatures near the melting point of the matrix material, the blowing agent decomposes and the released gas forces the compacted precursor material to expand. In the process, the resulting foam expansion depends, therefore, on the content of blowing agent, temperature, time, pressure, heating rate, size of the precursor, etc. Furthermore, other physical variables govern the dynamics of the gas bubbles in the foamed matrix of a precursor, such as the matrix state (solid, semi-solid or liquid), presence of solid particles on the bubble walls, fluid viscosity, etc. [34].

The high costs and the lack of control in the manufacturing process (in order to avoid foam-decay phenomena like drainage and coarsening) prevent the industrial production of metal foams. A mathematical model describing the manufacturing route of metal foams could help engineers in the study of the physical parameters that are involved in the evolution of the foam. We are interested in the study of the expansion stage of the foam within a hollow mold. As it will be described in Chapter 2, the mathematical modeling of the foam expansion stage can be reduced to the mathematical modeling of two-phase incompressible-compressible fluids: the incompressible part is the liquid metal, while the compressible part is the gas inside bubbles. The literature of multiphase flows includes many types of differential models. In a sharp-interface approach, the thickness of the interface between the two phases is small compared with other characteristic scales of the fluids. In recent years, diffuse-interface models have been successfully used to describe the flow of two or more immiscible fluids both for theoretical studies and numerical simulations. In this situation, the transition between the two phases takes place smoothly across an appropriate diffuse interface or layer (in contrast with the sharp-interface approach, in which the physical parameters characterizing the flow are discontinuous across the interface). These models are based on the observation that even for two (macroscopically) immiscible fluids there is a very thin interfacial region in which partial mixing of the

two fluids occurs. In [26] there is a comparison between sharp and diffuse-interface models.

Phase-field models belong to the diffuse-interface family of models. They have been used to describe a variety of physical problems in which phase transitions play a role, namely condensation, evaporation, crystallization, etc. The importance of phase-field techniques has grown considerably as they can be implemented numerically in an effective way. They are characterized by a scalar parameter, called order parameter, which differs in the two phases. There are different choices for the order parameter: for example, the average volume fraction of a phase [52] or the mass concentration of a phase [20, 38, 42, 43]. In both cases, the order parameter has a clear physical meaning and its evolution is described by a nonlinear diffusion equation. In Chapter 3 we have derived a thermodynamically consistent phase-field model for the description of the expansion stage of the foam. We have adopted mass concentration of the liquid phase as phase-field variable.

The system of equations associated the phase-field model for metal foams is an incompressible-compressible version of a Navier-Stokes-Cahn-Hilliard (NSCH) system. Several numerical approximations of the NSCH system have been proposed in literature in the case of incompressible two-phase fluids, but, up to our knowledge, the numerical analysis in the incompressible-compressible case is missing. Very recently (see [25] and [27]) numerical techniques have been developed for quasi-incompressible fluids, i.e., fluids in which both phases are incompressible, but the mixing is compressible. The main difficulties in the numerical approximation of these systems are represented by the presence of the pressure in the chemical potential definition and by the velocity field that is no longer divergence-free. The idea is to build a numerical scheme that, at the discrete level, preserves mass conservation and the energy dissipation law associated to the original system. The Lowengrub-Truskinovsky (LT) system described in [38] for quasi-incompressible fluids has many similarities with the NSCH system associated to the metal foaming model, so the numerical discretization of the LT system presented in Chapter 4 can be considered as a preliminary step towards the discretization of the incompressible-compressible system of equations for the metal foaming model described in Chapter 5.

This thesis is organised as follows. After describing the main properties and the different production routes of metal foams (Chapter 1), in Chapter 2 we will give a deeper description of the expansion stage of the foam within the so-called "powder metallurgical route". We will describe the experiments we have performed at MUSP laboratory in order to find suitable hypotheses for the construction of a mathematical model of metal foam expansion. Chapter 3 presents a thermodynamically consistent phase-field model for the description of metal foam expansion, from which an incompressible-compressible version of a Navier-Stokes-Cahn-Hilliard system arises. Chapter 4 describes an energy-based numerical method for the LT system for quasi-incompressible fluids using a modified-midpoint temporal discretization, similar to the one adopted in [27], and using Discontinuous Galerkin finite elements for the spatial discretization (as in [24] and [25]). In Chapter 5 we extend the numerical approximation to the incompressible-compressible case, that is the expansion model for metal foams presented in Chapter 3.

Chapter 1

Metal Foams.

When a modern man builds large load-bearing structures, he uses dense solids; steel, concrete, glass. When nature does the same, she generally uses cellular materials; wood, bone, coral. There must be good reasons for it.

Prof. M.F. Ashby, University of Cambridge

Foams can be found in our everyday life: from the milk foam in our coffee cups and soap froth (see Figures 1.1-1.2), to architectural and design elements (see Figure 1.3).

Figure 1.1: Milk foam.

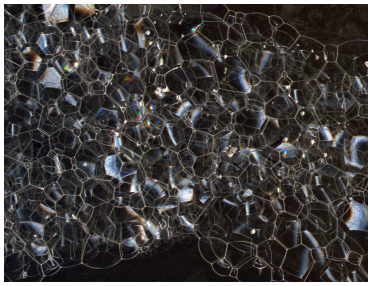

Figure 1.2: Soap froth.

Figure 1.3: The Beijing National Aquatics Center, also known as the Water Cube, was built for the swimming competitions of the 2008 Summer Olympics. The outer wall is based on the Weaire-Phelan structure, a structure devised from the natural pattern of bubbles in soap lather [63].

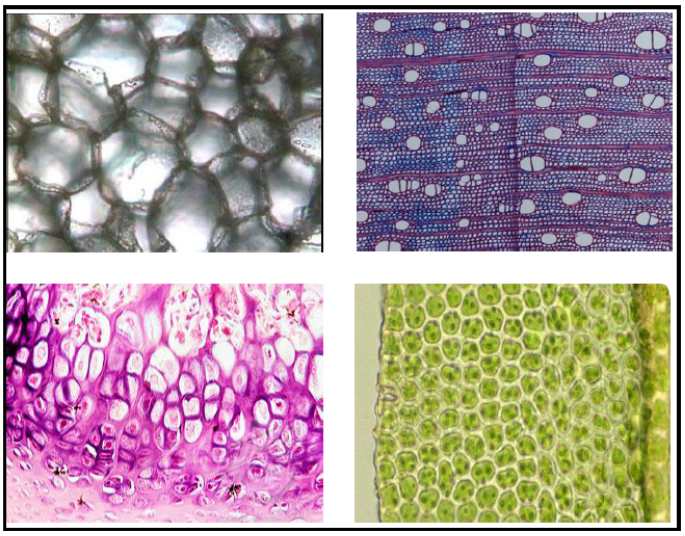

Figure 1.4: Cellular structure in nature: cork (top left), wood (top right), bone (bottom left), and leaf (bottom right) [10].

Nature is characterised by the presence of cellular structures: wood, bone, coral, cork, sponge, etc. (see Figure 1.4). Even the Universe structure could be considered foam-like [63]. The reason is that a cellular structure gives an optimization in the structural and mechanical properties, while lowering the weight. Researchers and engineers have started replying these natural cellular patterns in solid foaming materials. In this category the well-known polymeric foams and metal foams are included.

Metal foams are interesting materials with many potential applications [6, 7, 37]. They are characterised by a cellular structure, that is a metallic matrix including gas voids in the material. Thus, their density, or precisely, their relative density (foam density over the original metal density) can be considered as a new variable, with the real chance to modify ad hoc their physical properties. For industrial applications, metal foams offer attractive combinations of low density, high stiffness to weight ratio, good energy absorption and vibration damping capacity that cannot be obtained with other materials. If compared to

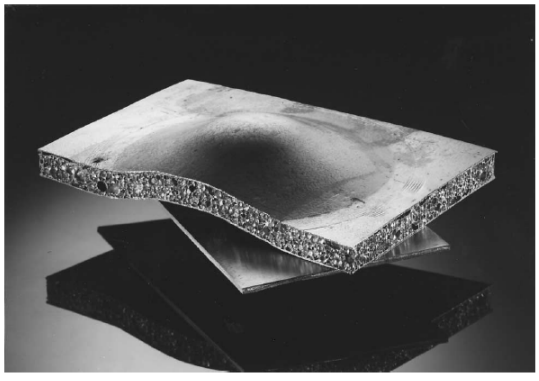

Figure 1.5: Sandwich panel having an aluminium foam core (thickness 12 mm) and two steel sheets [6].

polymers, metal foams maintain their mechanical properties at much higher temperatures and are generally more stable in harsh environments. As opposed to ceramics, they have the ability to deform plastically and absorb energy. Since the foaming of a metal decreases the density and increases the apparent thickness, a wide range of possibilities to use these materials arises in the automotive, aerospace, nautical, railway, building, civil engineering and medical industries. Metal foams can be used as reinforcement materials in hollow structure, to fill closed molds for manufacturing structural foam parts of complex shape or even for shaped sandwich panels with two dense face sheets and a cellular core (see Figure 1.5). Other applications could take advantage of the thermal and electrical conductivities of metal foams.

This chapter is entirely devoted to the description of the main properties, the processing routes and the applications of metal foams. After giving a definition for "metal(lic) foam" (Section 1.1), local equilibrium rules (Section 1.2) and foam phenomena (Section 1.3) will be recalled. A summary of the processing routes for metal foams is presented in Section 1.4. The enumeration of metal foam specific properties (Section 1.5) and foam characterisation through different methods (Section 1.6) will introduce the description of the most important applications (Section 1.7).

1.1 What are Metal Foams?

As reported in [6], if we consider all the possible dispersions of one phase into a second one -where each phase can be in one of the three states of matter- foams are uniform dispersions of a gaseous phase in either a liquid or a solid (as shown in Table 1.1). The single gas inclusions are separated from each other by portions of the liquid or solid, respectively. Thus the cells are entirely enclosed by the liquid or solid and are not interconnected. The term *foam*, in its original sense, is reserved for a dispersion of gas bubbles in a liquid. The morphology of such foams, however, can be preserved by letting the liquid solidify, thus obtaining what is called a *solid foam*.

	is dispersed in a gas	**is dispersed in a liquid**	**is dispersed in a solid**
when a gas	gas mixture	**foam**	**solid foam, cellular solid**
when a liquid	fog	emulsion	gel
when a solid	smoke	suspension slurry	embedded particles

Table 1.1: Dispersion of one phase into a second one. Each phase can be in one of the three states of matter [6].

When speaking of *metallic foams*, one generally means a solid foam. The *liquid metallic foam* is merely a stage that occurs during the fabrication of the material. Solid foams are special case of *cellular solid*. As in a liquid the minimisation of surface energy only allows for certain foam morphologies, the solid foam, which is just an image of its liquid counterpart, is restricted in the same way. In contrast, cellular solids are not necessarily made from the liquid state and can therefore have nearly any morphology, e.g. the typical open structure of sintered powders. Often such *porous structures* are also named foams, although the term *sponge* seems to be more appropriate. So, we can distinguish the following various expressions for metallic systems [3]:

- **cellular metal**: which are materials with a high volume fraction of voids made up of an interconnected network of struts and plates;
- **porous metal**: which have isolated, roughly spherical pores and a porosity level of usually less than about 70%. Mechanically, pores do not interact if the porosity is less than about 20%;
- **metal(lic) foam**: metallic foams are special cases of porous metals. They are also a subgroup of cellular metals, usually having polyhedral cells, but shapes may vary in cases where, e.g., directional solidification creates different morphologies. Cells may be either closed with membranes separating adjoining cells, or open, if there are no membranes across the faces of the cells so that the voids are interconnected. The expression metal foam, strictly valid only for the liquid phase, is often also used

to describe the solid product. Thus, the liquid counterpart is defined as *liquid-metal foam*;

- **metal sponge**: some prefer to call open-cell metallic structures metal sponges, not metal foams (see Fig. 1.6 and Fig. 1.7 for a comparison between closed-cell and open-cell metal foams).

These definitions are not mutually exclusive. A foam, e.g., is also a porous and a cellular structure, but a sponge does not necessarily have to contain cells. Moreover, as real materials are imperfect, the distinction is sometimes not easy.

Figure 1.6: An open-cell metal foam (metal sponge) (courtesy of MUSP).

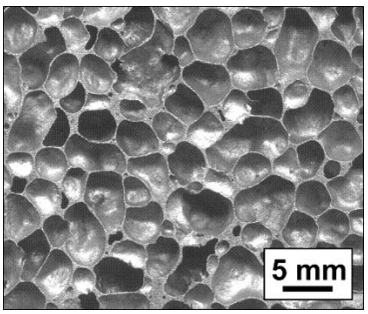

Figure 1.7: A closed-cell metal foam (metal foam) (courtesy of MUSP).

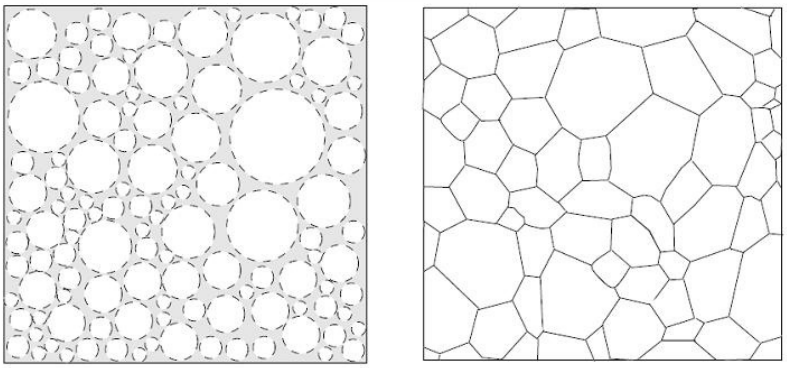

Figure 1.8: Wet foam and dry foam (courtesy of MUSP).

Another useful distinction is between *dry foams* and *wet foams* (see Fig. 1.8). A **dry foam** is a foam with little liquid. It consists of thin films which can be idealised as single surfaces. The bubbles take the form of polyhedral cells: the faces are the thin-film surfaces (which obviously are not flat), the films meet in lines (i.e., the edges of the polyhedra), the lines meet at vertices (see Fig. 1.9). The same terminology can be applied in the two-dimensional case, in which the bubbles are polygonal. Most foams owe their existence to the presence of *surfactants* molecules at bubble surfaces: they reduce the surface energy associated with surfaces and stabilise the thin films against rupture.

A foam that contains more than a percent of liquid by volume, does not completely conform to the description given above: the liquid can be found in the *Plateau borders* (Fig. 1.10), which are channels of finite width, replacing the lines of dry foams. The

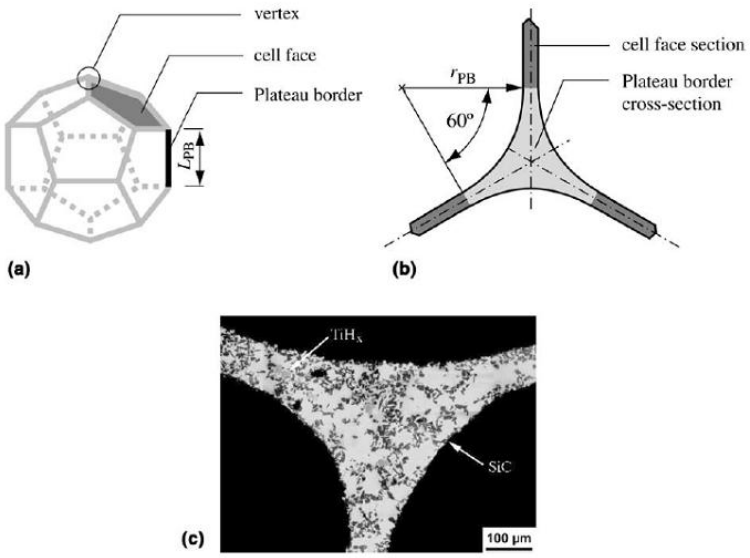

Figure 1.9: A dodecahedral cell with pentagonal faces and a microscope section of a Plateau border of an aluminium foam with the presence of tiny particles of SiC and TiH_2 (courtesy of MUSP).

polyhedral form of a bubble cell has its edges and corners rounded off. If the fraction of liquid further increases, the swelling of the Plateau borders leads to the extreme limit of a **wet foam**: in this case bubbles have a spherical shape. Foam loses its rigidity and is replaced by a bubbly liquid. In two-dimensional foams, the bubbles become circular at the limit of stability.

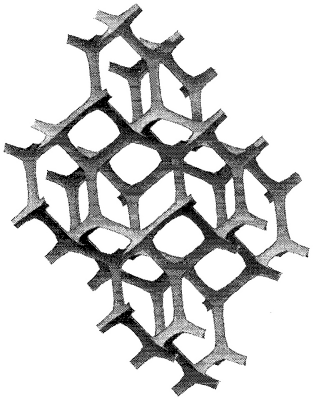

Figure 1.10: Plateau borders [63].

1.2 Local equilibrium rules.

In this section, following [63], we present the laws of Laplace and Plateau that rule the local equilibrium of a foam. Then we will describe the admissible (according to the local

equilibrium laws) topological changes for both dry and wet foams. This is useful in the study of some foam properties (e.g., coarsening, see Section 1.3).

1.2.1 The law of Laplace.

Gas-liquid interface must conform to the **law of Laplace**, expressing the balance of pressure difference across it, Δp, and the force of surface tension, acting upon an element of surface:

$$\Delta p = \frac{2\gamma}{r}, \tag{1.2.1}$$

where γ is the surface tension and r is the local radius of curvature of the surface. In a film within a foam, equation (1.2.1) must be adjusted to be

$$\Delta p = \frac{4\gamma}{r} \quad (3D) \tag{1.2.2}$$

on account of the two surfaces involved, although γ is sometimes used in place of 2γ in such a formula. In the case of two dimensions, we have

$$\Delta p = \frac{2\gamma}{r} \quad (2D). \tag{1.2.3}$$

If we apply the Laplace law to each single surface of the thin film, the pressure within the film is found to be the mean of the two gas pressures in the adjacent cells. This is obviously inconsistent with the equality of pressure throughout the liquid, since a much lower pressure p_b exists in the Plateau borders. In order to resolve this discrepancy, we need to recognise that the thin film is prevented from shrinking to zero thickness by repulsive forces between its two surfaces. The repulsive forces per unit area may be represented as a pressure to be included in the equilibrium condition. This is the **disjoining pressure** (see Fig. 1.11).

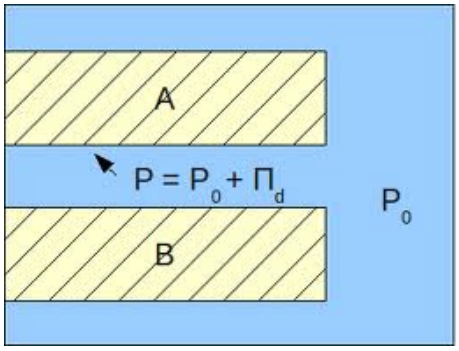

Figure 1.11: The pressure in a film can be viewed as $P = P_0 + \Pi_D$, where P_0 is the pressure in the bulk of the same phase as that of the film and Π_D is the disjoining pressure (courtesy of Stan J. Klimas).

1.2.2 The laws of Plateau.

The laws of Plateau, added to the law of Laplace, give some rules that are necessary for equilibrium. The first two rules relate to foams in the dry limit.

Equilibrium rule A1: *For a dry foam, the films can intersect only three at a time, and must do so at* 120°*(see Fig. 1.12). In two dimensions, this applies to the lines which define the cell boundaries.*

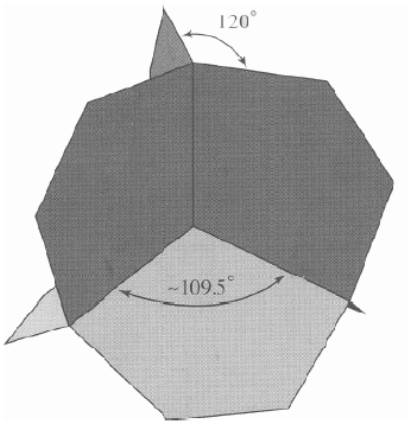

Figure 1.12: In a 3D dry foam, films meet at 120°, hence the vertex angles are 109.5° (the Maraldi angle) [63].

The 120° rule is required by the equilibrium of three equal surface tension force vectors acting at the intersection.

Equilibrium rule A2: *For a dry foam, at the vertices of the structure no more than four of the intersection lines (or six of the surfaces) can meet, and this tetrahedral vertex is perfectly symmetric. Its angles all have the value* $\phi = \cos^{-1}(-1/3)$, *sometimes called the Maraldi angle (see Fig. 1.12).*

The symmetry of the required tetrahedral vertex is dictated by the symmetry of the adjoining intersections (equilibrium rule A1).

For a wet foam, treating the film thickness as infinitesimal, the equilibrium of surface tension can be expressed by the following rule.

Equilibrium rule B: *Where a Plateau border joins an adjacent film, the surface is joined smoothly, that is, the surface normal is the same on both sides of the intersection.*

This means that the Plateau borders terminate in sharp cusps (see Fig. 1.13).

There are however *no* general stability rules for the multiplicity of the intersections at the Plateau borders, or their own intersections at junctions. We expect to find in a fairly dry foam only the features allowed in the dry foam, dressed with the Plateau borders of finite cross-section, and such is indeed observed. In two dimensions, this idea of dressing or *decorating* the dry foam structure with Plateau borders can be given an exact expression in the **decoration theorem**.

Decoration theorem: *Any two-dimensional dry foam structure can be decorated by the superposition of a Plateau border at each threefold vertex, to give an equilibrated wet foam structure, provided these Plateau borders do not overlap.*

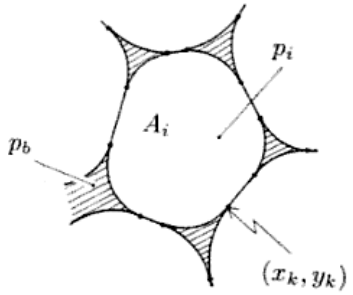

Figure 1.13: In a wet foam Plateau borders are smoothly joined to the adjacent films [63].

1.2.3 Osmotic pressure.

The bubbles in a foam with a very highly liquid content are spherical or nearly so. As the liquid drains out due to gravity, the individual bubbles are deformed into polyhedral shapes. The **osmotic pressure** (see Fig. 1.14) is the average force per unit area that is necessary to counter the increasing bubble-bubble repulsion, as they are squeezed together.

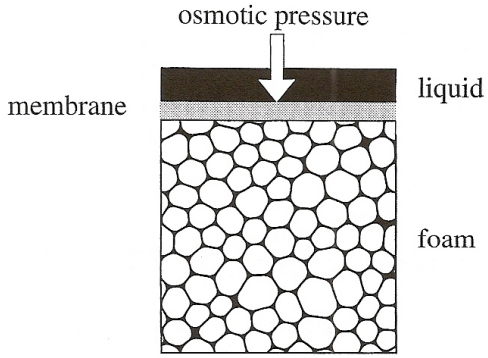

Figure 1.14: When a foam is in equilibrium in contact with a movable membrane porous to liquid (only), a force applied to the membrane is required to maintain equilibrium: expressed per unit area, this equals the osmotic pressure [63].

1.2.4 Topological changes.

A large part of foam properties is due to the role played by topological changes. For *two-dimensional* foams, two elementary changes (T1 and T2) can be defined: all the others may be regarded as a combination of these. For a dry foam, thanks to the Plateau laws, we observe that a fourfold vertex dissociates into two stable threefold vertices: this is a **T1 process** (see Fig. 1.15). So, the smooth changes in the structure of the foam due to coarsening or applied stress is punctuated by rapid T1 processes. For both dry and wet foams, a three sided cell may be removed: this is a **T2 process** (see Fig. 1.16). This is what occurs in coarsening. A two-dimensional wet foam is not subject to Plateau's requirement of threefold vertices. For this reason, the possibilities are much richer. Stable multiple vertices does exist. Hence the T1 process can be substituted with the one shown in the Figure 1.17.

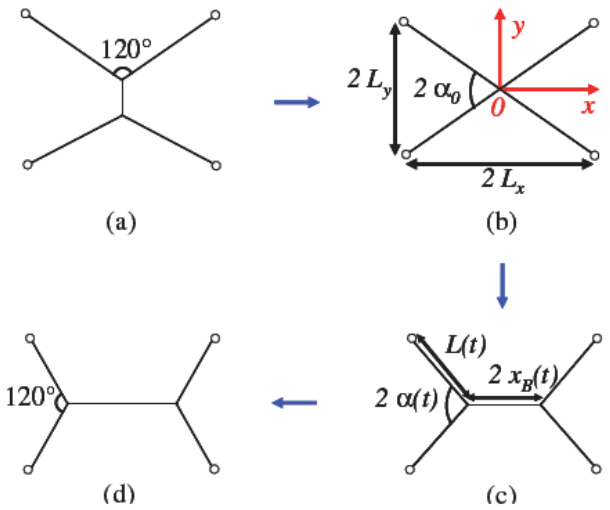

Figure 1.15: Schematic of the T1 transition. The initial configuration (a) evolves continuously through metastable states, for which Plateau laws are satisfied, to an unstable four-fold configuration (b). This unstable state spontaneously evolves into two three-fold junctions with creation of a new film (c) until a new metastable configuration (d) is reached, and Plateau laws are satisfied again [18].

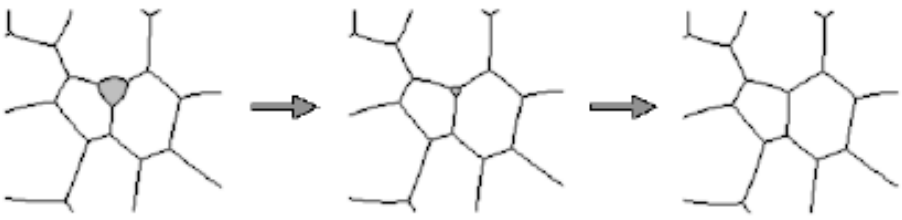

Figure 1.16: The T2 process for a 2D dry foam. When a threesided cell approaches zero area due to gas diffusion, it will perish [32].

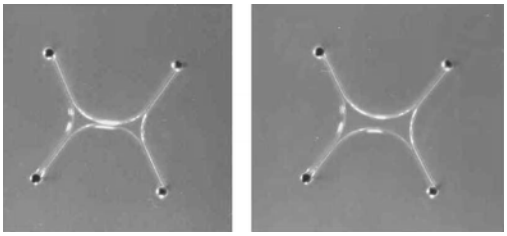

Figure 1.17: For a wet foam the intermediate configuration may be stable. A stable fourfold border is formed upon increasing the liquid fraction [62].

In a *three-dimensional* dry foam, the most elementary rearrangements are shown in Figure 1.18. It is often found to be combined with a second change (see Fig. 1.19). Again, wetting the foam allows multiple vertices to be stable, and the possibilities are richer. Figure 1.20 shows the vanishing of a three-dimensional cell, corresponding to a three-dimensional T2 change.

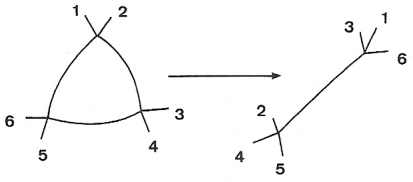

Figure 1.18: Elementary rearrangement in a three-dimensional dry foam, corresponding to the two-dimensional T1 process [63].

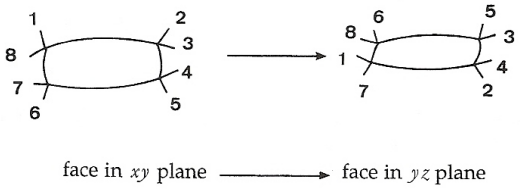

Figure 1.19: This type of rearrangement is more commonly observed than the more elementary form in Fig. 1.18 [63].

1.3 Essential properties of a foam.

1.3.1 Rheology.

Under low applied stress, a foam is a *solid* (see Fig. 1.21, on the left). We may attribute to it an elastic **shear modulus**, as for any isotropic solid material. It depends on bubble size and wetness.

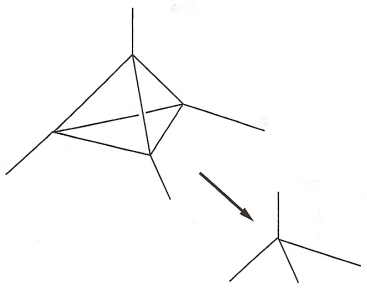

Figure 1.20: The T2 process in three dimensions [63].

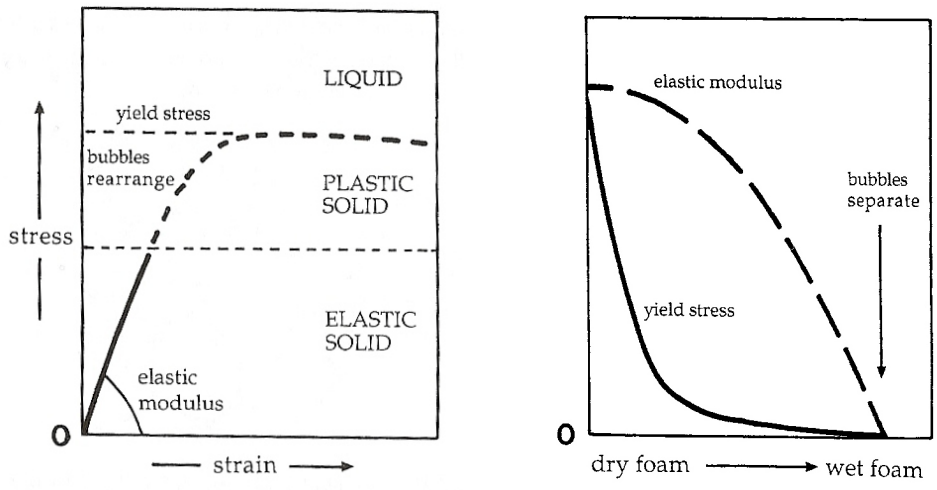

Figure 1.21: On the left, the stress-strain relation for a liquid foam. On the right the relation between the yield stress and the liquid fraction of the foam [63].

For sufficiently large deformations, topological changes are induced which are not immediately reversible if deformation is reduced. The foam becomes progressively *plastic*.

Beyond a certain **yield stress**, the foam flows, as topological changes are promoted indefinitely. Yield stress depends on bubble size, and also very strongly on wetness: for a dry foam it is of the same order as the shear modulus, for a wet foam is much less (see Fig. 1.21, on the right).

1.3.2 Drainage.

Foam drainage plays an important part in the formation and evolution of liquid foams. A freshly formed foam is not in equilibrium under gravity, and liquid drains out of it until such an equilibrium is attained. This is *free drainage*. Drainage causes a reduction in film thickness, rupture and coalescence of bubbles and a density gradient along the vertical direction of the foam.

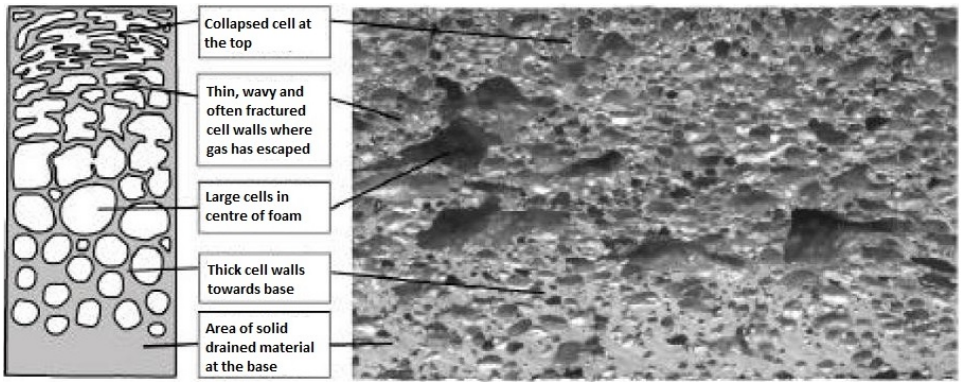

Figure 1.22: Transport of liquid through the foam (courtesy of MUSP).

1.3.3 Coalescence.

Coalescence is the fact that films crack when they become too thin and when they are stretched too much. As we can see from Fig. 1.23, coalescence of two bubbles is a highly dynamic process which impacts a larger neighborhood and eventually leads to sudden cascades of bubble coalescences. In between such cascades, the bubbles assume very quickly a perfect round shape.

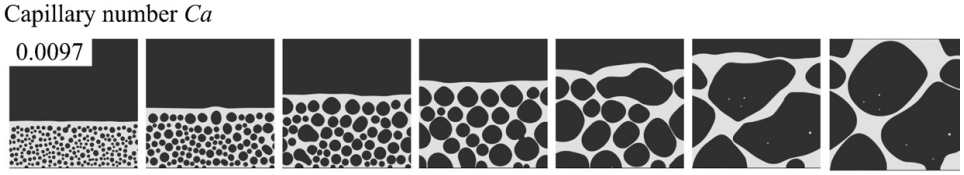

Figure 1.23: Coalescence of bubbles during aluminium foam evolution [33].

1.3.4 Coarsening.

The pressure differences between the cells of a disordered foam drive the diffusion of gas through the thin films which separate them. A single bubble will shrink and disappear for this reason and a similar fate awaits each bubble in a foam. While some will initially grow at the expense of others, all must eventually perish. This process is called coarsening. Pressure is proportional to the inverse of pore diameter: so, the smaller pore with the higher internal pressure disappears after giving its gas to the larger one (see Figure 1.24).

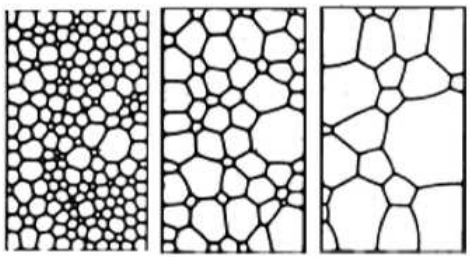

Figure 1.24: Schematic view of a 2D-foam coarsening process [39].

1.3.5 Collapse.

Most liquid foams do not last very long. Usually they collapse by the rupture of exposed films. Many factor can be adduced to account for this, singly or in combination. Drainage is important in reducing the film thickness, evaporation may reduce it further, the surfactant concentration may be inadequate, impurities may promote film instability. Foam collapse causes phenomena of bubble coalescence, loss of gas out of foam, a reduction in foam volume (see Figure 1.25).

Figure 1.26 shows the interdependence between foam decay phenomena.

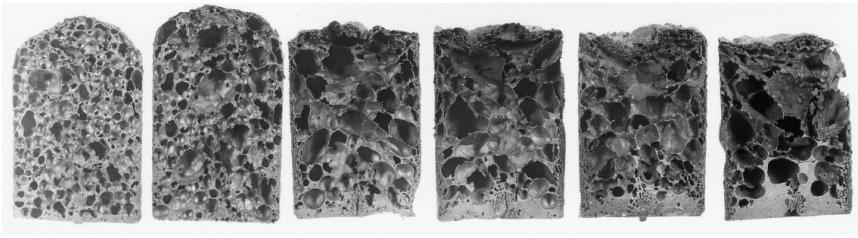

Figure 1.25: Aluminium foam collapse [17].

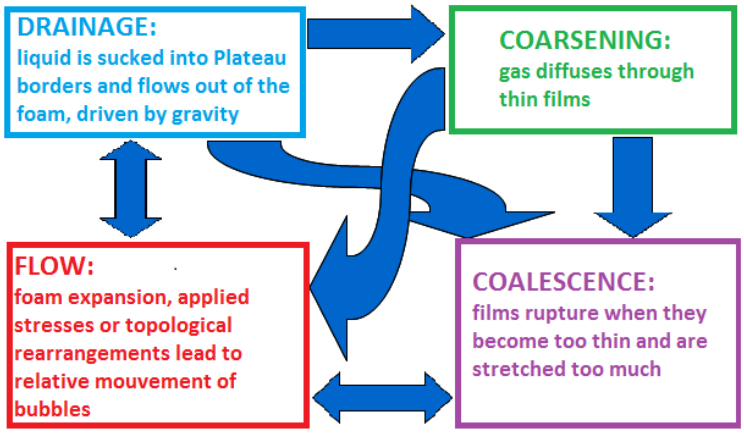

Figure 1.26: Phenomena which can occur during metal foam evolution [2].

1.4 Making foams.

As we previously discussed in Section 1.1, a metallic foam is a mixture of a gas and a solid phase in which the gas bubbles are isolated from each other while the solid matrix is contingent. In addition, we only consider foams originating from a liquid precursor in which gas bubbles can arrange freely without the help of a template.

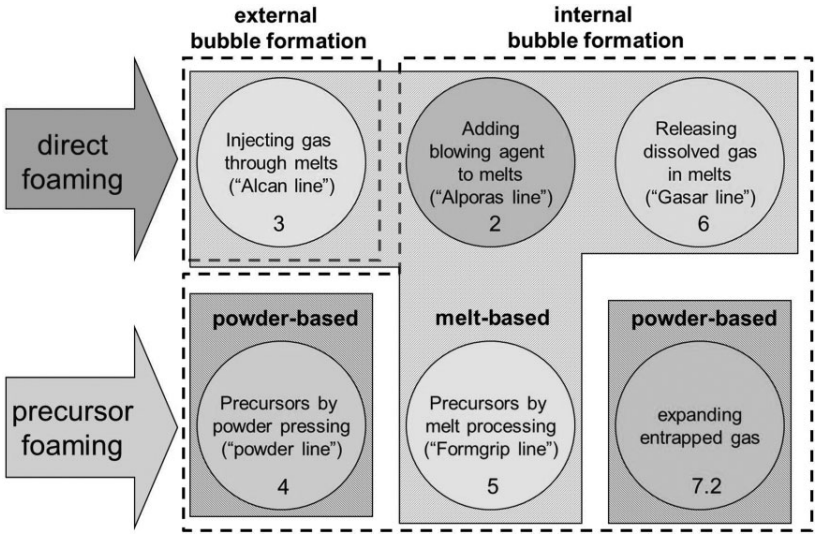

Figure 1.27: Principal methods for foaming metal [8].

In [8] Banhart grouped the different foaming techniques into various *lines*. Each method is named after a prototype of a process within a *line* (see Figure 1.27).

Direct foaming methods convert a liquid metal or alloy into foam without an interruption (look at the upper line in Figure 1.27). Depending on the gas source, we define the *Alcan line* in which the gas can be injected into the melt, the *Alporas line* in which a

chemical blowing agent can be added to the melt where it decomposes and liberates gas and the *Gasar line* characterized by the gas dissolution into the melt before its release during the foaming process.

Figure 1.28: On the left: aluminium foam blown with air from a particle-stabilised melt and beer; on the right: zinc foam and bread roll, both foamed by internal gas creation [2]. In the first case, gas is injected continuously to create foam. The foam accumulates to the surface and the result somewhat looks like a glass of draught beer. In the second case, gas-releasing propellants are added to the melt, very similar to the yeast of the baker.

Precursor foaming (*indirect foaming*) methods involve the melting of a solid material in which a gas source has been embedded that upon melting releases gas and drives the foaming process. The precursors can be made both by powder pressing (*Powder line*) or by melt processing (*Formgrip line*). In many cases the gas source is a blowing agent powder, but precursors are also made by entrapping gas in a powder mixture during densification and expanding the compact by subsequent thermal treatment.

Another distinction, from Figure 1.27, is between the different ways of bubble formation (*internal* from local sources or *external* at the gas injection points, see Figure 1.28) and between the states the base metal is during the processing (*melt* or *powder*).

The next subsections will briefly describe the historical evolution of the various foaming lines (see [8] for further details and references). The *powder line* will be studied more deeply in the next chapter.

1.4.1 Alporas line.

The first ideas of metal foaming techniques belong to De Meller in 1925 in France. He described a process in which there is an injection of inert gas into a molten metal or the addition of a blowing agent such as carbonate to a molten metal, during which the melt is stirred. His patent suggests also how to produce integral foams consisting of an inner foam core and a dense outer cover layer: De Meller claims that also complex parts can be made, but no real parts are shown. His knowledge of the feasibility of foaming aluminium with carbonates suggest that he worked on this fact, but he did not describe melt stabilisation which ensures that bubbles created in a melt remain stable during processing and do not rupture or coalesce. In addition it is known that bubbling inert gas through an Al melt does not produce stable foam, so the first variant that De Meller proposed (i.e. inert

Figure 1.29: Bjorksten demonstration of both lightness and stiffness of Al foams [8].

gas injection) cannot work in a simple way. De Meller talked about applications in the building industry and in airplanes, but no other technical details were given.

The next step in foaming history takes place in the USA in 1948. Benjamin Sosnick attempted to foam aluminium with mercury. He first melted a mix of Al and Hg in a closed chamber under high pressure. The pressure was released, leading to vaporisation of the mercury at the melting temperature of aluminium and to the formation of foam. In the mid 1950s it was well understood that liquid metals could be more easily foamed if they were pre-treated to modify their properties. This could be done by oxidising the melt or by adding solid particles. In 1951, John C. Elliott developed an aluminium foaming process at Bjorksten Research Laboratories (BRL) improving De Meller's process. He proposed to use TiH_2 or ZrH_2 as a blowing agent. As De Meller, he did not mention measures to stabilise foams. In addition he did not recognised the role of the oxides in the melt and the necessity of cooling the foam quickly in order to prevent foam decay indicates difficulties in the stabilisation of the foam. Beside Elliot, also William Stuart Fiedler, Stuart O. Fiedler and Johan Bjorksten (see Figure 1.29) are further inventors, first at BRL laboratories, then for the Lor Corporation to where the metal foam business is shifted for upscaling and commercial developments around 1960. They described the design of a continuous foaming process where granulated base metal and blowing agent are continuously heated and foamed.

As we previously mentioned, metal foams have to be cooled quickly after foaming. This leads to problem in foam stability, leading to non-uniform pore sizes and limitation in the production of small foam components. The high fraction of blowing agent used at that time inflates the pores but also ruptures the walls between bubbles and gives rise to big pores. John Ridgway of the Standard Oil Company proposed a solution based on dispersing a finely divided, wetted inert powder in the molten metal which remains solid there. In addition, he observed that the accidental entrainment of oxygen into the liquid metal during the addition of the blowing agent, which is usually accompanied by stirring, is a prerequisite for foaming. The entrained oxygen partially converts the blowing agent particles TiH_2 to TiO particles while hydrogen is liberated. These oxide particles stabilise the foam. Ridgway proposed to add MnO_2 to the aluminium alloy melt. It reacts with Al and leads to the formation of aluminium particles that are dispersed in the melt. In this way there is a reduction in the amount of blowing agent, more nucleation sites for bubbles, a more uniform distribution and smaller bubbles.

In the late 1960s at the Ethyl Corporation in Baton Rouge, Currie B. Berry proposed

thickening the metallic melts to be foamed by sparging oxygen, air or CO_2 through them as an alternative way to stabilise foams. A lot of work is done developing commercial uses for foamed aluminium, like large wall panels or energy absorbing bumpers for cars (see Figure 1.30).

Figure 1.30: Aluminium foam blocks produced in the 1970s by the Ethyl Corp. [8].

The Shinko Wire Co. Ltd., Osaka, Japan, a subsidiary of Kobe Steel, invented a process that is closely related to the one developed at the Ethyl Corporation and filed a patent in 1985 in Japan and later in Europe and USA. Metallic calcium is added to molten aluminium alloy after which the melt is stirred for several minutes at ambient atmosphere. During stirring the viscosity increases. After a predefined viscosity level has been reached, the thickened melt is poured into the foaming vessel and TiH_2 is admixed while stirring continues. After this, the melt is left for foaming for a quarter of hour. When the foam has filled the foaming vessel, the gas vents of the vessel are closed. Cooling the foam is done by air blowing. Cell sizes varies from 2 to 10 mm (see Figure 1.31). This type of foams is called **Alporas**. In [8], Banhart notice that the thickening is caused by the contact of

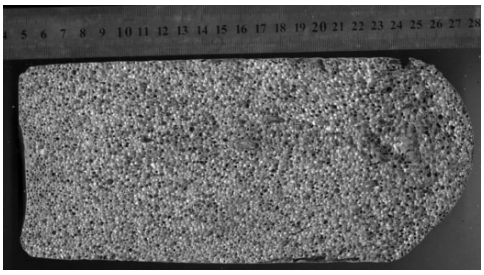

Figure 1.31: Alporas material: pure Al thickened with Ca and foamed with TiH_2 [8].

the melt with air and the oxidation causes the formation of particles that are crucial for the stabilisation of the foam. Calcium allows to obtain a sufficient number density of stabilising particles in the melt in a very short time. However, melt treatment with calcium is only one option. Further research is carried out to find alternate particles that are able to stabilise the foam. It is realised that solid particles in a metallic melt stabilise metallic films because they are situated at the gas-liquid interface. The blowing agent TiH_2 can be replaced by carbonates (especially $CaCO_3$) for reasons of safety and costs. However, the implementation of this technique, that goes back to De Meller's experiences, is not straightforward. It can be shown that melts can also be foamed without the addition of

blowing agent powders. Besides aluminium, also magnesium and zinc based foams have been studied.

1.4.2 Alcan line.

Gas can be injected from an external source through a nozzle into a metallic melt. This has been suggested by De Meller and later by Fiedler. The former proposed inert gas, the latter oxygen or steam. The gas blowing approach promises to replace potentially expensive blowing agents by cheap gases, but it is not easy to implement. The same melt that can be foamed by adding a blowing agent powder, might not be easy to be foamed by injection of gas from outside. The difference is that a multitude of gas bubbles are created locally in the former one, whereas in the latter, the gas bubbles are created at one, or few, points only and have to float through the melt from the injection point to their final position. Depending on the structure of the melt this might not happen and no foam is formed.

In 1989 there are patents from the Aluminium Company of Canada (**Alcan**) and from the Norwegian Norsk Hydro Company almost simultaneously. The Canadian group discovered this process quite accidentally, while processing liquid aluminium matrix composites (MMC). They observed that gas bubbles were remarkably stable in such melts and realised that foam could be produced by injecting gas into MMC melts instead of adding gas-releasing blowing agents. Figure 1.32, on the left, explains the process. Gas is injected

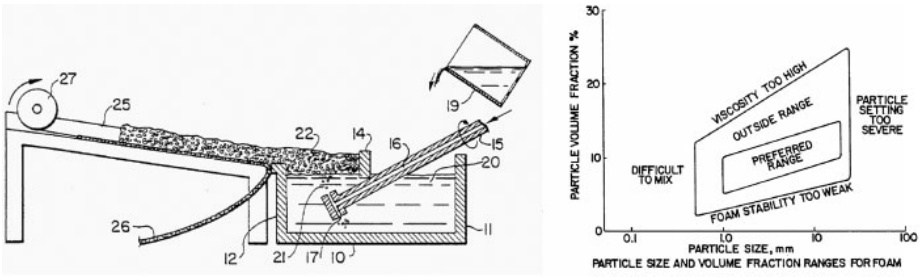

Figure 1.32: On the left, schematic of foam production taken from the patent of Alcan; on the right, relationship between particle fraction and size required for good foaming [8].

to below the surface of a melt and bubbles are formed that float to the top, accumulate there and form a metal foam layer. The particles dispersed in the liquid MMC act as stabilisers. They adhere to the gas/metal interfaces of rising bubbles. There is a minimum content of particles required for stability that depends on particle size (see Figure 1.32, on the right) and also on the distance between the injection point and the surface. Gas injection is done by a rotable air injection shaft connected to a number of outlet nozzles through which the gas (mostly air) escapes into the liquid. The use of a rotating shaft equipped with various blades is also suggested. The development at Norsk Hydro is very similar. Liquid aluminium based MMC alloys were foamed by injecting air or CO_2, after which the resulting foam layer formed on top of the melt is removed. Gas is injected through a rotor. However, foams produced by both the companies in 1990s (see Figure 1.33) had large pores and were not uniform. A gradient of pore size, shape and density from bottom to the top of the slabs was evident and mechanical properties were below expectations.

At Light Metal Competence Centre (LKR) in Ranshofen (Austria), to obtain uniform foam, researchers stated that it is more favorable to create and maintain individual equally sized bubbles. They proposed to use stationary injectors made of a ceramic material that

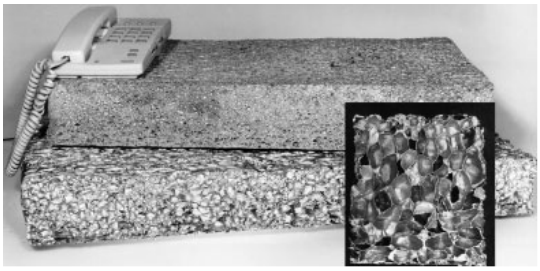

Figure 1.33: Foam samples made by Hydro Aluminium, by blowing gas into SiC containing Al MMCs. Inset: micrograph of similar Alcan type foam [8].

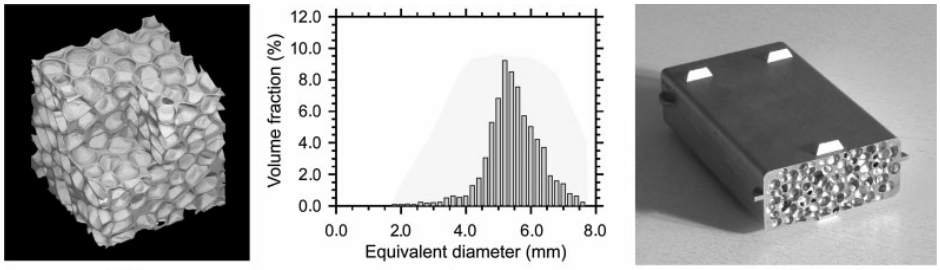

Figure 1.34: Foam made at LKR from aluminium alloy in which SiC particles are dispersed. On the left, a X-ray tomogram of a foam cube; in the middle, pore size distribution in that sample; on the right, a molded part of Al foam with dense outer skin [8].

have a defined conical geometry. This new nozzle design provides stable bubble separation criteria and allows one to make foam with a plurality of bubbles with almost the same volume. In another patent researchers proposed to blow bubbles from an array of the injectors described above, in order to increase bubble formation rate (see Figure 1.34).

1.4.3 Powder line.

The term **powder metallurgical** or **powder compact foaming** or, more simply, **powder** route is used for the foaming process in which a solid metallic precursor is first prepared and then expanded to a foam by thermal treatment. The precursors are made by processing blends of metal and blowing agent powders.

The first mention of the possibility to expand solid precursors made by consolidating powder mixtures and to fill closed molds with cellular material goes back to 1950s. John F. Pashak of the Dow Chemical Corporation proposed to mix Mg-base or Al-base metal powders with either $MgCO_3$ or other carbonates that can act as blowing agent, extruding these mixtures and then heat treating the extrusion below the melting temperature of the respective alloy. The blowing agent releases gas and the material expands in the solid state to form a foam, whose cells appeared to be irregular. Later Benjamin C. Allen of the United Corporation further developed these techniques, by mixing metal powders (e.g. aluminium) with a blowing agent (e.g. TiH_2, ZrH_2 or $CaCO_3$), extruding the mixture after an optional cold pre-compaction step and then foaming the extruded precursor by controlled heating to at least the melting point of the metal or alloy. The latter step is the main difference with the previous process (Pashak expanded the precursor in solid state). Allen observed that during the extrusion process the oxide films around each powder particle are broken and a good consolidation is achieved. Axial hot pressing of the

powders was insufficient, i.e., extrusion was essential.

The powder route process was later rediscovered in 1990s. Joachim Baumeister of the Fraunhofer-Institute in Bremen (Germany) redeveloped the powder process. In a first moment, he did not have the knowledge of the previous attempts in 1950s. The only difference of his technique is that the compaction temperature of the powder is higher. As a result, hot pressing yielded a good enough compaction to ensure very good foaming (in contrast with Allen's experiments). Initially compaction is done uniaxially, later extrusion is used to make foamable material more efficient. Production of foamable precursor by continuous extrusion is also developed, aiming at making large quantities of precursor material of small cross-section. Another way to produce foamable alloy is by powder rolling. Powders are filled into flat containers and then hot rolled and then densified in various passes. The container material remains as a dense outer skin.

For what concern the stabilisation, foams made from metal powders are stabilised by the natural oxide layers on the powder surface. One idea could be to tailor the oxide content of the metal powders in order to obtain maximum stability. For less than 0.3% oxide in Al precursor, poor stability was noted. More than 0.6% oxide contents compromises foam expansion indirectly by its negative impact on powder compaction. It is difficult to separate the direct influence of oxides on foam stability from other effects such as the quality of powder compaction. Additional particles can be added in order to further promote foam stability, e.g., SiC, Al_2O_3, TiB_2, soot, or metallic TiAl6V4. Foam stability may also depend on the presence of alloying elements. Magnesium is usually ascribed a positive influence on Al alloy foam stability.

We will give other details on the powder metallurgical route in the next chapter.

1.4.4 Formgrip line.

In the Alporas and Alcan lines a liquid foam is created in a foaming vessel in one step. The liquid foam is solidified to a block unless it is cast into a mold. Therefore, net-shaping of foams to complex components or thin sheets is difficult. The precursor processes avoid this problem since foam can be generated in molds or between face sheets of a sandwich panel by expanding a precursor. However, the necessity to use metal powders makes the process expensive. In order to combine the advantages of these approaches, the idea is to start processing by adding a blowing agent to a melt, but then to interrupt the incipient foaming process by swift cooling. The precursor obtained in this way will then be foamable upon reheating and can be further processed in analogy to the powder compacts of the powder line process. This way of processing has been proposed by William J. Ptashnik of the General Motors Corporation. He admixed blowing agent to an alloy melt held in the semi-solid state at a temperature at which the blowing agent does not decompose. The melt is solidified to a precursor in a second step. Foaming is done at a higher temperature than mixing, so that the blowing agent releases gas and creates bubbles.

The University of Cambridge, UK, in 1998, developed another way to make a foamable precursor. They considered a liquid aluminium alloy containing SiC particles. TiH_2 is added to the melt after being preoxidised in order to prevent it from releasing too much gas during mixing. In addition, to prevent burning of the hydride, TiH_2 powder is mixed with some Al powder and pressed to pellets that are added to the melt. After stir-homogenising, the melt is cast into a cold crucible and heat is removed as fast as possible. The resulting solid material contains some porosity but is predominantly dense. This precursor is converted into a foam during a foaming step very similar to the one adopted for the powder line. The result is a very uniform foam with all the advantages of the precursor route. This type of process is called **Formgrip**, which stands for *foaming*

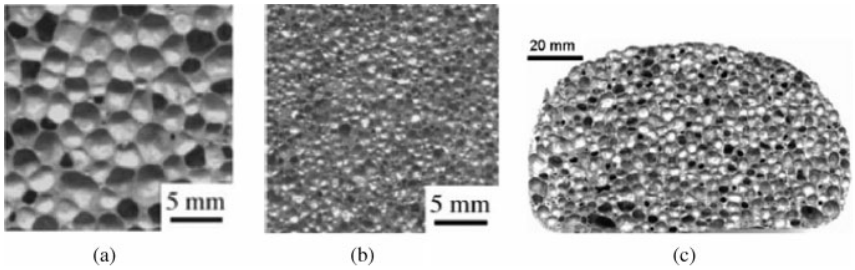

Figure 1.35: Foams made by the Formgrip process (a), the Foamcarp process (b) and the two-step (interrupted Alporas) process (c) [8].

of reinforced metals by gas release in precursors. If $CaCO_3$ is used as a blowing agent, the process is called **Foamcarp** (*foaming aluminium MMC by the chalk-aluminium reaction in precursors*); notice that reactions between the metal and the carbonate help in foam stabilisation.

Arnold Melzer of the Fraunhofer-Institute in Bremen, in 1998, developed another procedure in which aluminium alloy is injected into the die a cold-chamber die casting machine. At the entrance of the die, a small reservoir contains TiH_2 powders and some aluminium powders. During melt injection, the powders and the melt are intensely mixed. In the die, the metal solidifies quick enough to avoid notable decomposition of the blowing agent and therefore a largely dense precursor with embedded blowing agent particles is obtained that can be foamed by reheating. However, the resulting foam is not very stable if too little aluminium powder is added, as the oxide content in the cast material is low.

Some researchers (Babcsan, Kadoi et al.) proposed a modification of the Alporas-line techniques. They suggested to interrupt the foaming process immediately after adding the blowing agent and to obtain a solid precursor which can be foamed upon reheating. This method is called **two-step foaming** or also **interrupted Alporas** process. Figure 1.35 shows samples of foams produced with Formgrip, Foamcarp, and two-step foaming processes.

1.4.5 Gasar line.

Gas dissolved in a melt is a potential gas source that could blow metal foams. The solubility of most gases in metals is highly temperature dependent and shows abrupt changes at temperatures where transformations occur, e.g., at melting point. Solubility, according to Sievert's law, is pressure dependent. So, if one charges a metallic melt with gas and solidifies it, possibly with a pressure drop, gas will precipitate and it will be utilised for foam formation.

A different class of materials can be obtained by releasing gas from a gas-charged melt during solidification in a controlled way. Bubble growth is controlled by a directional solidification. This principle was first discovered by Vladimir Shapovalov in Dnepropetrovsk, Ukraine and was later developed by Hideo Nakajima in Osaka, Japan. The former scientist called these foams **Gasars**, whereas the latter **Lotus Metal**. The variety of metals, alloys and ceramics that can be processed is large: not only hydrogen, but also nitrogen and oxygen can be used as blowing agent. First Cu was used as material for this foaming process, later also Fe, Ni, Ag and brass.

1.4.6 Other foaming processes.

Amorphous metals (metallic glasses) shows exceptionally high strength levels compared to other crystalline metals. The use of these metallic glasses as matrix material for metallic foams promises strong foams, called **Amorphous (Metallic Glass) Foams**.

Sputter deposition is used to manufacture a metallic material in which a multitude of gas atoms are entrapped. If this material is heated to a temperature above the melting temperature of the metal and held there for a while, the gas will nucleate to small bubbles and form a porous body.

Spray forming involves atomising a melt and depositing the metallic spray on a substrate, forming a dense material. If one adds a blowing agent to the spray, a foam can be obtained.

1.4.7 Final overview.

Figure 1.36 reviews the historical development of metal foaming techniques.

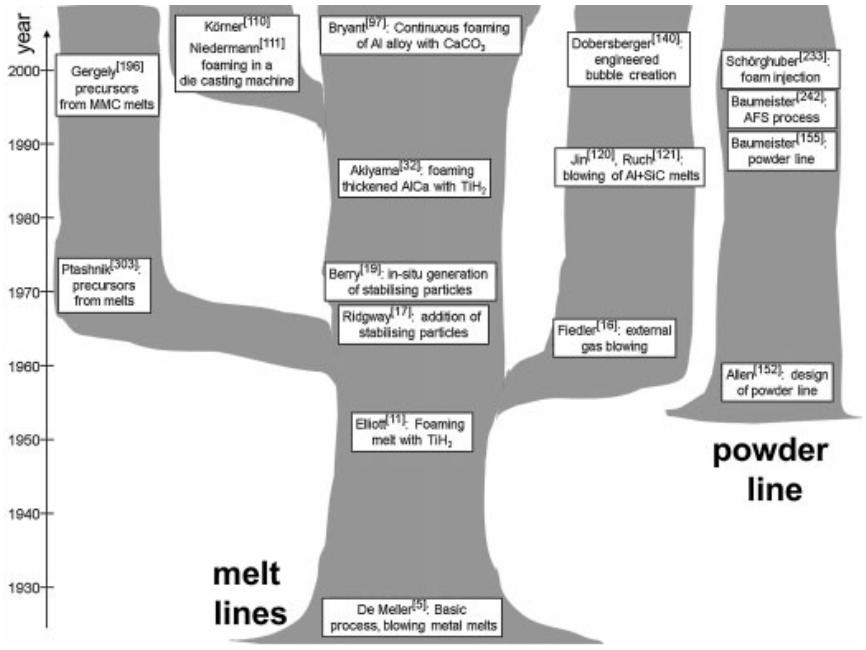

Figure 1.36: Overview of some important milestones in metal foaming technology until the year 2005 [8].

Banhart [8] observed that almost no literature describing details of the manufacture of metal foams and very little on metal foam properties is available before 1990. The reason is in the commercial and military interest of the companies, funding agencies and research institutes involved. A change came in 1990s when a Multidisciplinary University Research Initiative is created in the USA (MIT, Harvard and Virginia University) and in the UK (Cambridge University).

Nowadays metal foams have found niche market applications, even if there are available techniques for almost all the possible expectations (see Section 1.7 for a brief review on

metal foam applications). One of the principal reason of this fact is metal foam price. So, according to Banhart, future process developments should be done in the direction of reducing costs and not only in the improvement of foam properties. The problem of the costs and the standardisation of the production route are among the motivations for this research activity and will be better explained in the next chapter.

1.5 Specific properties of solid metal foams.

1.5.1 Density and porous structure.

The most prominent property of foamed metal is its low density: density values of aluminium range from 0.3 g/cm^3 to 1 g/cm^3 for foams produced by the powder method. The pores are predominantly closed and foams usually develop a closed outer skin hiding their porous structure. The porous structure is evident when the metal foam is cut apart. This

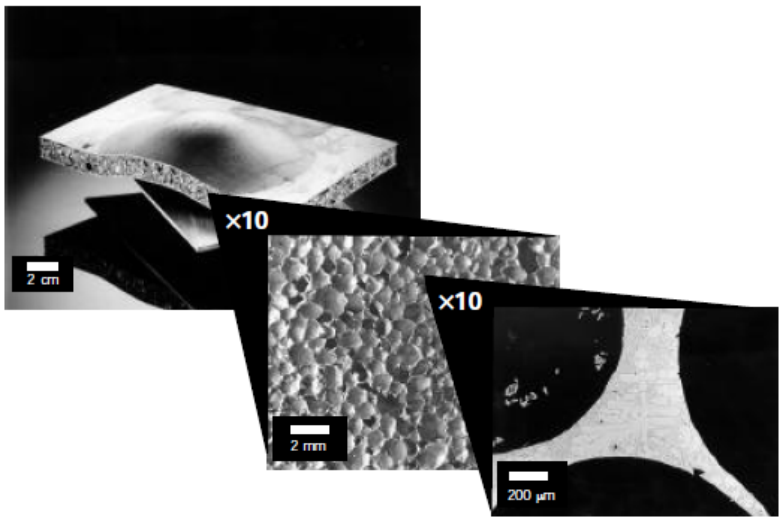

Figure 1.37: Sandwich part of a foamed aluminium layer [4].

can be seen in Figure 1.37: at the top left there is a sandwich part consisting of a foamed aluminium layer and two metallic face sheets. The saw cut of the sandwich has been enlarged by ten and reveals the highly porous nature of the material. Further magnification finally shows features like the intersection of three cell membranes - a so-called Plateau border - as shown at the lower right.

1.5.2 Mechanical properties.

The study of mechanical properties of metallic foams is an important topic, because foam applications, as we will see in the last section, are primarily load-bearing (e.g. for sandwich structures). Even foams whose main properties are functional (e.g., acoustic, thermal or surface area) require minimal mechanical properties to prevent damage or failure. The mechanical properties strongly depend on the apparent density of the foamed material. Quantities such as the Young's modulus, compression or tensile strength increase rapidly with increasing density. An example for a density dependence is shown in Figure 1.38, where the deformation strain of an aluminium foam is shown as a function of applied stress for various different densities. The deformation behaviour observed is typical for all kinds

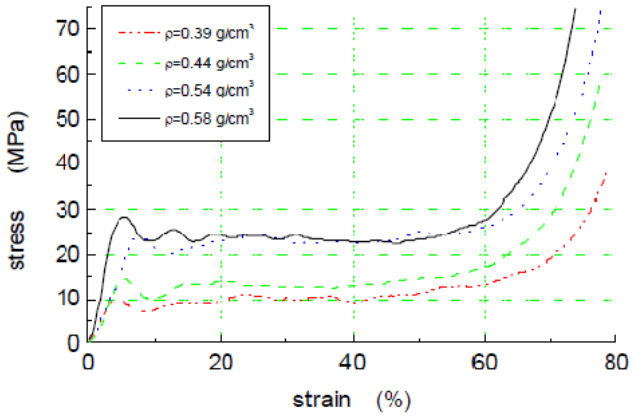

Figure 1.38: Deformation behavior of various aluminium foams. Deformation strain versus applied stress is shown [4].

of foams not only for metallic ones. There is a linear increase of stress at the beginning of the deformation and a plateau regime of nearly constant stress for deformations up to 60% followed by strong compaction for even higher deformations. Apart from density, mechanical properties are also influenced by the choice of the matrix alloy. Due to the special form of the compressive stress-strain curve, foamed materials have a high capability of absorbing large amounts of energy at a relatively low stress level.

1.5.3 Acoustic properties.

Metallic foams have been considered in various acoustic applications. On one hand, the unique structure of these materials can provide good sound absorption characteristics. On the other hand, their acoustic properties can be combined with other characteristics of the metallic foams (i.e., thermal and chemical stability, mechanical properties) to make them more attractive than common sound absorbers such as mineral wool or polymer foams. Budget associated with sound management being generally low, metallic foams will find applications when substantial improvements are observed or when the combination of the properties of the metallic foams represents an important benefit (i.e. standard sound absorbers are generally much cheaper than the most metallic foams).

1.5.4 Thermal properties.

Metallic foams are conductive, permeable and have high surface area. The combination of properties make them attractive for various thermal applications (heat exchangers, heat sink, heat pipes). Heat exchanges and conduction in metallic foams are complex phenomena. Heat exchange efficiency is affected by the conductivity of the foam, the heat exchange between the foam and the surrounding fluid and the pressure drop in the foam. These characteristics are all affected by various structural parameters (density, pore size distribution, cell connectivity, tortuosity, strut size, density and geometry, surface roughness) that are difficult to measure and to integrate.

1.5.5 Cell sizes and cell morphology.

Intuitively one tends to assume that metal foam properties are improved when all the individual cells of a foam have a similar size and a spherical shape. This, however, has not

really been verified experimentally. A clear influence of cell size distribution and morphological parameters on foam properties, however, has not yet been established. The reason for this is that it has not yet been possible to control these parameters during foaming. Therefore, studies of the interdependence of morphology and properties of foamed metals have in the past either been purely theoretical or have been concentrated on more simple systems such as open cell structures or honeycombs which can be manufactured in a more controlled way. Still, there are various opinions on what the ideal morphology of a closed - cell foam yielding the highest stiffness or strength at a given weight should be. Some authors find an insensitivity of strength on cell size distribution, others claim that a bimodal distribution of cell sizes is especially favourable. Irregular foams were found to have a higher tangent modulus at low strains, whereas regular foams with a more unique cell size were stronger at higher strains. A certain number of cells across a sample is necessary to ensure improved mechanical properties which make foams with small pores look more favourable. Importance has also been ascribed to the shape of cell walls. Especially corrugated cell walls seem to have a strong detrimental influence on foam properties. Foams with missing cell walls or cell walls containing holes or cracks were also studied and found to be mechanically weaker than perfect foams. The variability of mechanical properties in a group of specimens of identical nominal dimensions and densities has been analysed statistically and was found to be very large even for the most regular foams available at present. It is likely that more regular foams, even if they do not show better mechanical properties, lead to a lower variability of these properties, which would also be a very valuable feature.

1.5.6 Dependence on the production methods.

As the foaming process comprises various steps and each step can be influenced by many parameters, the properties of the final foamed part can vary very much if production conditions are changed. Especially in the early days of metal foaming, the search for appropriate foaming parameters was difficult because the mechanisms of metal foaming were unknown and the complex interdependence between parameters was not understood.

1.5.7 The quality of a foam.

There is no simple measure for the quality of a foam. Usually one assesses the uniformity of cells in a qualitative way by looking at sections through foamed specimens. Whenever a foam possesses many cells of a similar size it is often considered "good", if there are many obvious defects it is called "inferior". Figure 1.39 shows four samples as taken from different batches of aluminium foam sandwich (AFS) panels made by the company Applied Lightweight Materials (Saarbrücken, Germany) which clearly show a difference in foam quality. Another problem encountered is the very restricted significance of individual foaming trials. Systematic variations in foam quality associated with the change of a processing parameter are not easy to detect and require a large number of experiments. Finally, there also seems to be a size effect in foaming. The smaller the samples the more uniform the pore structure. The size of the sample makes a comparison of different results difficult.

1.6 Methods for characterising a foam.

Cellular metals can be characterised in many ways. The objective is either to obtain mechanical or physical data characteristic of the cellular material investigated or to carry out a technological characterisation of a component containing cellular metal. There are two ways to look at a cellular material:

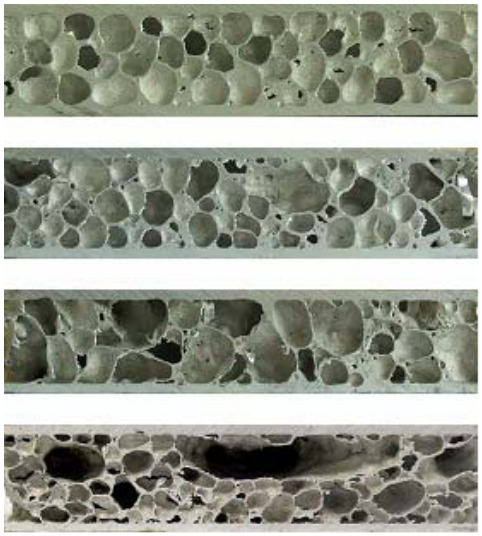

Figure 1.39: Sections of aluminium foam sandwich materials as obtained in industrial production. From bottom to top: improving quality [40].

- from an atomistic or molecular point of view, a cellular material is a *construction* consisting of a multitude of struts, membranes or other elements which themselves have the mechanical properties of some bulk metal: testing a cellular material is then equivalent to testing any engineering component;
- from a macroscopic point of view, the cellular structure is a *material*, and tests yield properties corresponding to the material: the cellular structure is a homogeneous medium which is represented by effective (or averaged) material parameters.

This section will describe the most important methods for the characterisation of cellular metals. In general, one can distinguish **destructive** and **non-destructive** methods according to whether the foam is irreversibly deformed or otherwise changed or remains unchanged or only minimally affected during characterisation.

1.6.1 Destructive testing.

Optical image analysis. The cell morphology and microstructure of metal foams can be analysed by optical observations (see Fig. 1.40). Although the actual analysis is non-destructive, sample preparation usually requires cutting, embedding or polishing of the materials and is therefore a destructive technique.
One can determine cell or pore size distribution or perform a shape analysis of the cell by using commercial image analysis programs. These programs are able to identify the individual cells in the preparation plane. However, meaningful results are difficult to obtain. A very careful preparation of the materials is required. Cell membranes and the interior must appear in different brightnesses. Some manual correction work is usually necessary to help the program in identifying individual pores and calculating the distribution of pore sizes. The intersections through the individual cells are randomly oriented in space: the results require some interpretation.

Mechanical testing. Mechanical testing of cellular metals is the prerequisite for any structural application. Mechanical data is either needed for the evaluation of the specific

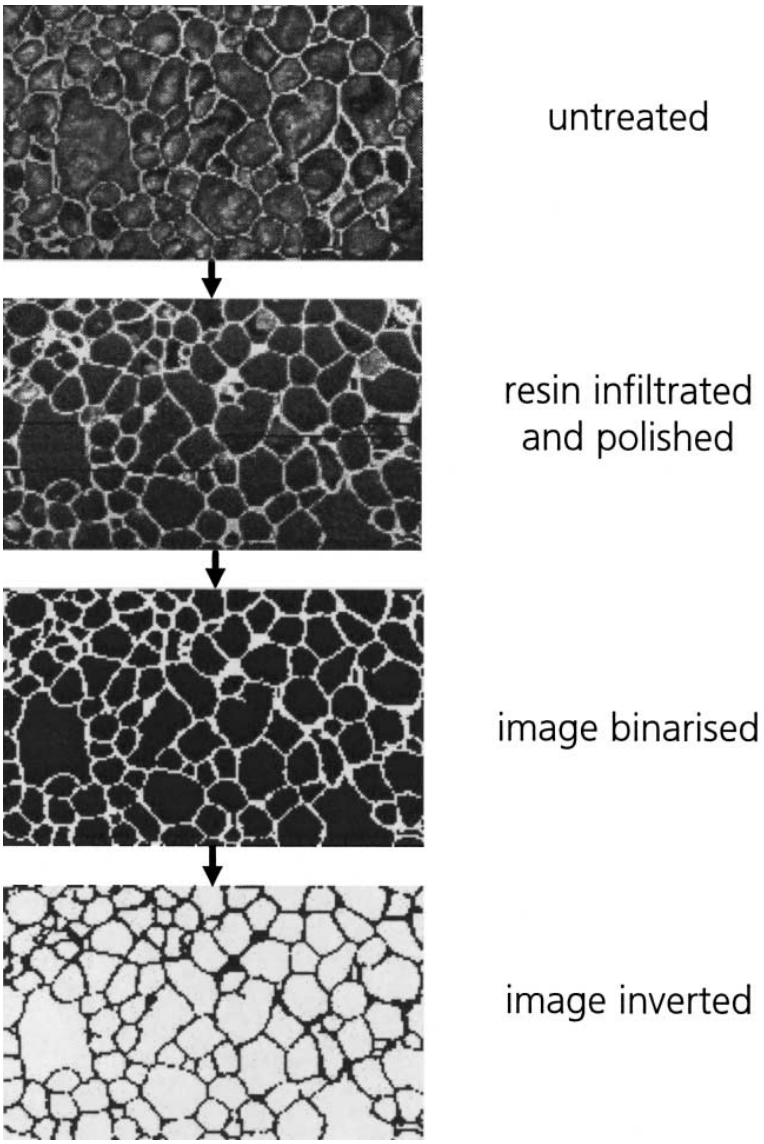

Figure 1.40: Optical image analysis of aluminium foams: various stages of sample preparation and image processing are shown [6].

applications or, more generally, to build databases which are needed for computer aided modeling of cellular materials or components containing such materials. In order to obtain meaningful results and to average out the "hidden" parameters (i.e. mass distribution, heterogeneous microstructure, etc. which distinguish various samples of the same overall density from each other), a large number of sample is required. The various different mechanical tests can be labelled by one of the following attributes:

- type of applied stress: uniaxial, biaxial, multiaxial, hydrostatic;
- mode of loading: compression, tension, shear, bending, torsion;
- time dependence of load: constant, slowly increasing (quasi-static), dynamic, cyclic.

1.6.2 Non-destructive testing.

Density measurements. The overall density of a porous material can be determined by weighing it and by measuring its volume using Archimedes' principle, i.e. by measuring its buoyancy in a liquid of given density. If the sample to be characterised does not have a closed outer skin, penetration of liquid into the pores has to be prevented by coating its surface, e.g., with a polymer skin.

Dye penetration measurements. In practice, imperfections occur while making foams. Such imperfections can include holes or crack in the cell walls or in the outer skin. Penetrant techniques are ideal for detecting such surface defects. A liquid chemical is first applied to the foam to be investigated. The chemical is eventually absorbed by the holes and the cracks. After drying the surface, a colouring developer is applied which creates colour where the penetrant chemical has been retained. In this way, one can obtains maps of the imperfections.

X-ray radiography and radioscopy. Cellular materials can be mapped by simple X-ray absorption techniques (transmission radiography). An X-ray beam is directed through a sample and its attenuation is measured. One averages over a certain lateral area and scans over two dimensions, thus obtaining a 2D absorption map of the foam. The method yields an integrated signal along the direction of the beam, i.e. the attenuation is related to the total mass in a column of material. If thin slices of foam are investigated, i.e. pieces with a thickness in the order of the average pore diameter, one can resolve individual pores and map the true pore morphology. However, if the slices are much thicker, single pores are not further distinguishable. Even features such as big pores or holes of a size of one fourth of the thickness of the foam cannot be resolved properly in some cases. Figure 1.41 shows an inhomogeneous lead foam in transmission: some of the very large pores can be seen, but is impossible to resolve most of the small pores, because many pore images are superimposed on each other.

X-ray computed tomography. Three-dimensional density distributions can be obtained by means of computed X-ray tomography (CT). X-ray images of a sample are taken from a large number of directions, usually by rotating and translating the source and the detector around the sample (spiral scanning, see Fig. 1.42). From the various images obtained, the attenuation of the rays at any point of the object and therefore the local density are reconstructed mathematically (see Fig. 1.43).

Vibrational analysis. Young's modulus and the loss factor of the material can be determined by vibrational analysis. A long bar of rectangular or round cross-section or a thin quadratic plate made of the material is forced into vibrations. Longitudinal, transverse or torsional excitations can be created. The sample can be clamped at one or two ends, or be supported by or suspended from thin wires. Measuring the properties of

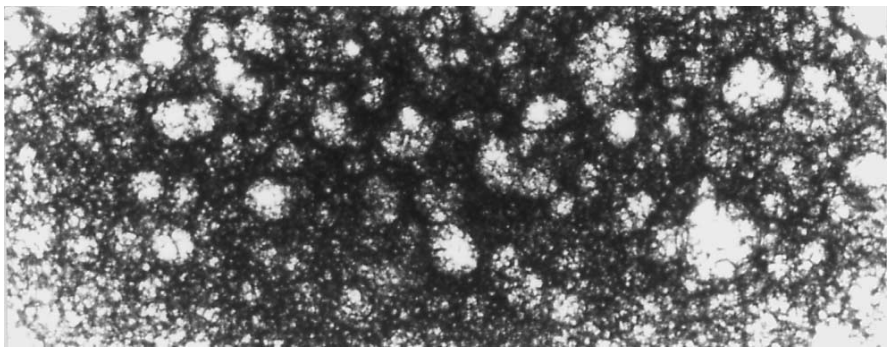

Figure 1.41: Image of a lead foam obtained by X-ray transmission radiography [6].

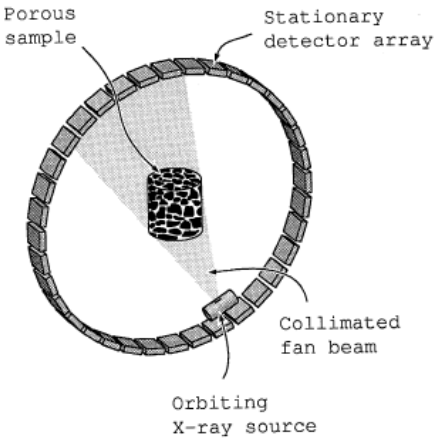

Figure 1.42: Experimental set-up in X-ray computed tomography [6].

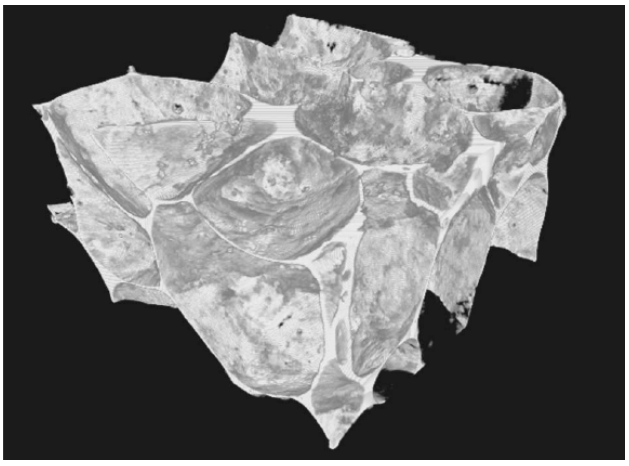

Figure 1.43: High resolution of a 3D-image of a zinc foam obtained by computed tomography [6].

cellular materials is not trivial. The materials are often inhomogeneous with an unknown mass distribution. The effective (average) Young's modulus then depends on the mass distribution.

Other methods. Other methods can be used for characterising cellular materials. Foam can be characterised by their relative density and pore size by carrying out multi-frequency electrical impedance measurements. The sound absorption properties of porous media are measured in an impedance tube. Also electrical and thermal conductivity have been measured on aluminium foam samples. More details can be found in [6].

1.6.3 Reproducibility tests.

A foam growth is a statistical process. So, two foaming experiments will never yield exactly the same result, even if the initial conditions were identical, i.e. the same within the limits of experimental accuracy. Accidental agglomerates of blowing agent particles in the foamable precursor or unpredictable heat transfer between the heat source and the foamable precursor samples are possible source for irreproducibility. Moreover, the experimental set-up might contain elements which limit reproducibility of foaming experiments, such as friction effects between foam and the mold in which the precursor is put. However, in practice, foaming tests can be carried out in a reproducible way. A minimum of two tests on identical samples is performed and the results are compared. If there seemed to be too much difference between the two results, further tests will be carried out. On the other hand, if the curves of the property tested were similar, an average curve will be calculated.

1.7 Applications of metal foams.

Metal foams have been commercially used for many years and various companies are producing these materials for different applications. Important commercial developments took place in the last 20 years on closed cell aluminium foams and sandwich panels for structural applications and various companies are now commercialising these materials. Aluminium foams, for example, are currently produced by a number of companies worldwide: there are companies in Germany, Austria, USA, Canada, Korea and China that are producing aluminium foams. In the following paragraphs, applications for metal foams are discussed.

Automotive industry. The increasing demand for safety of automobiles has lead to higher vehicle weight in many cases. This conflicts with further demand for low fuel consumption, necessitating additional measures for weight reduction. Moreover, cars weight reduced lengths are often desired. This reduction, however, should not take place at the expense of the size of the passenger compartment. One therefore tries to introduce new compact engines or reduce other structures to maintain passenger comfort. This creates new problems with heat dissipation in the engine compartment, because all aggregates are very closely spaced, or with crash safety owing to the reduced length of the crash zones. Finally, the need to reduce acoustic emissions from cars has led to a demand for new sound absorbers. Metal foams offer a possible solution for some of these problems. Figure 1.44 summarises the three application fields for metal foams, mostly aluminium foams, in the automotive industry. The inner circles represent the three fields which have to be distinguished and the outer boxes illustrate the foam properties which are responsible for the advantage in the given field. An ideal application would be a part which served as a light-weight panel, absorbed energy in crash situations and carried sound or heat absorbing functions (intersection of the three circles in the figure). Such multifunctional applications are, of course, difficult to find and one often would be satisfied with finding a

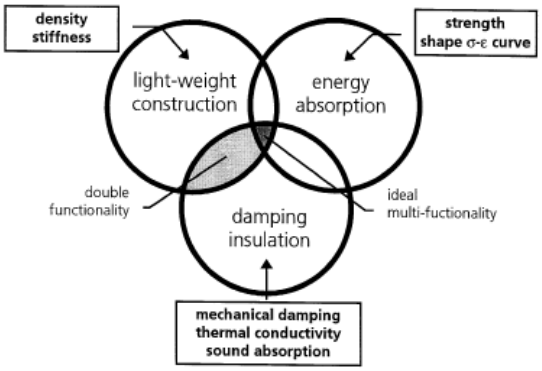

Figure 1.44: Automotive application fields of structural metal foams [6].

two-fold application where, e.g., a structural light-weight panel served as a sound absorber at the same time.

Light-weight construction. Light-weight construction depends on two properties of metallic foams: they exhibit a range of almost reversible, quasi-elastic deformation and their stiffness-to-mass ratio is high. In reality, foam-based structures have to compete with conventional structures with optimised mass distributions, i.e., aluminium foams have to be compared with aluminium extrusions, aluminium foam sandwiches with aluminium honeycombs panels. It has been shown that such structures can perform as well or better than foams. Foam-based structures nevertheless can be preferable for some reasons:

- they may be easier to manufacture in a given complicated geometry (and therefore may be cheaper);
- foam-based structures may be more robust and damage tolerant, and the failure behaviour less catastrophic;
- metallic foams may exhibit additional properties which are useful, e.g. heat resistance or acoustic properties.

Light, stiff structures made of aluminium foam-preferably in the form of sandwich panels-could therefore help to reduce weight in cars. Examples are bonnets, boot lids and sliding roofs, where a high stiffness is needed in order to avoid torsional deformation or to prevent these parts from vibrating. Because aluminium foam sandwich parts are more expensive than conventional stamped steel sheets, such an application would not be viable in spite of the weight reduction achieved if it only were a simple substitution of materials. However, by using very stiff sandwich structures for conventional sheets, one can introduce new constructional principles for the body frame of the vehicle. A consequence is that the number of components needed in the car can be significantly reduced if one applies the aluminium sandwich technology, hence decreasing construction costs.

Crash energy absorption. In energy absorption applications, the plastic, irreversible deformation regime of materials are exploited. Many cellular solids are excellent energy absorbers owing to their deformation at a nearly constant stress level over a wide range of strain. Metal foams might outperform conventional foams, e.g. polymer foams, because of their much higher strengths. What makes aluminium foams even more attractive is their low rebound in dynamic crash situations which has been determined to less than 3% in one study compared with 15% for a polyurethane foam. Therefore, an important application field for cellular metals in general and metal foams in particular is

energy absorption. Passive safety regulations for vehicles require that the collision energy is dissipated in designated areas and the rigid passenger cell is protected. Figure 1.45 shows an Alporas metal foam crash element in the front tip of the chassis of a racing car.

Figure 1.45: Crash protector in a model racing car built by students at the University of Technology of Stralsund, Germany; a. view of car with the front encasement taken off; b. full view [37].

Noise control. Polymer foams are often used for noise control. There are various ways in which aluminium foams could help reduce noise and care must be taken not to confuse the various ways of action. First of all, there is the problem of undesirable vibrations of a construction (machine, vehicle, etc.) which can cause damage and lead to the emission of sound waves (noise). Foams offer the possibility of avoiding noise problems. Sometimes, however, the task is to attenuate an incident or evanescent sound wave. Passengers have to be protected from noise coming from external sources or sound emissions from noisy machines (e.g. cars) must be prevented from propagating freely out into the environment. Sound absorption and insulation is a very important topic in the automotive industry. A problem often encountered is that sound absorbing elements have to be heat resistant and self-supporting. Combinations of polymer foams and aluminium foils might be a solution but are often not desirable. Aluminium foams at the current state-of-the-art technology do not exhibit excellent sound absorption properties due to their predominantly closed porosity but are at least heat resistant and self-supporting. Provided that one could sufficiently improve the sound absorption properties, an excellent material for such heat resistant sound absorbers could be obtained. Alporas foams are being used as sound absorbers along motorways and other busy roads in Japan to reduce traffic noise and in the Shinkansen railway tunnel to attenuate sonic shock waves. The combination of the given sound absorption properties with other characteristics such as fire resistance, resistance to weathering, non-generation of dangerous gases in the case of fires and the reported unproblematic cleaning of the foam panels makes Alporas a suitable material. Foam panels have also been used for indoor sound absorption purposes in entrance halls of public buildings. Also, the interesting visual appearance of the metal foam is likely an important aspect for some of these applications.

Aerospace industry. The light-weight constructional aspect of foamed metals is very similar in the aerospace and automotive sector. In aerospace applications, the replacement of expensive honeycomb structures by foamed aluminium sheets or metal foam sandwich panels could lead to higher performance at reduced costs. On one hand, a higher buckling and crippling resistance is sought, whereas on the other hand, an important advantage of foams is the isotropy of the mechanical properties of panels (with or without face sheets) and the possibility for making composite structures without adhesive bonding. The latter gives rise to a more benign behaviour in the case of fires where it is essential that the structure maintains its integrity as long as possible. Further applications include

structural parts in turbines where the enhanced stiffness in conjunction with increased damping is valuable. In space technology, aluminium foam has been evaluated for its use as an energy absorbing crash element for space vehicle landing pads and as reinforcement for load bearing structures in satellites, replacing materials which cause problems in the adverse environmental conditions in space (temperature changes, vacuum, etc.).

Ship building. Light-weight construction has gained importance in ship-building. Modern passenger ships can be entirely built from aluminium extrusions, aluminium sheets and aluminium honeycomb structures. Large panels of aluminium foam with aluminium cores promise to be an important element in some of these structures. If the face sheets are bonded to the core material with highly elastic polyurethane adhesives, one obtains light and stiff structures with an excellent damping behaviour, even at the low frequencies experienced in ships. Naval applications for cellular materials have also been identified.

Railway industry. The application of metal foams in railway equipment follows the same rules as for automotive industry concerning the three main application fields. Energy absorption is an issue especially for light railway sets and trams which operate in urban areas and for which collisions with cars might occur. Japanese trains have been equipped with a 2.3 m^3 block of Alporas foam to improve crash energy absorption. The advantages of foamed light-weight elements are the same as for cars, the main difference being that structures for railway wagons are much larger.

Building industry. There is a wide range of possible applications in the building industry. As modern office buildings are made of concrete, their facades are decorated with panels which hide the concrete and improve the appearance of the building. These panels have to be light, stiff and fire resistant. Quite frequently thin slices of marble or other decorative stones are joined to a support which is then fixed to the walls of the building. Such supports could be made of aluminium foam, replacing some of the expensive honeycombs presently used. Ballustrades of balconies have to satisfy rigorous safety regulations. Some of the materials used today are too heavy and are problematic in the case of fires. If they could be replaced by aluminium foam samples, some of the problems would be solved. Aluminium foams or foam panels could be very helpful in reducing the energy consumption of elevators. Because of frequent acceleration and slowing down and the high speed of modern elevators, light weight construction is an important issue. However, safety regulations often prevent an application of conventional light weight construction techniques. Because aluminium foams can act as energy absorbers and as stiff structural material at the same time, these applications seem very promising. Light weight firedoors and hatches make use of the relatively poor thermal conductivity and fire resistance of some of the low density aluminium foams. Aluminium foams are surprisingly stable when exposed to an open flame owing to a strong oxidation under such conditions.

Machine construction. There are some interesting applications for metallic foams in machine construction. Stiff foamed parts or foam-filled columns with reduced inertia and enhanced damping could replace axles, rolls or platforms presently made of conventional metal. Such components can be used in stationary drilling or milling machines, as well as in printing machines. Aluminium foams have also been used as supports for telescope mirrors.

General aspects of selecting applications. It is often quite difficult to find applications for a new material. Discussions in recent years have shown that the most promising applications are those where one makes use of various properties of metals foams. If only the low weight of the material is of interest, there will most probably already exist an established, cheaper material. If, however, low weight combined with good

energy absorption characteristics or heat resistance is required, then the competitiveness of metal foams will be significantly increased. Therefore, each new application idea has to be first evaluated by identifying the essential properties which are needed. Then one has to determine whether there is a cellular metal with the desired spectrum of properties and whether any established materials exist with comparable properties. If this is the case, other criteria such as cost will have to be considered to decide which solution is preferable.

Chapter 2

Powder route: towards a mathematical modeling.

Cell and tissue, shell and bone, leaf and flower are so many portions of matter, and it is in obedience to the laws of physics that their particles have been moved, moulded and conformed. [...] Their problems of form are in the first instance mathematical problems, their problems of growth are essentially physical problems, and the morphologist is, ipso facto, a student of physical science.

D'Arcy Wentworth Thompson

As Banhart reported in [6], current research on the improvement of the production processes concentrates on improving **process control** in order to produce higher quality materials and to achieve a better reproducibility and predictability of their properties. By *better quality* one usually means a good morphological and structural homogeneity of the cellular materials. For structural applications, curved or corrugated cell walls, inclusions, ruptured or missing cell walls, for example, should be avoided. For functional applications, a uniformity of pore or inter-pore channel size may be important. However, as Banhart remarked [6], for most processes, *there is no applicable theoretical or numerical model at the moment which allows for predicting the effect of parameter changes.* Improvements of production methods, that up to now are often made through a trial and error strategy, could be promoted.

MUSP laboratory in Piacenza is an applied research centre specialising in the study of machine tools and production systems, with a strong line of activity devoted to the study and development of innovative materials. It has been fully operative since 2006 and it is managed by the Consortium of the same name that unites the different operators that gave rise to the initiative: Universities (Politecnico di Milano and Università Cattolica del Sacro Cuore), enterprises in the machine tool industry (Capellini, Jobs, Lafer, Mandelli, MCM, Samputensili, Sandvik, Working Process), associations (UCIMU Sistemi per Produrre, Confindustria Piacenza) and institutions (Foundation of Piacenza and Vigevano, the Municipality and Province of Piacenza). Among its research fields there is the study of the powder metallurgical method for the production of foaming materials (see Figure 2.1) and their applications especially in field of machine tools. As we discussed above, process control is important in the improvement of the processing route. MUSP activity would receive some benefit if a mathematical model of the foaming process was available.

Figure 2.1: MUSP metal foams.

Together with MUSP researchers, we have worked in the derivation of a mathematical modeling of the expansion stage of the foam inside a mold. So, starting from the study of the main stages of powder route foaming process (Section 2.1), we have focused on the factors that influence foaming expansion (Section 2.2) and foam stabilisation (Section 2.3). Some experimental activities at MUSP laboratory (Section 2.4) helped us in the definition of reasonable hypotheses under which a mathematical model of foam expansion can be developed (Section 2.5).

2.1 Powder metallurgical route.

In this section the stages of foam production and evolution of the "powder metallurgical route" method will be described in details, according to the process studied at MUSP laboratory.

2.1.1 Main steps of the powder route process.

1. A **metal powder** (elementary metal powder, alloy powder, metal powder blend) is mixed with a powdered **blowing agent**, e.g., one mixes 99.5% aluminium powder and 0.5% titanium hydride powder (see Fig. 2.2).

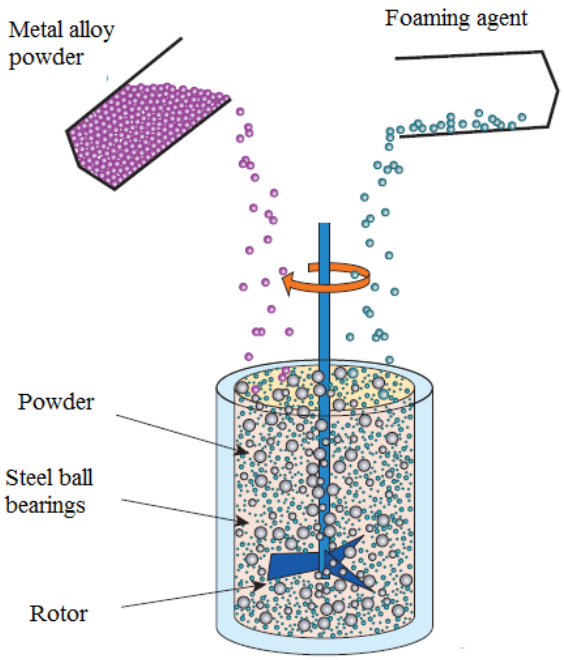

Figure 2.2: Mixing of the selected powders [41].

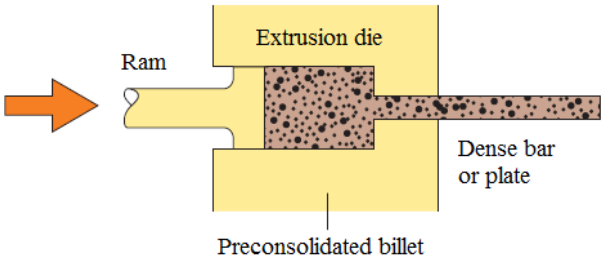

Figure 2.3: Pre-compaction and compaction [41].

2. The powder mixture is compacted into a semi-finished product, called **foamable precursor material**. In principle, the compaction can be done by any technique that ensures that the blowing agent is embedded into the metal matrix without any notable residual open porosity (e.g., by hot pressing, extrusion, powder rolling or other methods). Which compaction method is chosen depends on the required shape of precursor material. **Extrusion** seems to be the most economical method at the moment and is therefore the preferred way: after a pre-compaction phase at low temperatures, in which the powders are compacted into cylinder samples, the material is extruded in order to obtain bars or plates (see Fig. 2.3).

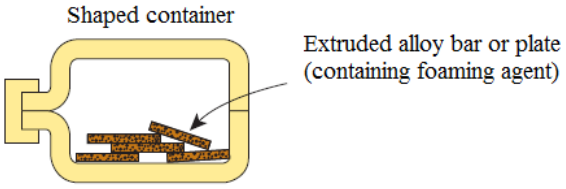

Figure 2.4: Precursors in a hollow mold [41].

3. The precursor is inserted into a hollow **mold** (see Fig. 2.4) and is heated up to the melting point of the metal inside a furnace (see Fig. 2.5). As the metal starts to

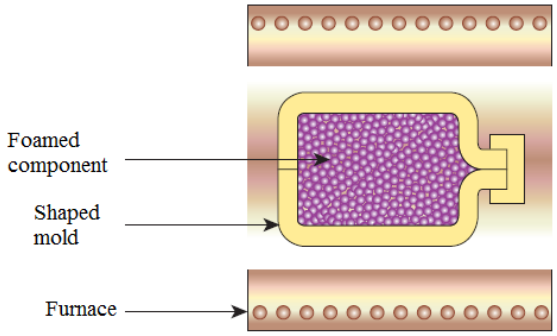

Figure 2.5: Expansion of the foam inside the mold [41].

melt into a semi-liquid viscous state, the blowing agent (which is homogeneously distributed within the dense metallic matrix) decomposes, thus releasing gas (in the case of titanium hydride, hydrogen is the gas released). The released gas forces the compacted precursor material to **expand** (see Fig. 2.5), thus forming its highly porous structure. The process takes place in the liquid phase, so the pores and the outer surface are closed owing to the effect of surface tension. The time needed for full expansion depends on temperature and size of the precursor and ranges from a few seconds to several minutes. After a maximum expansion, which corresponds to a fairly uniform foam morphology, the foam **collapses**.

4. Lowering the temperature, the foam structure can be frozen resulting in a **solid metallic foam**.

2.1.2 Powders.

The foamable precursor material is obtained from a homogeneous mixing of metal powders, blowing agent and other substances.

Metal powders.

This method is often called "powder metallurgical", because the starting materials are metal (or metal-alloy) powders. Although initial work concentrated on pure aluminium (see Fig. 2.6), then it was realised that aluminium alloys could offer advantages over pure metals: Al-Cu, Al-Si, Al-Mg, Al-Si-Cu, Al-Mg-Si, Al-Mg-Zn, Al-Sn are some examples. It was found that it was neither necessary nor desirable to use prealloyed powders, but one can mix elemental powders in appropriate fractions. Foaming aluminium alloys is mostly considered, but other metals can also be used: brass, bronze, zinc, for example, require minor adjustments of the hydride content and pressing and foaming temperature. Gold can be foamed with TiH_2 as a blowing agent after adding some silicon to lower the melting temperature. Pure magnesium was initially difficult to foam, better results were found adding Al. Lead and lead-tin foams can be produced by using lead carbonate as a blowing agent. Also the manufacture of iron and steel foam is studied.

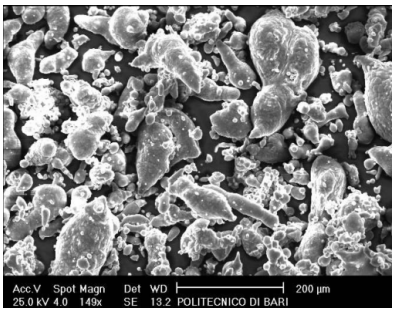

Figure 2.6: Aluminium- $45 - 150\mu m$- $150x$ (courtesy of MUSP).

Blowing agent.

For what concern the choice of blowing agent, different blowing agents are studied which are suitable for different metals, e.g., Ti, Zr, Hf, Ca, Sr, Ba, Ma, La, Li, carbonates of Mg, Ca, Sr, Ba, Li, Pb, Zn, Co and nitrides of Mn and Cr. For foaming aluminium foams, TiH_2 (see Figure 2.7) is the most suitable and the most used. In general, if metal hydride are used as blowing agent, a content of less than 1% is sufficient in most cases. However, the mismatch between the melting range of most Al alloys and the decomposition range of TiH_2 causes problems, because a gas pressure is built up in the precursor during heating before melting sets in. This can lead to the production of non-spherical and irregular pores. One possible remedy is to use alloy with a lower melting range that comes closer to the decomposition range of the blowing agent. Another possibility is to shift the range of hydrogen release to higher temperatures: one possibility is to oxidise the TiH_2 powders. Besides TiH_2, other hydrides are studied. But, in addition to metal hydrides, carbonates are frequently proposed as blowing agents, initially motivated by the much lower costs. As reported in [8] there are pronounced differences between carbonate and hydride driven foaming. A recent development is the possibility to foam without any chemical blowing agent. The reason is that metal powders release gas when they are heated due to the decomposition of reaction products on powder surfaces, e.g., hydroxides.

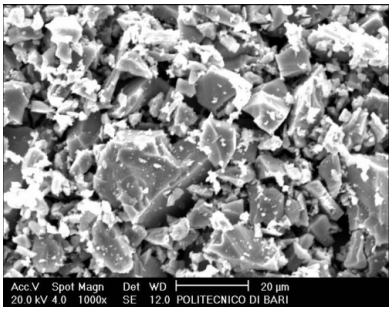

Figure 2.7: Titanium hydride- $40\mu m$- $1000x$ (courtesy of MUSP).

Solid particles.

Thin solid particles (for example, SiC, Al_2O_3, oxides, in addition to titanium-hydrure particles) on cell borders promote the foamability, lowering the surface tension, make a sort of barrier (*disjoining pressure*) against bubble coalescence (*repulsive action*), stabilise the foam and increase the foam viscosity (while the flow decreases).

2.1.3 Foam evolution.

The change of a foam from its formation until its collapse is called **foam evolution**. The foaming process is rather complicated, because at no time a thermodynamically equilibrium is assumed and the expanding foam is a complicated mixture of gaseous, liquid and solid phase (see Fig. 2.8). During the foaming of precursors containing a blowing agent,

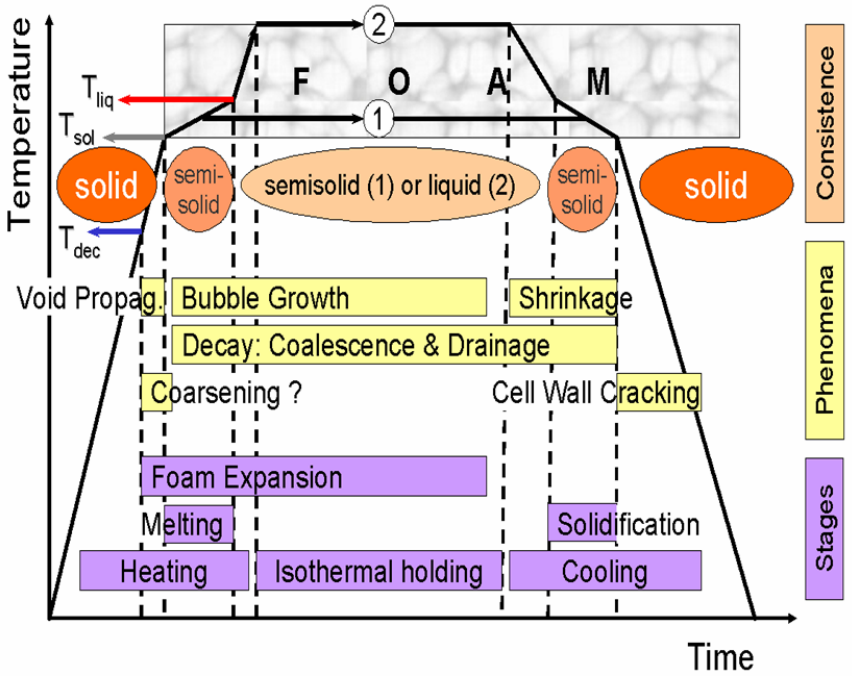

Figure 2.8: Stages during foam evolution [2].

foaming starts already during the heating of the precursor and the gas supply depends on the decomposition kinetics of the blowing agent. Development of a fully expanded foam can require several minutes. So, the study of foam evolution becomes difficult, because bubble nucleation and growth, drainage and coalescence overlap.

A three-phase system.

During the foaming process, the material is in a semi-solid state in which we can find the three phases (see Fig. 2.9):

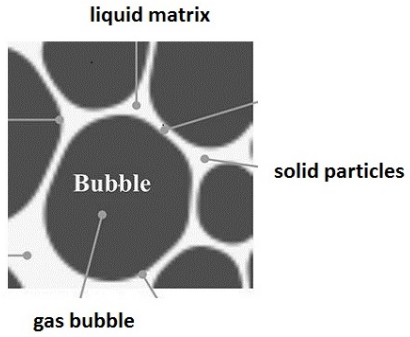

Figure 2.9: The foam as a three-phase system (courtesy of MUSP).

- **solid particles** that stabilise the foam (titanium-hydrure and other solid particles);
- **gas bubbles** that give the foam its final structure, drive the evolution of the cells during the foaming process: they are controlled by the surface tension, pressure, temperature, density, viscosity and time;
- **liquid matrix**, that is the medium in which the foam evolves: we can have wet foams or dry foams according to the liquid percentage inside the foam.

Foaming stages.

In Figure 2.10 some of the stages of the foaming process are shown.

a. The first stage is the **pore formation**: above the decomposition temperature of the blowing agent, the evolving gas accumulates in tiny voids of the precursor materials and forms a pore as pressure increases. As the solid precursor material was made by pressing powder, there is always a sufficient number of residual pores or oxide filaments which can act as centres of heterogeneous nucleation.

b. A further increase of the temperature increases the gas pressure and reduces the strength of the metal which practically vanishes at the melting point: **pore growth** sets in and the pores are inflated by the evolving gas. Growth may not be isotropic because of textures in the solid originating in the nature of precursor material.

c. A liquid foam is essentially unstable, so that the foaming process ends with **collapse** and a partial destruction of the structure.

The volume expansion.

In Figure 2.11 a time-resolved expansion curve of an aluminium foam is reported: here the volume and the temperature of an aluminium foam are represented as function of time.

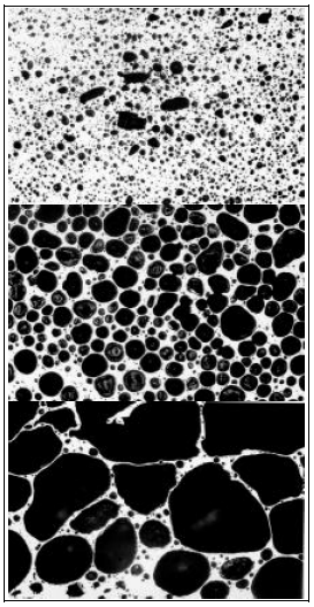

Figure 2.10: Stages in a zinc foam evolution. At the top, the early stage of foaming: there are tiny pores all over the sample. In the middle, there are greatly enlarged pores which fill most of space. Finally, a foam with a very coarse pore structure and some sign of collapse is shown at the bottom [4].

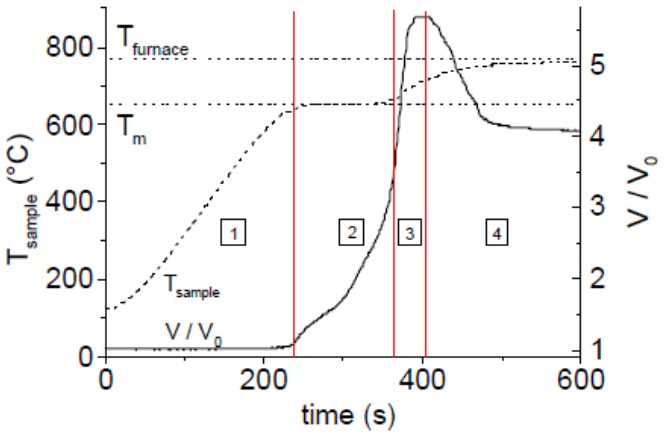

Figure 2.11: Stages of foaming [4].

1. At the beginning the piece of precursor is put into a pre-heated furnace at 780℃. As the material warms up, the volume first remains quite constant apart from the usual thermal expansion for temperatures up to the melting point (T_m=650℃) of the alloys (*stage* 1 in Figure 2.11).
2. Then, as the sample starts to melt, its volume increases due to the internal gas pressure as a consequence of the decomposition of TiH_2 to H_2 and Ti. During the melting the temperature remains almost constant (*stage* 2 in Figure 2.11).
3. After all the melt has been molten, the temperature begins to increase again and approaches the furnace temperature (780℃). The volume expansion speeds up and the volume finally reaches its maximum value of almost six times the original volume V_0 (*stage* 3 in Figure 2.11).
4. After this, the blowing agent is exhausted and no longer releases hydrogen: the unstable foam partially collapses (*stage* 4 in Figure 2.11).

Evolution of pore morphology.

In [17], in order to observe the evolution of pore morphology during foaming, a series of tests were performed on 6061 and AlSi7 aluminium alloys in a preheated furnace at 800 and 750℃. Figures 2.12 and 2.13 (a) show typical expansion curve for these alloys. The points marked with capital letters A-K and A'-K' indicate the different foaming stages. In Figures 2.12 and 2.13 (b) the corresponding micrographs of the various foaming stages are shown (the foamable precursor material is identified by "P"). As can be seen from the micrographs, the aluminium alloy shows the same foaming steps seen before, i.e.:

a. **pore formation**: pores elongated perpendicular to the compaction direction (which was from top to bottom) are formed (phase A and A' respectively);
b. **pore growth**: the pores are inflated by the evolving hydrogen and are increasingly rounded off as the foam expands (from B to G and from B' to G', respectively). The initial anisotropy starts to vanish until only a slight asphericity remains. Moreover, initially round pores are deformed to more polyhedral pores as the level of porosity increases and no more space can be filled by spherical pores;
c. **collapse**: after maximum expansion no more hydrogen gas is released and the foam begins to decay. This decay leads to foams with large and irregular pores, collapsed and oxidised pores especially at the top of the sample and a solid metal layer at the bottom (from H to K and from H' to K' respectively).

It is obvious that foam growth is neither isotropic nor uniform. The anisotropy has its origin in the texture created in the powder compact during solidification. In hot pressed tablets always oblate pores are formed and the following rise of the foam is along the original axis of pressing, whereas round extruded rods would rather expand in a radial direction. Non-uniformities in the emerging foam are probably caused by local agglomerates of the blowing agent or structural defects in the precursor material created by insufficient densification, impurities, or local oxidation. As the decomposition of TiH_2 starts rather early at about 380℃, i.e. in the solid state, tiny voids in the precursor material are formed, preferably near such structural defects, and lead to the formation of heterogeneous pore morphologies in the subsequent foam expansion.

The collapse of the foams is due to *drainage* and *coalescence* phenomena. For what concerns drainage, a thick metal layer at the bottom the two samples can be viewed (see H-K and H'-K'): the molten metal flows from the cell walls into the cell edges (driven by surface tension) and through cell edges downwards driven by gravity. It is thought that coalescence phenomena are due to cell ruptures, but no other information about this fact is known. From Figure 2.12 and 2.13, it can be seen that the collapse is quite different: after

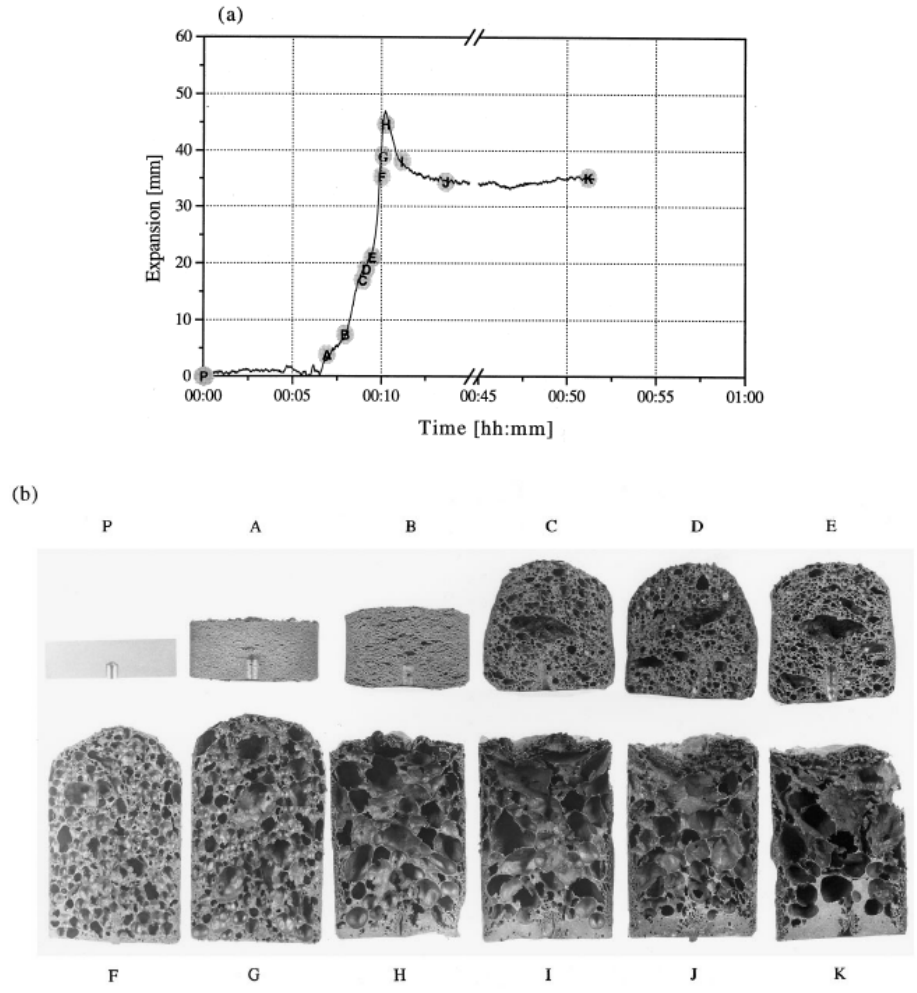

Figure 2.12: Expansion curve (a) and morphology at different foaming stages (b) for 6061 alloys using a pre-heated furnace at 800℃ [17].

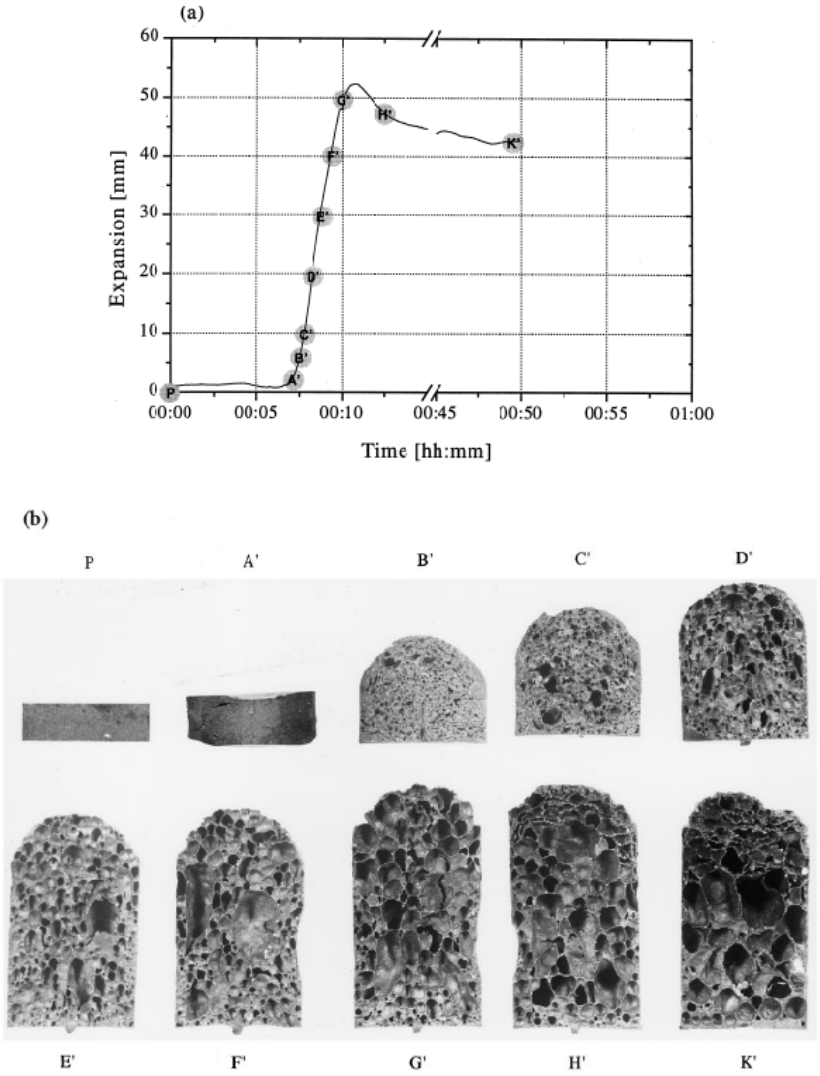

Figure 2.13: Expansion curve (a) and morphology at different foaming stages (b) for AlSi7 alloys using a pre-heated furnace at 750°C [17].

maximum expansion, AlSi7 foam does not loose its shape so much as the other sample. In addition, 6061 sample shows more decay in the upper surfaces and the vaulted shape disappears. AlSi7 sample remains vaulted and maintains a more regular cellular structure throughout the test.

2.2 Factors influencing foam expansion behavior.

In [17], factors influencing foam expansions are studied: aluminium alloy composition (they studied AlSi7 and 6061 samples), some of the pressing parameters of the foamable precursor material, the foaming temperature and the heating rate during foaming.

2.2.1 Compaction of the powder mixture.

The manufacture of the precursor (see Fig. 2.14) has to be carried out very carefully because any residual porosity or other defects will lead to poor results in further processing (see Fig. 2.15). Let us consider hot pressing. The hot pressing temperature (i.e., the compaction temperature during hot pressing) is a critical parameter for the foaming behavior (see Figure 2.16). The highest expansions are reached for hot pressing temperatures

Figure 2.14: Aluminium foamable precursor material (courtesy of MUSP).

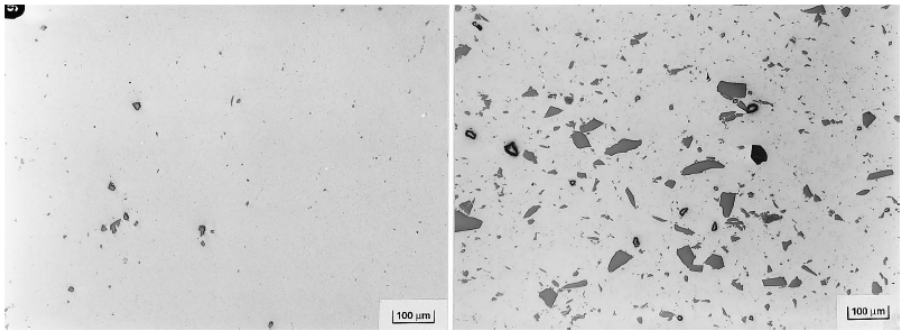

Figure 2.15: Foamable 6061 (on the left) and AlSi7 (on the right) precursor material containing 0.6 wt% TiH_2. Compacted powders are virtually pore free in both cases. Light grey TiH_2 particles can be seen in the metal matrix of both alloys. The darker angular shaped silicon particles are only observed in the metallic matrix of the AlSi7 alloy [17].

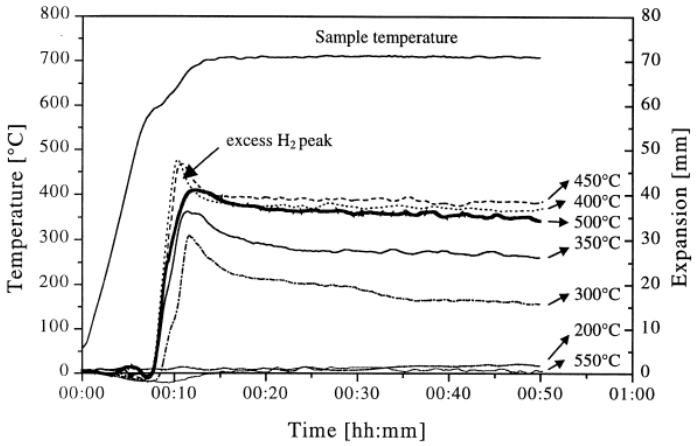

Figure 2.16: Expansion curves of AlSi7 samples prepared at different hot pressing temperatures [17].

between 400 and 450℃. For higher and lower temperatures, the maximum expansion is lower and in the extreme case, for 200 and 550℃, virtually no foaming can be observed. The reason for this is that for low compaction temperatures a high degree of residual open porosity is achieved, corresponding to a low density of the foamable precursor material. The hydrogen gas can escape from the melting precursor through the system of interconnected channels and it does not create and inflate bubbles. On the other hand, too high compaction temperatures also lead to lower maximum expansions, because hydrogen is lost already during hot compaction. This loss is almost complete for a compaction temperature of 550℃. Thermoanalysis of free TiH_2 powder shows that decomposition begins at 380℃ and continues up to 570℃. However, these results are valid only for free powders and depend also on the heating rates applied in the tests and on the environmental atmosphere. The optimum hot pressing temperature is around 400-450℃. It is interesting to note that the samples compacted at temperatures $T \leq 450$℃ show a transient expansion peak after which the foam quickly relaxes by a few millimetres to reach an almost constant volume. This peak could be a consequence of excess hydrogen in the precursor material which is weakly bound and is released at an early stage of foaming. The excess hydrogen could possibly cause a too quick inflation of pores and a corresponding partial collapse of some thin-walled membranes. The sample pressed at 500℃ does not show this behaviour and reaches a stable state without showing the transient peak. This is understandable since compaction of the powder mix at 500℃ is just sufficient to drive out this excess hydrogen, while this temperature is still too low to remove all the blowing gas. This, however, happens at 550℃ compaction temperature.

2.2.2 Furnace temperature.

The foaming process is sensitive to the foaming temperature chosen (see Fig. 2.17). If the final sample temperature is below the solidus temperature of the alloy (T1 for AlSi7, T2 for 6061, see Fig. 2.17) there is not very much more of an effect than a slight solid state expansion. If the final sample temperature lies in the solidus/liquidus interval (T2 for AlSi7, T4 for 6061, see Fig. 2.17) foam formation can be observed, but especially for 6061 it is limited to quite low expansions. The viscosity of the semi-molten material is still quite high at this temperature and surface oxidation leads to an additional resistance

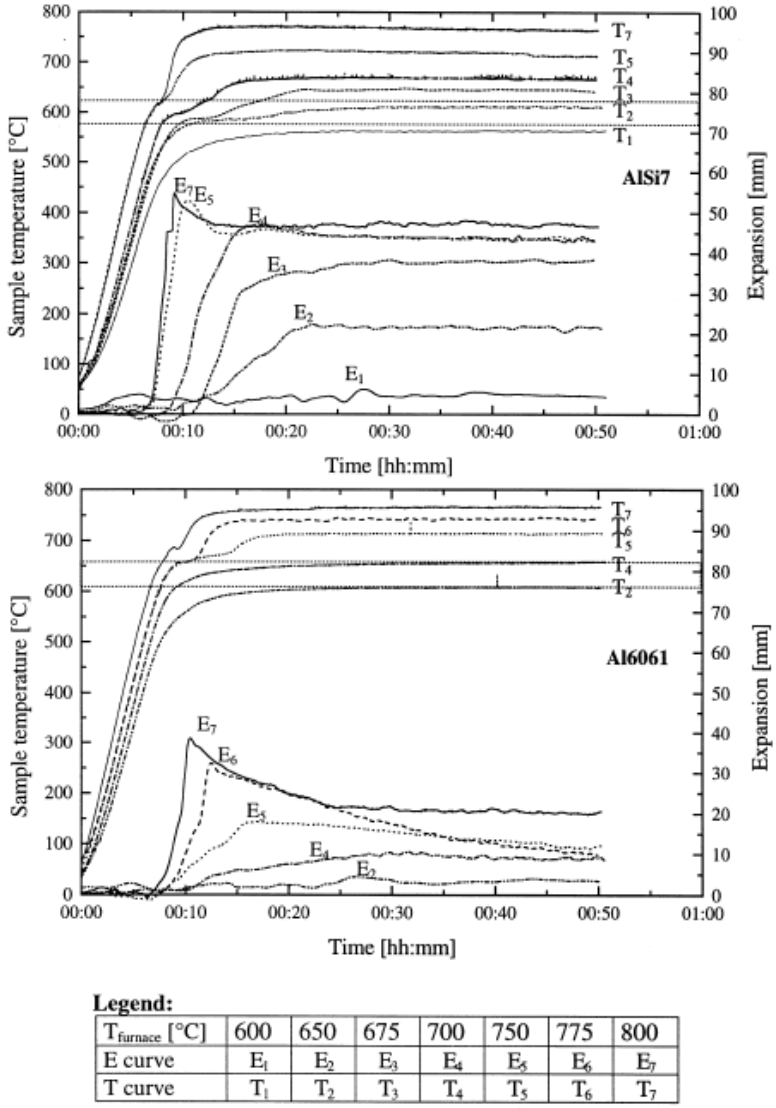

Figure 2.17: Expansion (E) and temperature (T) curves of AlSi7 and 6061 alloys foamed at different nominal furnace temperatures (600-800°C, values given in the legend). Solidus and liquidus temperatures of the two alloys are given as horizontal dotted lines [17].

towards bubble inflation, counteracting the internal gas pressure built up by the decomposing blowing agent. Increasingly higher temperatures reduce viscosity and promote gas production so that higher and higher volume expansions can be observed. Beside reducing viscosity, high furnace temperatures naturally also lead to high heating rates.

The volume expansion seems to almost saturate out for AlSi7 at 750°C, whereas the maximum of foam expansion for the 6061 alloy is presumably at temperatures above the maximum temperature at which the furnace can be operated (800°C), as can be seen from Fig. 2.18 which displays the maximum expansion as a function of nominal furnace temperature $T_{furnace}$, final temperature in the sample T_{final} and the temperature at the moment of maximum expansion $T_{max.exp.}$. Comparing the two temperatures T_{final} and $T_{max.exp.}$, one can see that they are almost identical for low furnace temperatures, i.e. the temperature does not rise anymore after the maximum of expansion has been reached, whereas for high furnace temperatures the sample temperature continues to increase after maximum expansion and therefore $T_{final} > T_{max.exp.}$. The latter situation seems to be a prerequisite for obtaining high expansion rates: one has to ensure a high heat flux into the sample up to maximum expansion by providing a furnace at a sufficiently high temperature.

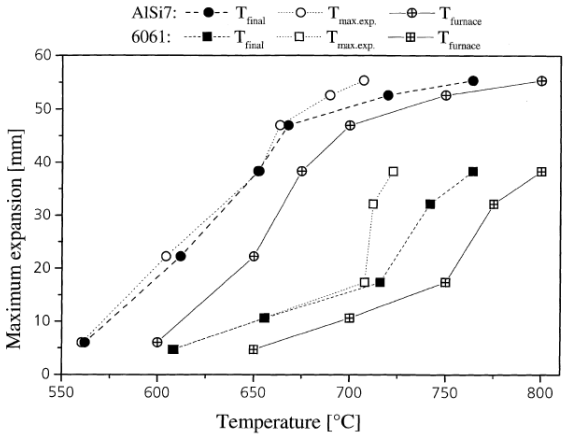

Figure 2.18: Maximum foam expansions of AlSi7 and 6061 alloys given as a function of various temperatures ($T_{furnace}$=nominal furnace temperature, T_{final}=final temperature in the samples after 50 min. of foaming, $T_{max.exp.}$=temperature in the sample in the moment of maximum expansion) [17].

2.2.3 Heating rate.

Different furnace temperatures lead to different heating rates and influence the foaming process this way. In order to evaluate the influence of the heating rate independently of temperature, foaming tests were carried out at 800°C at different heating rates (see [17]). Clearly, higher heating rates lead to an earlier expansion of the foamable precursor material because the melting temperature is reached at an earlier time. Only a significantly lower heating rate leads to a change in the expansion characteristics, namely a lower maximum expansion. The main possible reasons for the drop in foamability for low heating rates are:

(i) gas losses due to the decomposition of titanium hydride during the slow transition

through the temperature range from above 500℃, where decomposition is rapid and is the temperature at which foaming begins;

(ii) oxidation which could produce non-metallic layers on the surface of the precursor sample and even inside the sample in regions accessible to air by direct channels. Such oxide layers could contain alumina, magnesia or mixed oxides (6061 alloys contain magnesium), which remain solid throughout the foaming process and therefore mechanically hinder expansion.

2.3 Foam stabilisation.

In the previous section, some mechanisms responsible of the foaming process have been studied. Up to now, there is not a satisfactory comprehension of these phenomena. However it is generally accepted that the presence of particles plays an important role in foam evolution, but how these particles act is not well understood yet. In particular, researchers are interested in studying the role of the particles in foam stabilisation.

The term **foam stability** informs about the lifetime of a foam under given conditions and is related to the absence of cell wall ruptures and to a limitation to drainage effects which eventually destroy foam structure. Foams are unstable systems because their large surface area causes energy to be far from a minimum value. Foams can therefore be, at the most, metastable (this is the case of metal foams generated through the powder route, see [35]), constantly decaying at a certain rate. With foams, then, stability is the equivalent of slow decay. Metallic foams must be stabilised by different means. Like water, pure metallic melts cannot be foamed, but additives are required to act as stabilisers to create a foam. The stabilisation can be ascribed to **metal-oxide filaments** which reside in the powder compacts used, because oxides cover the surface of each powder particle prior to solidification and remain in the compact after pressing. These filaments are very thin, especially for aluminium where their thickness is believed to be well below 100 nm. The important role of these oxides in foam stabilisation is shown in Figure 2.19. Lead foams

Figure 2.19: Lead foams made from two different lead powders: (at the top) low-oxygen powder (0.06 wt.%) and (at the bottom) higher oxidised powder containing 0.46 wt.% of oxygen [5].

were manufactured by mixing lead powders with different degrees of oxidation with a blowing agent, compacting the mix, and foaming it. Powders with very low oxide contents lead to unstable foams; as the foam rises, liquid drains from it and limits its expansion. More stable foams result when powders with higher oxide contents are used and a large part of the liquid lead is kept in the foam structure at least until maximum expansion has

been reached. The action of foam stabilisation is not entirely understood yet. However, there is also some evidence that the same mechanisms described for lead foams are effective also for aluminium based foams. It is known that **surface tension** and **viscosity** of the melt determine its foamability. In this context, the role of the oxygen is postulated to increase the viscosity of the melt and/or decrease the surface tension. Körner [35] showed that neither an increased viscosity nor a decreased surface tension result in a stable foam. The only way to explain stability is to postulate the existence of an additional interfacial force which balances the suction of Plateau borders. This locally acting interfacial force, that is the **disjoining pressure**, describes the interaction of the two cell wall interfaces and it depends on the distance of the two neighboring interfaces. Körner also underlined that there is an evidence for this mechanism. Let us consider foams produced through the powder route: although there is no obvious addition of particles, the precursor material contains the oxides developed during metal powder production. The oxides, confined into cell walls during foam expansion, form network structures which have solid state character and generate a repulsive force (disjoining pressure) against further cell wall thinning. So, particle stabilisation is shown to be the universal mechanism of metal foam stabilisation.

2.4 The expansion step in powder route process: experimental results at MUSP.

Several experiments are reported in literature to describe the process of foam expansion starting from various composition of foaming precursors. Foaming process using Al6061, AlSi7, and Zn alloys showed a great foam expansion when the temperature in the liquid alloy rises to approach the furnace temperature [61]. A three steps foaming experiment consisting in heating, holding at around 600 °C for 100 s and cooling to room temperature on a AlSi6Cu4 alloy, highlighted a significant foam expansion during the holding time at constant temperature. In collaboration with MUSP researchers, we have performed similar experiments using an AlSi10 alloy. The aim is to analyse if, for this kind of alloy, most expansion takes place when the metal matrix is melted at (almost) constant temperature. This will be useful in the construction of a (simplified) model for foam expansion (see Section 2.5 and the next chapter).

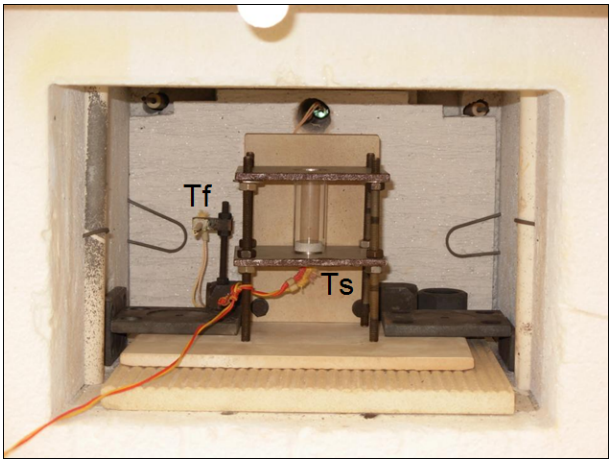

Figure 2.20: Experimental foaming set up at MUSP.

2.4.1 Experimental set up

Commercial foamable precursors of composition AlSi10 (0.8 wt.% TiH_2 as blowing agent), very close to the eutectic composition, have been foamed in a convection heating furnace pre-heated at 600, 650 and 700 ℃. To have the possibility of observing the volume expansion of the foam, pieces of precursor (diameter D_s=16.9 mm, thickness t_s= 5 mm, density ρ_s= 2,586 g/cm^3) have been inserted in a quartz tube (internal diameter D_{int}= 17 mm, external diameter D_{ext}= 20 mm, height h=50 mm) supported by two thin steel plates, as shown in Fig. 2.20. The upper side of the tube was open to the surrounding air. The

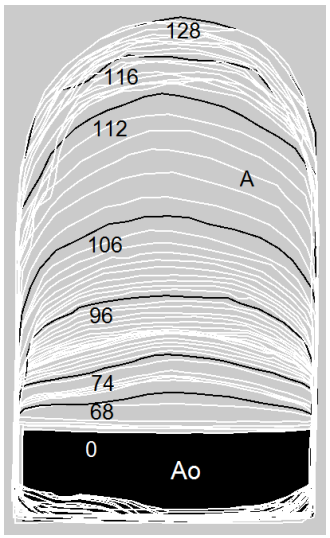

Figure 2.21: History of the evolution of the projected area expansion A/A_o (time measured in seconds) for foaming at 650 ℃: the black area represents the initial projected area A_o of the precursor, the foam contours (expansion and decay) are shown by white lines, while the black lines highlight some relevant contours of the expanded foam. The shape of the contour lines on the bottom is due to the stir up of the precursor at the beginning of the expansion process when the precursor is still in the solid state.

history of the thermal evolution has been followed by two thermocouples positioned as follows: one near the sample for measuring the temperature T_f inside the furnace while the other has been placed in touch with the bottom side of the sample for measuring the temperature T_s of the sample. Expansion of the foam was monitored by measuring the phenomenon with a camera positioned on the "peephole" of the oven door. An uEye fotocamera (2 Mega pixels UXGA Camera with 1/1.8" CCD Sensor) equipped with a precision lens (focal lens 25 mm) to focalize the area in the furnace and a protective filter for infrared radiation to improve the contrast between the foam and the background has been used. The process has been recorded at one frame per second (1 fps). A homemade software to connect temperature data to data acquired by the camera has been performed using Labview [36]. A quantitative analysis of the foam expansion was performed using the ImageJ [46] software for image analysis. In particular, volume expansion was measured by computing the increase of the two-dimensional projected area of the sample (Fig. 2.21). The projected area of the foam (A), normalized by that of the precursor (A_o), is defined as the area expansion (A/A_o).

2.4.2 Outcome of the experiments

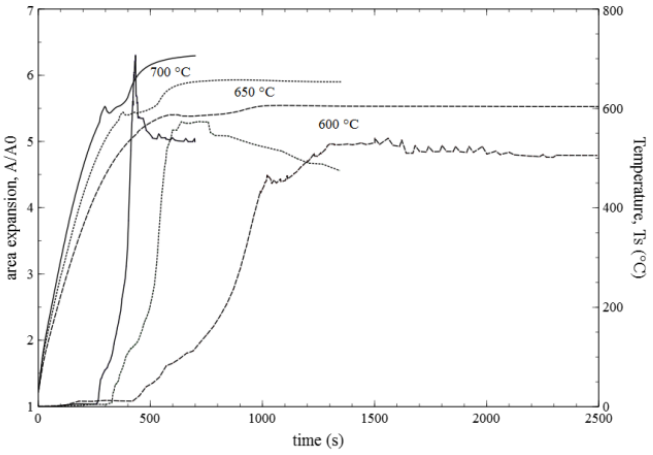

Figure 2.22: Evolution of the area expansion (A/A_o) with time (left vertical axis) and evolution of temperature in the sample (T_s) with time (right vertical axis) at three furnace temperatures: 600 (dashed curves), 650 (dotted curves) and 700 ℃ (solid curves).

In Figure 2.22 we report the foam expansion at three furnace temperatures (600, 650 and 700 ℃) by plotting the corresponding values of (A/A_o) as a function of time.
For increasing furnace temperatures, we observe a faster volume expansion and a higher foaming efficiency. On the other hand, the drop of A/A_o once the maximum has been reached suggests that the stability of the foam decreases in a faster way for higher furnace temperatures. If $A/A_o = 2$ is taken as a reference value at the beginning of the foam expansion, it could be observed that a consistent fraction of the foam expansion happens at constant temperature. Following the above considerations this behaviour is more evident for lower temperature (600 ℃). At higher temperature the phenomenon is influenced by the kinetics of the heating process.

In Fig. 2.23 the evolution of the area expansion, A/A_o, is reported as a function of temperature. The coloured upper bar shows the liquid percentage in the alloy with increasing temperature as calculated from the AlSi phase diagram. Red colour region is related to solid alloy while green region represents the liquid state. From the phase diagram of AlSi it is known that the solidus and the liquidus temperature[1] for AlSi10 are respectively: $T_{sol.}$= 575 ℃ and $T_{liq.}$= 595 ℃. At the solidus temperature the eutectic transformation occurs and consequently the temperature is stable. It can be observed that for A/A_o values higher than 3, in proximity of the liquidus temperature, the curve is both full green and nearly vertical suggesting that the alloy is already liquid and the temperature is approximately constant. This result is well fulfilled with the preheated furnace at temperature of 600 ℃.

So, from the outcome of the experiments, we conclude that most of the expansion takes place at almost constant temperature, when the metal matrix is already melted.

[1] The solidus temperature is the locus of temperatures (a curve on a phase diagram) below which a given substance is completely solid. The liquidus temperature specifies the temperature above which a material is completely liquid.

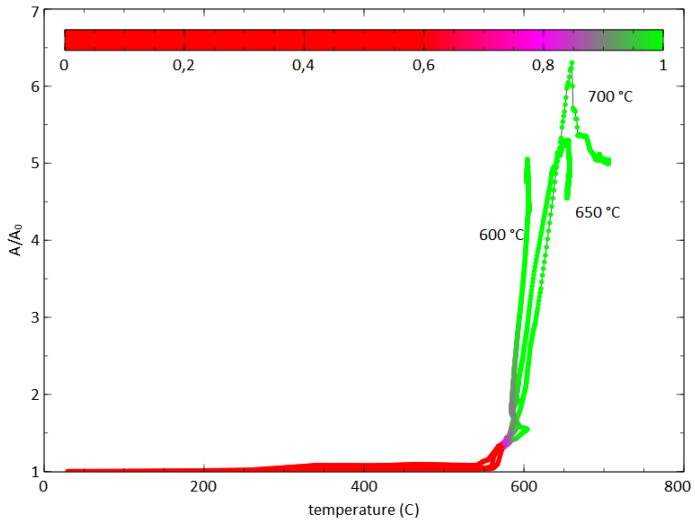

Figure 2.23: Evolution of area expansion (A/A_o) with sample temperature T_s. The colour bar is representative of the state of the alloy during the process: full red is related to solid while full green represents liquid.

2.5 The expansion step in powder route process: hypotheses for a mathematical modeling.

As we already discussed, the main difficulty in the industrial manufacturing of metal foams is the lack of control in the process. The aim of the engineers is to control the physical parameters involved in the foaming process in order to avoid foam decay phenomena and, at the same time, to study the mechanism of stabilisation of the foam. So, it would be useful for researchers to have a mathematical model which can predict the evolution of the foam, taking into account the physical parameters of the process.

To obtain a comprehensive description of foaming, all the physical mechanisms described in the previous sections should be incorporated in a model, but the effort has to be also pondered since the resulting computations are difficult to carry out due to the complexity of the system. Reviewing shortly the existing literature, Gergely and Cline [22] are the authors of a classical one-dimensional numerical model describing drainage in standing liquid metal foams. Their model allowed prediction of vertical density gradients as a function of geometrical and thermo-physical properties, giving numerical results which compared well with some experimental drainage data for metallic foams. In particular, the authors used an effective melt viscosity, which enhanced the dissipation mechanisms and controlled the gravity driven flows inside the foam. Adjusting the melt viscosity by stabilizing particles or promoting surface oxide skins in precursor foaming is the way to improve the foaming process. A more comprehensive model was developed by Thies [55] who applied the lattice Boltzmann method to study the precursor foaming by powder pressing, restricting his isothermal model to two dimensions, but including several physical mechanisms which govern the final structure. By his work it was possible to simulate the movement of a metal foam and demonstrate for the first time the pronounced impact of the disjoining pressure in the cell films on the foam stabilisation. Thies observed that only a drastically enlarged viscosity and in particular the static disjoining pressure in the films hinder the

gravitational and capillary drainage to cause foam collapse. Simulations showed that an increase of the viscosity leads to an increase of the maximum expansion and by decreasing the viscosity the resistance towards drainage was reduced. On the other hand, if the viscosity is too high, the foam is stiffer and compensation of film rupture events is more difficult. For what concerns the study of foam expansion, Bruchon [13] proposed a mathematical model for studying polymeric foam expansion with a sharp-interface approach.

In the next chapters, we aim at studying the foam evolution within a hollow mold, i.e. the expansion of one or more pieces of precursor material into a mold during heating. In this first effort for modeling the foaming process, we will neglect pore-formation, metal melting and foam-solidification stages, although they also play a key role in the quality of the evolving structure, as aforementioned in the previous sections. We will consider the foam growth, until the foam reaches the maximum expansion, that is before foam decay phenomena become predominant. The expansion represents the central step for metal foam processing at liquid state and drives mold filling.

Taking into account the outcomes of the experiments described in the previous section, we can think about studying a simplified mathematical model that describes the expansion stage of the foaming process on the basis of the following two limiting hypotheses:

1. the expansion takes place at constant temperature,
2. the metal alloy is completely melted during foam expansion,

i.e., most of the expansion takes place when the temperature is constant and when the metal alloy is already melted.

The hypothesis of melted metal allows us to ignore non-Newtonian effects during foam expansion, although the effective viscosity of the melted fluid surrounding the gas bubble depends both on the temperature (as aforementioned) and on the presence of solid particles next to the cell walls. Körner [34] reports some models describing the dependence of the melt viscosity on the particle volume contents, pointing out that the stabilising particles (for example, SiC, Al_2O_3, other oxides, etc.) added in metal foams manufacturing increase the viscosity and improve the stability of foams.

Chapter 3

Phase-field modeling of metal foaming process.

The great Galileo said that God wrote the book of nature in the form of the language of mathematics. He was convinced that God has given us two books: the book of Sacred Scripture and the book of nature. And the language of nature - this was his conviction - is mathematics, so it is a language of God, a language of the Creator. Let us now reflect on what mathematics is: in itself, it is an abstract system, an invention of the human spirit which as such in its purity does not exist. [...] The surprising thing is that this invention of our human intellect is truly the key to understanding nature, that nature is truly structured in a mathematical way, and that our mathematics, invented by our human mind, is truly the instrument for working with nature, to put it at our service, to use it through technology.

Benedict XVI

In this chapter we propose a thermodynamically consistent phase-field model for the description of the expansion stage of the foam inside a hollow mould, under the two limiting hypotheses of constant temperature and melted metal alloy that we discussed in the previous chapter. Phase-field models belong to the large family of diffuse-interface models, in which the interface separating two distinct phases is viewed as a narrow region within which sudden and yet continuous variations of the physical properties characterising the adjoining phases occur. This approach, pioneered by van der Waals (see [49]) at the end of the XIX century to model a gas-liquid interface, then rediscovered in a different context by Cahn and Hilliard (see [14]) is to be contrasted with the sharp interface view proposed by Gibbs (see [23]), according to which the properties of the phases remain those of a homogeneous substance up to a dividing surface where a discontinuous change occurs. Far from a phase transition, the choice of Gibbs's dividing surface seems more reasonable, though it is not exempt from serious conceptual difficulties when the interface is curved (for further details, see [50]).

Phase-field models are characterized by the fact that the phases involved are labelled by a scalar parameter, called the order parameter, that ranges in a fixed interval - $[0, 1]$ or $[-1, 1]$ are the typical choices - and such that it attains its maximum value at points lying in the bulk region occupied by a phase, say A, while it attains its minimum at points in the

bulk region occupied by the second phase, say B: generalisation to situations where $N > 2$ phases exist are straightforward as they only require the use of $N - 1$ order parameters.

Remaining for simplicity to biphasic systems, different phase-field models exist according to the choice of the order parameter, and for the problem at hand we recall two choices. The former, employed by Lowengrub and Truskinovsky [38] in their model of Cahn-Hilliard fluids, takes the mass concentration of a phase as the phase-field variable. This choice has the advantage that the order parameter has a clear physical meaning and that its evolution equation is a (nonlinear) diffusion equation. The latter choice [52] adopts the volume fraction of a phase as the order parameter. It should be noted that the volume fraction adopted in [52] and in subsequent papers by the same authors, [53], [54], is in fact an average volume fraction φ, defined as the statistical average of the indicator function pertaining to one of the phases involved. Actually, the phase-field model proposed in [52] is rooted in Drew and Passmann's [16] theory of multicomponent flows in which the equations for a multicomponent system are obtained by an averaging procedure performed upon the continuum equations for the separate components. As such, this theory falls into the realm of averaged methods and, as is known, the major problem with this approach is that on performing averages, information on the system gets partially lost and the averaged equations require a closure procedure which is tantamount as making further constitutive hypotheses upon the averaged variables. As a result, the phase-field approach proposed in [52] is characterised by two main features. At variance with standard mixture models, within the narrow layer separating two phases, these latter maintain their own velocities and pressures so that, besides the mixture velocity $\mathbf{u}$, also the velocity slip $\Delta\mathbf{u}$ should be taken into account. It should be noted that the averaging procedure is employed also to subsume the boundary conditions in the sharp-interface limit within the phase-field formulation. A second important procedure followed in [52] is the hybrid treatment of the φ profile across the transition layer: it is assumed that φ is the equilibrium profile φ_0 used to replace some differential operators acting on φ with algebraic expressions. On the other hand, φ does not disappear from the equations, since in some simpler terms the equilibrium profile φ_0 is not inserted. Such procedure can be justified by the fact that, in a thin interface limit, the equilibrium profile is the leading term in the formal asymptotic expansion of φ. It should be also noted that the possibility of expressing the averaged interface area as a treatable function of φ is, in fact, a closure requirement needed by the averaging approach. Consider the two species individually in a transition layer was mainly motivated by numerical requirements, most urgent when large contrasts exist among the properties of the phases [53]. In this case, dependence of the results upon the choice of the interface width was reported. Among the applications of their approach, Sun and Beckermann modelled a binary mixture formed by an ideal gas and a liquid metal [54] that is akin to modelling metal foams.

A different phase-field approach to liquid-gas systems was proposed by Naber, Liu and Feng in [44] where the phase-field parameter φ obeys a Cahn-Hilliard equation and attention is paid to embody Henry's law within the model. According to Henry's law, the pressure and the concentration of the gas are proportional, at the equilibrium. In a sharp-interface formulation, Henry's law acts as a boundary condition for the diffusion equation. From the structure of the stress tensor within the interface layer, Naber, Liu and Feng obtain a nonlinear relation between gas concentration and osmotic pressure that is taken as a substitute of Henry's law and is then employed as a restriction upon the parameters of the model.

In the case we are interested in, the metal foam can be viewed as a continuum medium which occurs in two different phases: a liquid phase (the melted metal) and a gas phase (the hydrogen in the bubbles). The liquid phase is incompressible, but the gas is compressible. We consider as phase-field function the concentration of the liquid phase: if we

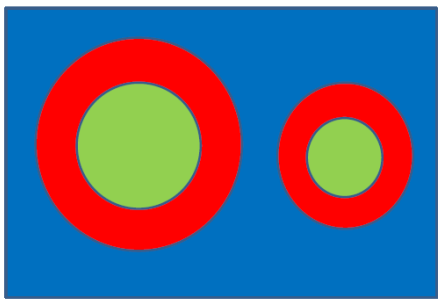

Figure 3.1: Phase-field model.

fix a spatial domain Ω and a time interval $[0, T]$, the phase-field function

$$c = c(\mathbf{x}, t) : \Omega \times [0, T] \to [0, 1] \tag{3.0.1}$$

is such that $c = 1$ if $\mathbf{x}$ belongs to the liquid phase (the blue one in Figure 3.1), $c = 0$ if $\mathbf{x}$ belongs to the gas phase (the green one in Figure 3.1), $0 < c < 1$ if $\mathbf{x}$ belongs to the transition layer between liquid and gas (the red one in Figure 3.1). To describe foam evolution, we will have to set mass balance and momentum balance equations (Navier-Stokes equations) for the two-phase incompressible-compressible system and a nonlinear evolution equation for the phase-field function c (Cahn-Hilliard equation).

In the following sections, after fixing tensor and vector notation (Section 3.1) and after recalling Truesdell's theory of mixtures (Section 3.2), we will find conditions to have a thermodynamically consistent phase-field model, obeying Clausius-Duhem inequality (Section 3.3). In Section 3.4, after introducing a suitable Gibbs free-energy, we will describe the correspondent incompressible-compressible Navier-Stokes-Cahn-Hilliard system of equations modelling the foam expansion process.

3.1 Tensor and vector notation.

Let us fix tensor notation that will be used in the following sections.

Let $\mathbf{x} = (x_1, ..., x_d)$ be a vector in $\mathbb{R}^d$, $v : \mathbb{R}^d \to \mathbb{R}$ a scalar function, $\mathbf{w} : \mathbb{R}^d \to \mathbb{R}^d$ a vector function and $\mathbf{A} : V \to Lin(V)$ a tensor-valued function, where V is a d-dimensional vector space and $Lin(V)$ is a second-rank tensor space:

1. the gradient of v is the vector ∇v:

$$(\nabla v)_i := \left(\frac{\partial v}{\partial x_i}\right)_{1\le i\le d}, \tag{3.1.1}$$

2. the divergence of $\mathbf{w}$ is the scalar $\operatorname{div}\mathbf{w}$:

$$\operatorname{div}\mathbf{w} := \sum_{i=1}^{d} \frac{\partial w_i}{\partial x_i}, \tag{3.1.2}$$

3. the gradient of $\mathbf{w}$ is the second-rank tensor $\nabla\mathbf{w}$ whose Cartesian components are:

$$(\nabla\mathbf{w})_{ij} := \left(\frac{\partial w_i}{\partial x_j}\right)_{1\le i,j\le d}, \tag{3.1.3}$$

4. the divergence of $\mathbf{A}$ is the vector $\operatorname{div}\mathbf{A}$:

$$(\operatorname{div}\mathbf{A})_i := \left(\sum_{j=1}^{d} \frac{\partial A_{ij}}{\partial x_j}\right)_{1\le i\le d}, \tag{3.1.4}$$

5. the Laplacian of v is the scalar Δv:

$$\Delta v := \sum_{i=1}^{d} \frac{\partial^2 v}{\partial x_i^2}, \tag{3.1.5}$$

6. the Laplacian of $\mathbf{w}$ is the vector $\Delta\mathbf{w}$:

$$(\Delta\mathbf{w})_i := \sum_{j=1}^{d} \frac{\partial^2 w_i}{\partial x_j^2}_{1\le i\le d}. \tag{3.1.6}$$

In addition, we will also use the following notation:

$$\int_\Omega |\nabla\mathbf{w}|^2\, dx := \int_\Omega \nabla\mathbf{w} : \nabla\mathbf{w}\, dx, \tag{3.1.7}$$

where

$$\int_\Omega \mathbf{A} : \mathbf{B}\, dx := \int_\Omega \sum_{1\le i,j\le d} A_{ij}B_{ij}\, dx \tag{3.1.8}$$

denotes the L^2 inner product of the two matrix functions $\mathbf{A}, \mathbf{B}$. In the model equations we will also use the tensor product $\mathbf{a}\otimes\mathbf{b}$ between two vectors $\mathbf{a}, \mathbf{b} \in \mathbb{R}^d$ whose action upon a vector $\mathbf{v} \in \mathbb{R}^d$ is defined by

$$(\mathbf{a}\otimes\mathbf{b})\mathbf{v} := (\mathbf{b}\cdot\mathbf{v})\mathbf{a}. \tag{3.1.9}$$

In Cartesian coordinates:

$$(\mathbf{a}\otimes\mathbf{b})_{ij} := a_i b_j. \tag{3.1.10}$$

3.2 Mixtures in a continuum model.

The theory of mixtures as a branch of Rational mechanics has probably its origins in two notes by Clifford Truesdell [57, 58] that will form the starting point of this section.

Truesdell states two basic principles that, later on, he will actually call three *metaphysical principles* ([59], p. 221):

1. *All properties of the mixture must be mathematical consequences of the properties of the constituents.*

2. *So as to describe the motion of a constituent, we may in imagination isolate it from the rest of the mixture, provided we allow properly for the actions of the other constituents upon it.*

3. The motion of the mixture is governed by the same equations as in a single body.

To justify the last principle, Truesdell mentions results by Noll who derived classical field equations of continuum mechanics starting from the statistical mechanics of an ensemble formed by an arbitrary number of molecules that might be different from one another.

3.2.1 Basic definitions.

Here we set our basic definitions by considering a mixture formed by ν species. It is assumed that any point in the space can be occupied by ν continua. If X_α is the Lagrangian coordinate of a particle belonging to the α component of the mixture, and $\mathbf{x}_\alpha$ is its position in space at time t, then we set

$$\mathbf{x}_\alpha = \chi_\alpha(X_\alpha, t)$$

and we define the **velocity** of the particle X_α as

$$\dot{\mathbf{x}}_\alpha := \left.\frac{\partial \chi_\alpha}{\partial t}\right|_{X_\alpha=\text{const.}}$$

and its **acceleration** as

$$(\mathbf{x}_\alpha)^{\cdot\cdot} := \left.\frac{\partial^2 \chi_\alpha}{\partial t^2}\right|_{X_\alpha=\text{const.}}.$$

The **bulk density** ρ_α of the α-th constituent is defined as the mass of the α-th component per unit volume of the *mixture*, whereas the **true density** γ_α of the α-th component is defined as the mass of the α-th component per unit volume of the α-component. The ratio

$$\phi_\alpha := \frac{\rho_\alpha}{\gamma_\alpha} \tag{3.2.1}$$

is called the **volume fraction** of the α-th component. In the following we shall consider mixtures having no voids and so

$$\sum \phi_\alpha = 1, \tag{3.2.2}$$

where a $\sum$ with unspecified index means summation over the different species forming the mixture.

The **total density** ρ of the mixture is defined as

$$\rho := \sum \rho_\alpha. \tag{3.2.3}$$

The **absolute concentration** or **mass fraction** of the α species is defined as the dimensionless ratio given by

$$c_\alpha := \frac{\rho_\alpha}{\rho} \tag{3.2.4}$$

and these concentrations obey the constraint

$$\sum c_\alpha = 1 \tag{3.2.5}$$

that follows from relation (3.2.3).

To describe the average motion of the mixture, we define an **average velocity** $\dot{\mathbf{x}}$ as the vector obeying

$$\rho\dot{\mathbf{x}} := \sum \rho_\alpha \dot{\mathbf{x}}_\alpha \tag{3.2.6}$$

or, by (3.2.4),

$$\dot{\mathbf{x}} := \sum c_\alpha \dot{\mathbf{x}}_\alpha. \tag{3.2.7}$$

Another important velocity is the **diffusive velocity** of the α species

$$\mathbf{u}_\alpha := \dot{\mathbf{x}}_\alpha - \dot{\mathbf{x}} \tag{3.2.8}$$

that, by (3.2.6) and (3.2.7), obeys

$$\sum \rho_\alpha \mathbf{u}_\alpha = 0 \qquad \text{or} \qquad \sum c_\alpha \mathbf{u}_\alpha = 0. \tag{3.2.9}$$

In traditional (i.e. one-component) continuum mechanics, there is just one definition of **material** or **substantial time derivative**; on the contrary, for mixtures, we can define a material derivative related to the average motion, and another related to the motion of the α species. Precisely, we have

$$\dot{Q} := \frac{\partial Q}{\partial t} + \nabla Q \cdot \dot{\mathbf{x}}; \qquad \grave{Q} := \frac{\partial Q}{\partial t} + \nabla Q \cdot \dot{\mathbf{x}}_\alpha. \tag{3.2.10}$$

where Q might be a scalar, a vector, or a tensor component. By (3.2.8), these material derivatives are related by

$$\grave{Q} - \dot{Q} = \nabla Q \cdot \mathbf{u}_\alpha. \tag{3.2.11}$$

3.2.2 Balance of mass.

We are now ready to state the **balance of mass** within mixtures. For any species α, we introduce the α-th **massive rapidity** $\hat{c}_\alpha$ such that $\rho\hat{c}_\alpha$ represents the mass per unit time and volume (of the mixture) that is injected into the α phase. Then, the balance of mass for the α-species amounts to

$$\frac{\partial \rho_\alpha}{\partial t} + \operatorname{div}(\rho_\alpha \dot{\mathbf{x}}_\alpha) = \rho\hat{c}_\alpha. \tag{3.2.12}$$

By summing over α and recalling (3.2.3) and (3.2.6), we obtain

$$\dot{\rho} + \rho \operatorname{div}(\dot{\mathbf{x}}) = \rho \sum \hat{c}_\alpha, \tag{3.2.13}$$

which is equivalent to local balance of mass for a *single* component if and only if

$$\sum \hat{c}_\alpha = 0. \tag{3.2.14}$$

In the following sections we shall adhere to this view and so we will write the averaged balance of mass as

$$\dot{\rho} + \rho \operatorname{div}(\dot{\mathbf{x}}) = 0. \tag{3.2.15}$$

3.2.3 Some useful identities.

With balance of mass at our disposal, we now obtain a *fundamental identity* that is rather useful in passing from balance equations for the single components to a balance equation involving mean quantities.

Let Q_α be a sufficiently smooth function and let us define

$$Q := \sum c_\alpha Q_\alpha. \tag{3.2.16}$$

Since

$$\rho_\alpha \dot{\grave{Q}}_\alpha = \frac{\partial}{\partial t}(\rho_\alpha Q_\alpha) + \mathrm{div}(\rho_\alpha Q_\alpha \dot{\grave{\mathbf{x}}}_\alpha) - Q_\alpha \left[\frac{\partial \rho_\alpha}{\partial t} + \mathrm{div}(\rho_\alpha \dot{\grave{\mathbf{x}}}_\alpha)\right]$$

or, by use of (3.2.8),

$$\rho_\alpha \dot{\grave{Q}}_\alpha = \frac{\partial}{\partial t}(\rho_\alpha Q_\alpha) + \mathrm{div}(\rho_\alpha Q_\alpha \dot{\mathbf{x}}) + \mathrm{div}(\rho_\alpha Q_\alpha \mathbf{u}_\alpha) - Q_\alpha \left[\frac{\partial \rho_\alpha}{\partial t} + \mathrm{div}(\rho_\alpha \dot{\grave{\mathbf{x}}}_\alpha)\right].$$

By adding over α and recalling (3.2.10), we also obtain

$$\sum c_\alpha \dot{\grave{Q}}_\alpha = \dot{Q} + \frac{Q}{\rho}\left[\frac{\partial \rho}{\partial t} + \mathrm{div}(\rho \dot{\mathbf{x}})\right] + \frac{1}{\rho}\sum \mathrm{div}(\rho_\alpha Q_\alpha \mathbf{u}_\alpha) - \sum \frac{Q_\alpha}{\rho}\left[\frac{\partial \rho_\alpha}{\partial t} + \mathrm{div}(\rho_\alpha \dot{\grave{\mathbf{x}}}_\alpha)\right] \tag{3.2.17}$$

that, by resorting to the balance equations (3.2.12) and (3.2.15), yields

$$\sum c_\alpha \dot{\grave{Q}}_\alpha = \dot{Q} + \frac{1}{\rho}\sum \mathrm{div}(\rho_\alpha Q_\alpha \mathbf{u}_\alpha) - \sum Q_\alpha \hat{c}_\alpha. \tag{3.2.18}$$

It is interesting to note that, if $Q_\alpha = \dot{\grave{\mathbf{x}}}_\alpha$, by (3.2.6), (3.2.8) and (3.2.9), we obtain

$$\sum c_\alpha (\mathbf{x}_\alpha)\dot{\grave{}}\grave{} = \ddot{\mathbf{x}} + \frac{1}{\rho}\sum \mathrm{div}(\rho_\alpha \mathbf{u}_\alpha \otimes \mathbf{u}_\alpha) - \sum \hat{c}_\alpha \mathbf{u}_\alpha \tag{3.2.19}$$

that shows that the mean acceleration $\ddot{\mathbf{x}}$ fails to be the weighted average value of the accelerations of the individual components.

3.2.4 Balance of linear momentum.

We now want to obtain the **balance of linear momentum** of the mixture, starting from the balance of linear momentum for any component. Actually, we suppose that

$$\rho_\alpha (\mathbf{x}_\alpha)\dot{\grave{}}\grave{} = \rho_\alpha \mathbf{b}_\alpha + \mathrm{div}\mathbf{T}_\alpha + \rho \hat{\mathbf{p}}_\alpha, \tag{3.2.20}$$

where $\hat{\mathbf{p}}_\alpha$ represents the impulsive rapidity of the α component and $\mathbf{b}_\alpha$ is the peculiar body force. If we now add over α, employ (3.2.19) and define

$$\mathbf{T} := \sum \mathbf{T}_\alpha - \rho_\alpha \mathbf{u}_\alpha \otimes \mathbf{u}_\alpha$$

together with $\mathbf{b} := \sum c_\alpha \mathbf{b}_\alpha$, we obtain

$$\rho(\ddot{\mathbf{x}} - \mathbf{b}) - \mathrm{div}\mathbf{T} = \rho \sum (\hat{\mathbf{p}}_\alpha + \hat{c}_\alpha \mathbf{u}_\alpha). \tag{3.2.21}$$

Hence, a necessary and sufficient condition for the validity of the third metaphysical principle is that

$$\sum (\hat{\mathbf{p}}_\alpha + \hat{c}_\alpha \mathbf{u}_\alpha) = 0 \tag{3.2.22}$$

which admits a clear physical meaning as it states that the sum of the linear momenta associated with interactions of the α- with other components and that associated to mass diffusion have to vanish.

3.2.5 Balance of energy.

Next, we consider **balance of energy** starting from its version for the α-constituent. To this aim we introduce e_α, the internal energy of the α-component, r_α the energy supply, $\mathbf{q}_\alpha$ the energy flux and the **energetic rapidity** $\hat{e}_\alpha$ whose meaning is that it vanishes if and only if the α-component is isolated from the others. Hence, we have

$$\rho\hat{e}_\alpha = \rho_\alpha(\grave{e}_\alpha - r_\alpha) - \mathbf{T}_\alpha \cdot \nabla\dot{\mathbf{x}}_\alpha + \mathrm{div}\mathbf{q}_\alpha = \rho_\alpha(\grave{e}_\alpha - r_\alpha) - \mathbf{T}_\alpha \cdot \nabla\mathbf{u}_\alpha - \mathbf{T}_\alpha \cdot \nabla\dot{\mathbf{x}} + \mathrm{div}\mathbf{q}_\alpha.$$

The total internal energy is not just the sum of e_α but also accounts for the kinetic energies of diffusion. Hence, we define

$$e := \sum c_\alpha \left(e_\alpha + \frac{1}{2}\mathbf{u}_\alpha^2 \right). \tag{3.2.23}$$

To proceed, we observe that, by definition,

$$\sum c_\alpha \overline{\frac{1}{2}\mathbf{u}_\alpha^2} = \sum c_\alpha \mathbf{u}_\alpha \cdot \left[(\mathbf{x}_\alpha)\grave{} - \frac{\partial\dot{\mathbf{x}}}{\partial t} - (\nabla\dot{\mathbf{x}})\dot{\mathbf{x}}_\alpha \right] = \sum c_\alpha \mathbf{u}_\alpha \cdot [(\mathbf{x}_\alpha)\grave{} - (\nabla\dot{\mathbf{x}})(\dot{\mathbf{x}} + \mathbf{u}_\alpha)]$$

where use of (3.2.9) has also been made. By repeated use of (3.2.9) we finally obtain

$$\sum c_\alpha \overline{\frac{1}{2}\mathbf{u}_\alpha^2} = \sum c_\alpha \mathbf{u}_\alpha \cdot [(\mathbf{x}_\alpha)\grave{} - \mathbf{D} \cdot (\mathbf{u}_\alpha \otimes \mathbf{u}_\alpha)], \tag{3.2.24}$$

where we defined

$$\mathbf{D} := \frac{1}{2}[\nabla\dot{\mathbf{x}} + (\nabla\dot{\mathbf{x}})^{\mathrm{T}}].$$

By recalling that

$$\mathbf{T}_\alpha \cdot \nabla\mathbf{u}_\alpha = \mathrm{div}(\mathbf{T}_\alpha^{\mathrm{T}}\mathbf{u}_\alpha) - \mathrm{div}(\mathbf{T}_\alpha) \cdot \mathbf{u}_\alpha$$

and applying (3.2.17) repeatedly, we obtain

$$\rho\dot{e} - \mathbf{T} \cdot \mathbf{D} + \mathrm{div}\mathbf{q} - \rho r = 0, \tag{3.2.25}$$

that is formally identical to the case of a unique continuum body, where

$$\mathbf{q} := \sum \left[\mathbf{q}_\alpha - \mathbf{T}_\alpha\mathbf{u}_\alpha + \rho_\alpha \left(e_\alpha + \frac{1}{2}\mathbf{u}_\alpha^2 \right) \mathbf{u}_\alpha \right],$$

$$r := \sum c_\alpha(r_\alpha + \mathbf{b}_\alpha \cdot \mathbf{u}_\alpha).$$

3.3 Thermodynamically consistent phase-field models.

In the sequel, we will derive the mathematical model for the description of metal foam expansion within a hollow mold, under the simplifying hypotheses of constant temperature and melted metal. The derivation of this model belongs to the framework of thermodynamically consistent phase-field models according to the results proved in [20], [42].

Let us consider a two-phase flow in which there is a fluid phase (hereafter, phase 1) and a gaseous phase (referred hereafter as phase 2). We also suppose that the mixture is non-reacting, so that $\hat{c}_\alpha$ can be set equal to zero. Hence, not only (3.2.15) holds, but (3.2.12) can be recast as

$$\frac{\partial\rho_\alpha}{\partial t} + \mathrm{div}(\rho_\alpha\dot{\mathbf{x}}_\alpha) = 0 \qquad \alpha = 1, 2. \tag{3.3.1}$$

We are concerned with the case in which the gaseous component is compressible, and so we cannot further simplify (3.3.1) by taking ρ_2 as constant: this is only possible for the liquid phase. As a phase-field variable we take

$$c = c_1 := \frac{\rho_1}{\rho},$$

the concentration of the liquid phase. Given a value of ρ, c and ρ_1 are simply proportional, but if ρ is unknown, c is another independent variable. By taking (3.3.1) and recalling (3.2.7), we readily obtain [42]

$$\rho\dot{c} = -\mathrm{div}\mathbf{j} \tag{3.3.2}$$

where $\mathbf{j} := \rho_1\mathbf{u}_1$ and $\mathbf{u}_1$ has been defined in (3.2.8). Equation (3.3.2) is taken as a postulate in the subsequent development, in the sense that we shall consider models in which the *scalar* phase-field variable is governed by an equation of the type

$$\rho\dot{c} = -\mathrm{div}\mathbf{j}(\rho, c, \theta, \nabla\rho, \nabla c, \nabla\theta), \tag{3.3.3}$$

neglecting, for simplicity, dependence on higher order gradients in the scalar fields. Together with (3.3.3), we shall also suppose that the averaged balance equations

$$\begin{cases} \dot{\rho} = -\rho\,\mathrm{div}(\mathbf{u}), \\ \rho\dot{\mathbf{v}} = \mathrm{div}\mathbf{T} + \rho b, \\ \rho\dot{e} = \mathbf{T}\cdot\mathbf{D} - \mathrm{div}\mathbf{q} + \rho r \end{cases} \tag{3.3.4}$$

hold in the mixture, in which $\mathbf{u} := \dot{\mathbf{x}}$.

In addition to these balance equations, we must ensure the validity of the second law of thermodynamics, through the **Clausius-Duhem** inequality, as explained in the following statement.

Entropy principle. *Let η be the entropy density. The Clausius-Duhem inequality*

$$\rho\dot{\eta} \geq -\mathrm{div}\left(\frac{\mathbf{q}}{\theta} + \mathbf{k}\right) + \frac{\rho r}{\theta} \tag{3.3.5}$$

must hold and must be compatible with the balance equations (3.3.4). The extra-entropy flux $\mathbf{k}$ is another constitutive quantity that accounts for entropy flux due to phase changes.

It is expedient to introduce the **Helmholtz free-energy** ψ defined by

$$\psi := e - \theta\eta$$

and then, by use of $(3.3.4)_2$, we transform (3.3.5) into

$$\rho(\dot{\psi} + \eta\dot{\theta}) - \mathbf{T}\cdot\mathbf{D} - \theta\mathrm{div}\mathbf{k} + \frac{1}{\theta}\mathbf{q}\cdot\nabla\theta \leq 0. \tag{3.3.6}$$

We suppose that $\psi = \psi(\rho, c, \theta, \nabla\theta, \mathbf{D}, \nabla c)$ and a similar functional dependence also for $\mathbf{T}$, η, $\mathbf{k}$, $\mathbf{q}$ and $\mathbf{j}$. The validity of the second law imposes appropriate restrictions on the constitutive functions $\mathbf{T}$, ψ, η, $\mathbf{k}$, $\mathbf{q}$ and $\mathbf{j}$, as will be proved by the next theorem (see [42]).

Theorem 3.3.1 (Restrictions imposed by Clausius-Duhem inequality)**.** *The functions $\mathbf{T}$, ψ, η, $\mathbf{k}$, $\mathbf{q}$ and $\mathbf{j}$ are compatible with the second law of thermodynamics in the form (3.3.6) if*

$$\psi_\theta + \eta = 0, \quad \psi_{\mathbf{D}} = 0, \quad \psi_{\nabla\theta} = 0, \tag{3.3.7}$$

$$\mathbf{q} = -\kappa(c, \rho, \theta)\nabla\theta, \tag{3.3.8}$$

$$\mathrm{div}\mathbf{j} = \hat{f}(c, \rho, \theta)\left(\frac{1}{\theta}\psi_c - \frac{1}{\rho}\mathrm{div}\left(\frac{\rho}{\theta}\psi_{\nabla c}\right)\right), \tag{3.3.9}$$

$$\mathbf{T} = -\rho^2\psi_\rho\mathbf{I} - \mathrm{sym}(\rho\nabla c\otimes\psi_{\nabla c}) + 2\mu\mathbf{D} + \lambda(\mathrm{div}\mathbf{v})\mathbf{I}, \tag{3.3.10}$$

where the functions κ and $\hat{f}$ are bound to be positive; μ and λ can be, in principle, taken as functions of ρ, θ, and c and must obey the constraints $\mu > 0$ and $2\mu + 3\lambda > 0$.

Proof. First we recall that, for any scalar function g, the following identity holds [20]:

$$\dot{\overline{\nabla g}} = \nabla \dot{g} - \mathbf{L}^{\mathrm{T}} \nabla g \tag{3.3.11}$$

where $\mathbf{L} := \nabla \mathbf{v}$. In fact, by definition,

$$\dot{\overline{\nabla g}} = \partial_t \nabla g + (\mathbf{v} \cdot \nabla) \nabla g.$$

The identity

$$(\mathbf{v} \cdot \nabla) \nabla g = \nabla (\mathbf{v} \cdot \nabla g) - \mathbf{L}^T \nabla g$$

gives

$$\dot{\overline{\nabla g}} = \nabla (\partial_t g + \mathbf{v} \cdot \nabla g) - \mathbf{L}^T \nabla g,$$

from which (3.3.11) follows.

By repeated use of the chain rule to compute $\dot{\psi}$ we can set (3.3.6) as

$$\begin{aligned} &\rho(\psi_\theta + \eta)\dot{\theta} + \rho\psi_c \dot{c} + \rho\psi_{\mathbf{D}} \cdot \dot{\mathbf{D}} + \rho\psi_{\nabla\theta} \dot{\overline{\nabla\theta}} \\ &+\rho\psi_{\nabla c} \cdot \dot{\overline{\nabla c}} - \operatorname{div}(\theta \mathbf{k}) + \mathbf{k} \cdot \nabla\theta + \tfrac{1}{\theta} \mathbf{q} \cdot \nabla\theta - (\mathbf{T} + \rho^2 \psi_\rho \mathbf{I}) \cdot \mathbf{L} \leq 0, \end{aligned} \tag{3.3.12}$$

where, according to [42], we restrict attention to symmetric stress tensors $\mathbf{T}$ and we also employed $(3.3.4)_1$ to get rid of $\dot{\rho}$. By also recalling (3.3.3), we conclude that

$$\begin{aligned} &-(\mathbf{T} + \rho^2 \psi_\rho \mathbf{I} + \rho \nabla c \otimes \psi_{\nabla c}) \cdot \mathbf{L} + \rho(\psi_\theta + \eta)\dot{\theta} + \rho\psi_c \dot{c} + \rho\psi_{\mathbf{D}} \cdot \dot{\mathbf{D}} + \rho\psi_{\nabla\theta} \dot{\overline{\nabla\theta}} \\ &+\rho\psi_{\nabla c} \cdot \nabla \dot{c} - \operatorname{div}(\theta \mathbf{k}) + \mathbf{k} \cdot \nabla\theta + \tfrac{1}{\theta} \mathbf{q} \cdot \nabla\theta \leq 0 \end{aligned} \tag{3.3.13}$$

should hold on all admissible processes that obey the averaged balance equations. We now observe that the left-hand side of (3.3.13) is linear in the fields $\dot{\mathbf{D}}$, $\dot{c}$, $\dot{\theta}$, and $\dot{\overline{\nabla\theta}}$ so that a sufficient condition for the fulfilment of (3.3.13) is that the corresponding coefficients vanish identically, yielding (3.3.7).

This fact reduces (3.3.13) to

$$-(\mathbf{T} + \rho^2 \psi_\rho \mathbf{I} + \rho \nabla c \otimes \psi_{\nabla c}) \cdot \mathbf{L} + \rho\psi_c \dot{c} + \rho\psi_{\nabla c} \cdot \nabla \dot{c} - \operatorname{div}(\theta \mathbf{k}) + \mathbf{k} \cdot \nabla\theta + \tfrac{1}{\theta} \mathbf{q} \cdot \nabla\theta \leq 0. \tag{3.3.14}$$

Following [42] we set

$$\widehat{\mathbf{T}} := \mathbf{T} + \rho^2 \psi_\rho \mathbf{I} + \rho \nabla c \otimes \psi_{\nabla c} \tag{3.3.15}$$

so that, by recalling (3.3.3) and after elementary manipulations we arrive at

$$-\widehat{\mathbf{T}} \cdot \mathbf{L} + (\rho\psi_c - \operatorname{div}(\rho\psi_{\nabla c})) \cdot \dot{c} + \operatorname{div}(\rho\psi_{\nabla c}\dot{c} - \theta\mathbf{k}) + \left(\mathbf{k} + \frac{\mathbf{q}}{\theta}\right) \cdot \nabla\theta \leq 0. \tag{3.3.16}$$

As in [20], it seems natural to set

$$\theta \mathbf{k} - \rho\psi_{\nabla c}\dot{c} = 0, \tag{3.3.17}$$

since the extra entropy-flux $\mathbf{k}$ is related to phase transformations and so should vanish whenever ∇c or $\dot{c}$ are equal to zero. Adhering to this view, we arrive at

$$-\widehat{\mathbf{T}} \cdot \mathbf{L} + (\rho\psi_c - \operatorname{div}(\rho\psi_{\nabla c})) \cdot \dot{c} + \left(\mathbf{k} + \frac{\mathbf{q}}{\theta}\right) \cdot \nabla\theta \leq 0 \tag{3.3.18}$$

or, by use of (3.3.17), and dividing by the positive quantity θ

$$-\frac{1}{\theta}\widehat{\mathbf{T}} \cdot \mathbf{L} - \left(\frac{1}{\theta}\psi_c - \frac{1}{\rho}\operatorname{div}\left(\frac{\rho}{\theta}\psi_{\nabla c}\right)\right) \cdot \operatorname{div}\mathbf{j} + \frac{\mathbf{q}}{\theta^2} \cdot \nabla\theta \leq 0 \tag{3.3.19}$$

which is the final version of the reduced Clausius-Duhem inequality. A possible way to obey it is by taking (3.3.8), (3.3.9) and (3.3.10), recalling that

$$\mathbf{D} \cdot \mathbf{L} = \mathbf{D} \cdot \mathbf{D} \quad \text{and} \quad \mathbf{I} \cdot \mathbf{D} = \operatorname{div} \mathbf{u}.$$

□

Remark 1. Since $\mathbf{L}$ might have a skew-symmetric part, we have the further restriction

$$\mathrm{skw}(\rho\nabla c \otimes \psi_{\nabla c}) = 0 \tag{3.3.20}$$

that, however, is easily accounted for. In fact, since the scalar function ψ can depend on the vector ∇c only through its scalar invariant, that is $|\nabla c|$, we can set $\psi_{\nabla c} = g(|\nabla c|)\nabla c$ and so (3.3.20) is automatically satisfied and (3.3.10) can be recast as

$$\mathbf{T} = \mathbf{T}_0 + \mathbf{T}_v, \tag{3.3.21}$$

where

$$\mathbf{T}_0 = -\rho^2\psi_\rho\mathbf{I} - \nu\rho\nabla c \otimes \nabla c \tag{3.3.22}$$

is the non-viscous part and

$$\mathbf{T}_v = 2\mu\mathbf{D} + \lambda(\mathrm{div}\mathbf{v})\mathbf{I} \tag{3.3.23}$$

is the viscous part.

Remark 2. Since in our problem the fluid component can be regarded as incompressible, while the gaseous phase is clearly compressible, we shall assume

$$\lambda = \lambda(c) = \lambda_g(1-c)$$

where λ_g is characteristic of the gas dispersed in the mixture. As to the viscosity μ, we take the simplest formula interpolating between the bulk values of the gas and the fluid phase:

$$\mu = \mu(c) := \mu_f c + \mu_g(1-c) \tag{3.3.24}$$

where μ_g and μ_f pertain to the gas and to the fluid phase, respectively. Following Lowengrub and Truskinovsky [38], we decompose the capillary stress into a pressure and into a shear component. Actually, we limit our attention to a free-energy ψ such that $\psi_{\nabla c} = \nu\nabla c$, with $\nu > 0$ a constant. Then, by limiting attention to non viscous terms $\mathbf{T}_0$ in $\mathbf{T}$ and setting $p_0 := \rho^2\psi_\rho$, we have

$$\mathbf{T}_0 = -(p_0 + \nu\rho|\nabla c|^2)\mathbf{I} + \nu\rho|\nabla c|^2\left(\mathbf{I} - \frac{\nabla c}{|\nabla c|} \otimes \frac{\nabla c}{|\nabla c|}\right). \tag{3.3.25}$$

Since $\frac{\nabla c}{|\nabla c|} = \mathbf{n}$, the unit normal to the interface, following the analogy with the level-set method described in [38] we also interpret the last term in (3.3.25) as a regularised extra-surface term, from which the surface tension can be derived (see [38]). It is tempting to interpret the phase-field dependent correction to the pressure $\nu\rho|\nabla c|^2$ as a disjoining pressure, but a more refined microscopic treatment would be needed to corroborate this claim. Nevertheless, at variance with [33], we do not add an extra term to account for disjoining pressure but we are content with the correction just found.

3.4 Phase-field model of two-phase incompressible-compressible fluids.

3.4.1 Gibbs free-energy.

Suppose that the incompressible phase (the liquid metal, phase 1) and the compressible phase (the hydrogen, phase 2) coexist at a given temperature θ. Up to now we have used Helmholtz free-energy $\psi(\rho, \theta, c, \nabla c)$ and we have defined pressure through the relation

$$p = \rho^2\partial_\rho\psi.$$

Actually this is possible only if the fluid is compressible and if the equation of state $p = p(\rho, T)$ can be inverted at a given temperature. For an incompressible fluid, however,

the density is constant at a given temperature and so $\rho = \rho(\theta)$, from which it is impossible to recover information about pressure. An avenue to overcome this difficulty, as remarked in [38], is reverting to Gibbs free-energy g which is usually related to Helmholtz free-energy via a Legendre transformation, whenever this is not singular. The knowledge of g makes it possible to recover ρ through

$$\rho^{-1} = \frac{\partial g}{\partial p}. \tag{3.4.1}$$

For future reference, we also list here the expressions it terms of g

$$\eta = -\frac{\partial g}{\partial \theta} \qquad \mu = \frac{\partial g}{\partial c}$$

where η is the specific internal entropy and μ is the (generalised) chemical potential. When g has been assigned, it is possible to turn back to ψ, now expressed in terms of p and θ as

$$\psi(p, \theta, c) = g(p, \theta, c) - p\frac{\partial g}{\partial p}. \tag{3.4.2}$$

By (3.4.1) we see that requiring $\rho = \text{const.}$ is tantamount as having

$$\frac{\partial^2 g}{\partial p^2} = 0. \tag{3.4.3}$$

In our context, it seems reasonable to set

$$\rho^{-1} = \frac{c}{\rho_1} + nR\theta(1-c)\frac{1}{p}, \tag{3.4.4}$$

so that, when $c \equiv 1$, $\rho = \rho_1$, the density of the fluid phase, whereas when $c \equiv 0$, ρ has the expression given by the equation of state of perfect gases. By use of (3.4.1), we obtain

$$g(p, \theta, c, \nabla c) = \frac{c}{\rho_1}p + nR\theta(1-c)\ln\frac{p}{p_0} + g_0(c, \theta) + g_1(c) + g_2(\nabla c),$$

where p_0 is a reference pressure. The term g_0 is set equal to

$$g_0(c, \theta) = (1-c)\left(\left(\frac{7}{2}nR - S_0\right)(\theta - \theta_0) + nR\theta\ln\left(\frac{\theta_0}{\theta}\right)^{\frac{7}{2}}\right)$$

so that, when $c \equiv 0$ the Gibbs free energy reduces to the standard expression for a perfect, diatomic gas ([47], p. 54): here S_0 and θ_0 are constants. As to g_1, we propose the standard double well potential

$$g_1(c) = \beta c^2(1-c)^2$$

since, on passing from the gas phase where $c = 0$ to a level surface for c, the Gibbs free energy changes from 0 to $\beta c^2(1-c)^2$ and we interpret this latter as an osmotic pressure

$$p_g = \beta c^2(1-c)^2. \tag{3.4.5}$$

If we only consider the leading term in (3.4.5) we find that

$$c = \sqrt{\frac{p_g}{\beta}} \tag{3.4.6}$$

at the interface between the gas and the liquid metal. Equation (3.4.6) shows the same relation between c and p_g as in Sievert's law. Sievert's law can be expressed by the relation

$$c(\theta, p_g) = K_s\sqrt{\frac{p_g}{p_a}} \tag{3.4.7}$$

where p_a is the atmospheric pressure and K_s is a temperature/dependent parameter that, in the case of hydrogen in liquid aluminium, is given by [54, 55]

$$K_s = 8.9 \cdot 10^{-5} \cdot 10^{-\frac{2760}{T}+2.796}.$$

Comparing (3.4.6) and (3.4.7), we find that

$$\beta = \frac{p_a}{K_s^2}$$

and so, also the Sievert's law is included in our model. The term $g_2(\nabla c)$ is defined by

$$g_2(\nabla c) = \frac{\gamma}{2}|\nabla c|^2.$$

Collecting together all the terms, the Gibbs free-energy is given by

$$\begin{aligned} g(p,\theta,c,\nabla c) &= \frac{c}{\rho_1}p + nR\theta(1-c)\ln\frac{p}{p_0} \\ &\quad +(1-c)\left(\left(\frac{7}{2}nR - S_0\right)(\theta-\theta_0) + nR\theta\ln\left(\frac{\theta_0}{\theta}\right)^{\frac{7}{2}}\right) \\ &\quad +\beta c^2(1-c)^2 + \frac{\gamma}{2}|\nabla c|^2. \end{aligned} \tag{3.4.8}$$

3.4.2 Metal-foam system of equations.

Using the Legendre transformation (3.4.2), we can rewrite (3.3.6) as

$$\rho\left(\dot{g} + \eta\dot{\theta} + \frac{1}{\rho^2}\dot{\rho}p - \frac{1}{\rho}\dot{p}\right) - \mathbf{T}\cdot\mathbf{D} - \theta\,\mathrm{div}\,\mathbf{k} + \frac{1}{\theta}\mathbf{q}\cdot\nabla\theta \leq 0. \tag{3.4.9}$$

We suppose that g and also $\mathbf{T}$, η, $\mathbf{k}$, $\mathbf{q}$ and $\mathbf{j}$ depend upon $p, c, \theta, \nabla\theta, \mathbf{D}, \nabla c$. In this case, the validity of the second law imposes appropriate restrictions on the constitutive functions $\mathbf{T}$, g, η, $\mathbf{k}$, $\mathbf{q}$ and $\mathbf{j}$. Similarly to the situation studied in the previous section, the following result can be proved (see [42]).

Theorem 3.4.1 (Validity of the Clausius-Duhem inequality - Gibbs free-energy). *The functions $\mathbf{T}$, g, η, $\mathbf{k}$, $\mathbf{q}$ and $\mathbf{j}$ are compatible with the second law of thermodynamics in the form (3.4.9) if*

$$g_\theta + \eta = 0, \quad g_{\mathbf{D}} = 0, \quad g_{\nabla\theta} = 0, \tag{3.4.10}$$

$$\mathbf{q} = -\kappa(c,p,\theta)\nabla\theta, \tag{3.4.11}$$

$$\mathrm{div}\mathbf{j} = \hat{f}(c,p,\theta)\left(\frac{1}{\theta}g_c - \frac{1}{\rho}\mathrm{div}\left(\frac{\rho}{\theta}g_{\nabla c}\right)\right), \tag{3.4.12}$$

$$\mathbf{T} = -p\mathbf{I} - \mathrm{sym}(\rho\nabla c\otimes g_{\nabla c}) + 2\mu\mathbf{D} + \lambda(\mathrm{div}\mathbf{v})\mathbf{I}, \tag{3.4.13}$$

where the functions κ and $\hat{f}$ are positive; μ and λ can be, in principle, taken as functions of p, θ, and c and must obey the constraints $\mu > 0$ and $2\mu + 3\lambda > 0$.

However, by using (3.3.20)-(3.3.23), (3.3.25) into (3.4.13), the stress tensor can be written as

$$\mathbf{T} = -p\mathbf{I} - \nu\rho\nabla c\otimes\nabla c + 2\mu c\mathbf{D},$$

where ν is a positive constant and we suppose that the viscosity is μ in the fluid phase, and 0 in the gas phase. No other viscosity is accounted for since the fluid phase is incompressible and Stokes relation forces $\lambda = 0$ in the gas phase, as soon as $\mu = 0$ is taken there. Actually, we started from the equation of state of perfect gas that contains the *thermodynamic pressure* which is conceptually different from the pressure arising as a Lagrange multiplier enforcing incompressibility. As proved in Chapter II of [60], these pressures coalesce together as soon as we assume that the bulk viscosity $\lambda + \frac{2}{3}\mu$ vanishes. The theory stemming from this assumption is named after Stokes and Kirchhoff.

Now, if we consider that the temperature θ is constant during the expansion of the foam (according to the model hypotheses we discussed in the previous chapter) and choosing $\hat{f} = \theta$, the set of Navier-Stokes-Cahn-Hilliard equations for incompressible-compressible fluids can be written in the form:

$$\rho^{-1} = \frac{c}{\rho_1} + \frac{(1-c)nR\theta}{p}, \tag{3.4.14}$$

$$\dot{\rho} = -\rho \operatorname{div} \mathbf{u}, \tag{3.4.15}$$

$$\rho\dot{\mathbf{u}} = \operatorname{div} \mathbf{T} + \rho\mathbf{b}, \tag{3.4.16}$$

$$\rho\dot{c} = \operatorname{div}\left(\zeta \nabla \left(\rho^{-1}\delta_c g\right)\right), \tag{3.4.17}$$

where ζ is a positive constant,

$$\mathbf{T} = -p\mathbf{I} - \nu\rho\nabla c \otimes \nabla c + 2\mu c\mathbf{D}, \tag{3.4.18}$$

$$\delta_c g := \rho g_c - \operatorname{div}\left(\rho g_{\nabla c}\right), \tag{3.4.19}$$

$$\begin{aligned} g(p,c,\nabla c) = {} & \frac{c}{\rho_1}p + nR\theta(1-c)\ln\frac{p}{p_0} \\ & +(1-c)\left(\left(\frac{7}{2}nR - S_0\right)(\theta-\theta_0) + nR\theta\ln\left(\frac{\theta_0}{\theta}\right)^{\frac{7}{2}}\right) \\ & +\beta c^2(1-c)^2 + \frac{\gamma}{2}|\nabla c|^2. \end{aligned} \tag{3.4.20}$$

3.4.3 Geometry and boundary-initial conditions.

We suppose that, at the initial time, we have a mixture of liquid metal and hydrogen, i.e. some bubbles are already present. The mixture is in a rectangular box $\mathcal{B}$ (see Figure 3.2). For simplicity, we consider a 2D geometry and this box, open at the top, models the mould in which the foaming expansion evolves. Hydrogen can be found both in the upper part of the box and inside the bubbles.

We have now to impose a suitable set of boundary conditions on the fields $\mathbf{u}$, p, and c characterising our system. We first consider the rigid portions of the boundary, $\partial\mathcal{B}_l$ and $\partial\mathcal{B}_b$ for the lateral part and the bottom part of the boundary, respectively. For the

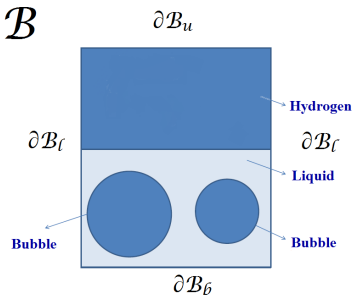

Figure 3.2: Test case for the metal-foam model.

velocity field we enforce

$$\mathbf{u} = \mathbf{0} \qquad \text{on } \partial\mathcal{B}_b, \tag{3.4.21}$$

$$\mathbf{u}\cdot\mathbf{n} = 0 \qquad \text{on } \partial\mathcal{B}_l, \tag{3.4.22}$$

and

$$\mathbf{T}\mathbf{n}\cdot\boldsymbol{\tau}=0 \qquad \text{on } \partial\mathcal{B}_l, \tag{3.4.23}$$

where $\mathbf{T}\mathbf{n}\cdot\boldsymbol{\tau}$ identifies the tangential component of $\mathbf{T}\mathbf{n}$. We also suppose that

$$\mathbf{T}\mathbf{n}=\mathbf{0} \qquad \text{on } \partial\mathcal{B}_u \tag{3.4.24}$$

on the upper part of the box.

For the concentration c, we have two types of boundary conditions. First, we suppose that

$$\nabla c\cdot\mathbf{n}=0 \qquad \text{on } \partial\mathcal{B}. \tag{3.4.25}$$

Moreover, we recall that the evolution of c is ruled by

$$\rho\dot{c}=-\mathrm{div}\mathbf{j} \tag{3.4.26}$$

where the current $\mathbf{j}$ is given by

$$\mathbf{j}:=\zeta\nabla\left(\frac{1}{\rho}\delta_c g\right).$$

By integrating on $\mathcal{B}$ and using both Reynolds' transport theorem and the divergence theorem, we arrive at

$$\frac{\mathrm{d}}{\mathrm{d}t}\int_{\mathcal{B}}\rho c\mathrm{d}V=\int_{\partial\mathcal{B}}\mathbf{j}\cdot\mathbf{n}\mathrm{d}A:$$

imposing

$$\mathbf{j}\cdot\mathbf{n}=0 \qquad \text{on } \partial\mathcal{B} \tag{3.4.27}$$

amounts at saying that there is no flux across the boundaries of the box.

As initial conditions, we have to set an initial configuration c_0 of the bubbles and we can suppose that the initial velocity is equal to zero.

3.4.4 Dimensionless equations.

Let us consider the following characteristic quantities: the length L^*, the velocity V^*, the density ρ^*, the chemical potential μ^*, the temperature θ^*.

They induce a characteristic time $t^*=\frac{L^*}{V^*}$ and a characteristic pressure $p^*=\rho^*\mu^*$. In the new dimensionless variables, the continuity equation does not change:

$$\dot{\rho}=-\rho\,\mathrm{div}\,\mathbf{u}. \tag{3.4.28}$$

Momentum balance equation, in which we do not include body forces for simplicity, can be written as

$$\rho\dot{\mathbf{u}}=\mathrm{div}\,\mathbf{T}, \tag{3.4.29}$$

where

$$\mathbf{T}=-\frac{1}{\mathbb{M}}\left(p\mathbf{I}+\mathbb{C}\rho\nabla c\otimes\nabla c\right)+\frac{2}{\mathbb{R}e}c\mathbf{D}, \tag{3.4.30}$$

$\mathbb{M}=\frac{\mu^*}{V^*}$ is the Mach number and $\mathbb{C}=\frac{\nu}{\mu^*L^{*2}}$ is the Cahn number (or capillary number), whereas $\mathbb{R}e=\frac{\rho^*V^*L^*}{\mu}$ is the Reynolds number.
The evolution of c is governed by

$$\rho\dot{c}=\mathrm{div}\left(\frac{1}{\mathbb{P}e}\,\nabla\left(\rho^{-1}\delta_c g\right)\right), \tag{3.4.31}$$

where $\mathbb{P}e=\frac{\rho^*V^*L^*}{\zeta\mu^*}$ is the Péclet number,

$$g(p,c,\nabla c)=\frac{c}{\rho_1}p+N_1\theta(1-c)\ln\frac{p}{p_0}+g_0(c)+g_1(c)+g_2(\nabla c), \tag{3.4.32}$$

where $N_1 = \frac{R\theta_0}{M_w \mu^*}$, θ_0 a reference temperature and M_w molecular weight of the gas,

$$g_0(c) = (1-c)\left(\left(\frac{7}{2}N_1 - \sigma_0\right)(\theta - 1) + N_1\theta \ln\left(\frac{\theta_0}{\theta}\right)^{\frac{7}{2}}\right), \tag{3.4.33}$$

$\sigma_0 = \frac{S_0\theta_0}{\mu^*}$,

$$g_1(c) = bc^2(1-c)^2, \tag{3.4.34}$$

with $b = \frac{\beta}{\mu^*}$, and

$$g_2(\nabla c) = \frac{\mathbb{C}}{2}|\nabla c|^2. \tag{3.4.35}$$

In conclusion, the incompressible-compressible version of the Navier-Stokes-Cahn-Hilliard system of equations in dimensionless form is given by

$$\dot{\rho} = -\rho \operatorname{div} \mathbf{u}, \tag{3.4.36}$$

$$\rho\dot{\mathbf{u}} = \operatorname{div} \mathbf{T}, \tag{3.4.37}$$

$$\rho\dot{c} = \operatorname{div}\left(\frac{1}{\mathbb{P}e}\nabla\left(\rho^{-1}\delta_c g\right)\right), \tag{3.4.38}$$

where

$$\rho^{-1} = \frac{c}{\rho_1} + \frac{(1-c)N_1\theta}{p} \tag{3.4.39}$$

$$\mathbf{T} = -\frac{1}{\mathbb{M}}\left(p\mathbf{I} + \mathbb{C}\rho\nabla c \otimes \nabla c\right) + \frac{2}{\mathbb{R}e}c\mathbf{D}, \tag{3.4.40}$$

$$\delta_c g = \rho g_c - \operatorname{div}\left(\rho g_{\nabla c}\right), \tag{3.4.41}$$

$$g(p, c, \nabla c) = \frac{c}{\rho_1}p + N_1\theta(1-c)\ln\frac{p}{p_0} \tag{3.4.42}$$

$$+(1-c)\left(\left(\frac{7}{2}N_1 - \sigma_0\right)(\theta - 1) + N_1\theta\ln\left(\frac{\theta_0}{\theta}\right)^{\frac{7}{2}}\right) \tag{3.4.43}$$

$$+bc^2(1-c)^2 + \frac{\mathbb{C}}{2}|\nabla c|^2, \tag{3.4.44}$$

together with the following boundary conditions:

$$\mathbf{u} = \mathbf{0} \quad \text{on } \partial\mathcal{B}_b, \tag{3.4.45}$$

$$\mathbf{u}\cdot\mathbf{n} = 0 \quad \text{on } \partial\mathcal{B}_l, \tag{3.4.46}$$

$$\mathbf{T}\mathbf{n}\cdot\boldsymbol{\tau} = 0 \quad \text{on } \partial\mathcal{B}_l, \tag{3.4.47}$$

$$\mathbf{T}\mathbf{n} = \mathbf{0} \quad \text{on } \partial\mathcal{B}_u, \tag{3.4.48}$$

$$\nabla c\cdot\mathbf{n} = 0 \quad \text{on } \partial\mathcal{B}, \tag{3.4.49}$$

$$\mathbf{j}\cdot\mathbf{n} = 0 \quad \text{on } \partial\mathcal{B}. \tag{3.4.50}$$

Chapter 4

Numerical methods for the Lowengrub-Truskinovsky system of equations.

Banach once told me, "Good mathematicians see analogies between theorems or theories, the very best ones see analogies between analogies."

Stanislaw Ulam

The system of equations (3.4.36)-(3.4.38) arising from the phase-field model proposed in the previous chapter is an incompressible-compressible version of Navier-Stokes-Cahn-Hilliard (NSCH) system. Several numerical discretisations of the NSCH system have been proposed in literature in the case of incompressible two-phase fluids (see, for example, [11, 21, 31, 51]), but, up to our knowledge, the numerical analysis related to the approximation of the incompressible-compressible case is missing.

Very recently (see [25] and [27]) numerical techniques have been developed for quasi-incompressible fluids. The notion of quasi-incompressibility was originally proposed by Joseph [30] and then was developed by Lowengrub-Truskinovsky [38]. Quasi-incompressibility means that two incompressible fluids can be mixed together and form a mixture whose velocity field fails to be solenoidal because of concentration gradients. Fluids in both phases are incompressible, but the mixing is compressible. The major difficulties in the numerical simulation of these systems are represented by the presence of the pressure in the chemical potential definition and by the velocity field that is no longer divergence-free. The key idea is to build a numerical scheme that, at the discrete level, preserves mass conservation and the energy dissipation law associated to the original system.

In this chapter, we propose a numerical discretisation of the Lowengrub-Truskinovsky (LT) system of equations in presence of gravity (see [27] and [38] for the derivation of the mathematical model). We will use a modified-midpoint temporal discretisation, similar to the one adopted in [27], but with a slightly different semi-discrete in time mixed formulation, and Discontinuous Galerkin finite elements for the spatial discretisation, in which the calculation of numerical fluxes has been inspired by [24] and [25]. This can be considered as a first step towards a numerical approximation of the metal foaming problem presented

in the previous chapter. In fact, the Lowengrub-Truskinovsky model has many similarities with the metal foaming model, but it has the advantage to be simpler. For example, as we will see in the following, there is no degenerate viscosity, the density is constant within each phase and the Gibbs free-energy does not include logarithmic terms.

In the sequel, after recalling some useful definitions about Sobolev spaces (Section 4.1), we will describe in details the equations of the LT model (Section 4.2) and prove, at the continuous level, mass conservation, momentum balance and an energy law. Section 4.3 will present a semi-discrete in space scheme conserving the mass and preserving the energy law, inspired by [24]. Section 4.4 will propose a semi-discrete in time scheme conserving the mass and preserving the energy law, that is a slight modification of the one adopted in [27]. Section 4.5 will propose a fully discrete numerical scheme for the LT model, based on the results proved in the previous sections. Numerical simulations have been carried out, in the case of conforming finite elements, using the software FreeFem++ [28], proving the good properties of mass conservation and energy law decreasing (see Section 4.6).

4.1 Sobolev spaces.

In this section we want to recall some definitions about Sobolev spaces. For further references, see [12], [45].

Let us consider a bounded domain $\Omega \subset \mathbb{R}^d$ and a time interval $(0,T)$. We suppose that the boundary $\partial\Omega$ is sufficiently smooth. The Sobolev space $W^{k,p}(\Omega)$, where k is a non-negative integer and $1 \leq p \leq \infty$ is defined by:

$$W^{k,p}(\Omega) := \{v \in L^p(\Omega) |\, D^{\boldsymbol{\alpha}} v \in L^p(\Omega) \text{ for } |\boldsymbol{\alpha}| \leq k\}, \tag{4.1.1}$$

where $\boldsymbol{\alpha} = (\alpha_1, ..., \alpha_d)$ is a multi-index, α_i are non-negative integers, $|\boldsymbol{\alpha}| = \alpha_1 + ... + \alpha_d$ is the length of $\boldsymbol{\alpha}$ and

$$D^{\boldsymbol{\alpha}} v := \frac{\partial^{|\boldsymbol{\alpha}|} v}{\partial x_1^{\alpha_1} ... \partial x_d^{\alpha_d}}.$$

For each p, $1 \leq p \leq \infty$, $W^{0,p}(\Omega) = L^p(\Omega)$ and $W^{k_2,p}(\Omega) \subset W^{k_1,p}(\Omega)$ when $k_1 \leq k_2$. For $1 \leq p < \infty$ it is a Banach space with respect to the norm

$$\|v\|_{k,p,\Omega} := \left(\sum_{|\boldsymbol{\alpha}| \leq k} \|D^{\boldsymbol{\alpha}} v\|^p_{L^p(\Omega)} \right)^{\frac{1}{p}}. \tag{4.1.2}$$

The seminorm is defined by

$$|v|_{k,p,\Omega} := \left(\sum_{|\boldsymbol{\alpha}| = k} \|D^{\boldsymbol{\alpha}} v\|^p_{L^p(\Omega)} \right)^{\frac{1}{p}}. \tag{4.1.3}$$

$W^{k,\infty}(\Omega)$ is a Banach space with respect to the norm

$$\|v\|_{k,\infty,\Omega} := \max_{|\boldsymbol{\alpha}| \leq k} \|D^{\boldsymbol{\alpha}} v\|_{L^\infty(\Omega)}, \tag{4.1.4}$$

while its seminorm is

$$|v|_{k,\infty,\Omega} := \max_{|\boldsymbol{\alpha}| = k} \|D^{\boldsymbol{\alpha}} v\|_{L^\infty(\Omega)}. \tag{4.1.5}$$

In particular, if $p = 2$, we set $H^k(\Omega) := W^{k,2}(\Omega)$, $\|\cdot\|_{k,\Omega} := \|\cdot\|_{k,2,\Omega}$ and $|\cdot|_{k,\Omega} := |\cdot|_{k,2,\Omega}$. We will also use, for vector-valued functions the space

$$H(\mathrm{div};\Omega) := \left\{ \mathbf{w} \in (L^2(\Omega))^d |\, \mathrm{div}\, \mathbf{w} \in L^2(\Omega) \right\} \tag{4.1.6}$$

with the norm

$$\|\mathbf{w}\|_{H(\mathrm{div};\Omega)} := \left(\|\mathbf{w}\|^2_{0,\Omega} + \|\mathrm{div}\, \mathbf{w}\|^2_{0,\Omega} \right)^{\frac{1}{2}}. \tag{4.1.7}$$

For space-time functions $v = v(x,t)$, $(x,t) \in \Omega \times (0,T)$, we can consider the space

$$\begin{aligned} L^q(0,T;W^{s,p}(\Omega)) \quad := \quad & \{v : (0,T) \to W^{s,p}(\Omega) |\, v \text{ is measurable and} \\ & \int_0^T \|v(t)\|^q_{s,p,\Omega}\, dt < \infty \Big\}, \end{aligned} \tag{4.1.8}$$

for $1 \leq q < \infty$ with the norm

$$\|v\|_{L^q(0,T;W^{s,p}(\Omega))} := \left(\int_0^T \|v(t)\|^q_{s,p,\Omega}\, dt \right)^{\frac{1}{q}}. \tag{4.1.9}$$

In a similar way we could define $L^\infty(0,T;W^{s,p}(\Omega))$. If the boundary of Ω is Lipschitz continuous we can also define

$$H^1_0(\Omega) := \left\{ v \in H^1(\Omega) : \gamma_0 v = 0 \right\} \text{ and } H^1_{\mathbf{n}}(\Omega) := \left\{ \mathbf{w} \in (H^1(\Omega))^d : \gamma^* \mathbf{w} = 0 \right\}, \tag{4.1.10}$$

where $\mathbf{n}$ is the outward pointing normal to $\partial\Omega$, $\gamma_0 v$ is the trace of the scalar function v on $\partial\Omega$ and $\gamma^* \mathbf{w}$ is the normal trace of the vector function $\mathbf{w}$ on $\partial\Omega$.

4.2 Quasi-incompressible Lowengrub-Truskinovsky model equations.

Here we will describe the mathematical model for quasi-incompressible isothermal binary fluids presented in [27], that is the Lowengrub-Truskinovsky model originally derived in [38] with the addition of gravity. We will rewrite the resulting system of equations, a Navier-Stokes-Cahn-Hilliard system (NSCH), in a suitable mixed form and we will derive the corresponding continuous energy dissipation law. The proof of the energy law and the structure of the mixed formulation will be useful in the construction of a discrete energy law preserving numerical scheme.

4.2.1 A quasi-incompressible model for binary fluids.

Let us consider, as order parameter, the concentration $c : \Omega \times (0,T) \to [0,1]$ of one fluid (e.g. fluid 1), where Ω is a bidimensional spatial domain: c is equal to 1 in the regions of Ω corresponding to fluid 1, is equal to 0 in the regions corresponding to fluid 2 and varies smoothly between 0 and 1 in the diffuse interfacial region. Let ρ_1 and ρ_2 be the densities of the two incompressible constituents ($\rho_1, \rho_2 > 0$). The total density $\rho(c)$ of the mixture is given by the relation

$$\frac{1}{\rho(c)} = \frac{1}{\rho_1} c + \frac{1}{\rho_2}(1-c). \tag{4.2.1}$$

The derivative $\partial\rho/\partial c$ satisfies the following identity

$$\frac{\partial \rho}{\partial c} = -\alpha \rho^2, \tag{4.2.2}$$

where the constant $\alpha = (\rho_2 - \rho_1)/(\rho_1\rho_2)$. Now, we are able to write the dimensionless NSCH system of equations for the Lowengrub-Truskinovsky (LT) model with the effects of gravity (see [27]):

$$\begin{aligned}
\rho \dot{c} &= \frac{1}{\mathbb{P}e} \Delta \mu, && (4.2.3)\\
\rho \dot{\mathbf{u}} &= -\frac{1}{\mathbb{M}} \left(\nabla p + \mathbb{C} \operatorname{div}(\rho \nabla c \otimes \nabla c) \right) + \frac{1}{\mathbb{R}e} \left(\Delta \mathbf{u} + \frac{1}{3} \nabla \operatorname{div} \mathbf{u} \right) \\
&\quad - \frac{1}{\mathbb{F}r^2} (\rho - \rho_0)\, \hat{\mathbf{j}}, && (4.2.4)\\
\operatorname{div} \mathbf{u} &= \frac{\alpha}{\mathbb{P}e} \Delta \mu, && (4.2.5)\\
\mu &= \mu_0(c) + \alpha\, p - \frac{\mathbb{C}}{\rho} \operatorname{div}(\rho \nabla c) - \frac{\mathbb{M}\, \rho_0\, \alpha}{\mathbb{F}r^2}\, y, && (4.2.6)
\end{aligned}$$

where $\mathbf{u} : \Omega \times (0,T) \to \mathbb{R}^2$ denotes the velocity of the mixture, $\dot{x} = x_t + (\mathbf{u} \cdot \nabla)x$ is the material derivative of a generic quantity x, $p : \Omega \times (0,T) \to \mathbb{R}$ is the pressure, $\mu : \Omega \times (0,T) \to \mathbb{R}$ is called (generalized) chemical potential, $\mu_0(c)$ is the derivative of $g_1(c)$, where

$$g_1(c) := \frac{1}{4} c^2 (c-1)^2 \tag{4.2.7}$$

is a double-well potential, ρ_0 is a reference density, $\hat{\mathbf{j}}$ is the vertical component of the unit vector (in a Cartesian coordinate system), y is the vertical coordinate. The Reynolds number $\mathbb{R}e$, the Froude number $\mathbb{F}r$, the Péclet number $\mathbb{P}e$, the Cahn number $\mathbb{C}$, the Mach number $\mathbb{M}$ are also used.

We can associate the following initial conditions

$$\mathbf{u}(x,0) = \mathbf{u}_0(x), \quad c(x,0) = c_0(x), \quad \text{for all } x \in \Omega \tag{4.2.8}$$

and the boundary conditions

$$\mathbf{u} = \mathbf{0}, \quad \nabla c \cdot \mathbf{n} = \nabla \mu \cdot \mathbf{n} = 0, \quad \text{on } \partial\Omega \times (0,T) \tag{4.2.9}$$

to the NSCH system (4.2.3)-(4.2.6).

4.2.2 Mass conservation.

If we multiply equation (4.2.3) by $\alpha\rho$ and equation (4.2.5) by ρ, and take the difference, we obtain

$$\alpha\rho^2\dot{c} - \rho \operatorname{div}\mathbf{u} = 0. \tag{4.2.10}$$

Using the relation (4.2.2), we obtain the local conservation of mass

$$\partial_t\rho + \operatorname{div}(\rho\mathbf{u}) = 0. \tag{4.2.11}$$

This fact means that local mass conservation is included in the model equations (4.2.3)-(4.2.6). From (4.2.11), using boundary conditions (4.2.9), we can prove the global conservation of mass (see [24]).

Theorem 4.2.1 (Conservation of mass). *If $(c, \mathbf{u}, p, \mu)$ is a strong solution of the system (4.2.3)-(4.2.6) which satisfies the boundary conditions (4.2.9), then*

$$\frac{d}{dt}\left(\int_\Omega \rho(c)\,dx\right) = 0. \tag{4.2.12}$$

Proof. Let us consider the local mass conservation equation (4.2.11) and integrate it over the domain Ω:

$$\int_\Omega \left(\partial_t\rho + \operatorname{div}(\rho\mathbf{u})\right)\,dx = 0. \tag{4.2.13}$$

But, due to the boundary conditions (4.2.9),

$$\int_\Omega \operatorname{div}(\rho\mathbf{u})\,dx = \int_{\partial\Omega} \rho\mathbf{u}\cdot\mathbf{n}\,ds = 0, \tag{4.2.14}$$

so equation (4.2.13) can be rewritten as

$$\int_\Omega \partial_t\rho\,dx = 0 \tag{4.2.15}$$

that yields the global mass conservation relation (4.2.12). □

4.2.3 Transformations on the momentum equation.

In this section three transformations on the pressure terms will be proposed in order to write the LT system in a mixed form suitable for the sequent numerical approximation. The first two pressure transformations have been also performed in [27], whereas the third one is the quasi-incompressible counterpart of the one proposed in [21] for the incompressible case.

A first pressure transformation. Let us consider the following tensor identity:

$$\operatorname{div}(\rho\nabla c\otimes\nabla c) = \operatorname{div}(\rho\nabla c)\nabla c + \frac{1}{2}\rho\nabla(|\nabla c|^2). \tag{4.2.16}$$

Similarly to what is done in [21] in the case of incompressible fluids, if we introduce the following pressure $\hat{p}$

$$\hat{p} := p + \frac{\mathbb{C}}{2}\rho|\nabla c|^2 \tag{4.2.17}$$

and observe that

$$p = \hat{p} - \frac{\mathbb{C}}{2}\,\rho\,|\nabla c|^2 \quad \text{and} \quad \nabla p = \nabla \hat{p} - \frac{\mathbb{C}}{2}\,\nabla\left(\rho\,|\nabla c|^2\right), \tag{4.2.18}$$

momentum equation (4.2.4), using the identity (4.2.16), can be rewritten in terms of $\hat{p}$:

$$\begin{aligned}\rho\dot{\mathbf{u}} &= -\frac{1}{\mathbb{M}}\left(\nabla\hat{p} - \frac{\mathbb{C}}{2}|\nabla c|^2\nabla\rho + \mathbb{C}\,\mathrm{div}\,(\rho\,\nabla c)\,\nabla c\right)\\ &\quad + \frac{1}{\mathbb{R}e}\left(\Delta\mathbf{u} + \frac{1}{3}\nabla\,\mathrm{div}\,\mathbf{u}\right) - \frac{1}{\mathbb{F}r^2}(\rho-\rho_0)\,\hat{\mathbf{j}}.\end{aligned} \tag{4.2.19}$$

The chemical potential equation (4.2.6) in terms of $\hat{p}$ is

$$\mu = \mu_0(c) + \alpha\left(\hat{p} - \frac{\mathbb{C}}{2}\rho\,|\nabla c|^2\right) - \frac{\mathbb{C}}{\rho}\,\mathrm{div}(\rho\,\nabla c) - \frac{\mathbb{M}\,\rho_0\,\alpha}{\mathbb{F}r^2}\,y. \tag{4.2.20}$$

A second pressure transformation. We can perform a second pressure transformation

$$\tilde{p} := \hat{p} + \rho g_1(c) = p + \frac{\mathbb{C}}{2}\,\rho\,|\nabla c|^2 + \rho g_1(c) \tag{4.2.21}$$

and note that

$$\hat{p} = \tilde{p} - \rho g_1(c) \quad \text{and} \quad \nabla\hat{p} = \nabla\tilde{p} - g_1(c)\nabla\rho - \rho\mu_0(c)\nabla c. \tag{4.2.22}$$

The chemical potential equation (4.2.6) in term of $\tilde{p}$ is

$$\mu = \mu_0(c) + \alpha\left(\tilde{p} - \rho g_1(c) - \frac{\mathbb{C}}{2}\rho\,|\nabla c|^2\right) - \frac{\mathbb{C}}{\rho}\,\mathrm{div}(\rho\,\nabla c) - \frac{\mathbb{M}\,\rho_0\,\alpha}{\mathbb{F}r^2}\,y. \tag{4.2.23}$$

If we multiply each term in (4.2.23) by $\rho\,\nabla c$, we obtain that

$$\begin{aligned}\mathbb{C}\,\mathrm{div}(\rho\,\nabla c)\nabla c &= -\rho\mu\nabla c + \rho\mu_0(c)\nabla c + (\alpha\rho)\;\tilde{p}\,\nabla c - \left(\alpha\rho^2\right) g_1(c)\nabla c\\ &\quad - \left(\alpha\rho^2\right)\frac{\mathbb{C}}{2}|\nabla c|^2\nabla c - \frac{\mathbb{M}\,\rho_0\,\alpha}{\mathbb{F}r^2}\,\rho y\nabla c.\end{aligned} \tag{4.2.24}$$

Using (4.2.22) and (4.2.24) into (4.2.19), and the fact that

$$\nabla\rho = \frac{\partial\rho}{\partial c}\nabla c = -\alpha\rho^2\nabla c, \tag{4.2.25}$$

we obtain

$$\begin{aligned}\rho\dot{\mathbf{u}} &= -\frac{1}{\mathbb{M}}\left(\nabla\tilde{p} + (\alpha\rho)\;\tilde{p}\,\nabla c - \rho\mu\nabla c\right) + \frac{1}{\mathbb{R}e}\left(\Delta\mathbf{u} + \frac{1}{3}\nabla\,\mathrm{div}\,\mathbf{u}\right)\\ &\quad - \frac{\rho_0}{\mathbb{F}r^2\rho}\,y\nabla\rho - \frac{1}{\mathbb{F}r^2}(\rho-\rho_0)\,\hat{\mathbf{j}}.\end{aligned} \tag{4.2.26}$$

Relations (4.2.2) and (4.2.25) can be used to verify the following identities:

$$\nabla\tilde{p} + (\alpha\rho)\;\tilde{p}\,\nabla c = \nabla\tilde{p} - \nabla\rho\frac{\tilde{p}}{\rho} \tag{4.2.27}$$

and

$$\nabla\left(\rho\,\frac{\tilde{p}}{\rho}\right) = \nabla\tilde{p} = \nabla\rho\,\frac{\tilde{p}}{\rho} + \rho\nabla\left(\frac{\tilde{p}}{\rho}\right). \tag{4.2.28}$$

From these identities we can deduce that

$$\nabla\tilde{p} + (\alpha\rho)\;\tilde{p}\,\nabla c = \rho\nabla\left(\frac{\tilde{p}}{\rho}\right). \tag{4.2.29}$$

Using (4.2.29), equation (4.2.26) can be rewritten as

$$\begin{aligned}\rho\dot{\mathbf{u}} &= -\frac{1}{\mathbb{M}}\left(\rho\nabla\left(\frac{\tilde{p}}{\rho}\right) - \rho\mu\nabla c\right) + \frac{1}{\mathbb{R}e}\left(\Delta\mathbf{u} + \frac{1}{3}\nabla\,\mathrm{div}\,\mathbf{u}\right)\\ &\quad - \frac{\rho_0}{\mathbb{F}r^2\rho}\,y\nabla\rho - \frac{1}{\mathbb{F}r^2}(\rho-\rho_0)\,\hat{\mathbf{j}}.\end{aligned} \tag{4.2.30}$$

A third pressure transformation. Equation (4.2.30) is in the form used in the paper [27]. As remarked at the beginning of this section, we propose another pressure transformation, similar to what is done by [21] in the incompressible case, in which the gradient of the chemical potential μ enters the momentum equation (4.2.30).
Let us consider this third pressure transformation:

$$\bar{p} := \frac{\tilde{p}}{\rho} - \mu c = \frac{p}{\rho} + \frac{\mathbb{C}}{2}|\nabla c|^2 + g_1(c) - \mu c. \tag{4.2.31}$$

From this relation we can deduce that

$$\tilde{p} = \rho\,\bar{p} + \rho\mu c \quad \text{and} \quad \nabla\left(\frac{\tilde{p}}{\rho}\right) = \nabla\bar{p} + \mu\nabla c + c\nabla\mu. \tag{4.2.32}$$

Using (4.2.32) into (4.2.30) we obtain

$$\begin{aligned}\rho\dot{\mathbf{u}} \;=\; & -\frac{1}{\mathbb{M}}\left(\rho\nabla\bar{p} + \rho c\nabla\mu\right) + \frac{1}{\mathbb{R}e}\left(\Delta\mathbf{u} + \frac{1}{3}\nabla\,\mathrm{div}\,\mathbf{u}\right)\\ & -\frac{\rho_0}{\mathbb{F}r^2\rho}\,y\nabla\rho - \frac{1}{\mathbb{F}r^2}(\rho-\rho_0)\,\hat{\mathbf{j}}.\end{aligned} \tag{4.2.33}$$

The chemical potential equation in terms of $\bar{p}$ is

$$\left(\rho + \frac{\partial\rho}{\partial c}c\right)\mu = \rho\mu_0(c) - \frac{\partial\rho}{\partial c}\left(\bar{p} - g_1(c) - \frac{\mathbb{C}}{2}|\nabla c|^2\right) - \mathbb{C}\,\mathrm{div}(\rho\,\nabla c) - \frac{\mathbb{M}\,\rho_0\,\alpha}{\mathbb{F}r^2}\,\rho y. \tag{4.2.34}$$

4.2.4 Continuous mixed formulation.

We now introduce a mixed formulation of the NSCH system of equations for the Lowengrub-Truskinovsky model (4.2.3)-(4.2.6) taking into account the mass conservation property in Section 4.2.2 and pressure transformations in Section 4.2.3. The strong problem reads as follows. Find $(c, \mathbf{u}, \bar{p}, \mu, \mathbf{q})$ such that

$$0 = \rho\,\partial_t c + \rho(\mathbf{u}\cdot\nabla)c - \frac{1}{\mathbb{P}e}\Delta\mu, \tag{4.2.35}$$

$$\begin{aligned}\mathbf{0} = \; & \sqrt{\rho}\,\partial_t\left(\sqrt{\rho}\mathbf{u}\right) + \rho(\mathbf{u}\cdot\nabla)\mathbf{u} + \frac{1}{2}\,\mathrm{div}(\rho\mathbf{u})\mathbf{u} + \frac{1}{\mathbb{M}}\rho\,\nabla\bar{p} + \frac{1}{\mathbb{M}}\rho c\,\nabla\mu\\ & + \frac{\rho_0}{\mathbb{F}r^2\rho}\,y\nabla\rho + \frac{1}{\mathbb{F}r^2}(\rho-\rho_0)\,\hat{\mathbf{j}} - \frac{1}{\mathbb{R}e}\left(\Delta\mathbf{u} + \frac{1}{3}\nabla\,\mathrm{div}\,\mathbf{u}\right),\end{aligned} \tag{4.2.36}$$

$$0 = \partial_t\rho + \mathrm{div}(\rho\mathbf{u}), \tag{4.2.37}$$

$$\begin{aligned}0 = \; & \left(\rho + \frac{\partial\rho}{\partial c}c\right)\mu - \rho\mu_0(c) + \frac{\partial\rho}{\partial c}\left(\bar{p} - g_1(c) - \frac{\mathbb{C}}{2}|\mathbf{q}|^2\right)\\ & + \mathbb{C}\,\mathrm{div}(\,\rho\,\mathbf{q}\,) + \frac{\mathbb{M}\,\rho_0\,\alpha}{\mathbb{F}r^2}\,\rho y,\end{aligned} \tag{4.2.38}$$

$$\mathbf{0} = \mathbf{q} - \nabla c, \tag{4.2.39}$$

with the following initial and boundary conditions, consistent with (4.2.8) and (4.2.9):

$$\mathbf{u}(x,0) = \mathbf{u}_0(x), \quad c(x,0) = c_0(x), \quad \text{for all } x\in\Omega, \tag{4.2.40}$$

$$\mathbf{u} = \mathbf{0}, \quad \mathbf{q}\cdot\mathbf{n} = \nabla\mu\cdot\mathbf{n} = 0, \quad \text{on } \partial\Omega\times(0,T). \tag{4.2.41}$$

Notice that we have introduced a new variable, $\mathbf{q}$, defined in (4.2.39). Equation (4.2.37) is the local mass conservation equation that arises from the combination of (4.2.3) and (4.2.5) (see Section 4.2.2).
We remark that equation (4.2.36) is a modified version of the momentum equation (4.2.33). In fact, let us multiply the local mass conservation equation (4.2.37) by $\mathbf{u}/2$:

$$\frac{1}{2}(\partial_t\rho)\mathbf{u} + \frac{1}{2}\,\mathrm{div}(\rho\mathbf{u})\mathbf{u} = 0. \tag{4.2.42}$$

Adding this equation to (4.2.33), we obtain equation (4.2.36). This new form of the momentum equation will be very useful in the next sections in deriving a numerical scheme preserving a discrete energy dissipation law.

4.2.5 Momentum balance.

Let us prove a momentum balance for the NSCH system of equations (4.2.35)-(4.2.39). The proof has been inspired by the proof proposed in [24] for a Navier-Stokes-Korteweg system.

Theorem 4.2.2 (Momentum balance). *If $(c, \mathbf{u}, \bar{p}, \mu, \mathbf{q})$ is a strong solution of the NSCH system of equations (4.2.35)-(4.2.39), together with boundary conditions (4.2.41), then*

$$\begin{aligned}\frac{d}{dt}\left(\int_\Omega \rho(c)\mathbf{u}\,dx\right) &= -\int_\Omega \frac{1}{\mathbb{F}r^2}(\rho-\rho_0)\hat{\mathbf{j}}\,dx \\ &\quad -\int_{\partial\Omega}\frac{\rho(c)}{\mathbb{M}}(\bar{p}+c\mu-g_1(c))\mathbf{n}\,ds+\int_{\partial\Omega}\frac{1}{\mathbb{R}e}\left(\nabla\mathbf{u}+\frac{1}{3}(\operatorname{div}\mathbf{u})\mathbb{I}\right)\mathbf{n}\,ds.\end{aligned} \tag{4.2.43}$$

Proof. Let $\mathbf{e}_i$ be the $i-$th coordinate vector in $\mathbb{R}^d$. Then

$$\frac{d}{dt}\left(\int_\Omega \rho(c)\mathbf{u}\cdot\mathbf{e}_i\,dx\right)=\int_\Omega\left((\partial_t\rho)\mathbf{u}\cdot\mathbf{e}_i+\rho(\partial_t\mathbf{u})\cdot\mathbf{e}_i\right)dx. \tag{4.2.44}$$

From (4.2.36) multiplied by $\mathbf{e}_i$, it is simple to check that

$$\begin{aligned}\sqrt{\rho}\,\partial_t(\sqrt{\rho}\mathbf{u})\cdot\mathbf{e}_i &= \frac{1}{2}(\partial_t\rho)\mathbf{u}\cdot\mathbf{e}_i+\rho(\partial_t\mathbf{u})\cdot\mathbf{e}_i \\ &= -\rho(\mathbf{u}\cdot\nabla)\mathbf{u}\cdot\mathbf{e}_i-\frac{1}{2}\operatorname{div}(\rho\mathbf{u})\mathbf{u}\cdot\mathbf{e}_i-\frac{1}{\mathbb{M}}\rho\nabla\bar{p}\cdot\mathbf{e}_i \\ &\quad -\frac{1}{\mathbb{M}}\rho c\nabla\mu\cdot\mathbf{e}_i-\frac{\rho_0 y}{\mathbb{F}r^2\rho}\nabla\rho\cdot\mathbf{e}_i-\frac{1}{\mathbb{F}r^2}(\rho-\rho_0)\hat{\mathbf{j}}\cdot\mathbf{e}_i \\ &\quad +\frac{1}{\mathbb{R}e}\left(\Delta\mathbf{u}+\frac{1}{3}\nabla\operatorname{div}\mathbf{u}\right)\cdot\mathbf{e}_i.\end{aligned} \tag{4.2.45}$$

If we multiply each term in (4.2.37) by $\dfrac{\mathbf{u}\cdot\mathbf{e}_i}{2}$, we have that

$$\frac{1}{2}(\partial_t\rho)\mathbf{u}\cdot\mathbf{e}_i=-\frac{1}{2}\operatorname{div}(\rho\mathbf{u})\,\mathbf{u}\cdot\mathbf{e}_i. \tag{4.2.46}$$

Using (4.2.45) and (4.2.46) into (4.2.44), we obtain

$$\begin{aligned}\frac{d}{dt}\left(\int_\Omega\rho(c)\mathbf{u}\cdot\mathbf{e}_i\,dx\right) &= \int_\Omega\Big(-\rho(\mathbf{u}\cdot\nabla)\mathbf{u}\cdot\mathbf{e}_i-\operatorname{div}(\rho\mathbf{u})\mathbf{u}\cdot\mathbf{e}_i \\ &\quad -\frac{1}{\mathbb{M}}\rho\nabla\bar{p}\cdot\mathbf{e}_i-\frac{1}{\mathbb{M}}\rho c\nabla\mu\cdot\mathbf{e}_i-\frac{\rho_0 y}{\mathbb{F}r^2\rho}\nabla\rho\cdot\mathbf{e}_i \\ &\quad -\frac{1}{\mathbb{F}r^2}(\rho-\rho_0)\hat{\mathbf{j}}\cdot\mathbf{e}_i+\frac{1}{\mathbb{R}e}\left(\Delta\mathbf{u}+\frac{1}{3}\nabla\operatorname{div}\mathbf{u}\right)\cdot\mathbf{e}_i\Big)\,dx.\end{aligned} \tag{4.2.47}$$

Since

$$\int_\Omega\left(\rho(\mathbf{u}\cdot\nabla)\mathbf{u}\cdot\mathbf{e}_i+\operatorname{div}(\rho\mathbf{u})\,\mathbf{u}\cdot\mathbf{e}_i\right)dx=0, \tag{4.2.48}$$

then we can rewrite (4.2.47) as

$$\begin{aligned}\frac{d}{dt}\left(\int_\Omega \rho(c)\mathbf{u}\cdot\mathbf{e}_i\,dx\right) &= \int_\Omega \left(-\frac{1}{\mathbb{M}}\rho\nabla\bar{p}\cdot\mathbf{e}_i - \frac{1}{\mathbb{M}}\rho c\nabla\mu\cdot\mathbf{e}_i - \frac{\rho_0 y}{\mathbb{F}r^2\rho}\nabla\rho\cdot\mathbf{e}_i\right.\\ &\left. -\frac{1}{\mathbb{F}r^2}(\rho-\rho_0)\hat{\mathbf{j}}\cdot\mathbf{e}_i + \frac{1}{\mathbb{R}e}\left(\Delta\mathbf{u}+\frac{1}{3}\nabla\operatorname{div}\mathbf{u}\right)\cdot\mathbf{e}_i\right)dx.\end{aligned} \tag{4.2.49}$$

Integration by parts of the first two terms in the right-hand side, leads to:

$$\begin{aligned}\frac{d}{dt}\left(\int_\Omega \rho(c)\mathbf{u}\cdot\mathbf{e}_i\,dx\right) &= \int_\Omega \left(\frac{1}{\mathbb{M}}\bar{p}\nabla\rho\cdot\mathbf{e}_i + \frac{1}{\mathbb{M}}\mu\nabla(\rho c)\cdot\mathbf{e}_i - \frac{\rho_0 y}{\mathbb{F}r^2\rho}\nabla\rho\cdot\mathbf{e}_i\right.\\ &\left. -\frac{1}{\mathbb{F}r^2}(\rho-\rho_0)\hat{\mathbf{j}}\cdot\mathbf{e}_i + \frac{1}{\mathbb{R}e}\left(\Delta\mathbf{u}+\frac{1}{3}\nabla\operatorname{div}\mathbf{u}\right)\cdot\mathbf{e}_i\right)dx.\\ &+\int_{\partial\Omega} -\frac{1}{\mathbb{M}}\rho(\bar{p}+c\mu)n_i\,ds,\end{aligned} \tag{4.2.50}$$

where n_i is the i-th component of $\boldsymbol{n}$. If we notice that

$$\begin{aligned}\frac{1}{\mathbb{M}}\mu\nabla(\rho c)\cdot\mathbf{e}_i &= \frac{1}{\mathbb{M}}\mu(c\nabla\rho+\rho\nabla c)\cdot\mathbf{e}_i\\ &= \frac{1}{\mathbb{M}}\mu\left(\frac{\partial\rho}{\partial c}c+\rho\right)\nabla c\cdot\mathbf{e}_i,\end{aligned} \tag{4.2.51}$$

then (4.2.50), using also (4.2.38), can be rewritten as

$$\begin{aligned}\frac{d}{dt}\left(\int_\Omega \rho(c)\mathbf{u}\cdot\mathbf{e}_i\,dx\right) &= \int_\Omega \left(\frac{1}{\mathbb{M}}\rho\mu_0(c)\nabla c\cdot\mathbf{e}_i + \frac{1}{\mathbb{M}}\frac{\partial\rho}{\partial c}g_1(c)\nabla c\cdot\mathbf{e}_i\right.\\ &\quad + \frac{\mathbb{C}}{2\mathbb{M}}\frac{\partial\rho}{\partial c}|\mathbf{q}|^2\nabla c\cdot\mathbf{e}_i - \frac{\mathbb{C}}{\mathbb{M}}\operatorname{div}(\rho\mathbf{q})\nabla c\cdot\mathbf{e}_i\\ &\quad \left. -\frac{1}{\mathbb{F}r^2}(\rho-\rho_0)\hat{\mathbf{j}}\cdot\mathbf{e}_i + \frac{1}{\mathbb{R}e}\left(\Delta\mathbf{u}+\frac{1}{3}\nabla\operatorname{div}\mathbf{u}\right)\cdot\mathbf{e}_i\right)dx\\ &+\int_{\partial\Omega} -\frac{1}{\mathbb{M}}\rho(\bar{p}+c\mu)n_i\,ds,\end{aligned} \tag{4.2.52}$$

where we have used the fact that

$$-\frac{\rho_0 y}{\mathbb{F}r^2\rho}\nabla\rho = \frac{\rho_0\alpha}{\mathbb{F}r^2}\rho y\nabla c. \tag{4.2.53}$$

The fact that

$$\begin{aligned}&\int_\Omega \frac{1}{\mathbb{M}}\left(\rho\mu_0(c)\nabla c\cdot\mathbf{e}_i + \frac{\partial\rho}{\partial c}g_1(c)\nabla c\cdot\mathbf{e}_i\right)dx\\ =\ &\int_\Omega \frac{1}{\mathbb{M}}\left(\rho\mu_0(c)\nabla c\cdot\mathbf{e}_i + g_1(c)\nabla\rho\cdot\mathbf{e}_i\right)dx\\ =\ &\int_{\partial\Omega}\frac{1}{\mathbb{M}}\rho g_1(c)\,n_i\,ds\end{aligned} \tag{4.2.54}$$

and

$$\begin{aligned}
&\int_\Omega \left(\frac{\mathbb{C}}{2\mathbb{M}} \frac{\partial \rho}{\partial c} |\mathbf{q}|^2 \nabla c \cdot \mathbf{e}_i - \frac{\mathbb{C}}{\mathbb{M}} \operatorname{div}(\rho \mathbf{q}) \nabla c \cdot \mathbf{e}_i \right) dx \\
= &\int_\Omega \left(\frac{\mathbb{C}}{2\mathbb{M}} |\mathbf{q}|^2 \nabla \rho \cdot \mathbf{e}_i - \frac{\mathbb{C}}{\mathbb{M}} \operatorname{div}(\rho \mathbf{q}) \mathbf{q} \cdot \mathbf{e}_i \right) dx \\
= &\int_\Omega \left(-\frac{\mathbb{C}}{2\mathbb{M}} \rho \operatorname{div}(|\mathbf{q}|^2 \mathbf{e}_i) - \frac{\mathbb{C}}{\mathbb{M}} \operatorname{div}(\rho \mathbf{q}) \mathbf{q} \cdot \mathbf{e}_i \right) dx \\
= &\int_\Omega \left(-\frac{\mathbb{C}}{2\mathbb{M}} \rho \nabla(|\mathbf{q}|^2) \cdot \mathbf{e}_i - \frac{\mathbb{C}}{\mathbb{M}} \operatorname{div}(\rho \mathbf{q}) \mathbf{q} \cdot \mathbf{e}_i \right) dx \\
= &\int_\Omega \left(-\frac{\mathbb{C}}{\mathbb{M}} \operatorname{div}(\rho \mathbf{q} \otimes \mathbf{q}) \cdot \mathbf{e}_i \right) dx = 0 \qquad (4.2.55)
\end{aligned}$$

into (4.2.52) leads to (4.2.43). □

4.2.6 Continuous energy dissipation law.

Now let us derive the continuous energy dissipation law for the NSCH system of equations of the Lowengrub-Truskinovsky model. The derivation will be consistent with the mixed formulation (4.2.35)-(4.2.39) given in Section 4.2.4. In the sequel, for simplicity of notation, $\rho := \rho(c)$. A proof of the energy law for the LT system has been proposed in [27]. However, we will reorganise the proof (following a scheme that is similar to the one proposed in [25]) in such a way it will be useful in proving the semi-discrete in space and time energy laws.

The total energy associated to the system (4.2.35)-(4.2.39) is given by:

$$E := E_{kin} + E_{free} + E_g = \int_\Omega \left(\frac{1}{2} \rho |\mathbf{u}|^2 + \frac{1}{\mathbb{M}} \rho\, g_1(c) + \frac{\mathbb{C}}{2\,\mathbb{M}} \rho |\mathbf{q}|^2 + \frac{1}{\mathbb{F}r^2} \rho y \right) dx, \quad (4.2.56)$$

where

$$E_{kin} := \int_\Omega \frac{1}{2} \rho |\mathbf{u}|^2 \, dx \qquad (4.2.57)$$

denotes the kinetic energy of the mixture,

$$E_{free} := \int_\Omega \left(\frac{1}{\mathbb{M}} \rho\, g_1(c) + \frac{\mathbb{C}}{2\,\mathbb{M}} \rho |\mathbf{q}|^2 \right) dx \qquad (4.2.58)$$

is the Cahn-Hilliard free energy, while

$$E_g := \int_\Omega \frac{1}{\mathbb{F}r^2} \rho\, y \, dx \qquad (4.2.59)$$

is the gravitational potential energy.

Now, let us suppose that ρ is a nonnegative function with

$$\rho \in L^\infty(0,T; L^\infty(\Omega));$$

we will also consider

$$g_1(c) \in L^1(0,T; L^1(\Omega)) \quad \text{and} \quad \mu_0(c) \in L^2(0,T; L^2(\Omega)).$$

Theorem 4.2.3 (Continuous energy dissipation law). *Let* $(c, \mathbf{u}, \bar{p}, \mu, \mathbf{q}) \in L^2(0,T; H^1(\Omega)) \times L^2(0,T; (H^2(\Omega) \cap H_0^1(\Omega))^2) \times L^2(0,T; H^1(\Omega)) \times L^2(0,T; H^2(\Omega)) \times L^2(0,T; H^1_{\mathbf{n}}(\Omega))$ *be a strong solution of the system (4.2.35)-(4.2.39), such that* $(\partial_t c, \partial_t \mathbf{u}) \in L^2(0,T; L^2(\Omega)) \times$

$L^2(0,T;(L^2(\Omega))^2)$. *Then*

$$\begin{aligned}\frac{dE}{dt} &= \frac{d}{dt}\left(\int_\Omega \left(\frac{\rho(c)}{2}|\mathbf{u}|^2 + \frac{\rho(c)}{\mathbb{M}}g_1(c) + \frac{\mathbb{C}}{2\,\mathbb{M}}\rho(c)|\mathbf{q}|^2 + \frac{1}{\mathbb{F}r^2}\rho(c)y\right)dx\right)\\ &= -\frac{1}{\mathbb{P}e\mathbb{M}}\int_\Omega |\nabla\mu|^2\,dx - \frac{1}{\mathbb{R}e}\int_\Omega\left(|\nabla\mathbf{u}|^2 + \frac{1}{3}|\operatorname{div}\mathbf{u}|^2\right)dx. \qquad (4.2.60)\end{aligned}$$

Proof. Let us test (4.2.35) by $\frac{\mu}{\mathbb{M}}$ and (4.2.36) by $\mathbf{u}$ and sum them together:

$$\begin{aligned}0 &= \int_\Omega\Big(\frac{1}{\mathbb{M}}\rho\mu(\partial_t c) + \frac{\mu}{\mathbb{M}}\rho(\mathbf{u}\cdot\nabla)c - \frac{1}{\mathbb{P}e\mathbb{M}}\mu\Delta\mu + \sqrt{\rho}\,\partial_t(\sqrt{\rho}\mathbf{u})\cdot\mathbf{u} + \rho(\mathbf{u}\cdot\nabla)\mathbf{u}\cdot\mathbf{u}\\ &\quad + \frac{1}{2}\operatorname{div}(\rho\mathbf{u})\mathbf{u}\cdot\mathbf{u} + \frac{1}{\mathbb{M}}\rho\nabla\bar{p}\cdot\mathbf{u} + \frac{1}{\mathbb{M}}\rho c\nabla\mu\cdot\mathbf{u}\\ &\quad + \frac{\rho_0}{\mathbb{F}r^2\rho}y\nabla\rho\cdot\mathbf{u} + \frac{1}{\mathbb{F}r^2}(\rho-\rho_0)\hat{\mathbf{j}}\cdot\mathbf{u}\\ &\quad - \frac{1}{\mathbb{R}e}\left(\Delta\mathbf{u}\cdot\mathbf{u} + \frac{1}{3}\nabla\operatorname{div}\mathbf{u}\cdot\mathbf{u}\right)\Big)\,dx. \qquad (4.2.61)\end{aligned}$$

Integration by parts of the terms containing, respectively, $\nabla\bar{p}$ and $\Delta\mu$, and of the viscous terms leads to

$$\begin{aligned}0 &= \int_\Omega\Big(\frac{1}{\mathbb{M}}\rho\mu(\partial_t c) + \frac{\mu}{\mathbb{M}}\rho(\mathbf{u}\cdot\nabla)c + \sqrt{\rho}\,\partial_t(\sqrt{\rho}\mathbf{u})\cdot\mathbf{u} + \rho(\mathbf{u}\cdot\nabla)\mathbf{u}\cdot\mathbf{u}\\ &\quad + \frac{1}{2}\operatorname{div}(\rho\mathbf{u})\mathbf{u}\cdot\mathbf{u} - \frac{1}{\mathbb{M}}\bar{p}\operatorname{div}(\rho\mathbf{u}) + \frac{1}{\mathbb{M}}\rho c\nabla\mu\cdot\mathbf{u}\\ &\quad + \frac{\rho_0}{\mathbb{F}r^2\rho}y\nabla\rho\cdot\mathbf{u} + \frac{1}{\mathbb{F}r^2}(\rho-\rho_0)\hat{\mathbf{j}}\cdot\mathbf{u}\\ &\quad + \frac{1}{\mathbb{P}e\mathbb{M}}|\nabla\mu|^2 + \frac{1}{\mathbb{R}e}\left(|\nabla\mathbf{u}|^2 + \frac{1}{3}|\operatorname{div}\mathbf{u}|^2\right)\Big)\,dx, \qquad (4.2.62)\end{aligned}$$

where we have used boundary conditions (4.2.41). Using local mass conservation equation (4.2.37) into (4.2.62), we obtain:

$$\begin{aligned}0 &= \int_\Omega\Big(\frac{1}{\mathbb{M}}\rho\mu(\partial_t c) + \frac{\mu}{\mathbb{M}}\rho(\mathbf{u}\cdot\nabla)c + \sqrt{\rho}\,\partial_t(\sqrt{\rho}\mathbf{u})\cdot\mathbf{u} + \frac{\bar{p}}{\mathbb{M}}(\partial_t\rho) + \frac{1}{\mathbb{M}}\rho c\nabla\mu\cdot\mathbf{u}\\ &\quad + \rho(\mathbf{u}\cdot\nabla)\mathbf{u}\cdot\mathbf{u} + \frac{1}{2}\operatorname{div}(\rho\mathbf{u})\mathbf{u}\cdot\mathbf{u} + \frac{\rho_0}{\mathbb{F}r^2\rho}y\nabla\rho\cdot\mathbf{u} + \frac{1}{\mathbb{F}r^2}(\rho-\rho_0)\hat{\mathbf{j}}\cdot\mathbf{u}\\ &\quad + \frac{1}{\mathbb{P}e\mathbb{M}}|\nabla\mu|^2 + \frac{1}{\mathbb{R}e}\left(|\nabla\mathbf{u}|^2 + \frac{1}{3}|\operatorname{div}\mathbf{u}|^2\right)\Big)\,dx. \qquad (4.2.63)\end{aligned}$$

If we notice that

$$\int_\Omega\left(\rho(\mathbf{u}\cdot\nabla)\mathbf{u}\cdot\mathbf{u} + \frac{1}{2}\operatorname{div}(\rho\mathbf{u})\mathbf{u}\cdot\mathbf{u}\right)dx = 0 \qquad (4.2.64)$$

and if we use the definition of $\rho\mu$ from (4.2.38), we can rewrite (4.2.63) as

$$\begin{aligned}0 &= \int_\Omega\Big(\sqrt{\rho}\,\partial_t(\sqrt{\rho}\mathbf{u})\cdot\mathbf{u} + \frac{1}{\mathbb{M}}\rho\mu_0(c)(\partial_t c) + \frac{1}{\mathbb{M}}g_1(c)(\partial_t\rho)\\ &\quad + \frac{\mathbb{C}}{2\,\mathbb{M}}|\mathbf{q}|^2(\partial_t\rho) - \frac{\mathbb{C}}{\mathbb{M}}\operatorname{div}(\rho\mathbf{q})(\partial_t c)\\ &\quad + \frac{\rho_0}{\mathbb{F}r^2\rho}y(\partial_t\rho) + \frac{\rho_0}{\mathbb{F}r^2\rho}y\nabla\rho\cdot\mathbf{u} + \frac{1}{\mathbb{F}r^2}(\rho-\rho_0)\hat{\mathbf{j}}\cdot\mathbf{u}\\ &\quad - \frac{1}{\mathbb{M}}c\mu(\partial_t\rho) + \frac{\mu}{\mathbb{M}}\rho(\mathbf{u}\cdot\nabla)c + \frac{1}{\mathbb{M}}\rho c\nabla\mu\cdot\mathbf{u}\\ &\quad + \frac{1}{\mathbb{P}e\mathbb{M}}|\nabla\mu|^2 + \frac{1}{\mathbb{R}e}\left(|\nabla\mathbf{u}|^2 + \frac{1}{3}|\operatorname{div}\mathbf{u}|^2\right)\Big)\,dx. \qquad (4.2.65)\end{aligned}$$

We get the following relations:

(I) the first term in (4.2.65) is

$$\int_\Omega \sqrt{\rho}\,\partial_t(\sqrt{\rho}\mathbf{u})\cdot\mathbf{u}\,dx = \int_\Omega \partial_t\left(\frac{\rho(c)}{2}|\mathbf{u}|^2\right)dx, \tag{4.2.66}$$

(II) the terms containing the double-well potential $g_1(c)$ and its derivative $\mu_0(c)$ are

$$\int_\Omega \left(\frac{1}{\mathbb{M}}\rho\mu_0(c)(\partial_t c) + \frac{1}{\mathbb{M}}g_1(c)(\partial_t\rho)\right)dx = \int_\Omega \partial_t\left(\frac{\rho(c)}{\mathbb{M}}g_1(c)\right)dx, \tag{4.2.67}$$

(III) integrating by parts and remembering boundary conditions (4.2.41), the terms containing the variable $\mathbf{q}$ are equal to

$$\begin{aligned}&\int_\Omega \left(\frac{\mathbb{C}}{2\,\mathbb{M}}|\mathbf{q}|^2(\partial_t\rho) - \frac{\mathbb{C}}{\mathbb{M}}\,\mathrm{div}(\rho\mathbf{q})(\partial_t c)\right)dx \quad = \\ &= \int_\Omega \left(\frac{\mathbb{C}}{2\,\mathbb{M}}|\mathbf{q}|^2(\partial_t\rho) + \frac{\mathbb{C}}{\mathbb{M}}\,(\rho\mathbf{q})\cdot(\partial_t\mathbf{q})\right)dx \quad = \quad \int_\Omega \partial_t\left(\frac{\mathbb{C}}{2\,\mathbb{M}}\rho|\mathbf{q}|^2\right)dx,\end{aligned} \tag{4.2.68}$$

(IV) integrating by parts, using boundary conditions (4.2.41), the definition of $\hat{\mathbf{j}}$ and local mass conservation (4.2.37), gravity terms can be rewritten as

$$\begin{aligned}&\int_\Omega \left(\frac{\rho_0}{\mathbb{F}r^2\rho}y(\partial_t\rho) + \frac{\rho_0}{\mathbb{F}r^2\rho}y\nabla\rho\cdot\mathbf{u} + \frac{1}{\mathbb{F}r^2}(\rho-\rho_0)\,\hat{\mathbf{j}}\cdot\mathbf{u}\right)dx = \\ &= \int_\Omega \left(\frac{\rho_0}{\mathbb{F}r^2\rho}y(\partial_t\rho) + \frac{\rho_0}{\mathbb{F}r^2\rho}y\nabla\rho\cdot\mathbf{u} - \frac{1}{\mathbb{F}r^2}y\,\mathrm{div}(\rho\mathbf{u}) + \frac{\rho_0 y}{\mathbb{F}r^2}\,\mathrm{div}\,\mathbf{u}\right)dx = \\ &= \int_\Omega \left(\frac{\rho_0}{\mathbb{F}r^2\rho}\,(\partial_t\rho + \nabla\rho\cdot\mathbf{u} + \rho\,\mathrm{div}\,\mathbf{u})\,y + \frac{1}{\mathbb{F}r^2}(\partial_t\rho)y\right)dx = \\ &= \int_\Omega \partial_t\left(\frac{1}{\mathbb{F}r^2}\rho y\right)dx,\end{aligned} \tag{4.2.69}$$

(V) using integration by parts, boundary conditions (4.2.41) and local mass conservation (4.2.37),

$$\begin{aligned}&\int_\Omega \left(-\frac{1}{\mathbb{M}}c\mu(\partial_t\rho) + \frac{\mu}{\mathbb{M}}\rho(\mathbf{u}\cdot\nabla)c + \frac{1}{\mathbb{M}}\rho c\nabla\mu\cdot\mathbf{u}\right)dx = \\ &= \int_\Omega \left(-\frac{1}{\mathbb{M}}c\mu(\partial_t\rho) + \frac{1}{\mathbb{M}}(\rho\mathbf{u})\cdot(\mu\nabla c + c\nabla\mu)\right)dx = \\ &= \int_\Omega \left(-\frac{1}{\mathbb{M}}c\mu\,(\partial_t\rho + \mathrm{div}(\rho\mathbf{u}))\right)dx = 0.\end{aligned} \tag{4.2.70}$$

Employing identities (4.2.66)-(4.2.70) into (4.2.65) gives

$$\begin{aligned}0 \quad = \quad &\int_\Omega \partial_t\left(\frac{\rho(c)}{2}|\mathbf{u}|^2 + \frac{\rho(c)}{\mathbb{M}}g_1(c) + \frac{\mathbb{C}}{2\,\mathbb{M}}\rho(c)|\mathbf{q}|^2 + \frac{1}{\mathbb{F}r^2}\rho(c)y\right)dx \\ &+ \frac{1}{\mathbb{P}e\mathbb{M}}\int_\Omega |\nabla\mu|^2\,dx + \frac{1}{\mathbb{R}e}\int_\Omega \left(|\nabla\mathbf{u}|^2 + \frac{1}{3}|\,\mathrm{div}\,\mathbf{u}|^2\right)dx,\end{aligned} \tag{4.2.71}$$

that is equivalent to the thesis (4.2.60). □

4.3 Spatial DG discretisation.

In this section we will design a novel Discontinuous Galerkin (DG) spatial approximation of the mixed NSCH system of equations (4.2.35)-(4.2.39). This DG discrete formulation will be consistent with the mass conservation and energy dissipation properties of the original system (see [24] and [25] for other examples of mass-energy consistent DG schemes for a Navier-Stokes-Korteweg system and a volume-fraction based quasi-incompressible model).

4.3.1 DG definitions, spaces and notation.

Discretisation. Let $\mathscr{T}_h$ be a conforming, shape-regular family of partitions of Ω into disjoint open triangles T such that $\bar{\Omega} = \bigcup_{T\in\mathscr{T}_h} \bar{T}$. Let us denote with h_T the diameter of an element T of $\mathscr{T}_h$ and let h be the maximum element diameter. Let e denote an edge of the triangulation and $\mathcal{E}$ the set of all interior edges of $\mathcal{T}_h$.

Broken Sobolev spaces. Let us recall the definition of some useful broken Sobolev spaces:

$$H^k(\mathscr{T}_h) := \left\{ v \in L^2(\Omega) : v|_T \in H^k(T),\ \forall T \in \mathscr{T}_h \right\}, \tag{4.3.1}$$

$$H(\mathrm{div};\mathscr{T}_h) := \left\{ \mathbf{w} \in (L^2(\Omega))^2 : \mathrm{div}(\mathbf{w}|_T) \in L^2(T),\ \forall T \in \mathscr{T}_h \right\}, \tag{4.3.2}$$

$$H^1_0(\mathscr{T}_h) := \left\{ v \in H^1(\mathscr{T}_h) : \gamma_0 v = 0 \right\}, \tag{4.3.3}$$

$$H^1_{\mathbf{n}}(\mathscr{T}_h) := \left\{ \mathbf{w} \in (H^1(\mathscr{T}_h))^2 : \gamma^* \mathbf{w} = 0 \right\}. \tag{4.3.4}$$

If v is a scalar function in $H^1(\mathscr{T}_h)$, we can define the piecewise gradient $\nabla_h v$ to be the function whose restriction to every element $T \in \mathscr{T}_h$ is equal to ∇v. In the same way, we can define the piecewise divergence $\mathrm{div}_h \mathbf{w}$ of a vector function $\mathbf{w} \in H(\mathrm{div};\mathscr{T}_h)$ as the function whose restriction to every element $T \in \mathscr{T}_h$ is equal to $\mathrm{div}\,\mathbf{w}$. In the rest of the section, for ease of writing, we will suppress the subscript h in the notation of both the piecewise gradient and the piecewise divergence.

The traces of functions in $H^1(\mathscr{T}_h)$ belong to the trace space

$$\mathbb{T}(\mathcal{E}\cup\partial\Omega) := \prod_{T\in\mathscr{T}_h} L^2(\partial T). \tag{4.3.5}$$

Finite element spaces. Let $\mathbb{P}^p(\mathscr{T}_h)$ denote the space of piecewise polynomials of degree p over $\mathscr{T}_h$. Then we can define the following finite element spaces:

$$\mathbb{V} := \mathbb{P}^p(\mathscr{T}_h),\quad \mathbb{V}_0 := \mathbb{V}\cap H^1_0(\mathscr{T}_h),\quad \mathbb{V}_{\mathbf{n}} := \mathbb{V}^2 \cap H^1_{\mathbf{n}}(\mathscr{T}_h). \tag{4.3.6}$$

For simplicity we assume that $\mathbb{V}$ is constant in time.

Jumps and averages. For $\varphi \in \mathbb{T}(\mathcal{E}\cup\partial\Omega)$, we define the jump $[\![\varphi]\!] \in (L^2(\mathcal{E}\cup\partial\Omega))^2$ and average $\{\!\{\varphi\}\!\} \in L^2(\mathcal{E}\cup\partial\Omega)$ of φ as follows. For every $e \in \mathcal{E}$ shared by the (open) triangles T^+ and T^-,

$$[\![\varphi]\!]_e := (\varphi^+|_e)\mathbf{n}^+ + (\varphi^-|_e)\mathbf{n}^-, \qquad \{\!\{\varphi\}\!\}_e := \frac{1}{2}(\varphi^+|_e + \varphi^-|_e), \tag{4.3.7}$$

where, for $i = +,-, v^i = v|_{\bar{T^i}}$ and $\mathbf{n}^i$ is the unit normal vector on e pointing outward of T^i. If $e \in \partial\Omega$, then

$$[\![\varphi]\!]_e := \varphi\mathbf{n}, \qquad \{\!\{\varphi\}\!\}_e := \varphi, \tag{4.3.8}$$

where $\mathbf{n}$ is the outward unit normal.
In the same way, we can define the jumps $[\![\boldsymbol{\varphi}]\!] \in L^2(\mathcal{E}\cup\partial\Omega)$, $[\![\boldsymbol{\varphi}]\!]_{\otimes} \in (L^2(\mathcal{E}\cup\partial\Omega))^{2\times 2}$ and average $\{\!\{\boldsymbol{\varphi}\}\!\} \in (L^2(\mathcal{E}\cup\partial\Omega))^2$ of the vector function $\boldsymbol{\varphi} \in (\mathbb{T}(\mathcal{E}\cup\partial\Omega))^2$ as follows. For every $e \in \mathcal{E}$ shared by the (open) triangles T^+ and T^-,

$$[\![\boldsymbol{\varphi}]\!]_e := (\boldsymbol{\varphi}^+|_e)\cdot\mathbf{n}^+ + (\boldsymbol{\varphi}^-|_e)\cdot\mathbf{n}^-, \tag{4.3.9}$$

$$[\![\boldsymbol{\varphi}]\!]_{e\otimes} := (\boldsymbol{\varphi}^+|_e)\otimes\mathbf{n}^+ + (\boldsymbol{\varphi}^-|_e)\otimes\mathbf{n}^-, \tag{4.3.10}$$

$$\{\!\{\boldsymbol{\varphi}\}\!\}_e := \frac{1}{2}(\boldsymbol{\varphi}^+|_e + \boldsymbol{\varphi}^-|_e). \tag{4.3.11}$$

If $e \in \partial\Omega$, then

$$[\![\boldsymbol{\varphi}]\!]_e := \boldsymbol{\varphi}\cdot\mathbf{n}, \quad [\![\boldsymbol{\varphi}]\!]_{e\otimes} := \boldsymbol{\varphi}\otimes\mathbf{n}, \quad \{\!\{\boldsymbol{\varphi}\}\!\}_e := \boldsymbol{\varphi}. \tag{4.3.12}$$

In the next sections we will suppress the subscript e in the notations of jumps and averages.

Elementwise formulation and numerical fluxes. We can give the elementwise variational formulation of the problem (4.2.35)-(4.2.39) in mixed form. Let us suppose that

$$\rho \in L^\infty(0,T;L^\infty(\mathscr{T}_h)),$$
$$g_1(c) \in L^1(0,T;L^1(\mathscr{T}_h)), \quad \mu_0(c) \in L^2(0,T;L^2(\mathscr{T}_h)).$$

We have to find

$$\begin{aligned}(c,\mathbf{u},\bar{p},\mu,\mathbf{q}) \quad \in \quad & L^2(0,T;H^1(\mathscr{T}_h)) \times L^2(0,T;(H^1_0(\mathscr{T}_h))^2) \times L^2(0,T;H^1(\mathscr{T}_h)) \times \\ & L^2(0,T;H^1(\mathscr{T}_h)) \times L^2(0,T;H^1_{\mathbf{n}}(\mathscr{T}_h))\end{aligned}$$

such that

$$(\partial_t c, \partial_t \mathbf{u}) \in L^2(0,T;L^2(\mathscr{T}_h)) \times L^2(0,T;(L^2(\mathscr{T}_h))^2)$$

and

$$\begin{aligned}0 = & \sum_{T\in\mathscr{T}_h}\int_T (\rho(\partial_t c)X + \rho(\mathbf{u}\cdot\nabla)cX)\,dx - \frac{1}{\mathbb{P}e}\mathcal{A}(\mu,X) \\ & + \int_{\mathcal{E}} F_1(c,\mathbf{u},\bar{p},\mu,\mathbf{q},X)\,ds, \end{aligned}\tag{4.3.13}$$

$$\begin{aligned}0 = & \sum_{T\in\mathscr{T}_h}\int_T \Big(\sqrt{\rho}\,\partial_t(\sqrt{\rho}\mathbf{u})\cdot\boldsymbol{\xi} + \rho(\mathbf{u}\cdot\nabla)\mathbf{u}\cdot\boldsymbol{\xi} + \frac{1}{2}\operatorname{div}(\rho\mathbf{u})\mathbf{u}\cdot\boldsymbol{\xi} \\ & + \frac{1}{\mathbb{M}}\rho\nabla\bar{p}\cdot\boldsymbol{\xi} + \frac{1}{\mathbb{M}}\rho c\nabla\mu\cdot\boldsymbol{\xi} + \frac{\rho_0}{\mathbb{F}r^2\rho}\,y\nabla\rho\cdot\boldsymbol{\xi} + \frac{1}{\mathbb{F}r^2}(\rho-\rho_0)\hat{\mathbf{j}}\cdot\boldsymbol{\xi}\Big)dx \\ & - \frac{1}{\mathbb{R}e}\mathcal{B}(\mathbf{u},\boldsymbol{\xi}) + \int_{\mathcal{E}} F_2(c,\mathbf{u},\bar{p},\mu,\mathbf{q},\boldsymbol{\xi})\,ds, \end{aligned}\tag{4.3.14}$$

$$0 = \sum_{T\in\mathscr{T}_h}\int_T ((\partial_t\rho)\,Z + \operatorname{div}(\rho\mathbf{u})Z)\,dx + \int_{\mathcal{E}} F_3(c,\mathbf{u},\bar{p},\mu,\mathbf{q},Z)\,ds, \tag{4.3.15}$$

$$\begin{aligned}0 = & \sum_{T\in\mathscr{T}_h}\int_T \Big(\Big(\rho + \frac{\partial\rho}{\partial c}c\Big)\mu\psi - \rho\mu_0(c)\psi + \frac{\partial\rho}{\partial c}\Big(\bar{p} - g_1(c) - \frac{\mathbb{C}}{2}|\mathbf{q}|^2\Big)\psi \\ & + \mathbb{C}\operatorname{div}(\rho\,\mathbf{q})\psi + \frac{\mathbb{M}\,\rho_0\,\alpha}{\mathbb{F}r^2}\rho y\psi\Big)\,dx + \int_{\mathcal{E}} F_4(c,\mathbf{u},\bar{p},\mu,\mathbf{q},\psi)\,ds, \end{aligned}\tag{4.3.16}$$

$$0 = \sum_{T\in\mathscr{T}_h}\int_T (\mathbf{q}\cdot\mathbf{T} - \nabla c\cdot\mathbf{T})\,dx + \int_{\mathcal{E}} F_5(c,\mathbf{u},\bar{p},\mu,\mathbf{q},\mathbf{T})\,ds, \tag{4.3.17}$$

$$\forall\,(X,\boldsymbol{\xi},Z,\psi,\mathbf{T})\in H^1(\mathscr{T}_h)\times(H^1_0(\mathscr{T}_h))^2\times H^1(\mathscr{T}_h)\times H^1(\mathscr{T}_h)\times H^1_{\mathbf{n}}(\mathscr{T}_h),$$

in which

$$\begin{aligned}
\mathcal{A}(\mu,X) &= -\sum_{T\in\mathscr{T}_h}\int_T \nabla\mu\cdot\nabla X\,dx+\int_{\mathcal{E}}\{\!\{\nabla X\}\!\}\cdot[\![\mu]\!]\,ds\\
&\quad+\int_{\mathcal{E}}[\![X]\!]\cdot\{\!\{\nabla\mu\}\!\}\,ds-\int_{\mathcal{E}}\frac{\sigma}{h}[\![\mu]\!]\cdot[\![X]\!]\,ds, \qquad (4.3.18)\\
\mathcal{B}(\mathbf{u},\boldsymbol{\xi}) &= -\sum_{T\in\mathscr{T}_h}\int_T\left(\left(\nabla\mathbf{u}+\frac{1}{3}(\operatorname{div}\mathbf{u})\mathbb{I}\right):\nabla\boldsymbol{\xi}\right)dx\\
&\quad+\int_{\mathcal{E}\cup\partial\Omega}\left(\left\{\!\!\left\{\nabla\boldsymbol{\xi}+\frac{1}{3}(\operatorname{div}\boldsymbol{\xi})\mathbb{I}\right\}\!\!\right\}:[\![\mathbf{u}]\!]_{\otimes}\right)ds\\
&\quad+\int_{\mathcal{E}\cup\partial\Omega}\left(\left\{\!\!\left\{\nabla\mathbf{u}+\frac{1}{3}(\operatorname{div}\mathbf{u})\mathbb{I}\right\}\!\!\right\}:[\![\boldsymbol{\xi}]\!]_{\otimes}\right)ds\\
&\quad-\int_{\mathcal{E}\cup\partial\Omega}\frac{\gamma}{h}\left([\![\mathbf{u}]\!]_{\otimes}:[\![\boldsymbol{\xi}]\!]_{\otimes}+\frac{1}{3}[\![\mathbf{u}]\!][\![\boldsymbol{\xi}]\!]\right)ds \qquad (4.3.19)
\end{aligned}$$

are the symmetric interior penalty discretisation of the laplacian of the chemical potential μ (see [1], [48]) and the DG formulation of the viscous terms (see [64]), where σ and γ are sufficiently large parameters.
The elementwise numerical fluxes F_i, for $i=1,...,5$, will be chosen in the next sections according to the properties that our discrete formulation will have to obey. We suppose that the numerical fluxes only depend on the traces of their arguments and are linear in the test functions.

4.3.2 Spatially discrete mixed formulation.

Let us give a spatially discrete DG mixed formulation of (4.3.13)-(4.3.17): find

$$\begin{aligned}
(c_h,\mathbf{u}_h,\bar{p}_h,\mu_h,\mathbf{q}_h) \;\in\;& L^2(0,T;\mathbb{V})\times L^2(0,T;\mathbb{V}_0^2)\times L^2(0,T;\mathbb{V})\times\\
& L^2(0,T;\mathbb{V})\times L^2(0,T;\mathbb{V}_{\mathbf{n}})
\end{aligned}$$

such that

$$\begin{aligned}
0 =\;& \sum_{T\in\mathscr{T}_h}\int_T(\rho_h(\partial_t c_h)X+\rho_h(\mathbf{u}_h\cdot\nabla)c_hX)\,dx-\frac{1}{\mathbb{P}e}\mathcal{A}(\mu_h,X)\\
&+\int_{\mathcal{E}}F_1(c_h,\mathbf{u}_h,\bar{p}_h,\mu_h,\mathbf{q}_h,X)\,ds, \qquad (4.3.20)\\
0 =\;& \sum_{T\in\mathscr{T}_h}\int_T\Big(\sqrt{\rho_h}\,\partial_t\left(\sqrt{\rho_h}\mathbf{u}_h\right)\cdot\boldsymbol{\xi}+\rho_h(\mathbf{u}_h\cdot\nabla)\mathbf{u}_h\cdot\boldsymbol{\xi}+\frac{1}{2}\operatorname{div}(\rho_h\mathbf{u}_h)\mathbf{u}_h\cdot\boldsymbol{\xi}\\
&+\frac{1}{\mathbb{M}}\rho_h\nabla\bar{p}_h\cdot\boldsymbol{\xi}+\frac{1}{\mathbb{M}}\rho_h c_h\nabla\mu_h\cdot\boldsymbol{\xi}+\frac{\rho_0}{\mathbb{F}r^2\rho_h}y\nabla\rho_h\cdot\boldsymbol{\xi}+\frac{1}{\mathbb{F}r^2}(\rho_h-\rho_0)\hat{\mathbf{j}}\cdot\boldsymbol{\xi}\Big)dx\\
&-\frac{1}{\mathbb{R}e}\mathcal{B}(\mathbf{u}_h,\boldsymbol{\xi})+\int_{\mathcal{E}}F_2(c_h,\mathbf{u}_h,\bar{p}_h,\mu_h,\mathbf{q}_h,\boldsymbol{\xi})\,ds, \qquad (4.3.21)\\
0 =\;& \sum_{T\in\mathscr{T}_h}\int_T((\partial_t\rho_h)\,Z+\operatorname{div}(\rho_h\mathbf{u}_h)Z)\,dx+\int_{\mathcal{E}}F_3(c_h,\mathbf{u}_h,\bar{p}_h,\mu_h,\mathbf{q}_h,Z)\,ds, \qquad (4.3.22)\\
0 =\;& \sum_{T\in\mathscr{T}_h}\int_T\Big(\Big(\rho_h+\frac{\partial\rho_h}{\partial c_h}c_h\Big)\mu_h\psi-\rho_h\mu_0(c_h)\psi+\frac{\partial\rho_h}{\partial c_h}\left(\bar{p}_h-g_1(c_h)-\frac{\mathbb{C}}{2}|\mathbf{q}_h|^2\right)\psi\\
&+\mathbb{C}\operatorname{div}(\rho_h\,\mathbf{q}_h)\psi+\frac{\mathbb{M}\,\rho_0\,\alpha}{\mathbb{F}r^2}\,\rho_h y\psi\Big)\,dx+\int_{\mathcal{E}}F_4(c_h,\mathbf{u}_h,\bar{p}_h,\mu_h,\mathbf{q}_h,\psi)\,ds, \qquad (4.3.23)
\end{aligned}$$

$$0 = \sum_{T\in\mathscr{T}_h}\int_T (\mathbf{q}_h\cdot\mathbf{T} - \nabla c_h\cdot\mathbf{T})\,dx + \int_{\mathcal{E}} F_5(c_h,\mathbf{u}_h,\bar{p}_h,\mu_h,\mathbf{q}_h,\mathbf{T})\,ds, \tag{4.3.24}$$

$$\forall\,(X,\boldsymbol{\xi},Z,\psi,\mathbf{T})\in\mathbb{V}\times\mathbb{V}_0^2\times\mathbb{V}\times\mathbb{V}\times\mathbb{V}_{\mathbf{n}}.$$

In the DG formulation (4.3.20)-(4.3.24) we have used, for simplicity, the notation ρ_h that means $\rho(c_h)$. Now we will recall a proposition that will be used to prove the discrete mass conservation property and the discrete version of the energy law for the spatially discrete DG formulation (4.3.20)-(4.3.24) (see [1], [24]).

Proposition 4.3.1. *If $\mathbf{w}\in H(\mathrm{div};\mathscr{T}_h)$ and $v\in H^1(\mathscr{T}_h)$, then*

$$\sum_{T\in\mathscr{T}_h}\int_T \mathrm{div}(\mathbf{w})v\,dx = \sum_{T\in\mathscr{T}_h}\left(-\int_T \mathbf{w}\cdot\nabla v\,dx + \int_{\partial T} v\mathbf{w}\cdot\mathbf{n}_T\,ds\right). \tag{4.3.25}$$

In particular, $\mathbf{w}\in(\mathbb{T}(\mathcal{E}\cup\partial\Omega))^2$, $v\in\mathbb{T}(\mathcal{E}\cup\partial\Omega)$ and

$$\sum_{T\in\mathscr{T}_h}\int_{\partial T} v\mathbf{w}\cdot\mathbf{n}\,ds = \int_{\mathcal{E}}[\![\mathbf{w}]\!]\{\!\{v\}\!\}\,ds + \int_{\mathcal{E}\cup\partial\Omega}[\![v]\!]\cdot\{\!\{\mathbf{w}\}\!\}\,ds = \int_{\mathcal{E}\cup\partial\Omega}[\![v\mathbf{w}]\!]\,ds. \tag{4.3.26}$$

The fluxes will be chosen in the next sections by imposing:

- spatially discrete mass conservation,
- spatially discrete energy dissipation law,
- consistency of the discrete DG formulation (4.3.20)-(4.3.24), i.e.

$$F_i(c,\mathbf{u},\bar{p},\mu,\mathbf{q},\cdot) = 0 \tag{4.3.27}$$

for $i=1,\dots,5$ and for all smooth functions $c,\mathbf{u},\bar{p},\mu,\mathbf{q}$.

4.3.3 Spatially discrete mass conservation.

Now we want to give conditions on the numerical fluxes $F_i, i=1,\dots,5$, in order to ensure that a mass conservation relation holds for the spatial discretisation (4.3.20)-(4.3.24). The proof is reported in [24] for a Navier-Stokes-Korteweg system.

Theorem 4.3.2 (Spatially discrete conservation of mass)**.** *If $(c_h,\mathbf{u}_h,\bar{p}_h,\mu_h,\mathbf{q}_h)$ is a solution of the spatially discrete system (4.3.20)-(4.3.24) then*

$$\frac{d}{dt}\left(\sum_{T\in\mathscr{T}_h}\int_T \rho(c_h)\,dx\right) = 0 \tag{4.3.28}$$

if and only if

$$\int_{\mathcal{E}} F_3(c_h,\mathbf{u}_h,\bar{p}_h,\mu_h,\mathbf{q}_h,1)\,ds = -\int_{\mathcal{E}}[\![\rho_h\mathbf{u}_h]\!]\,ds. \tag{4.3.29}$$

Proof. Let $Z=1$ be the scalar function equal to 1 everywhere on the spatial domain Ω. Using $Z=1$ in (4.3.22), we obtain

$$0 = \sum_{T\in\mathscr{T}_h}\int_T(\partial_t\rho_h + \mathrm{div}(\rho_h\mathbf{u}_h))\,dx + \int_{\mathcal{E}} F_3(c_h,\mathbf{u}_h,\bar{p}_h,\mu_h,\mathbf{q}_h,1)\,ds. \tag{4.3.30}$$

Integration by parts of the second term leads to

$$0 = \sum_{T\in\mathscr{T}_h}\int_T \partial_t\rho_h\,dx + \int_{\mathcal{E}}[\![\rho_h\mathbf{u}_h]\!]\,ds + \int_{\mathcal{E}} F_3(c_h,\mathbf{u}_h,\bar{p}_h,\mu_h,\mathbf{q}_h,1)\,ds \tag{4.3.31}$$

which implies the thesis. □

4.3.4 Spatially discrete energy dissipation law.

Let us define the spatially discrete total energy of the system (4.3.20)-(4.3.24) as

$$E_h := \sum_{T\in\mathscr{T}_h}\int_T\left(\frac{1}{2}\rho(c_h)\,|\mathbf{u}_h|^2+\frac{1}{\mathbb{M}}\rho(c_h)\,g_1(c_h)+\frac{\mathbb{C}}{2\,\mathbb{M}}\rho(c_h)\,|\nabla c_h|^2+\frac{1}{\mathbb{F}r^2}\rho(c_h)y\right)dx, \tag{4.3.32}$$

that is the spatially discrete version of the continuous total energy (4.2.56). The next theorem will set conditions on the numerical fluxes F_i, $i=1,\dots,5$, under which the spatially discrete system (4.3.20)-(4.3.24) preserves a spatially discrete form of the energy dissipation law (4.2.60). The proof will have the same structure as in the continuous case and has been inspired from the proof given in [25] for a volume-fraction based quasi-incompressible phase-field model. For simplicity of notation, we will set

$$F_i(\cdot) := F_i(c_h,\mathbf{u}_h,\bar{p}_h,\mu_h,\mathbf{q}_h,\cdot),\ \text{for all } i=1,\dots,5.$$

Theorem 4.3.3 (Spatially discrete energy dissipation law)**.** *If $(c_h,\mathbf{u}_h,\bar{p}_h,\mu_h,\mathbf{q}_h)$ is a solution of the spatially discrete system (4.3.20)-(4.3.24) then*

$$\begin{aligned}\frac{dE_h}{dt} &= \frac{d}{dt}\left(\sum_{T\in\mathscr{T}_h}\int_T\left(\frac{\rho(c_h)}{2}|\mathbf{u}_h|^2+\frac{\rho(c_h)}{\mathbb{M}}g_1(c_h)+\frac{\mathbb{C}}{2\,\mathbb{M}}\rho(c_h)|\mathbf{q}_h|^2+\frac{1}{\mathbb{F}r^2}\rho(c_h)y\right)dx\right)\\ &= \frac{1}{\mathbb{P}e\mathbb{M}}\mathcal{A}(\mu_h,\mu_h)+\frac{1}{\mathbb{R}e}\mathcal{B}(\mathbf{u}_h,\mathbf{u}_h)\end{aligned} \tag{4.3.33}$$

if and only if the following conditions on the numerical fluxes F_i, for $i=1,\dots,5$, are satisfied:

a.

$$\begin{aligned}0=\int_{\mathcal{E}}\Bigg(&F_1\left(\frac{\mu_h}{\mathbb{M}}\right)+F_2\left(\mathbf{u}_h\right)+F_3\left(\frac{c_h\mu_h}{\mathbb{M}}+\frac{\bar{p}_h}{\mathbb{M}}+\frac{y}{\mathbb{F}r^2}-\frac{\rho_0 y}{\mathbb{F}r^2\rho_h}\right)\\ &+\frac{1}{\mathbb{M}}[\![\rho_h\mu_h c_h\mathbf{u}_h]\!]+\frac{1}{\mathbb{M}}[\![\rho_h\bar{p}_h\mathbf{u}_h]\!]+\frac{1}{\mathbb{F}r^2}[\![(\rho_h-\rho_0)y\,\mathbf{u}_h]\!]\Bigg)\,ds,\end{aligned} \tag{4.3.34}$$

b.

$$0 = \int_{\mathcal{E}}\left(\partial_t F_5\left(\frac{\mathbb{C}}{\mathbb{M}}\,\rho_h\mathbf{q}_h\right)-\frac{\mathbb{C}}{\mathbb{M}}\,[\![\rho_h\mathbf{q}_h(\partial_t c_h)]\!]-F_4\left(\frac{1}{\mathbb{M}}\partial_t c_h\right)\right)ds. \tag{4.3.35}$$

Remark. Notice that $\mathcal{A}$ and $\mathcal{B}$, by definition, are negative definite.

Proof. Let us test (4.3.20) by $\dfrac{\mu_h}{\mathbb{M}}$ and (4.3.21) by $\mathbf{u}_h$ and sum them together:

$$\begin{aligned}0 = \sum_{T\in\mathscr{T}_h}\int_T\Bigg(&\frac{1}{\mathbb{M}}\rho_h\mu_h(\partial_t c_h)+\frac{\mu_h}{\mathbb{M}}\rho_h(\mathbf{u}_h\cdot\nabla)c_h+\sqrt{\rho_h}\,\partial_t(\sqrt{\rho_h}\mathbf{u}_h)\cdot\mathbf{u}_h\\ &+\rho_h(\mathbf{u}_h\cdot\nabla)\mathbf{u}_h\cdot\mathbf{u}_h+\frac{1}{2}\,\mathrm{div}(\rho_h\mathbf{u}_h)\mathbf{u}_h\cdot\mathbf{u}_h\\ &+\frac{1}{\mathbb{M}}\rho_h\nabla\bar{p}_h\cdot\mathbf{u}_h+\frac{1}{\mathbb{M}}\rho_h c_h\nabla\mu_h\cdot\mathbf{u}_h\\ &+\frac{\rho_0}{\mathbb{F}r^2\rho_h}y\nabla\rho_h\cdot\mathbf{u}_h+\frac{1}{\mathbb{F}r^2}(\rho_h-\rho_0)\hat{\mathbf{j}}\cdot\mathbf{u}_h\Bigg)\,dx\\ &+\int_{\mathcal{E}}\left(F_1\left(\frac{\mu_h}{\mathbb{M}}\right)+F_2\left(\mathbf{u}_h\right)\right)ds-\frac{1}{\mathbb{P}e\mathbb{M}}\mathcal{A}(\mu_h,\mu_h)-\frac{1}{\mathbb{R}e}\mathcal{B}(\mathbf{u}_h,\mathbf{u}_h).\end{aligned} \tag{4.3.36}$$

Integration by parts of the term containing $\nabla \bar{p}_h$ leads to

$$\begin{aligned} 0 \;=\; & \sum_{T\in\mathscr{T}_h}\int_T \Big(\frac{1}{\mathbb{M}}\rho_h\mu_h(\partial_t c_h) + \frac{\mu_h}{\mathbb{M}}\rho_h(\mathbf{u}_h\cdot\nabla)c_h + \sqrt{\rho_h}\,\partial_t(\sqrt{\rho_h}\mathbf{u}_h)\cdot\mathbf{u}_h \\ & \quad +\rho_h(\mathbf{u}_h\cdot\nabla)\mathbf{u}_h\cdot\mathbf{u}_h + \frac{1}{2}\operatorname{div}(\rho_h\mathbf{u}_h)\mathbf{u}_h\cdot\mathbf{u}_h \\ & \quad -\frac{1}{\mathbb{M}}\bar{p}_h\operatorname{div}(\rho_h\mathbf{u}_h) + \frac{1}{\mathbb{M}}\rho_h c_h\nabla\mu_h\cdot\mathbf{u}_h \\ & \quad +\frac{\rho_0}{\mathbb{F}r^2\rho_h}y\nabla\rho_h\cdot\mathbf{u}_h + \frac{1}{\mathbb{F}r^2}(\rho_h-\rho_0)\hat{\mathbf{j}}\cdot\mathbf{u}_h\Big)\,dx \\ & +\int_{\mathcal{E}}\Big(F_1\left(\frac{\mu_h}{\mathbb{M}}\right)+F_2\left(\mathbf{u}_h\right)+\frac{1}{\mathbb{M}}\left[\!\left[\rho_h\bar{p}_h\mathbf{u}_h\right]\!\right]\Big)\,ds \\ & -\frac{1}{\mathbb{P}e\mathbb{M}}\mathcal{A}(\mu_h,\mu_h)-\frac{1}{\mathbb{R}e}\mathcal{B}(\mathbf{u}_h,\mathbf{u}_h). \end{aligned} \tag{4.3.37}$$

Using the spatially discrete local mass conservation equation (4.3.22) into (4.3.37), we obtain:

$$\begin{aligned} 0 \;=\; & \sum_{T\in\mathscr{T}_h}\int_T \Big(\frac{1}{\mathbb{M}}\rho_h\mu_h(\partial_t c_h) + \frac{\mu_h}{\mathbb{M}}\rho_h(\mathbf{u}_h\cdot\nabla)c_h + \sqrt{\rho_h}\,\partial_t(\sqrt{\rho_h}\mathbf{u}_h)\cdot\mathbf{u}_h \\ & \quad +\frac{\bar{p}_h}{\mathbb{M}}(\partial_t\rho_h) + \frac{1}{\mathbb{M}}\rho_h c_h\nabla\mu_h\cdot\mathbf{u}_h \\ & \quad +\rho_h(\mathbf{u}_h\cdot\nabla)\mathbf{u}_h\cdot\mathbf{u}_h + \frac{1}{2}\operatorname{div}(\rho_h\mathbf{u}_h)\mathbf{u}_h\cdot\mathbf{u}_h \\ & \quad +\frac{\rho_0}{\mathbb{F}r^2\rho_h}y\nabla\rho_h\cdot\mathbf{u}_h + \frac{1}{\mathbb{F}r^2}(\rho_h-\rho_0)\hat{\mathbf{j}}\cdot\mathbf{u}_h\Big)\,dx \\ & +\int_{\mathcal{E}}\Big(F_1\left(\frac{\mu_h}{\mathbb{M}}\right)+F_2\left(\mathbf{u}_h\right)+F_3\left(\frac{\bar{p}_h}{\mathbb{M}}\right)+\frac{1}{\mathbb{M}}\left[\!\left[\rho_h\bar{p}_h\mathbf{u}_h\right]\!\right]\Big)\,ds \\ & -\frac{1}{\mathbb{P}e\mathbb{M}}\mathcal{A}(\mu_h,\mu_h)-\frac{1}{\mathbb{R}e}\mathcal{B}(\mathbf{u}_h,\mathbf{u}_h). \end{aligned} \tag{4.3.38}$$

If we notice that

$$\sum_{T\in\mathscr{T}_h}\int_T\Big(\rho_h(\mathbf{u}_h\cdot\nabla)\mathbf{u}_h\cdot\mathbf{u}_h+\frac{1}{2}\operatorname{div}(\rho_h\mathbf{u}_h)\mathbf{u}_h\cdot\mathbf{u}_h\Big)\,dx=\int_{\mathcal{E}}\frac{1}{2}\left[\!\left[\rho_h(\mathbf{u}_h\cdot\mathbf{u}_h)\mathbf{u}_h\right]\!\right]ds \tag{4.3.39}$$

and if we use the definition of $\rho_h\mu_h$ from (4.3.23), with $\psi = (\partial_t c_h)/\mathbb{M}$, we can rewrite (4.3.38):

$$\begin{aligned} 0 = & \sum_{T\in\mathscr{T}_h}\int_T\Big(\sqrt{\rho_h}\,\partial_t(\sqrt{\rho_h}\mathbf{u}_h)\cdot\mathbf{u}_h + \frac{1}{\mathbb{M}}\rho_h\mu_0(c_h)(\partial_t c_h) + \frac{1}{\mathbb{M}}g_1(c_h)(\partial_t\rho_h) \\ & \quad +\frac{\mathbb{C}}{2\,\mathbb{M}}|\mathbf{q}_h|^2(\partial_t\rho_h) - \frac{\mathbb{C}}{\mathbb{M}}\operatorname{div}(\rho_h\mathbf{q}_h)(\partial_t c_h) \\ & \quad +\frac{\rho_0}{\mathbb{F}r^2\rho_h}y(\partial_t\rho_h) + \frac{\rho_0}{\mathbb{F}r^2\rho_h}y\nabla\rho_h\cdot\mathbf{u}_h + \frac{1}{\mathbb{F}r^2}(\rho_h-\rho_0)\hat{\mathbf{j}}\cdot\mathbf{u}_h \\ & \quad -\frac{1}{\mathbb{M}}c_h\mu_h(\partial_t\rho_h) + \frac{\mu_h}{\mathbb{M}}\rho_h(\mathbf{u}_h\cdot\nabla)c_h + \frac{1}{\mathbb{M}}\rho_h c_h\nabla\mu_h\cdot\mathbf{u}_h\Big)\,dx \\ & +\int_{\mathcal{E}}\Big(F_1\left(\frac{\mu_h}{\mathbb{M}}\right)+F_2\left(\mathbf{u}_h\right)+F_3\left(\frac{\bar{p}_h}{\mathbb{M}}\right)-F_4\left(\frac{1}{\mathbb{M}}\partial_t c_h\right) \\ & \quad +\frac{1}{\mathbb{M}}\left[\!\left[\rho_h\bar{p}_h\mathbf{u}_h\right]\!\right]+\frac{1}{2}\left[\!\left[\rho_h(\mathbf{u}_h\cdot\mathbf{u}_h)\mathbf{u}_h\right]\!\right]\Big)\,ds \\ & -\frac{1}{\mathbb{P}e\mathbb{M}}\mathcal{A}(\mu_h,\mu_h)-\frac{1}{\mathbb{R}e}\mathcal{B}(\mathbf{u}_h,\mathbf{u}_h). \end{aligned} \tag{4.3.40}$$

Let us rewrite terms in (4.3.40) in a more useful form:

(I) the first term is

$$\sum_{T\in\mathscr{T}_h}\int_T \sqrt{\rho_h}\,\partial_t(\sqrt{\rho_h}\mathbf{u}_h)\cdot\mathbf{u}_h\,dx = \sum_{T\in\mathscr{T}_h}\int_T \partial_t\left(\frac{\rho(c_h)}{2}|\mathbf{u}_h|^2\right)dx, \tag{4.3.41}$$

(II) the terms containing the spatially discrete double-well potential $g_1(c_h)$ and its derivative $\mu_0(c_h)$ are

$$\sum_{T\in\mathscr{T}_h}\int_T \left(\frac{1}{\mathbb{M}}\rho\mu_0(c_h)(\partial_t c_h)+\frac{1}{\mathbb{M}}g_1(c_h)(\partial_t\rho_h)\right)dx = \sum_{T\in\mathscr{T}_h}\int_T \partial_t\left(\frac{\rho(c_h)}{\mathbb{M}}g_1(c_h)\right)dx, \tag{4.3.42}$$

(III) integrating by parts the terms containing the variable $\mathbf{q}_h$ and using (4.3.24):

$$\begin{aligned}
&\sum_{T\in\mathscr{T}_h}\int_T \left(\frac{\mathbb{C}}{2\,\mathbb{M}}|\mathbf{q}_h|^2(\partial_t\rho_h)-\frac{\mathbb{C}}{\mathbb{M}}\,\mathrm{div}(\rho_h\mathbf{q}_h)(\partial_t c_h)\right)dx\\
&=\sum_{T\in\mathscr{T}_h}\int_T \left(\frac{\mathbb{C}}{2\,\mathbb{M}}|\mathbf{q}_h|^2(\partial_t\rho_h)+\frac{\mathbb{C}}{\mathbb{M}}\,\rho_h\mathbf{q}_h\cdot\nabla(\partial_t c_h)\right)dx-\int_{\mathcal{E}}\frac{\mathbb{C}}{\mathbb{M}}\,[\![\rho_h\mathbf{q}_h(\partial_t c_h)]\!]\,ds\\
&=\sum_{T\in\mathscr{T}_h}\int_T \left(\frac{\mathbb{C}}{2\,\mathbb{M}}|\mathbf{q}_h|^2(\partial_t\rho_h)+\frac{\mathbb{C}}{\mathbb{M}}\,\rho_h\mathbf{q}_h\cdot(\partial_t\mathbf{q}_h)\right)dx\\
&\quad+\int_{\mathcal{E}}\left(\partial_t F_5\left(\frac{\mathbb{C}}{\mathbb{M}}\,\rho_h\mathbf{q}_h\right)-\frac{\mathbb{C}}{\mathbb{M}}\,[\![\rho_h\mathbf{q}_h(\partial_t c_h)]\!]\right)ds\\
&=\sum_{T\in\mathscr{T}_h}\int_T \frac{\mathbb{C}}{2\,\mathbb{M}}\partial_t\left(\rho_h|\mathbf{q}_h|^2\right)dx+\int_{\mathcal{E}}\left(\partial_t F_5\left(\frac{\mathbb{C}}{\mathbb{M}}\,\rho_h\mathbf{q}_h\right)-\frac{\mathbb{C}}{\mathbb{M}}\,[\![\rho_h\mathbf{q}_h(\partial_t c_h)]\!]\right)ds,
\end{aligned} \tag{4.3.43}$$

(IV) integrating by parts, using the definition of $\hat{\mathbf{j}}$ and local mass conservation (4.3.22), gravity terms can be rewritten as

$$\begin{aligned}
&\sum_{T\in\mathscr{T}_h}\int_T \left(\frac{\rho_0}{\mathbb{F}r^2\rho_h}y(\partial_t\rho_h)+\frac{\rho_0}{\mathbb{F}r^2\rho_h}y\nabla\rho_h\cdot\mathbf{u}_h+\frac{1}{\mathbb{F}r^2}(\rho_h-\rho_0)\hat{\mathbf{j}}\cdot\mathbf{u}_h\right)dx\\
&=\sum_{T\in\mathscr{T}_h}\int_T \left(\frac{\rho_0}{\mathbb{F}r^2\rho_h}y(\partial_t\rho_h)+\frac{\rho_0}{\mathbb{F}r^2\rho_h}y\nabla\rho_h\cdot\mathbf{u}_h-\frac{1}{\mathbb{F}r^2}y\,\mathrm{div}(\rho_h\mathbf{u}_h)+\frac{\rho_0 y}{\mathbb{F}r^2}\,\mathrm{div}\,\mathbf{u}_h\right)dx\\
&\quad+\int_{\mathcal{E}}\frac{1}{\mathbb{F}r^2}\,[\![(\rho_h-\rho_0)y\,\mathbf{u}_h]\!]\,ds\\
&=\sum_{T\in\mathscr{T}_h}\int_T \left(\frac{\rho_0}{\mathbb{F}r^2\rho_h}\left(\partial_t\rho_h+\nabla\rho_h\cdot\mathbf{u}_h+\rho_h\,\mathrm{div}\,\mathbf{u}_h\right)y+\frac{1}{\mathbb{F}r^2}(\partial_t\rho_h)y\right)dx\\
&\quad+\int_{\mathcal{E}}F_3\left(\frac{y}{\mathbb{F}r^2}\right)+\frac{1}{\mathbb{F}r^2}\,[\![(\rho_h-\rho_0)y\,\mathbf{u}_h]\!]\,ds\\
&=\sum_{T\in\mathscr{T}_h}\int_T \partial_t\left(\frac{1}{\mathbb{F}r^2}\rho_h y\right)dx+\int_{\mathcal{E}}\left(F_3\left(\frac{y}{\mathbb{F}r^2}-\frac{\rho_0 y}{\mathbb{F}r^2\rho_h}\right)+\frac{1}{\mathbb{F}r^2}\,[\![(\rho_h-\rho_0)y\,\mathbf{u}_h]\!]\right)ds,
\end{aligned} \tag{4.3.44}$$

(V) using integration by parts and local mass conservation (4.2.37),

$$\begin{aligned}
&\sum_{T\in\mathscr{T}_h}\int_T\left(-\frac{1}{\mathbb{M}}c_h\mu_h(\partial_t\rho_h)+\frac{\mu_h}{\mathbb{M}}\rho_h(\mathbf{u}_h\cdot\nabla)c_h+\frac{1}{\mathbb{M}}\rho_h c_h\nabla\mu_h\cdot\mathbf{u}_h\right)dx\\
&=\sum_{T\in\mathscr{T}_h}\int_T\left(-\frac{1}{\mathbb{M}}c_h\mu_h(\partial_t\rho_h)+\frac{1}{\mathbb{M}}(\rho_h\mathbf{u}_h)\cdot(\mu_h\nabla c_h+c_h\nabla\mu_h)\right)dx\\
&=\sum_{T\in\mathscr{T}_h}\int_T\left(-\frac{1}{\mathbb{M}}c_h\mu_h\left(\partial_t\rho_h+\operatorname{div}(\rho_h\mathbf{u}_h)\right)\right)dx+\int_{\mathcal{E}}\frac{1}{\mathbb{M}}\left[\!\left[\rho_h\mu_h c_h\mathbf{u}_h\right]\!\right]ds\\
&=\int_{\mathcal{E}}\left(F_3\left(\frac{c_h\mu_h}{\mathbb{M}}\right)+\frac{1}{\mathbb{M}}\left[\!\left[\rho_h\mu_h c_h\mathbf{u}_h\right]\!\right]\right)ds. \qquad (4.3.45)
\end{aligned}$$

Identities (4.3.41)-(4.3.45) into (4.3.40) give

$$\begin{aligned}
0 \;=\;& \sum_{T\in\mathscr{T}_h}\int_T\partial_t\left(\frac{\rho(c_h)}{2}|\mathbf{u}_h|^2+\frac{\rho(c_h)}{\mathbb{M}}g_1(c_h)+\frac{\mathbb{C}}{2\,\mathbb{M}}\rho(c_h)|\mathbf{q}_h|^2+\frac{1}{\mathbb{F}r^2}\rho(c_h)y\right)dx\\
&+\int_{\mathcal{E}}\left(F_1\left(\frac{\mu_h}{\mathbb{M}}\right)+F_2\left(\mathbf{u}_h\right)+F_3\left(\frac{c_h\mu_h}{\mathbb{M}}+\frac{\bar{p}_h}{\mathbb{M}}+\frac{y}{\mathbb{F}r^2}-\frac{\rho_0 y}{\mathbb{F}r^2\rho_h}\right)\right.\\
&\quad -F_4\left(\frac{1}{\mathbb{M}}\partial_t c_h\right)+\partial_t F_5\left(\frac{\mathbb{C}}{\mathbb{M}}\rho_h\mathbf{q}_h\right)\\
&\quad -\frac{\mathbb{C}}{\mathbb{M}}\left[\!\left[\rho_h\mathbf{q}_h(\partial_t c_h)\right]\!\right]+\frac{1}{\mathbb{M}}\left[\!\left[\rho_h\mu_h c_h\mathbf{u}_h\right]\!\right]+\frac{1}{2}\left[\!\left[\rho_h(\mathbf{u}_h\cdot\mathbf{u}_h)\mathbf{u}_h\right]\!\right]\\
&\quad \left.+\frac{1}{\mathbb{M}}\left[\!\left[\rho_h\bar{p}_h\mathbf{u}_h\right]\!\right]+\frac{1}{\mathbb{F}r^2}\left[\!\left[(\rho_h-\rho_0)y\,\mathbf{u}_h\right]\!\right]\right)ds\\
&-\frac{1}{\mathbb{P}e\mathbb{M}}\mathcal{A}(\mu_h,\mu_h)-\frac{1}{\mathbb{R}e}\mathcal{B}(\mathbf{u}_h,\mathbf{u}_h). \qquad (4.3.46)
\end{aligned}$$

The scheme (4.3.20)-(4.3.24) preserves the energy law at the spatially discrete level iff

$$\begin{aligned}
0=\;& \int_{\mathcal{E}}\left(F_1\left(\frac{\mu_h}{\mathbb{M}}\right)+F_2\left(\mathbf{u}_h\right)+F_3\left(\frac{c_h\mu_h}{\mathbb{M}}+\frac{\bar{p}_h}{\mathbb{M}}+\frac{y}{\mathbb{F}r^2}-\frac{\rho_0 y}{\mathbb{F}r^2\rho_h}\right)+\frac{1}{\mathbb{M}}\left[\!\left[\rho_h\mu_h c_h\mathbf{u}_h\right]\!\right]\right.\\
&\left.+\frac{1}{2}\left[\!\left[\rho_h(\mathbf{u}_h\cdot\mathbf{u}_h)\mathbf{u}_h\right]\!\right]+\frac{1}{\mathbb{M}}\left[\!\left[\rho_h\bar{p}_h\mathbf{u}_h\right]\!\right]+\frac{1}{\mathbb{F}r^2}\left[\!\left[(\rho_h-\rho_0)y\,\mathbf{u}_h\right]\!\right]\right)ds\\
&+\int_{\mathcal{E}}\left(\partial_t F_5\left(\frac{\mathbb{C}}{\mathbb{M}}\rho_h\mathbf{q}_h\right)-\frac{\mathbb{C}}{\mathbb{M}}\left[\!\left[\rho_h\mathbf{q}_h(\partial_t c_h)\right]\!\right]-F_4\left(\frac{1}{\mathbb{M}}\partial_t c_h\right)\right)ds. \qquad (4.3.47)
\end{aligned}$$

From (4.3.20)-(4.3.24) it is clear that the trace of $\partial_t c_h$ does not depend from the other variables; so conditions (a) and (b) of the thesis are satisfied. □

4.3.5 Choice of the numerical fluxes.

In view of the computations performed in the previous sections, here we address the question of how practically choosing the numerical fluxes $F_i, i=1,...,5$. From the spatially discrete mass conservation theorem (Theorem 4.3.2), it follows that we have mass conservation for the spatially discrete scheme (4.3.20)-(4.3.24) iff

$$\int_{\mathcal{E}}F_3(c_h,\mathbf{u}_h,\bar{p}_h,\mu_h,\mathbf{q}_h,1)\,ds=-\int_{\mathcal{E}}\left[\!\left[\rho_h\mathbf{u}_h\right]\!\right]ds. \qquad (4.3.48)$$

So, we can choose:

$$F_3(c_h,\mathbf{u}_h,\bar{p}_h,\mu_h,\mathbf{q}_h,Z)=-\left[\!\left[\rho_h\mathbf{u}_h\right]\!\right]\left\{\!\left\{Z\right\}\!\right\}. \qquad (4.3.49)$$

Let us recall the condition (b) in the spatially discrete energy law, i.e.,

$$0 = \int_{\mathcal{E}} \left(\partial_t F_5 \left(\frac{\mathbb{C}}{\mathbb{M}} \rho_h \mathbf{q}_h \right) - \frac{\mathbb{C}}{\mathbb{M}} \left[\!\left[\rho_h \mathbf{q}_h (\partial_t c_h) \right]\!\right] - F_4 \left(\frac{1}{\mathbb{M}} \partial_t c_h \right) \right) ds. \quad (4.3.50)$$

If we choose

$$F_5(c_h, \mathbf{u}_h, \bar{p}_h, \mu_h, \mathbf{q}_h, \mathbf{T}) = \left[\!\left[c_h \right]\!\right] \cdot \left\{\!\left\{ \mathbf{T} \right\}\!\right\}, \quad (4.3.51)$$

then the first two terms in (4.3.50) can be written as:

$$\begin{aligned} & \int_{\mathcal{E}} \left(\partial_t F_5 \left(\frac{\mathbb{C}}{\mathbb{M}} \rho_h \mathbf{q}_h \right) - \frac{\mathbb{C}}{\mathbb{M}} \left[\!\left[\rho_h \mathbf{q}_h (\partial_t c_h) \right]\!\right] \right) ds \\ = & \int_{\mathcal{E}} \left(-\frac{\mathbb{C}}{\mathbb{M}} \left[\!\left[\rho_h \mathbf{q}_h \right]\!\right] \left\{\!\left\{ \partial_t c_h \right\}\!\right\} \right) ds. \end{aligned} \quad (4.3.52)$$

This fact implies that

$$\int_{\mathcal{E}} F_4 \left(c_h, \mathbf{u}_h, \bar{p}_h, \mu_h, \mathbf{q}_h, \frac{1}{\mathbb{M}} (\partial_t c_h) \right) ds = \int_{\mathcal{E}} \left(-\frac{\mathbb{C}}{\mathbb{M}} \left[\!\left[\rho_h \mathbf{q}_h \right]\!\right] \left\{\!\left\{ \partial_t c_h \right\}\!\right\} \right) ds. \quad (4.3.53)$$

So,

$$F_4(c_h, \mathbf{u}_h, \bar{p}_h, \mu_h, \mathbf{q}_h, \psi) = -\mathbb{C} \left[\!\left[\rho_h \mathbf{q}_h \right]\!\right] \left\{\!\left\{ \psi \right\}\!\right\}. \quad (4.3.54)$$

The condition (a) in the spatially discrete energy law is:

$$\begin{aligned} 0 = \int_{\mathcal{E}} \Bigg(& F_1 \left(\frac{\mu_h}{\mathbb{M}} \right) + F_2 \left(\mathbf{u}_h \right) + F_3 \left(\frac{c_h \mu_h}{\mathbb{M}} + \frac{\bar{p}_h}{\mathbb{M}} + \frac{y}{\mathbb{F}r^2} - \frac{\rho_0 y}{\mathbb{F}r^2 \rho_h} \right) \\ & + \frac{1}{2} \left[\!\left[\rho_h |\mathbf{u}_h|^2 \mathbf{u}_h \right]\!\right] + \frac{1}{\mathbb{M}} \left[\!\left[\rho_h \mu_h c_h \mathbf{u}_h \right]\!\right] + \frac{1}{\mathbb{M}} \left[\!\left[\rho_h \bar{p}_h \mathbf{u}_h \right]\!\right] + \frac{1}{\mathbb{F}r^2} \left[\!\left[(\rho_h - \rho_0) y \, \mathbf{u}_h \right]\!\right] \Bigg) ds. \end{aligned} \quad (4.3.55)$$

If we consider gravity terms, with the definition of the flux F_3, we have that

$$\begin{aligned} & \int_{\mathcal{E}} \left(\frac{1}{\mathbb{F}r^2} \left[\!\left[(\rho_h - \rho_0) y \mathbf{u}_h \right]\!\right] + F_3 \left(\frac{y}{\mathbb{F}r^2} - \frac{\rho_0 y}{\mathbb{F}r^2 \rho_h} \right) \right) ds \\ = & \int_{\mathcal{E}} \left(-\frac{\rho_0 y}{\mathbb{F}r^2} \left[\!\left[\mathbf{u}_h \right]\!\right] + \frac{\rho_0 y}{\mathbb{F}r^2} \left[\!\left[\rho_h \mathbf{u}_h \right]\!\right] \left\{\!\left\{ \frac{1}{\rho_h} \right\}\!\right\} \right) ds \\ = & \int_{\mathcal{E}} -\frac{\rho_0 y}{\mathbb{F}r^2} \left[\!\left[\frac{1}{\rho_h} \right]\!\right] \cdot \left\{\!\left\{ \rho_h \mathbf{u}_h \right\}\!\right\} ds \end{aligned} \quad (4.3.56)$$

and, if we notice that

$$\begin{aligned} & \int_{\mathcal{E}} \left(F_3 \left(\frac{c_h \mu_h}{\mathbb{M}} + \frac{\bar{p}_h}{\mathbb{M}} \right) \right) ds \\ = & \int_{\mathcal{E}} \left(-\frac{1}{\mathbb{M}} \left[\!\left[\rho_h \mathbf{u}_h \right]\!\right] \left\{\!\left\{ c_h \mu_h \right\}\!\right\} - \frac{1}{\mathbb{M}} \left[\!\left[\rho_h \mathbf{u}_h \right]\!\right] \left\{\!\left\{ \bar{p}_h \right\}\!\right\} \right) ds, \end{aligned} \quad (4.3.57)$$

then we get

$$\begin{aligned} & \int_{\mathcal{E}} \left(F_1 \left(\frac{\mu_h}{\mathbb{M}} \right) + F_2 \left(\mathbf{u}_h \right) \right) ds \\ = & \int_{\mathcal{E}} \Bigg(-\frac{1}{\mathbb{M}} \left[\!\left[\bar{p}_h \right]\!\right] \cdot \left\{\!\left\{ \rho_h \mathbf{u}_h \right\}\!\right\} - \frac{1}{2} \left[\!\left[\rho_h |\mathbf{u}_h|^2 \mathbf{u}_h \right]\!\right] \\ & + \frac{1}{\mathbb{M}} \left[\!\left[\rho_h \mathbf{u}_h \right]\!\right] \left\{\!\left\{ c_h \mu_h \right\}\!\right\} - \frac{1}{\mathbb{M}} \left[\!\left[\rho_h c_h \mu_h \mathbf{u}_h \right]\!\right] + \frac{\rho_0 y}{\mathbb{F}r^2} \left[\!\left[\frac{1}{\rho_h} \right]\!\right] \cdot \left\{\!\left\{ \rho_h \mathbf{u}_h \right\}\!\right\} \Bigg) ds. \end{aligned} \quad (4.3.58)$$

So, a possible choice of the numerical fluxes (notice it is not unique) in order to have a consistent, mass conservative, and energy law preserving spatially discrete numerical scheme is the following:

$$F_1(c_h,\mathbf{u}_h,\bar{p}_h,\mu_h,\mathbf{q}_h,X) = [\![\rho_h\mathbf{u}_h]\!]\{\!\{c_hX\}\!\} - [\![c_h\mathbf{u}_h]\!]\{\!\{\rho_hX\}\!\}\,, \tag{4.3.59}$$

$$\begin{aligned} F_2(c_h,\mathbf{u}_h,\bar{p}_h,\mu_h,\mathbf{q}_h,\boldsymbol{\xi}) = &-\frac{1}{\mathbb{M}}[\![\bar{p}_h]\!]\cdot\{\!\{\rho_h\boldsymbol{\xi}\}\!\} - (\{\!\{\boldsymbol{\xi}\}\!\}\otimes\{\!\{\rho_h\mathbf{u}_h\}\!\}) : [\![\mathbf{u}_h]\!]_{\otimes} \\ &- \frac{1}{2}[\![\rho_h\mathbf{u}_h]\!]\{\!\{\mathbf{u}_h\cdot\boldsymbol{\xi}\}\!\} - \frac{1}{\mathbb{M}}[\![\rho_h\mu_h]\!]\cdot\{\!\{c_h\boldsymbol{\xi}\}\!\} \\ &+ \frac{\rho_0\, y}{\mathbb{F}r^2}\left[\!\!\left[\frac{1}{\rho_h}\right]\!\!\right]\cdot\{\!\{\rho_h\boldsymbol{\xi}\}\!\}\,, \end{aligned} \tag{4.3.60}$$

$$F_3(c_h,\mathbf{u}_h,\bar{p}_h,\mu_h,\mathbf{q}_h,Z) = -[\![\rho_h\mathbf{u}_h]\!]\{\!\{Z\}\!\}\,, \tag{4.3.61}$$

$$F_4(c_h,\mathbf{u}_h,\bar{p}_h,\mu_h,\mathbf{q}_h,\psi) = -\mathbb{C}[\![\rho_h\mathbf{q}_h]\!]\{\!\{\psi\}\!\}\,, \tag{4.3.62}$$

$$F_5(c_h,\mathbf{u}_h,\bar{p}_h,\mu_h,\mathbf{q}_h,\mathbf{T}) = [\![c_h]\!]\cdot\{\!\{\mathbf{T}\}\!\}\,. \tag{4.3.63}$$

In the choice of F_2 we have used the following identity:

$$\int_{\mathcal{E}}\left((\{\!\{\mathbf{u}_h\}\!\}\otimes\{\!\{\rho_h\mathbf{u}_h\}\!\}) : [\![\mathbf{u}_h]\!]_{\otimes} - \frac{1}{2}[\![|\mathbf{u}_h|^2]\!]\cdot\{\!\{\rho_h\mathbf{u}_h\}\!\}\right) ds = 0. \tag{4.3.64}$$

In view of the above discussion, the spatially mixed discrete scheme for the Lowengrub-Truskinovsky model equations can be rewritten as follows. Find

$$\begin{aligned} (c_h,\mathbf{u}_h,\bar{p}_h,\mu_h,\mathbf{q}_h) \quad \in \quad & L^2(0,T;\mathbb{V})\times L^2(0,T;\mathbb{V}_0^2)\times L^2(0,T;\mathbb{V})\times \\ & L^2(0,T;\mathbb{V})\times L^2(0,T;\mathbb{V}_{\mathbf{n}}) \end{aligned}$$

such that

$$0 = \sum_{T\in\mathscr{T}_h}\int_T (\rho_h(\partial_t c_h)X + \rho_h(\mathbf{u}_h\cdot\nabla)c_hX)\,dx$$
$$+\int_{\mathcal{E}}([\![\rho_h\mathbf{u}_h]\!]\{\!\{c_hX\}\!\} - [\![c_h\mathbf{u}_h]\!]\{\!\{\rho_hX\}\!\})\,ds - \frac{1}{\mathbb{P}e}\mathcal{A}(\mu_h,X), \tag{4.3.65}$$

$$\begin{aligned} 0 = \sum_{T\in\mathscr{T}_h}\int_T \Big(&\sqrt{\rho_h}\,\partial_t(\sqrt{\rho_h}\mathbf{u}_h)\cdot\boldsymbol{\xi} + \rho_h(\mathbf{u}_h\cdot\nabla)\mathbf{u}_h\cdot\boldsymbol{\xi} + \frac{1}{2}\operatorname{div}(\rho_h\mathbf{u}_h)\mathbf{u}_h\cdot\boldsymbol{\xi} \\ &+\frac{1}{\mathbb{M}}\rho_h\nabla\bar{p}_h\cdot\boldsymbol{\xi} + \frac{1}{\mathbb{M}}\rho_hc_h\nabla\mu_h\cdot\boldsymbol{\xi} \\ &+\frac{\rho_0}{\mathbb{F}r^2\rho_h}y\nabla\rho_h\cdot\boldsymbol{\xi} + \frac{1}{\mathbb{F}r^2}(\rho_h-\rho_0)\hat{\mathbf{j}}\cdot\boldsymbol{\xi}\Big)dx \\ +\int_{\mathcal{E}}\Big(&-\frac{1}{\mathbb{M}}[\![\bar{p}_h]\!]\cdot\{\!\{\rho_h\boldsymbol{\xi}\}\!\} - (\{\!\{\boldsymbol{\xi}\}\!\}\otimes\{\!\{\rho_h\mathbf{u}_h\}\!\}) : [\![\mathbf{u}_h]\!]_{\otimes} - \frac{1}{2}[\![\rho_h\mathbf{u}_h]\!]\{\!\{\mathbf{u}_h\cdot\boldsymbol{\xi}\}\!\} \\ &-\frac{1}{\mathbb{M}}[\![\rho_h\mu_h]\!]\cdot\{\!\{c_h\boldsymbol{\xi}\}\!\} + \frac{\rho_0\,y}{\mathbb{F}r^2}\left[\!\!\left[\frac{1}{\rho_h}\right]\!\!\right]\cdot\{\!\{\rho_h\boldsymbol{\xi}\}\!\}\Big)\,ds - \frac{1}{\mathbb{R}e}\mathcal{B}(\mathbf{u}_h,\boldsymbol{\xi}), \end{aligned} \tag{4.3.66}$$

$$0 = \sum_{T\in\mathscr{T}_h}\int_T ((\partial_t\rho_h)\,Z + \operatorname{div}(\rho_h\mathbf{u}_h)Z)\,dx + \int_{\mathcal{E}}(-[\![\rho_h\mathbf{u}_h]\!]\{\!\{Z\}\!\})\,ds, \tag{4.3.67}$$

$$\begin{aligned} 0 = \sum_{T\in\mathscr{T}_h}\int_T \Big(&\Big(\rho_h + \frac{\partial\rho_h}{\partial c_h}c_h\Big)\mu_h\psi - \rho_h\mu_0(c_h)\psi + \frac{\partial\rho_h}{\partial c_h}\Big(\bar{p}_h - g_1(c_h) - \frac{\mathbb{C}}{2}|\mathbf{q}_h|^2\Big)\psi \\ &+\mathbb{C}\operatorname{div}(\rho_h\,\mathbf{q}_h)\psi + \frac{\mathbb{M}\,\rho_0\,\alpha}{\mathbb{F}r^2}\rho_hy\psi\Big)\,dx + \int_{\mathcal{E}}(-\mathbb{C}[\![\rho_h\mathbf{q}_h]\!]\{\!\{\psi\}\!\})\,ds, \end{aligned} \tag{4.3.68}$$

$$0 = \sum_{T\in\mathscr{T}_h}\int_T (\mathbf{q}_h\cdot\mathbf{T} - \nabla c_h\cdot\mathbf{T})\,dx + \int_{\mathcal{E}}([\![c_h]\!]\cdot\{\!\{\mathbf{T}\}\!\})\,ds, \tag{4.3.69}$$

$$\forall\,(X,\boldsymbol{\xi},Z,\psi,\mathbf{T})\in\mathbb{V}\times\mathbb{V}_0^2\times\mathbb{V}\times\mathbb{V}\times\mathbb{V}_{\mathbf{n}}.$$

Remark. The semi-discrete in space numerical scheme (4.3.65)-(4.3.69) preserves, at the spatially discrete level, the mass conservation property and the energy law associated to the original system. However, it does not seem possible to find numerical fluxes that, in addition to the energy law, also preserve the momentum balance, as happens in [24] and [25].

4.4 Temporal discretisation.

In this section we propose a semi-discretisation in time for our mixed formulation (4.2.35)-(4.2.39) based on a modified midpoint type scheme (see [19] and [56]) used in [27].

4.4.1 Temporally discrete mixed formulation.

Let us subdivide the time interval $[0,T]$ into N equally spaced subintervals whose endpoints are $t_0 = 0 < t_1 < \ldots < t_N = T$ and denote with Δt the timestep size, such that $t^{n+1} = t^n + \Delta t$ for all $n = 0, 1, ..., N-1$; let $h^n(\cdot)$ denote $h(\cdot, t^n)$ for a generic time-dependent function h. The temporally discrete scheme for (4.2.35)-(4.2.39) is written as follows.
Given initial conditions $(c^0, \mathbf{u}^0, \bar{p}^0, \mu^0, \mathbf{q}^0)$, for all $n = 0, 1, ..., N-1$, find

$$(c^{n+1}, \mathbf{u}^{n+1}, \bar{p}^{n+1}, \mu^{n+1}, \mathbf{q}^{n+1}) \in H^1(\Omega) \times (H^2(\Omega) \cap H_0^1(\Omega))^2 \times H^1(\Omega) \times H^2(\Omega) \times H^1_{\mathbf{n}}(\Omega)$$

such that

$$\begin{aligned}
0 &= -\frac{r(c^{n+1}, c^n)}{\alpha \rho^{n+\frac{1}{2}}} c_{\bar{t}}^{n+1} + \frac{1}{2\rho^{n+\frac{1}{2}}} \left(\left(\rho^{n+1}\right)^2 \left((\sqrt{\rho}\mathbf{u})^{n+1} \cdot \nabla \right) c^{n+1} \right. \\
&\quad \left. + (\rho^n)^2 \left((\sqrt{\rho}\mathbf{u})^{n+1} \cdot \nabla \right) c^n \right) - \frac{1}{\mathbb{P}e} \Delta \mu^{n+\frac{1}{2}}, \qquad (4.4.1) \\
\mathbf{0} &= \sqrt{\rho}^{\,n+\frac{1}{2}} (\sqrt{\rho}\mathbf{u})_{\bar{t}}^{n+1} + \rho^{n+\frac{1}{2}} \left((\sqrt{\rho}\mathbf{u})^{n+1} \cdot \nabla \right) (\sqrt{\rho}\mathbf{u})^{n+1} \\
&\quad + \frac{1}{2} \operatorname{div} \left(\rho^{n+\frac{1}{2}} (\sqrt{\rho}\mathbf{u})^{n+1} \right) (\sqrt{\rho}\mathbf{u})^{n+1} + \frac{1}{\mathbb{M}} \rho^{n+\frac{1}{2}} \nabla \bar{p}^{n+\frac{1}{2}} \\
&\quad + \frac{1}{\mathbb{M}} \rho^{n+\frac{1}{2}} c^{n+\frac{1}{2}} \nabla \mu^{n+\frac{1}{2}} + \frac{\rho_0}{\mathbb{F}r^2} y \frac{\nabla \rho^{n+\frac{1}{2}}}{\rho^{n+\frac{1}{2}}} + \frac{1}{\mathbb{F}r^2} \left(\rho^{n+\frac{1}{2}} - \rho_0 \right) \hat{\mathbf{j}} \\
&\quad - \frac{1}{\mathbb{R}e} \left(\Delta (\sqrt{\rho}\mathbf{u})^{n+1} + \frac{1}{3} \nabla \operatorname{div} (\sqrt{\rho}\mathbf{u})^{n+1} \right), \qquad (4.4.2) \\
0 &= \rho_{\bar{t}}^{n+1} + \operatorname{div} \left(\rho^{n+\frac{1}{2}} (\sqrt{\rho}\mathbf{u})^{n+1} \right), \qquad (4.4.3) \\
0 &= \left(-\frac{r(c^{n+1}, c^n)}{\alpha \rho^{n+\frac{1}{2}}} + r(c^{n+1}, c^n) c^{n+\frac{1}{2}} \right) \mu^{n+\frac{1}{2}} - \rho^{n+\frac{1}{2}} G(c^{n+1}, c^n) \\
&\quad + r(c^{n+1}, c^n) \left(\bar{p}^{n+\frac{1}{2}} - \frac{1}{2} \left(g_1 \left(c^{n+1} \right) + g_1 \left(c^n \right) \right) - \frac{\mathbb{C}}{4} \left(\mathbf{q}^{n+1} \cdot \mathbf{q}^{n+1} + \mathbf{q}^n \cdot \mathbf{q}^n \right) \right) \\
&\quad + \mathbb{C} \operatorname{div} \left(\rho^{n+\frac{1}{2}} \mathbf{q}^{n+\frac{1}{2}} \right) - \frac{\mathbb{M}\, \rho_0}{\mathbb{F}r^2}\, y\, \frac{r(c^{n+1}, c^n)}{\rho^{n+\frac{1}{2}}}, \qquad (4.4.4) \\
\mathbf{0} &= \mathbf{q}^{n+\frac{1}{2}} - \nabla c^{n+\frac{1}{2}}. \qquad (4.4.5)
\end{aligned}$$

In (4.4.1)-(4.4.5) we have considered

$$c_{\bar{t}}^{n+1} := \frac{c^{n+1} - c^n}{\Delta t}, \quad \rho_{\bar{t}}^{n+1} := \frac{\rho^{n+1} - \rho^n}{\Delta t}, \quad (\sqrt{\rho}\mathbf{u})_{\bar{t}}^{n+1} := \frac{\sqrt{\rho^{n+1}}\mathbf{u}^{n+1} - \sqrt{\rho^n}\mathbf{u}^n}{\Delta t},$$
$$\rho^{n+1} := \frac{\rho_1 \rho_2}{(\rho_2 - \rho_1) c^{n+1} + \rho_1}, \qquad (\sqrt{\rho}\mathbf{u})^{n+1} := \frac{\sqrt{\rho^{n+1}}\mathbf{u}^{n+1} + \sqrt{\rho^n}\mathbf{u}^n}{\sqrt{\rho^{n+1}} + \sqrt{\rho^n}}.$$

We have used, for simplicity,

$$h^{n+\frac{1}{2}} := \frac{h^n + h^{n+1}}{2}$$

for a generic function h. In the temporal scheme, the modified midpoint approximation $G(c^{n+1}, c^n)$ of the potential term has been used:

$$G(c^{n+1}, c^n) := \frac{g_1\left(c^{n+1}\right) - g_1\left(c^n\right)}{c^{n+1} - c^n} \tag{4.4.6}$$

$$= \frac{1}{4}\left(c^{n+1}\left(c^{n+1} - 1\right) + c^n\left(c^n - 1\right)\right)\left(c^{n+1} + c^n - 1\right). \tag{4.4.7}$$

In addition, we considered the following notation

$$r(c^{n+1}, c^n) := \frac{\rho(c^{n+1}) - \rho(c^n)}{c^{n+1} - c^n} \tag{4.4.8}$$

$$= -\frac{\rho_1\rho_2(\rho_2 - \rho_1)}{\left(\left(\rho_2 - \rho_1\right)c^{n+1} + \rho_1\right)\left(\left(\rho_2 - \rho_1\right)c^n + \rho_1\right)} \tag{4.4.9}$$

as an approximation to $\partial\rho/\partial c$. Lastly we have used the following approximations for the density $\rho(c)$:

$$-\frac{r(c^{n+1}, c^n)}{\alpha\rho^{n+\frac{1}{2}}}, \quad \frac{\left(\rho^{n+1}\right)^2}{\rho^{n+\frac{1}{2}}}, \quad \frac{(\rho^n)^2}{\rho^{n+\frac{1}{2}}}. \tag{4.4.10}$$

4.4.2 Temporally discrete mass conservation.

We want to prove that the temporally discrete scheme (4.4.1)-(4.4.5) satisfies the mass conservation law.

Theorem 4.4.1 (Temporally discrete conservation of mass). *The temporally discrete scheme (4.4.1)-(4.4.5) is mass-conservative, i.e.*

$$\int_\Omega \rho(c^{n+1})\,dx = \int_\Omega \rho(c^n)\,dx, \qquad \textit{for all } n = 0, 1, ..., N-1. \tag{4.4.11}$$

Proof. Let us integrate equation (4.4.3) over the spatial domain Ω:

$$\int_\Omega \left(\rho_{\tilde{t}}^{n+1} + \operatorname{div}\left(\rho^{n+\frac{1}{2}}(\sqrt{\rho}\mathbf{u})^{n+1}\right)\right) dx = 0. \tag{4.4.12}$$

Using the fact that

$$\int_\Omega \operatorname{div}\left(\rho^{n+\frac{1}{2}}(\sqrt{\rho}\mathbf{u})^{n+1}\right) dx = \int_{\partial\Omega} \rho^{n+\frac{1}{2}}(\sqrt{\rho}\mathbf{u})^{n+1}\cdot\mathbf{n}\,ds = 0, \tag{4.4.13}$$

equation (4.4.12) can be rewritten as

$$\int_\Omega \frac{\rho(c^{n+1}) - \rho(c^n)}{\Delta t}\,dx = 0, \tag{4.4.14}$$

which implies the thesis. □

4.4.3 Temporally discrete energy dissipation law.

Let

$$E^n := \int_\Omega \left(\frac{1}{2}\rho(c^n)\left|\mathbf{u}^n\right|^2 + \frac{1}{\mathbb{M}}\rho(c^n)g_1\left(c^n\right) + \frac{\mathbb{C}}{2\,\mathbb{M}}\rho(c^n)\left|\mathbf{q}^n\right|^2 + \frac{1}{\mathbb{F}r^2}\rho(c^n)y\right) dx \tag{4.4.15}$$

be the temporally discrete version of the total energy (4.2.56), for $n = 0, 1, ..., N$. The next theorem will prove that our temporal scheme (4.4.1)-(4.4.5) preserves a temporally discrete formulation of the continuous energy dissipation law (4.2.60).

Theorem 4.4.2 (Temporally discrete energy dissipation law). *If* $(c^{n+1}, \mathbf{u}^{n+1}, \bar{p}^{n+1}, \mu^{n+1}, \mathbf{q}^{n+1})$ *is a solution of the temporally discrete system (4.4.1)-(4.4.5), then*

$$E_{\bar{t}}^{n+1} = -\frac{1}{\mathbb{P}e\mathbb{M}} \int_\Omega \left(\nabla \mu^{n+\frac{1}{2}}\right)^2 dx - \frac{1}{\mathbb{R}e} \int_\Omega \left(\left(\nabla (\sqrt{\rho}\mathbf{u})^{n+1}\right)^2 + \frac{1}{3}\left(\operatorname{div}(\sqrt{\rho}\mathbf{u})^{n+1}\right)^2 \right) dx, \tag{4.4.16}$$

for all $n = 0, 1, ..., N-1$, *where*

$$E_{\bar{t}}^{n+1} := \frac{E^{n+1} - E^n}{\Delta t}.$$

Proof. Let us test (4.4.1) by $\dfrac{\mu^{n+\frac{1}{2}}}{\mathbb{M}}$ and (4.4.2) by $(\sqrt{\rho}\mathbf{u})^{n+1}$ and sum them together:

$$\begin{aligned}
0 = \int_\Omega \Bigg(& -\frac{1}{\mathbb{M}} \frac{r(c^{n+1}, c^n)}{\alpha \rho^{n+\frac{1}{2}}} \mu^{n+\frac{1}{2}} \frac{c^{n+1} - c^n}{\Delta t} + \frac{\mu^{n+\frac{1}{2}}}{2\rho^{n+\frac{1}{2}}\mathbb{M}} \left(\left(\rho^{n+1}\right)^2 \left((\sqrt{\rho}\mathbf{u})^{n+1} \cdot \nabla \right) c^{n+1} \right. \\
& \left. + (\rho^n)^2 \left((\sqrt{\rho}\mathbf{u})^{n+1} \cdot \nabla \right) c^n \right) - \frac{1}{\mathbb{P}e\mathbb{M}} \mu^{n+\frac{1}{2}} \Delta \mu^{n+\frac{1}{2}} + \sqrt{\rho}^{\,n+\frac{1}{2}} ((\sqrt{\rho}\mathbf{u})_{\bar{t}}^{n+1}) \cdot (\sqrt{\rho}\mathbf{u})^{n+1} \\
& + \rho^{n+\frac{1}{2}} \left((\sqrt{\rho}\mathbf{u})^{n+1} \cdot \nabla \right) (\sqrt{\rho}\mathbf{u})^{n+1} \cdot (\sqrt{\rho}\mathbf{u})^{n+1} \\
& + \frac{1}{2} \operatorname{div}\left(\rho^{n+\frac{1}{2}} (\sqrt{\rho}\mathbf{u})^{n+1} \right) (\sqrt{\rho}\mathbf{u})^{n+1} \cdot (\sqrt{\rho}\mathbf{u})^{n+1} \\
& + \frac{1}{\mathbb{M}} \rho^{n+\frac{1}{2}} \nabla \bar{p}^{n+\frac{1}{2}} \cdot (\sqrt{\rho}\mathbf{u})^{n+1} + \frac{1}{\mathbb{M}} \rho^{n+\frac{1}{2}} c^{n+\frac{1}{2}} \nabla \mu^{n+\frac{1}{2}} \cdot (\sqrt{\rho}\mathbf{u})^{n+1} \\
& - \frac{1}{\mathbb{R}e} \left(\Delta (\sqrt{\rho}\mathbf{u})^{n+1} \cdot (\sqrt{\rho}\mathbf{u})^{n+1} + \frac{1}{3} \nabla \operatorname{div} (\sqrt{\rho}\mathbf{u})^{n+1} \cdot (\sqrt{\rho}\mathbf{u})^{n+1} \right) \\
& + \frac{\rho_0\, y}{\mathbb{F}r^2 \rho^{n+\frac{1}{2}}} \nabla \rho^{n+\frac{1}{2}} \cdot (\sqrt{\rho}\mathbf{u})^{n+1} + \frac{1}{\mathbb{F}r^2} \left(\rho^{n+\frac{1}{2}} - \rho_0 \right) \hat{\mathbf{j}} \cdot (\sqrt{\rho}\mathbf{u})^{n+1} \Bigg)\, dx.
\end{aligned} \tag{4.4.17}$$

Integration by parts of the terms containing, respectively, $\nabla \bar{p}^{n+\frac{1}{2}}$ and $\Delta \mu^{n+\frac{1}{2}}$, and of viscous terms leads to

$$\begin{aligned}
0 = \int_\Omega \Bigg(& -\frac{1}{\mathbb{M}} \frac{r(c^{n+1}, c^n)}{\alpha \rho^{n+\frac{1}{2}}} \mu^{n+\frac{1}{2}} \frac{c^{n+1} - c^n}{\Delta t} + \frac{\mu^{n+\frac{1}{2}}}{2\rho^{n+\frac{1}{2}}\mathbb{M}} \left(\left(\rho^{n+1}\right)^2 \left((\sqrt{\rho}\mathbf{u})^{n+1} \cdot \nabla \right) c^{n+1} \right. \\
& \left. + (\rho^n)^2 \left((\sqrt{\rho}\mathbf{u})^{n+1} \cdot \nabla \right) c^n \right) + \sqrt{\rho}^{\,n+\frac{1}{2}} ((\sqrt{\rho}\mathbf{u})_{\bar{t}}^{n+1}) \cdot (\sqrt{\rho}\mathbf{u})^{n+1} \\
& + \rho^{n+\frac{1}{2}} \left((\sqrt{\rho}\mathbf{u})^{n+1} \cdot \nabla \right) (\sqrt{\rho}\mathbf{u})^{n+1} \cdot (\sqrt{\rho}\mathbf{u})^{n+1} \\
& + \frac{1}{2} \operatorname{div}\left(\rho^{n+\frac{1}{2}} (\sqrt{\rho}\mathbf{u})^{n+1} \right) (\sqrt{\rho}\mathbf{u})^{n+1} \cdot (\sqrt{\rho}\mathbf{u})^{n+1} \\
& - \frac{1}{\mathbb{M}} \bar{p}^{n+\frac{1}{2}} \operatorname{div}\left(\rho^{n+\frac{1}{2}} (\sqrt{\rho}\mathbf{u})^{n+1} \right) + \frac{1}{\mathbb{M}} \rho^{n+\frac{1}{2}} c^{n+\frac{1}{2}} \nabla \mu^{n+\frac{1}{2}} \cdot (\sqrt{\rho}\mathbf{u})^{n+1} \\
& + \frac{\rho_0\, y}{\mathbb{F}r^2 \rho^{n+\frac{1}{2}}} \nabla \rho^{n+\frac{1}{2}} \cdot (\sqrt{\rho}\mathbf{u})^{n+1} + \frac{1}{\mathbb{F}r^2} \left(\rho^{n+\frac{1}{2}} - \rho_0 \right) \hat{\mathbf{j}} \cdot (\sqrt{\rho}\mathbf{u})^{n+1} \\
& + \frac{1}{\mathbb{P}e\mathbb{M}} \left(\nabla \mu^{n+\frac{1}{2}} \right)^2 + \frac{1}{\mathbb{R}e} \left(\left(\nabla (\sqrt{\rho}\mathbf{u})^{n+1} \right)^2 + \frac{1}{3} \left(\operatorname{div} (\sqrt{\rho}\mathbf{u})^{n+1} \right)^2 \right) \Bigg)\, dx.
\end{aligned} \tag{4.4.18}$$

Using local mass conservation equation (4.4.3) into (4.4.18), we obtain:

$$
\begin{aligned}
0 = \int_\Omega \Bigg(& -\frac{\mu^{n+\frac{1}{2}}}{\mathbb{M}} \frac{r(c^{n+1},c^n)}{\alpha\rho^{n+\frac{1}{2}}} \frac{c^{n+1}-c^n}{\Delta t} + \frac{\mu^{n+\frac{1}{2}}}{2\rho^{n+\frac{1}{2}}\mathbb{M}} \left(\left(\rho^{n+1}\right)^2 \left((\sqrt{\rho}\mathbf{u})^{n+1}\cdot\nabla\right) c^{n+1}\right. \\
& \left. + (\rho^n)^2 \left((\sqrt{\rho}\mathbf{u})^{n+1}\cdot\nabla\right) c^n\right) + \sqrt{\rho}^{\,n+\frac{1}{2}} (\sqrt{\rho}\mathbf{u})^{n+1}\cdot(\sqrt{\rho}\mathbf{u})_{\bar{t}}^{n+1} \\
& + \rho^{n+\frac{1}{2}} \left((\sqrt{\rho}\mathbf{u})^{n+1}\cdot\nabla\right)(\sqrt{\rho}\mathbf{u})^{n+1}\cdot(\sqrt{\rho}\mathbf{u})^{n+1} \\
& + \frac{1}{2}\,\mathrm{div}\left(\rho^{n+\frac{1}{2}}(\sqrt{\rho}\mathbf{u})^{n+1}\right)(\sqrt{\rho}\mathbf{u})^{n+1}\cdot(\sqrt{\rho}\mathbf{u})^{n+1} \\
& + \frac{\bar{p}^{n+\frac{1}{2}}}{\mathbb{M}}(\rho_{\bar{t}}^{n+1}) + \frac{1}{\mathbb{M}}\rho^{n+\frac{1}{2}} c^{n+\frac{1}{2}} \nabla\mu^{n+\frac{1}{2}}\cdot(\sqrt{\rho}\mathbf{u})^{n+1} \\
& + \frac{\rho_0\, y}{\mathbb{F}r^2\rho^{n+\frac{1}{2}}}\nabla\rho^{n+\frac{1}{2}}\cdot(\sqrt{\rho}\mathbf{u})^{n+1} + \frac{1}{\mathbb{F}r^2}\left(\rho^{n+\frac{1}{2}}-\rho_0\right)\hat{\mathbf{j}}\cdot(\sqrt{\rho}\mathbf{u})^{n+1} \\
& + \frac{1}{\mathbb{P}e\mathbb{M}}\left(\nabla\mu^{n+\frac{1}{2}}\right)^2 + \frac{1}{\mathbb{R}e}\left(\left(\nabla(\sqrt{\rho}\mathbf{u})^{n+1}\right)^2 + \frac{1}{3}\left(\mathrm{div}(\sqrt{\rho}\mathbf{u})^{n+1}\right)^2\right)\Bigg)\, dx.
\end{aligned}
\tag{4.4.19}
$$

If we notice that

$$
\begin{aligned}
& \int_\Omega \Big(\rho^{n+\frac{1}{2}} \left((\sqrt{\rho}\mathbf{u})^{n+1}\cdot\nabla\right)(\sqrt{\rho}\mathbf{u})^{n+1}\cdot(\sqrt{\rho}\mathbf{u})^{n+1} \\
& + \frac{1}{2}\,\mathrm{div}\left(\rho^{n+\frac{1}{2}}(\sqrt{\rho}\mathbf{u})^{n+1}\right)(\sqrt{\rho}\mathbf{u})^{n+1}\cdot(\sqrt{\rho}\mathbf{u})^{n+1}\Big) \quad = \quad 0
\end{aligned}
\tag{4.4.20}
$$

and if we use the definition of $-\dfrac{r(c^{n+1},c^n)}{\alpha\rho^{n+\frac{1}{2}}}\mu^{n+\frac{1}{2}}$ from (4.4.4), we can rewrite (4.4.19) as

$$
\begin{aligned}
0 = \int_\Omega \Bigg(& \sqrt{\rho}^{\,n+\frac{1}{2}} (\sqrt{\rho}\mathbf{u})_{\bar{t}}^{n+1}\cdot(\sqrt{\rho}\mathbf{u})^{n+1} + \rho^{n+\frac{1}{2}} \frac{g_1\left(c^{n+1}\right)-g_1\left(c^n\right)}{c^{n+1}-c^n}\frac{c^{n+1}-c^n}{\mathbb{M}\Delta t} \\
& + r(c^{n+1},c^n)\frac{g_1\left(c^{n+1}\right)+g_1\left(c^n\right)}{2}\frac{c^{n+1}-c^n}{\mathbb{M}\Delta t} \\
& + \frac{\mathbb{C}(c^{n+1}-c^n)}{\mathbb{M}\Delta t}\frac{r(c^{n+1},c^n)}{4}\left(|\mathbf{q}^{n+1}|^2+|\mathbf{q}^n|^2\right) - \frac{\mathbb{C}(c^{n+1}-c^n)}{\mathbb{M}\Delta t}\,\mathrm{div}(\rho^{n+\frac{1}{2}}\mathbf{q}^{n+\frac{1}{2}}) \\
& + \frac{\rho_0}{\mathbb{F}r^2}\frac{r(c^{n+1},c^n)}{\rho^{n+\frac{1}{2}}} y \frac{c^{n+1}-c^n}{\mathbb{M}\Delta t} + \frac{\rho_0\, y}{\mathbb{F}r^2\rho^{n+\frac{1}{2}}}\nabla\rho^{n+\frac{1}{2}}\cdot(\sqrt{\rho}\mathbf{u})^{n+1} \\
& + \frac{1}{\mathbb{F}r^2}\left(\rho^{n+\frac{1}{2}}-\rho_0\right)\hat{\mathbf{j}}\cdot(\sqrt{\rho}\mathbf{u})^{n+1} - \mu^{n+\frac{1}{2}}c^{n+\frac{1}{2}}r(c^{n+1},c^n)\frac{c^{n+1}-c^n}{\mathbb{M}\Delta t} \\
& + \frac{\mu^{n+\frac{1}{2}}}{2\mathbb{M}\rho^{n+\frac{1}{2}}}\left(\left(\rho^{n+1}\right)^2\left((\sqrt{\rho}\mathbf{u})^{n+1}\cdot\nabla\right)c^{n+1} + (\rho^n)^2\left((\sqrt{\rho}\mathbf{u})^{n+1}\cdot\nabla\right)c^n\right) \\
& + \frac{1}{\mathbb{M}}\rho^{n+\frac{1}{2}}c^{n+\frac{1}{2}}\nabla\mu^{n+\frac{1}{2}}\cdot(\sqrt{\rho}\mathbf{u})^{n+1} \\
& + \frac{1}{\mathbb{P}e\mathbb{M}}\left(\nabla\mu^{n+\frac{1}{2}}\right)^2 + \frac{1}{\mathbb{R}e}\left(\left(\nabla(\sqrt{\rho}\mathbf{u})^{n+1}\right)^2 + \frac{1}{3}\left(\mathrm{div}(\sqrt{\rho}\mathbf{u})^{n+1}\right)^2\right)\Bigg)\, dx.
\end{aligned}
\tag{4.4.21}
$$

We obtain the following relations:

(I) the first term in (4.4.21) is

$$
\int_\Omega \sqrt{\rho}^{\,n+\frac{1}{2}}(\sqrt{\rho}\mathbf{u})_{\bar{t}}^{n+1}\cdot(\sqrt{\rho}\mathbf{u})^{n+1}\,dx = \int_\Omega \frac{1}{2\Delta t}\left(\rho^{n+1}\left(\mathbf{u}^{n+1}\right)^2 - \rho^n\left(\mathbf{u}^n\right)^2\right)\,dx,
\tag{4.4.22}
$$

(II) the terms containing the double-well potential $g_1\left(c^{n+1}\right)$ are

$$\begin{aligned}
&\int_\Omega\left(\rho^{n+\frac{1}{2}}\frac{g_1\left(c^{n+1}\right)-g_1\left(c^n\right)}{\mathbb{M}\Delta t}+r(c^{n+1},c^n)\frac{g_1\left(c^{n+1}\right)+g_1\left(c^n\right)}{2}\frac{c^{n+1}-c^n}{\mathbb{M}\Delta t}\right)dx\\
=\;&\int_\Omega\left(\frac{1}{\mathbb{M}\Delta t}\left(\rho^{n+1}g_1\left(c^{n+1}\right)-\rho^n g_1\left(c^n\right)\right)\right)dx, \qquad (4.4.23)
\end{aligned}$$

(III) integrating by parts, the terms containing the variable $\mathbf{q}^{n+1}$ are

$$\begin{aligned}
&\int_\Omega\left(\frac{\mathbb{C}(c^{n+1}-c^n)}{\mathbb{M}\Delta t}\frac{r(c^{n+1},c^n)}{4}\left(|\mathbf{q}^{n+1}|^2+|\mathbf{q}^n|^2\right)\right.\\
&\qquad\left.-\frac{\mathbb{C}(c^{n+1}-c^n)}{\mathbb{M}\Delta t}\operatorname{div}(\rho^{n+\frac{1}{2}}\mathbf{q}^{n+\frac{1}{2}})\right)dx\\
=\;&\int_\Omega\left(\frac{\rho^{n+1}-\rho^n}{\mathbb{M}\Delta t}\frac{\mathbb{C}}{4}\left(|\mathbf{q}^{n+1}|^2+|\mathbf{q}^n|^2\right)\right.\\
&\qquad\left.+\left(\rho^{n+1}+\rho^n\right)\frac{\mathbb{C}(\mathbf{q}^{n+1}-\mathbf{q}^n)}{4\mathbb{M}\Delta t}\cdot\left(\mathbf{q}^{n+1}+\mathbf{q}^n\right)\right)dx\\
=\;&\int_\Omega\frac{\mathbb{C}}{\mathbb{M}\Delta t}\frac{1}{2}\left(\rho^{n+1}(\mathbf{q}^{n+1})^2-\rho^n(\mathbf{q}^n)^2\right)dx, \qquad (4.4.24)
\end{aligned}$$

(IV) integrating by parts, using the definition of $\hat{\mathbf{j}}$ and local mass conservation (4.4.3), gravity terms can be rewritten as

$$\begin{aligned}
&\int_\Omega\left(\frac{\rho_0}{\mathbb{F}r^2}\frac{r(c^{n+1},c^n)}{\rho^{n+\frac{1}{2}}}y\frac{c^{n+1}-c^n}{\mathbb{M}\Delta t}+\frac{\rho_0\,y}{\mathbb{F}r^2\rho^{n+\frac{1}{2}}}\nabla\rho^{n+\frac{1}{2}}\cdot(\sqrt{\rho}\mathbf{u})^{n+1}\right.\\
&\qquad\left.+\frac{1}{\mathbb{F}r^2}\left(\rho^{n+\frac{1}{2}}-\rho_0\right)\hat{\mathbf{j}}\cdot(\sqrt{\rho}\mathbf{u})^{n+1}\right)dx\\
=\;&\int_\Omega\left(\frac{\rho_0}{\mathbb{F}r^2\rho^{n+\frac{1}{2}}}\left(\rho_{\bar{t}}^{n+1}+\nabla\rho^{n+\frac{1}{2}}\cdot(\sqrt{\rho}\mathbf{u})^{n+1}+\rho^{n+\frac{1}{2}}\operatorname{div}\left((\sqrt{\rho}\mathbf{u})^{n+1}\right)\right)y\right.\\
&\qquad\left.+\frac{1}{\mathbb{F}r^2}\rho_{\bar{t}}^{n+1}y\right)dx\\
=\;&\int_\Omega\left(\frac{1}{\mathbb{F}r^2}\frac{\rho^{n+1}-\rho^n}{\Delta t}y\right)dx, \qquad (4.4.25)
\end{aligned}$$

(V) using integration by parts and local mass conservation (4.4.3),

$$\begin{aligned}
&\int_\Omega\left(\frac{\mu^{n+\frac{1}{2}}}{2\mathbb{M}\rho^{n+\frac{1}{2}}}\left(\left(\rho^{n+1}\right)^2\left((\sqrt{\rho}\mathbf{u})^{n+1}\cdot\nabla\right)c^{n+1}+\left(\rho^n\right)^2\left((\sqrt{\rho}\mathbf{u})^{n+1}\cdot\nabla\right)c^n\right)\right.\\
&\qquad\left.+\frac{1}{\mathbb{M}}\rho^{n+\frac{1}{2}}c^{n+\frac{1}{2}}\nabla\mu^{n+\frac{1}{2}}\cdot(\sqrt{\rho}\mathbf{u})^{n+1}\right)dx\\
=&\int_\Omega\left(-\frac{\rho^{n+1}-\rho^n}{\mathbb{M}\Delta t}\mu^{n+\frac{1}{2}}c^{n+\frac{1}{2}}\right.\\
&\qquad\left.+\frac{1}{\mathbb{M}}\left(\rho^{n+\frac{1}{2}}(\sqrt{\rho}\mathbf{u})^{n+1}\right)\cdot(\mu^{n+\frac{1}{2}}\nabla c^{n+\frac{1}{2}}+c^{n+\frac{1}{2}}\nabla\mu^{n+\frac{1}{2}})\right)dx\\
=&\int_\Omega\left(-\frac{1}{\mathbb{M}}c^{n+\frac{1}{2}}\mu^{n+\frac{1}{2}}\left(\rho_{\bar{t}}^{n+1}+\operatorname{div}(\rho^{n+\frac{1}{2}}(\sqrt{\rho}\mathbf{u})^{n+1})\right)\right)dx=0. \qquad (4.4.26)
\end{aligned}$$

Identities (4.4.22)-(4.4.26) into (4.4.21) give

$$\begin{aligned} 0 \;=\; & \int_\Omega \frac{1}{\Delta t}\left(\frac{1}{2}\left(\rho^{n+1}(\mathbf{u}^{n+1})^2-\rho^n(\mathbf{u}^n)^2\right)+\frac{1}{\mathbb{M}\Delta t}\left(\rho^{n+1}g_1\left(c^n\right)-\rho^n g_1\left(c^n\right)\right)\right. \\ & \left.+\frac{\mathbb{C}}{\mathbb{M}\Delta t}\left(\rho^{n+1}(\mathbf{q}^{n+1})^2-\rho^n(\mathbf{q}^n)^2\right)+\frac{1}{\mathbb{F}r^2\Delta t}(\rho^{n+1}-\rho^n)y\right)dx \\ & +\frac{1}{\mathbb{P}e\mathbb{M}}\int_\Omega\left(\nabla\mu^{n+\frac{1}{2}}\right)^2dx+\frac{1}{\mathbb{R}e}\int_\Omega\left(\left(\nabla(\sqrt{\rho}\mathbf{u})^{n+1}\right)^2+\frac{1}{3}\left(\mathrm{div}(\sqrt{\rho}\mathbf{u})^{n+1}\right)^2\right)dx \end{aligned} \tag{4.4.27}$$

that is equivalent to the thesis (4.4.16). □

4.5 Fully discrete energy consistent DG numerical method.

In this section we propose a fully discretisation of the mixed system (4.2.35)-(4.2.39), based on the spatial discretisation presented in Section 4.3 and on the temporal discretisation introduced in Section 4.4.

4.5.1 Fully discrete mixed formulation.

The fully discrete mixed formulation of (4.2.35)-(4.2.39) can be written as follows: given initial conditions $(c_h^0,\mathbf{u}_h^0,\bar{p}_h^0,\mu_h^0,\mathbf{q}_h^0)$, for all $n=0,1,...,N-1$, find

$$(c_h^{n+1},\mathbf{u}_h^{n+1},\bar{p}_h^{n+1},\mu_h^{n+1},\mathbf{q}_h^{n+1})\in\mathbb{V}\times\mathbb{V}_0^2\times\mathbb{V}\times\mathbb{V}\times\mathbb{V}_{\mathbf{n}}$$

such that

$$\begin{aligned} 0 \;=\; & \sum_{T\in\mathscr{T}_h}\int_T\left(-\frac{r(c_h^{n+1},c_h^n)}{\alpha\rho_h^{n+\frac{1}{2}}}(c_h)_{\bar{t}}^{n+1}+\frac{1}{2\rho_h^{n+\frac{1}{2}}}\left(\left(\rho_h^{n+1}\right)^2\left((\sqrt{\rho_h}\mathbf{u}_h)^{n+1}\cdot\nabla\right)c_h^{n+1}\right.\right. \\ & \left.\left.+\left(\rho_h^n\right)^2\left((\sqrt{\rho_h}\mathbf{u}_h)^{n+1}\cdot\nabla\right)c_h^n\right)\right)Xdx-\frac{1}{\mathbb{P}e}\mathcal{A}(\mu_h^{n+\frac{1}{2}},X) \\ & +\int_{\mathcal{E}}\left(\left[\!\left[\rho_h^{n+\frac{1}{2}}(\sqrt{\rho_h}\mathbf{u}_h)^{n+1}\right]\!\right]\left\{\!\left\{c_h^{n+\frac{1}{2}}X\right\}\!\right\}\right. \\ & \left.-\left[\!\left[c_h^{n+\frac{1}{2}}(\sqrt{\rho_h}\mathbf{u}_h)^{n+1}\right]\!\right]\left\{\!\left\{\rho_h^{n+\frac{1}{2}}X\right\}\!\right\}\right)ds \end{aligned} \tag{4.5.1}$$

$$
\begin{aligned}
0 \;=\; & \sum_{T\in\mathscr{T}_h}\int_T \Big(\sqrt{\rho_h}^{\,n+\frac12}(\sqrt{\rho_h}\mathbf{u}_h)_{\bar t}^{n+1}+\rho_h^{n+\frac12}\big((\sqrt{\rho_h}\mathbf{u}_h)^{n+1}\cdot\nabla\big)(\sqrt{\rho_h}\mathbf{u}_h)^{n+1}\\
&\quad+\frac12\,\mathrm{div}\left(\rho_h^{n+\frac12}(\sqrt{\rho_h}\mathbf{u}_h)^{n+1}\right)(\sqrt{\rho_h}\mathbf{u}_h)^{n+1}\\
&\quad+\frac{1}{\mathbb{M}}\rho_h^{n+\frac12}\nabla\bar p_h^{n+\frac12}+\frac{1}{\mathbb{M}}\rho_h^{n+\frac12}c_h^{n+\frac12}\nabla\mu_h^{n+\frac12}\\
&\quad+\frac{\rho_0}{\mathbb{F}r^2}y\frac{\nabla\rho_h^{n+\frac12}}{\rho_h^{n+\frac12}}+\frac{1}{\mathbb{F}r^2}\left(\rho_h^{n+\frac12}-\rho_0\right)\hat{\mathbf{j}}\Big)\cdot\boldsymbol{\xi}\,dx-\frac{1}{\mathbb{R}e}\mathcal{B}((\sqrt{\rho_h}\mathbf{u}_h)^{n+1},\boldsymbol{\xi})\\
&+\int_{\mathcal{E}}\Big(-\frac{1}{\mathbb{M}}\left[\!\left[\bar p_h^{n+\frac12}\right]\!\right]\cdot\left\{\!\left\{\rho_h^{n+\frac12}\boldsymbol{\xi}\right\}\!\right\}\\
&\quad-\left(\{\!\{\boldsymbol{\xi}\}\!\}\otimes\left\{\!\left\{\rho_h^{n+\frac12}(\sqrt{\rho_h}\mathbf{u}_h)^{n+1}\right\}\!\right\}\right):[\![(\sqrt{\rho_h}\mathbf{u}_h)^{n+1}]\!]_{\otimes}\\
&\quad-\frac12\left[\!\left[\rho_h^{n+\frac12}(\sqrt{\rho_h}\mathbf{u}_h)^{n+1}\right]\!\right]\{\!\{(\sqrt{\rho_h}\mathbf{u}_h)^{n+1}\cdot\boldsymbol{\xi}\}\!\}\\
&\quad+\frac{\rho_0\,y}{\mathbb{F}r^2}\left[\!\left[\frac{1}{\rho_h^{n+\frac12}}\right]\!\right]\cdot\left\{\!\left\{\rho_h^{n+\frac12}\boldsymbol{\xi}\right\}\!\right\}-\frac{1}{\mathbb{M}}\left[\!\left[\rho_h^{n+\frac12}\mu_h^{n+\frac12}\right]\!\right]\cdot\left\{\!\left\{c_h^{n+\frac12}\boldsymbol{\xi}\right\}\!\right\}\Big)\,ds,
\end{aligned}
\tag{4.5.2}
$$

$$
0 \;=\; \sum_{T\in\mathscr{T}_h}\int_T\Big((\rho_h)_{\bar t}^{n+1}+\mathrm{div}\Big(\rho_h^{n+\frac12}(\sqrt{\rho_h}\mathbf{u}_h)^{n+1}\Big)\Big)Z\,dx-\int_{\mathcal{E}}\left[\!\left[\rho_h^{n+\frac12}(\sqrt{\rho_h}\mathbf{u}_h)^{n+1}\right]\!\right]\{\!\{Z\}\!\}\,ds,
\tag{4.5.3}
$$

$$
\begin{aligned}
0 \;=\; & \sum_{T\in\mathscr{T}_h}\int_T\Bigg(\left(-\frac{r(c_h^{n+1},c_h^n)}{\alpha\rho_h^{n+\frac12}}+r(c_h^{n+1},c_h^n)c_h^{n+\frac12}\right)\mu_h^{n+\frac12}-\rho_h^{n+\frac12}G(c_h^{n+1},c_h^n)\\
&\quad+r(c_h^{n+1},c_h^n)\Big(\bar p_h^{n+\frac12}-\frac12\left(g_1\left(c_h^{n+1}\right)+g_1\left(c_h^n\right)\right)-\frac{\mathbb{C}}{4}\left(\mathbf{q}_h^{n+1}\cdot\mathbf{q}_h^{n+1}+\mathbf{q}_h^n\cdot\mathbf{q}_h^n\right)\Big)\\
&\quad+\mathbb{C}\,\mathrm{div}\left(\rho_h^{n+\frac12}\,\mathbf{q}_h^{n+\frac12}\right)-\frac{\mathbb{M}\,\rho_0}{\mathbb{F}r^2}\;y\;\frac{r(c_h^{n+1},c_h^n)}{\rho_h^{n+\frac12}}\Bigg)\psi\,dx\\
&-\mathbb{C}\int_{\mathcal{E}}\left[\!\left[\rho_h^{n+\frac12}\mathbf{q}_h^{n+\frac12}\right]\!\right]\{\!\{\psi\}\!\}\,ds
\end{aligned}
\tag{4.5.4}
$$

$$
0 \;=\; \sum_{T\in\mathscr{T}_h}\int_T\left(\mathbf{q}_h^{n+\frac12}-\nabla c_h^{n+\frac12}\right)\cdot\mathbf{T}\,dx+\int_{\mathcal{E}}\left[\!\left[c_h^{n+\frac12}\right]\!\right]\cdot\{\!\{\mathbf{T}\}\!\}\,ds,
\tag{4.5.5}
$$

$$
\forall\,(X,\boldsymbol{\xi},Z,\psi,\mathbf{T})\in\mathbb{V}\times\mathbb{V}_0^2\times\mathbb{V}\times\mathbb{V}\times\mathbb{V}_{\mathbf{n}}.
$$

4.5.2 Fully discrete mass conservation and energy law.

Now we can state mass conservation property and energy dissipation law for the fully discrete scheme. The proofs of these results follow from the combination of the corresponding propositions in the spatial (Theorems 4.3.2, 4.3.3) and temporal (Theorems 4.4.1, 4.4.2) approximation.

Theorem 4.5.1 (Fully discrete conservation of mass). *The fully discrete scheme (4.5.1)-(4.5.5) is mass-conservative, i.e.*

$$
\sum_{T\in\mathscr{T}_h}\int_T\rho(c_h^{n+1})\,dx=\sum_{T\in\mathscr{T}_h}\int_T\rho(c_h^n)\,dx,\qquad \textit{for all } n=0,1,...,N-1.
\tag{4.5.6}
$$

Proof. The proof follows from the results proposed by Theorems 4.3.2 and 4.4.1 which provide a spatial and a temporal semidiscrete mass conservation result, respectively. □

Theorem 4.5.2 (Fully discrete energy dissipation law). *Let*

$$E_h^n := \sum_{T\in\mathcal{T}_h}\int_T\left(\frac{1}{2}\rho(c_h^n)|\mathbf{u}_h^n|^2+\frac{1}{\mathbb{M}}\rho(c_h^n)g_1\left(c_h^n\right)+\frac{\mathbb{C}}{2\,\mathbb{M}}\rho(c_h^n)|\mathbf{q}_h^n|^2+\frac{1}{\mathbb{F}r^2}\rho(c_h^n)y\right)dx \quad (4.5.7)$$

be the fully discrete version of the total energy (4.2.56), for $n=0,1,...,N$. If $(c_h^{n+1},\mathbf{u}_h^{n+1},\bar{p}_h^{n+1},\mu_h^{n+1},\mathbf{q}_h^{n+1})$ is a solution of the fully discrete system (4.5.1)-(4.5.5), then

$$(E_h)_{\bar{t}}^{n+1} \quad = \quad \frac{1}{\mathbb{P}e\mathbb{M}}\mathcal{A}(\mu_h^{n+\frac{1}{2}},\mu_h^{n+\frac{1}{2}})+\frac{1}{\mathbb{R}e}\mathcal{B}((\sqrt{\rho_h}\mathbf{u}_h)^{n+1},(\sqrt{\rho_h}\mathbf{u}_h)^{n+1}), \quad (4.5.8)$$

for all $n=0,1,...,N-1$, where

$$(E_h)_{\bar{t}}^{n+1} := \frac{E_h^{n+1}-E_h^n}{\Delta t}$$

and $\mathcal{A},\mathcal{B}$ are negative definite, by definition.

Proof. The proof consists in the application of the results proposed by Theorems 4.3.3 and 4.4.2 which provide a spatial and a temporal semidiscrete energy dissipation law, respectively. □

4.6 Numerical experiments.

Numerical simulations have been performed using FreeFem++ platform [28]. FreeFem++ has the possibility to implement a Discontinuous Galerkin algorithm. However, some technical difficulties have arisen in the implementation of the non-conventional numerical fluxes $F_1,...,F_5$. This fact, together with the high computational cost required for this kind of problems suggested us to use conforming finite elements to perform the first numerical tests. So, using the consistency property of numerical fluxes $F_1,...,F_5$, we can rewrite the fully discrete formulation as follows. If $\mathbb{V}^*,\mathbb{V}_0^*$ and $\mathbb{V}_{\mathbf{n}}^*$ are the **continuous** counterparts of $\mathbb{V},\mathbb{V}_0$ and $\mathbb{V}_{\mathbf{n}}$, given initial conditions $(c_h^0,\mathbf{u}_h^0,\bar{p}_h^0,\mu_h^0,\mathbf{q}_h^0)$, for all $n=0,1,...,N-1$, we have to find

$$(c_h^{n+1},\mathbf{u}_h^{n+1},\bar{p}_h^{n+1},\mu_h^{n+1},\mathbf{q}_h^{n+1})\in\mathbb{V}^*\times(\mathbb{V}_0^*)^2\times\mathbb{V}^*\times\mathbb{V}^*\times\mathbb{V}_{\mathbf{n}}^*$$

such that

$$\begin{aligned}0 \;=\int_\Omega\Bigg(&-\frac{r(c_h^{n+1},c_h^n)}{\alpha\rho_h^{n+\frac{1}{2}}}(c_h)_{\bar{t}}^{n+1}X+\frac{1}{2\rho_h^{n+\frac{1}{2}}}\left(\left(\rho_h^{n+1}\right)^2\left((\sqrt{\rho_h}\mathbf{u}_h)^{n+1}\cdot\nabla\right)c_h^{n+1}\right.\\&\left.+\left(\rho_h^n\right)^2\left((\sqrt{\rho_h}\mathbf{u}_h)^{n+1}\cdot\nabla\right)c_h^n\right)X+\frac{1}{\mathbb{P}e}\nabla\mu_h^{n+\frac{1}{2}}\cdot\nabla X\Bigg)\,dx\end{aligned} \quad (4.6.1)$$

$$
\begin{aligned}
0 \;=& \int_\Omega \Bigg(\sqrt{\rho_h}^{\,n+\frac{1}{2}} (\sqrt{\rho_h}\mathbf{u}_h)_{\bar{t}}^{n+1} \cdot \boldsymbol{\xi} + \rho_h^{n+\frac{1}{2}} \big((\sqrt{\rho_h}\mathbf{u}_h)^{n+1} \cdot \nabla \big) (\sqrt{\rho_h}\mathbf{u}_h)^{n+1} \cdot \boldsymbol{\xi} \\
&+ \frac{1}{2} \operatorname{div} \left(\rho_h^{n+\frac{1}{2}} (\sqrt{\rho_h}\mathbf{u}_h)^{n+1} \right) (\sqrt{\rho_h}\mathbf{u}_h)^{n+1} \cdot \boldsymbol{\xi} \\
&+ \frac{1}{\mathbb{M}} \rho_h^{n+\frac{1}{2}} \nabla \bar{p}_h^{n+\frac{1}{2}} \cdot \boldsymbol{\xi} + \frac{1}{\mathbb{M}} \rho_h^{n+\frac{1}{2}} c_h^{n+\frac{1}{2}} \nabla \mu_h^{n+\frac{1}{2}} \cdot \boldsymbol{\xi} \\
&+ \frac{\rho_0}{\mathbb{F}r^2} y \frac{\nabla \rho_h^{n+\frac{1}{2}}}{\rho_h^{n+\frac{1}{2}}} \cdot \boldsymbol{\xi} + \frac{1}{\mathbb{F}r^2} \left(\rho_h^{n+\frac{1}{2}} - \rho_0 \right) \hat{\mathbf{j}} \cdot \boldsymbol{\xi} \\
&+ \frac{1}{\mathbb{R}e} \left(\nabla (\sqrt{\rho_h}\mathbf{u}_h)^{n+1} + \frac{1}{3} \operatorname{div} ((\sqrt{\rho_h}\mathbf{u}_h)^{n+1}) \mathbb{I} \right) : \nabla \boldsymbol{\xi} \Bigg) \, dx
\end{aligned} \tag{4.6.2}
$$

$$
0 = \int_\Omega \left((\rho_h)_{\bar{t}}^{n+1} + \operatorname{div} \left(\rho_h^{n+\frac{1}{2}} (\sqrt{\rho_h}\mathbf{u}_h)^{n+1} \right) \right) Z \, dx \tag{4.6.3}
$$

$$
\begin{aligned}
0 \;=& \int_\Omega \Bigg(\left(-\frac{r(c_h^{n+1}, c_h^n)}{\alpha \rho_h^{n+\frac{1}{2}}} + r(c_h^{n+1}, c_h^n) c_h^{n+\frac{1}{2}} \right) \mu_h^{n+\frac{1}{2}} - \rho_h^{n+\frac{1}{2}} G(c_h^{n+1}, c_h^n) \\
&+ r(c_h^{n+1}, c_h^n) \left(\bar{p}_h^{n+\frac{1}{2}} - \frac{1}{2} \left(g_1 \left(c_h^{n+1} \right) + g_1 \left(c_h^n \right) \right) - \frac{\mathbb{C}}{4} \left(\mathbf{q}_h^{n+1} \cdot \mathbf{q}_h^{n+1} + \mathbf{q}_h^n \cdot \mathbf{q}_h^n \right) \right) \\
&+ \mathbb{C} \operatorname{div} \left(\rho_h^{n+\frac{1}{2}} \, \mathbf{q}_h^{n+\frac{1}{2}} \right) - \frac{\mathbb{M} \, \rho_0}{\mathbb{F}r^2} \, y \, \frac{r(c_h^{n+1}, c_h^n)}{\rho_h^{n+\frac{1}{2}}} \Bigg) \psi \, dx
\end{aligned} \tag{4.6.4}
$$

$$
0 = \int_\Omega \left(\mathbf{q}_h^{n+\frac{1}{2}} - \nabla c_h^{n+\frac{1}{2}} \right) \cdot \mathbf{T} \, dx \tag{4.6.5}
$$

$$
\forall \, (X, \boldsymbol{\xi}, Z, \psi, \mathbf{T}) \in \mathbb{V}^* \times (\mathbb{V}_0^*)^2 \times \mathbb{V}^* \times \mathbb{V}^* \times \mathbb{V}_{\mathbf{n}}^*.
$$

This fully discrete formulation is very similar to the one studied in [27]: the difference is in the choice of pressure transformations and in the introduction of the auxiliary variable $\mathbf{q}$. As in [27], in the implementation, it has been useful to introduce the auxiliary variable $\tilde{\mathbf{u}} = \sqrt{\rho}\mathbf{u}$. Due to the nonlinearity of the numerical scheme (4.6.1)-(4.6.5), we adopted a Newton's method to linearize the time-dependent NSCH system. In the numerical tests, only two or three Newton steps for each timestep were necessary. In order to have an accurate description of the evolution of the quasi-incompressible system, we used P_2 (piecewise quadratic) continuous finite elements for all the variables and we finely refined the interface between the two bubbles using the adaptive mesh tools of FreeFem++.

For a first test case we adopted one of the test cases used in [27]. Inside the spatial domain $\Omega = [-1, 1] \times [-1, 1]$ we studied the coalescence of two kissing bubbles, where the heavier drops are set in a lighter medium. If fluid 2 are the two bubbles, we can consider $\rho_2 = 10$ and $\rho_1 = 1$. The initial configuration of the two bubbles is described by

$$
c = \frac{1}{2} \tanh \left(\frac{-r + \sqrt{(x - a_x)^2 + (y - a_y)^2}}{2\sqrt{2}\varepsilon} \right) + \frac{1}{2} \tanh \left(\frac{-r + \sqrt{(x - b_x)^2 + (y - b_y)^2}}{2\sqrt{2}\varepsilon} \right), \tag{4.6.6}
$$

where r is the drop radius, (a_x, a_y), (b_x, b_y) are the initial centre positions of the two drops, with $r = 0.2\sqrt{2}$, $(a_x, a_y) = (-r/\sqrt{2}, r/\sqrt{2})$, $(b_x, b_y) = (r/\sqrt{2}, -r/\sqrt{2})$ and $\varepsilon = 0.01$. We chose $\mathbb{C} = 100\varepsilon^2$, $\mathbb{M} = 1/(10\varepsilon)$, $\mathbb{P}e = 100/\varepsilon$, $\mathbb{R}e = 10$. We neglected the influence of gravitational forces. The timestep used for the numerical simulation is $\Delta t = 0.01$.

The evolution of the concentration c over the time and the pattern of the streamlines are shown in Figures 4.1-4.3. Figure 4.4 shows that $\int \rho(c) \, dx \approx 7.64$. The decrease of the

total energy associated to the system (see Figure 4.5) in addition to mass conservation reveals the good properties of the algorithm (4.6.1)-(4.6.5) that have been theoretically proved in the previous sections.

However, we expect that increasing values of the density jump ρ_2-ρ_1 will make necessary the use of DG discretisation as the one considered in the previous section. Indeed, as it is well known, DG schemes have built-in stabilizations properties that make these kind of schemes particularly suitable to deal with highly jumping density values. Further investigations will be performed in the future along these lines.

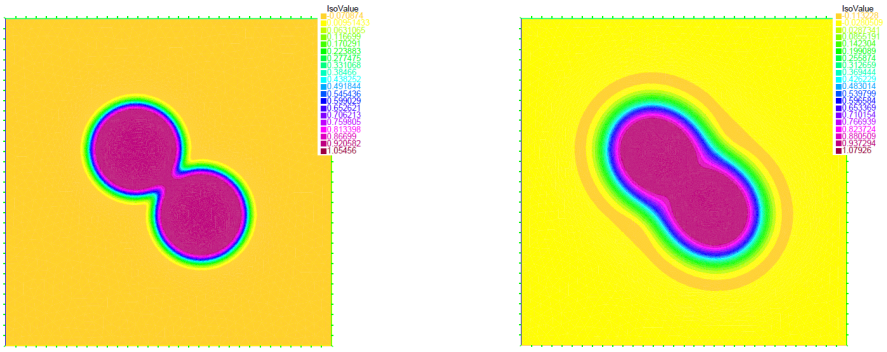

Figure 4.1: Concentration c at times t=0.1 and t=5.

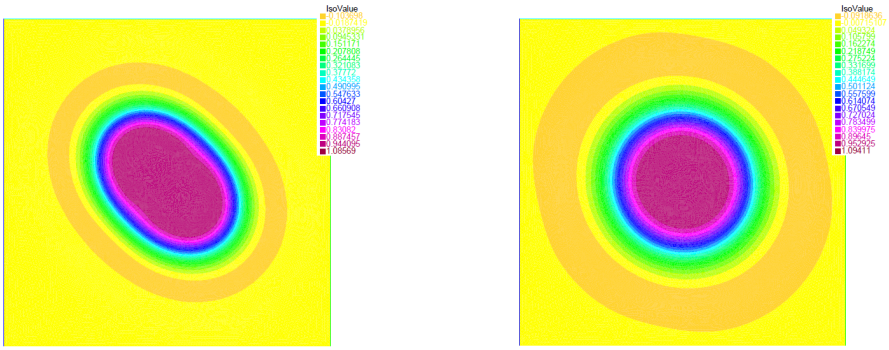

Figure 4.2: Concentration c at times t=13.5 and t=75.

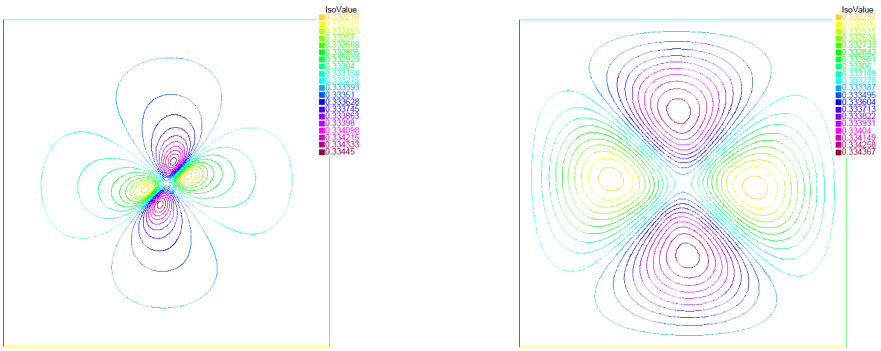

Figure 4.3: Streamlines at times t=0.1 and t=13.5.

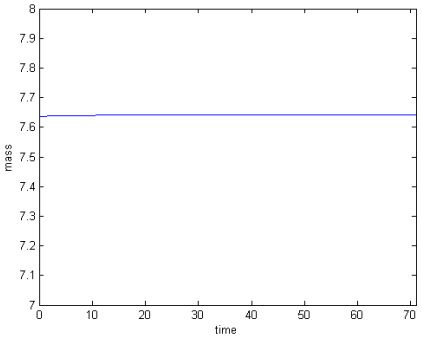

Figure 4.4: Mass conservation.

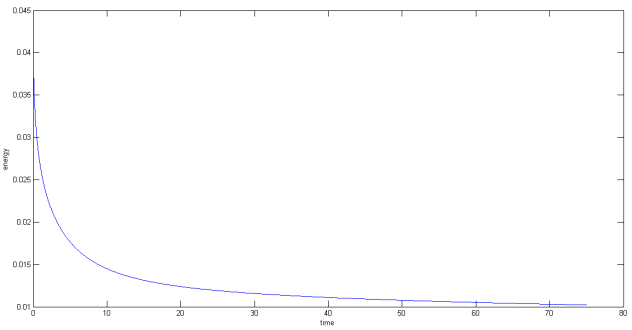

Figure 4.5: Energy decrease.

Chapter 5

Numerical methods for the metal foam system of equations.

Scientists are not passive recipients of the unexpected; rather, they actively create the conditions for discovering the unexpected and have a robust mental toolkit that makes discovery possible.

Kevin Dunbar and Jonathan Fugelsang

In this chapter we will extend the energy-based numerical scheme that we have derived for the Lowengrub-Truskinvosky system to the metal foam model. This causes the introduction of some technical difficulties, especially in proving the energy law, due to the presence of logarithmic pressure terms in the Gibbs free-energy associated to our model and due to the fact that we have a degenerate viscosity in the gas phase. Again, we will use a DG spatial approximation and a modified-midpoint based temporal approximation. The structure of the numerical fluxes for the metal foam system will be similar to the one of the LT system. In extending the modified-midpoint scheme, suitable approximations for the logarithmic terms will be used.

This chapter is organised as follows. In Section 5.1 we give a mixed formulation for the metal foam system. Starting from this formulation, mass conservation property and an energy law will be derived. In Section 5.2 we calculate numerical fluxes for the DG spatial approximation, in order to preserve mass conservation and the energy law at the semi-discrete level. In Section 5.3 we extend the modified-midpoint time scheme to the case of metal foam system, preserving mass conservation and the energy law. In Section 5.4, collecting the previous results, we propose a fully discrete approximation of the metal foam system which preserves the mass conservation property and the energy law of the original system.

5.1 Metal foam system of equations.

In this section we propose a suitable continuous mixed formulation for the metal foam (MF) system. From this formulation, a mass conservation property and a continuous energy dissipation law will be derived.

5.1.1 Metal foam system of equations.

In Chapter 3 we have written the MF system of equations through (3.4.36)-(3.4.38). By introducing the chemical potential definition, as for the LT system, we can rewrite the MF system as follows:

$$
\begin{aligned}
0 &= \rho(\partial_t c) + \rho(\mathbf{u}\cdot\nabla)c - \frac{1}{\mathbb{P}e}\Delta\mu, && (5.1.1)\\
\mathbf{0} &= \sqrt{\rho}\partial_t(\sqrt{\rho}\mathbf{u}) + \rho(\mathbf{u}\cdot\nabla)\mathbf{u} + \frac{1}{2}\operatorname{div}(\rho\mathbf{u})\mathbf{u} + \frac{1}{\mathbb{M}}\nabla p \\
&\quad + \frac{\mathbb{C}}{\mathbb{M}}\operatorname{div}(\rho\nabla c\otimes\nabla c) - \frac{2}{\mathbb{R}e}\operatorname{div}(c\mathbf{D}), && (5.1.2)\\
0 &= \partial_t\rho + \operatorname{div}(\rho\mathbf{u}), && (5.1.3)\\
0 &= \mu - \mu_0(c) - \frac{p}{\rho_1} + N_1\theta\ln p + \frac{\mathbb{C}}{\rho}\operatorname{div}(\rho\nabla c) + K && (5.1.4)
\end{aligned}
$$

where

$$
\begin{aligned}
\rho^{-1} &= \frac{c}{\rho_1} + \frac{(1-c)N_1\theta}{p}, && (5.1.5)\\
K &= \left(\frac{7}{2}N_1 - \sigma_0\right)(\theta-1) + N_1\theta\ln\left(\frac{\theta_0}{\theta}\right)^{\frac{7}{2}}, && (5.1.6)\\
\mu_0(c) &= \frac{dg_1(c)}{dc}. && (5.1.7)\\
& && (5.1.8)
\end{aligned}
$$

Notice that, for ease of notation, we have supposed that the reference pressure p_0 is equal to 1. For the analysis, we will consider the following initial and boundary conditions:

$$
\mathbf{u}(x,0) = \mathbf{u}_0(x), \quad c(x,0) = c_0(x), \quad \text{for all } x\in\Omega, \tag{5.1.9}
$$

$$
\mathbf{u} = \mathbf{0}, \quad \nabla c\cdot\mathbf{n} = \nabla\mu\cdot\mathbf{n} = 0, \quad \text{on } \partial\Omega\times(0,T). \tag{5.1.10}
$$

Conditions (5.1.10) are simplified boundary conditions with respect to the ones used in Section 3.4.4. However, the analysis can be extended to the original boundary conditions.

Remark. Notice that the phase-field variable c enters the viscous term in the right-hand side of (5.1.2). Due to the choice of $g_1(c)$ as a double-well potential, it is not guaranteed that the variable c belongs to the interval $[0,1]$. In order to enforce this constraint, another choice of $g_1(c)$ has to be done, e.g. a logarithmic potential (see [15], [9]). In order to reduce the complexity of the problem, it is well accepted in the literature the use of double-well potentials. The fact that c is guaranteed to remain in the interval $[0,1]$ influences the validity of the energy law (see Theorem 5.1.2).

Transformations on the momentum equation. We propose some transformations on the momentum equation (5.1.2), similar to the ones introduced in Section 4.2.3. For the MF system, it does not seem useful to introduce new pressures, because in

this case the expression of the density depends on the pressure and because of the presence of a logarithmic term in the chemical potential definition (5.1.4). Using identity (4.2.16), we can rewrite (5.1.2) as follows:

$$\begin{aligned}\mathbf{0} &= \sqrt{\rho}\partial_t(\sqrt{\rho}\mathbf{u}) + \rho(\mathbf{u}\cdot\nabla)\mathbf{u} + \frac{1}{2}\,\mathrm{div}(\rho\mathbf{u})\mathbf{u} + \frac{1}{\mathbb{M}}\nabla p \\ &\quad + \frac{\mathbb{C}}{\mathbb{M}}\,\mathrm{div}(\rho\nabla c)\nabla c + \frac{\mathbb{C}}{2\,\mathbb{M}}\rho\nabla\left(|\nabla c|^2\right) - \frac{2}{\mathbb{R}e}\,\mathrm{div}(c\mathbf{D}). \end{aligned} \tag{5.1.11}$$

Using, from equation (5.1.4), the fact that

$$\begin{aligned}\frac{\mathbb{C}}{\mathbb{M}}\,\mathrm{div}(\rho\nabla c)\nabla c &= \frac{1}{\mathbb{M}}\rho\mu_0(c)\nabla c - \frac{1}{\mathbb{M}}\rho\mu\nabla c + \frac{1}{\mathbb{M}}\frac{1}{\rho_1}\rho p\nabla c \\ &\quad - \frac{1}{\mathbb{M}}N_1\theta\rho\ln p\nabla c - \frac{1}{\mathbb{M}}K\rho\nabla c, \end{aligned} \tag{5.1.12}$$

we can rewrite equation (5.1.11) as

$$\begin{aligned}\mathbf{0} &= \sqrt{\rho}\,\partial_t\left(\sqrt{\rho}\mathbf{u}\right) + \rho(\mathbf{u}\cdot\nabla)\mathbf{u} + \frac{1}{2}\,\mathrm{div}(\rho\mathbf{u})\mathbf{u} + \frac{1}{\mathbb{M}}\nabla p - \frac{1}{\mathbb{M}}\rho\mu\,\nabla c \\ &\quad + \frac{1}{\mathbb{M}}\frac{1}{\rho_1}\rho p\nabla c - \frac{1}{\mathbb{M}}N_1\theta\rho\ln p\nabla c - \frac{1}{\mathbb{M}}K\rho\nabla c \\ &\quad + \frac{\mathbb{C}}{2\mathbb{M}}\rho\nabla(|\nabla c|^2) + \frac{1}{\mathbb{M}}\rho\mu_0(c)\nabla c - \frac{2}{\mathbb{R}e}\,\mathrm{div}(c\mathbf{D}). \end{aligned} \tag{5.1.13}$$

5.1.2 Continuous mixed formulation.

We now introduce a mixed formulation of the MF system of equations (5.1.1)-(5.1.4) taking into account the transformations performed in the previous section. The strong problem reads as follows. Find $(c, \mathbf{u}, p, \mu, \mathbf{q})$ such that

$$0 = \rho\,\partial_t c + \rho(\mathbf{u}\cdot\nabla)c - \frac{1}{\mathbb{P}e}\Delta\mu, \tag{5.1.14}$$

$$\begin{aligned}\mathbf{0} &= \sqrt{\rho}\,\partial_t\left(\sqrt{\rho}\mathbf{u}\right) + \rho(\mathbf{u}\cdot\nabla)\mathbf{u} + \frac{1}{2}\,\mathrm{div}(\rho\mathbf{u})\mathbf{u} + \frac{1}{\mathbb{M}}\nabla p - \frac{1}{\mathbb{M}}\rho\mu\,\nabla c \\ &\quad + \frac{1}{\mathbb{M}}\frac{1}{\rho_1}\rho p\nabla c - \frac{1}{\mathbb{M}}N_1\theta\rho\ln p\nabla c - \frac{1}{\mathbb{M}}K\rho\nabla c \\ &\quad + \frac{\mathbb{C}}{2\mathbb{M}}\rho\nabla(|\mathbf{q}|^2) + \frac{1}{\mathbb{M}}\rho\mu_0(c)\nabla c - \frac{2}{\mathbb{R}e}\,\mathrm{div}(c\mathbf{D}), \end{aligned} \tag{5.1.15}$$

$$0 = \partial_t\rho + \mathrm{div}(\rho\mathbf{u}), \tag{5.1.16}$$

$$0 = \rho\mu - \rho\mu_0(c) - \frac{p}{\rho_1}\rho + N_1\theta\rho\ln p + \mathbb{C}\,\mathrm{div}(\,\rho\,\mathbf{q}\,) + K\rho, \tag{5.1.17}$$

$$\mathbf{0} = \mathbf{q} - \nabla c, \tag{5.1.18}$$

with the following initial and boundary conditions:

$$\mathbf{u}(x,0) = \mathbf{u}_0(x), \quad c(x,0) = c_0(x), \quad \text{for all } x \in \Omega, \tag{5.1.19}$$

$$\mathbf{u} = \mathbf{0}, \quad \mathbf{q}\cdot\mathbf{n} = \nabla\mu\cdot\mathbf{n} = 0, \quad \text{on } \partial\Omega\times(0,T). \tag{5.1.20}$$

Notice that we have introduced a new variable, $\mathbf{q}$, defined in (5.1.18), as for the LT system.

5.1.3 Continuous mass conservation.

Let us write the mass conservation property of the MF system (5.1.14)-(5.1.18). The proof is the same as the one presented for the LT system in Section 4.2.2.

Theorem 5.1.1 (Conservation of mass.). *If $(c, \mathbf{u}, p, \mu, \mathbf{q})$ is a strong solution of the system (5.1.14)-(5.1.18) which satisfies the boundary conditions (5.1.20), then*

$$\frac{d}{dt}\left(\int_\Omega \rho\, dx\right) = 0. \tag{5.1.21}$$

5.1.4 Continuous energy dissipation law.

Let us derive the continuous energy dissipation law for the MF system. The derivation will be consistent with the mixed formulation (5.1.14)-(5.1.18) given in Section 5.1.2. The proof will be similar to the one proposed for the LT system: the main differences (and the main technical difficulties) are due to the presence of logarithmic pressure terms both in the momentum equation (5.1.15) and in the chemical potential definition (5.1.17).

Let us introduce the total energy associated to the system (5.1.14)-(5.1.18):

$$E := \int_\Omega \left(\frac{1}{2}\rho\,|\mathbf{u}|^2 + \frac{1}{\mathbb{M}}\rho\, g(p, c, \mathbf{q}) - \frac{1}{\mathbb{M}}p\right) dx, \tag{5.1.22}$$

where

$$\begin{aligned}
g(p, c, \mathbf{q}) &= \frac{c}{\rho_1}p + N_1\theta(1-c)\ln p + g_0(c) + g_1(c) + g_2(\mathbf{q}) && (5.1.23)\\
g_0(c) &= (1-c)K, && (5.1.24)\\
g_1(c) &= \frac{1}{4}c^2(1-c)^2, && (5.1.25)\\
g_2(\mathbf{q}) &= \frac{\mathbb{C}}{2}|\mathbf{q}|^2. && (5.1.26)
\end{aligned}$$

Theorem 5.1.2 (Continuous energy dissipation law). *Let $(c, \mathbf{u}, p, \mu, \mathbf{q}) \in L^2(0,T;H^1(\Omega)) \times L^2(0,T;(H^2(\Omega)\cap H_0^1(\Omega))^2) \times L^2(0,T;H^1(\Omega)) \times L^2(0,T;H^2(\Omega)) \times L^2(0,T;H^1_{\mathbf{n}}(\Omega))$ be a strong solution of the system (5.1.14)-(5.1.18). Then*

$$\begin{aligned}
\frac{dE}{dt} &= \frac{d}{dt}\left(\int_\Omega \left(\frac{1}{2}\rho\,|\mathbf{u}|^2 + \frac{1}{\mathbb{M}}\rho\, g(p, c, \mathbf{q}) - \frac{1}{\mathbb{M}}p\right) dx\right)\\
&= -\frac{1}{\mathbb{P}e\mathbb{M}}\int_\Omega |\nabla\mu|^2\, dx - \frac{2}{\mathbb{R}e}\int_\Omega c\,(\mathbf{D}:\mathbf{D})\, dx. && (5.1.27)
\end{aligned}$$

Proof. Let us test equation (5.1.14) with $\frac{\mu}{\mathbb{M}}$ and equation (5.1.15) with $\mathbf{u}$ and sum them together. If we use the following identity

$$\int_\Omega \left(\rho\,(\mathbf{u}\cdot\nabla)\,\mathbf{u}\cdot\mathbf{u} + \frac{1}{2}\,\mathrm{div}(\rho\mathbf{u})\mathbf{u}\cdot\mathbf{u}\right) dx = 0, \tag{5.1.28}$$

we obtain:

$$\begin{aligned}
0 = \int_\Omega \Bigg(&\frac{1}{\mathbb{M}}\rho\mu(\partial_t c) - \frac{1}{\mathbb{P}e\mathbb{M}}\mu\Delta\mu + \sqrt{\rho}\,\partial_t\left(\sqrt{\rho}\mathbf{u}\right)\cdot\mathbf{u} + \frac{1}{\mathbb{M}}\nabla p\cdot\mathbf{u}\\
&+ \frac{1}{\mathbb{M}}\frac{1}{\rho_1}\rho p\nabla c\cdot\mathbf{u} - \frac{1}{\mathbb{M}}N_1\theta\rho\ln p\nabla c\cdot\mathbf{u} - \frac{1}{\mathbb{M}}K\rho\nabla c\cdot\mathbf{u}\\
&+ \frac{\mathbb{C}}{2\mathbb{M}}\rho\nabla(|\mathbf{q}|^2)\cdot\mathbf{u} + \frac{1}{\mathbb{M}}\rho\mu_0(c)\nabla c\cdot\mathbf{u} - \frac{2}{\mathbb{R}e}\,\mathrm{div}(c\mathbf{D})\cdot\mathbf{u}\Bigg)\, dx. \qquad (5.1.29)
\end{aligned}$$

Using equation (5.1.17) for the first term of (5.1.29) and integrating by parts the viscous term and term containing $\Delta\mu$, we obtain:

$$\begin{aligned} 0 \;=\; & \int_\Omega \Big(\sqrt{\rho}\,\partial_t\left(\sqrt{\rho}\mathbf{u}\right)\cdot\mathbf{u} + \frac{1}{\mathbb{M}}\nabla p\cdot\mathbf{u} + \frac{1}{\mathbb{M}}\frac{1}{\rho_1}\rho p\nabla c\cdot\mathbf{u} - \frac{1}{\mathbb{M}}N_1\theta\rho\ln p\nabla c\cdot\mathbf{u} \\ & + \frac{1}{\mathbb{M}}\frac{1}{\rho_1}\rho p(\partial_t c) - \frac{1}{\mathbb{M}}N_1\theta\rho\ln p(\partial_t c) + \frac{1}{\mathbb{M}}\rho\mu_0(c)\nabla c\cdot\mathbf{u} + \frac{1}{\mathbb{M}}\rho\mu_0(c)(\partial_t c) \\ & + \frac{\mathbb{C}}{2\,\mathbb{M}}\rho\nabla(|\mathbf{q}|^2)\cdot\mathbf{u} - \frac{\mathbb{C}}{\mathbb{M}}\,\mathrm{div}(\rho\mathbf{q})(\partial_t c) - \frac{1}{\mathbb{M}}K\rho\nabla c\cdot\mathbf{u} - \frac{1}{\mathbb{M}}K\rho(\partial_t c) \\ & + \frac{1}{\mathbb{P}e\mathbb{M}}|\nabla\mu|^2 + \frac{2}{\mathbb{R}e}c\mathbf{D}:\mathbf{D}\Big)\,dx. \end{aligned} \tag{5.1.30}$$

We get the following relations:

(I) the first term in (5.1.30) is

$$\int_\Omega \sqrt{\rho}\,\partial_t(\sqrt{\rho}\mathbf{u})\cdot\mathbf{u}\,dx = \int_\Omega \partial_t\left(\frac{\rho}{2}|\mathbf{u}|^2\right)\,dx, \tag{5.1.31}$$

(II) integrating by parts, using the boundary conditions (5.1.20) and the mass conservation equation (5.1.16), the terms containing $\mu_0(c)$ are equal to

$$\begin{aligned} & \int_\Omega \left(\frac{1}{\mathbb{M}}\rho\mu_0(c)\nabla c\cdot\mathbf{u} + \frac{1}{\mathbb{M}}\rho\mu_0(c)(\partial_t c)\right)\,dx \\ = \;& \int_\Omega \left(\frac{1}{\mathbb{M}}\nabla(g_1(c))\cdot(\rho\mathbf{u}) + \frac{1}{\mathbb{M}}\rho\mu_0(c)(\partial_t c)\right)\,dx \\ = \;& \int_\Omega \left(-\frac{1}{\mathbb{M}}g_1(c)\,\mathrm{div}(\rho\mathbf{u}) + \frac{1}{\mathbb{M}}\rho\partial_t(g_1(c))\right)\,dx \\ = \;& \int_\Omega \left(\frac{1}{\mathbb{M}}g_1(c)(\partial_t\rho) + \frac{1}{\mathbb{M}}\rho\partial_t(g_1(c))\right)\,dx \\ = \;& \int_\Omega \partial_t\left(\frac{1}{\mathbb{M}}\rho g_1(c)\right)\,dx, \end{aligned} \tag{5.1.32}$$

(III) integrating by parts, using the boundary conditions (5.1.20) and the mass conservation equation (5.1.16), the terms containing the variable $\mathbf{q}$ are equal to

$$\begin{aligned} & \int_\Omega \left(\frac{\mathbb{C}}{2\,\mathbb{M}}\rho\nabla(|\mathbf{q}|^2)\cdot\mathbf{u} - \frac{\mathbb{C}}{\mathbb{M}}\,\mathrm{div}(\rho\mathbf{q})(\partial_t c)\right)\,dx \\ = \;& \int_\Omega \left(-\frac{\mathbb{C}}{2\,\mathbb{M}}|\mathbf{q}|^2\,\mathrm{div}(\rho\mathbf{u}) + \frac{\mathbb{C}}{\mathbb{M}}\,\rho\mathbf{q}\cdot(\partial_t\mathbf{q})\right)\,dx \\ = \;& \int_\Omega \left(\frac{\mathbb{C}}{2\,\mathbb{M}}|\mathbf{q}|^2(\partial_t\rho) + \frac{\mathbb{C}}{\mathbb{M}}\,\rho\mathbf{q}\cdot(\partial_t\mathbf{q})\right)\,dx \\ = \;& \int_\Omega \partial_t\left(\frac{1}{\mathbb{M}}\rho g_2(\mathbf{q})\right)\,dx, \end{aligned} \tag{5.1.33}$$

(IV) integrating by parts, using the boundary conditions (5.1.20) and the mass conser-

vation equation (5.1.16), the terms containing the constant K are equal to

$$\begin{aligned}
&\int_\Omega \left(-\frac{1}{\mathbb{M}}K\rho\nabla c\cdot\mathbf{u}-\frac{1}{\mathbb{M}}K\rho(\partial_t c)\right)dx\\
=&\int_\Omega \left(\frac{1}{\mathbb{M}}K\rho\nabla(1-c)\cdot\mathbf{u}+\frac{1}{\mathbb{M}}K\rho\partial_t(1-c)\right)dx\\
=&\int_\Omega \left(-\frac{1}{\mathbb{M}}K(1-c)\operatorname{div}(\rho\mathbf{u})+\frac{1}{\mathbb{M}}K\rho\partial_t(1-c)\right)dx\\
=&\int_\Omega \left(\frac{1}{\mathbb{M}}K(1-c)(\partial_t\rho)+\frac{1}{\mathbb{M}}K\rho\partial_t(1-c)\right)dx\\
=&\int_\Omega \partial_t\left(\frac{1}{\mathbb{M}}\rho g_0(c)\right)dx. \qquad (5.1.34)
\end{aligned}$$

Now, let us consider pressure terms:

$$\begin{aligned}
\int_\Omega\Big(&\frac{1}{\mathbb{M}}\nabla p\cdot\mathbf{u}+\frac{1}{\mathbb{M}}\frac{1}{\rho_1}\rho p\nabla c\cdot\mathbf{u}-\frac{1}{\mathbb{M}}N_1\theta\rho\ln p\nabla c\cdot\mathbf{u}\\
&+\frac{1}{\mathbb{M}}\frac{1}{\rho_1}\rho p(\partial_t c)-\frac{1}{\mathbb{M}}N_1\theta\rho\ln p(\partial_t c)\Big)\,dx. \qquad (5.1.35)
\end{aligned}$$

Notice that, integrating by parts, using boundary conditions (5.1.20) and mass conservation equation (5.1.16):

(a)

$$\begin{aligned}
&\int_\Omega\left(\frac{1}{\mathbb{M}}\frac{1}{\rho_1}\rho p\nabla c\cdot\mathbf{u}\right)dx\\
=&\int_\Omega\left(-\frac{1}{\mathbb{M}}\frac{1}{\rho_1}cp\operatorname{div}(\rho\mathbf{u})-\frac{1}{\mathbb{M}}\frac{1}{\rho_1}c\rho\mathbf{u}\cdot\nabla p\right)dx\\
=&\int_\Omega\left(\frac{1}{\mathbb{M}}\frac{1}{\rho_1}cp(\partial_t\rho)-\frac{1}{\mathbb{M}}\frac{1}{\rho_1}\rho c\mathbf{u}\cdot\nabla p\right)dx, \qquad (5.1.36)
\end{aligned}$$

(b)

$$\begin{aligned}
&\int_\Omega\left(-\frac{1}{\mathbb{M}}N_1\theta\rho\ln p\nabla c\cdot\mathbf{u}\right)dx\\
=&\int_\Omega\left(\frac{1}{\mathbb{M}}N_1\theta\rho\ln p\nabla(1-c)\cdot\mathbf{u}\right)dx\\
=&\int_\Omega\left(-\frac{1}{\mathbb{M}}N_1\theta(1-c)\ln p\operatorname{div}(\rho\mathbf{u})-\frac{1}{\mathbb{M}}N_1\theta\rho(1-c)\frac{\nabla p}{p}\cdot\mathbf{u}\right)dx\\
=&\int_\Omega\left(\frac{1}{\mathbb{M}}N_1\theta(1-c)\ln p(\partial_t\rho)-\frac{1}{\mathbb{M}}N_1\theta\rho(1-c)\frac{\nabla p}{p}\cdot\mathbf{u}\right)dx. \qquad (5.1.37)
\end{aligned}$$

Using (5.1.36) and (5.1.37) into (5.1.35) we obtain:

$$\begin{aligned}
\int_\Omega\Big(&\frac{1}{\mathbb{M}}\nabla p\cdot\mathbf{u}-\frac{1}{\mathbb{M}}\frac{1}{\rho_1}\rho c\mathbf{u}\cdot\nabla p-\frac{1}{\mathbb{M}}N_1\theta\rho(1-c)\frac{\nabla p}{p}\cdot\mathbf{u}\\
&+\frac{1}{\mathbb{M}}\frac{1}{\rho_1}cp(\partial_t\rho)+\frac{1}{\mathbb{M}}\frac{1}{\rho_1}\rho p(\partial_t c)\\
&+\frac{1}{\mathbb{M}}N_1\theta(1-c)\ln p(\partial_t\rho)-\frac{1}{\mathbb{M}}N_1\theta\rho\ln p(\partial_t c)\Big)\,dx. \qquad (5.1.38)
\end{aligned}$$

If we notice the fact that, remembering the definition of ρ,

$$\begin{aligned}
&\int_\Omega\left(\frac{1}{\mathbb{M}}\nabla p\cdot\mathbf{u}-\frac{1}{\mathbb{M}}\frac{1}{\rho_1}\rho c\mathbf{u}\cdot\nabla p-\frac{1}{\mathbb{M}}N_1\theta\rho(1-c)\frac{\nabla p}{p}\cdot\mathbf{u}\right)dx\\
=&\int_\Omega\left(\frac{1}{\mathbb{M}}\nabla p\cdot\mathbf{u}-\frac{1}{\mathbb{M}}\left(\frac{c}{\rho_1}+\frac{N_1\theta(1-c)}{p}\right)\rho\mathbf{u}\cdot\nabla p\right)dx=0, \qquad (5.1.39)
\end{aligned}$$

then (5.1.38) can be rewritten as

$$\int_\Omega \left(\frac{1}{\mathbb{M}}\frac{1}{\rho_1} cp(\partial_t \rho) + \frac{1}{\mathbb{M}}\frac{1}{\rho_1} p\rho(\partial_t c) - \frac{1}{\mathbb{M}} N_1 \theta \rho (1-c)\frac{\partial_t p}{p} \right.$$
$$+ \frac{1}{\mathbb{M}} N_1 \theta \rho (1-c)\frac{\partial_t p}{p} + \frac{1}{\mathbb{M}} N_1 \theta (1-c)\ln p(\partial_t \rho)$$
$$\left. - \frac{1}{\mathbb{M}} N_1 \theta \rho \ln p(\partial_t c) \right) dx, \tag{5.1.40}$$

in which we have added and subtracted the quantity $\frac{1}{\mathbb{M}} N_1 \theta \rho (1-c)\frac{\partial_t p}{p}$. Using the fact that p can be written, in terms of ρ and c, as

$$p = \frac{N_1 \theta \rho_1 \rho (1-c)}{\rho_1 - \rho c}, \tag{5.1.41}$$

we obtain:

$$\int_\Omega \left(-\frac{1}{\mathbb{M}} N_1 \theta \rho (1-c)\frac{\partial_t p}{p} \right) dx = \int_\Omega \left(-\frac{1}{\mathbb{M}}\partial_t p + \frac{1}{\mathbb{M}}\frac{1}{\rho_1}\rho c(\partial_t p) \right) dx. \tag{5.1.42}$$

Using (5.1.42) into (5.1.40), we obtain:

$$\begin{aligned} & \int_\Omega \left(\frac{1}{\mathbb{M}}\frac{1}{\rho_1} cp(\partial_t \rho) + \frac{1}{\mathbb{M}}\frac{1}{\rho_1} \rho p(\partial_t c) + \frac{1}{\mathbb{M}}\frac{1}{\rho_1}\rho c(\partial_t p) \right. \\ & \quad + \frac{1}{\mathbb{M}} N_1 \theta (1-c)\ln p(\partial_t \rho) + \frac{1}{\mathbb{M}} N_1 \theta \rho \ln p \partial_t (1-c) \\ & \quad \left. + \frac{1}{\mathbb{M}} N_1 \theta \rho (1-c)\frac{\partial_t p}{p} - \frac{1}{\mathbb{M}}\partial_t p \right) dx \\ = & \int_\Omega \frac{1}{\mathbb{M}}\partial_t \left(\frac{c}{\rho_1} p\rho + N_1 \theta \rho (1-c)\ln p - p \right) dx. \end{aligned} \tag{5.1.43}$$

Using (5.1.31)-(5.1.34) and (5.1.35)-(5.1.43) into (5.1.30), we obtain:

$$\int_\Omega \partial_t \left(\frac{\rho}{2}|\mathbf{u}|^2 + \frac{1}{\mathbb{M}}\rho g(p,c,\mathbf{q}) - \frac{1}{\mathbb{M}} p \right) dx = -\int_\Omega \frac{1}{\mathbb{P}e\mathbb{M}} |\nabla \mu|^2 \, dx - \int_\Omega \frac{2}{\mathbb{R}e} c\mathbf{D} : \mathbf{D} \, dx, \tag{5.1.44}$$

that is equivalent to the thesis (5.1.27). □

5.2 Spatial DG discretisation.

In this section we propose a Discontinuous Galerkin spatial approximation of the MF system of equations (5.1.14)-(5.1.18). As for the case of the LT system, this DG discrete formulation will be consistent with the mass conservation and energy dissipation properties of the original system. In the sequel we will use the same DG notation introduced in the previous chapter.

5.2.1 Elementwise formulation.

We can give the elementwise variational formulation of the problem (5.1.14)-(5.1.18) in mixed form. We have to find

$$\begin{aligned} (c, \mathbf{u}, p, \mu, \mathbf{q}) \quad \in \quad & L^2(0,T; H^1(\mathscr{T}_h)) \times L^2(0,T; (H_0^1(\mathscr{T}_h))^2) \times L^2(0,T; H^1(\mathscr{T}_h)) \times \\ & L^2(0,T; H^1(\mathscr{T}_h)) \times L^2(0,T; H^1_{\mathbf{n}}(\mathscr{T}_h)) \end{aligned}$$

such that

$$0 = \sum_{T\in\mathscr{T}_h}\int_T \left(\rho\,(\partial_t c)\,X + \rho(\mathbf{u}\cdot\nabla)cX\right)\,dx - \frac{1}{\mathbb{P}e}\mathcal{A}(\mu,X) + \int_{\mathcal{E}} F_1(c,\mathbf{u},p,\mu,\mathbf{q},X)\,ds, \tag{5.2.1}$$

$$\begin{aligned} 0 = \sum_{T\in\mathscr{T}_h}\int_T \Big(&\sqrt{\rho}\,\partial_t\left(\sqrt{\rho}\mathbf{u}\right)\cdot\boldsymbol{\xi} + \rho(\mathbf{u}\cdot\nabla)\mathbf{u}\cdot\boldsymbol{\xi} + \frac{1}{2}\,\mathrm{div}(\rho\mathbf{u})\mathbf{u}\cdot\boldsymbol{\xi} + \frac{1}{\mathbb{M}}\nabla p\cdot\boldsymbol{\xi} - \frac{1}{\mathbb{M}}\rho\mu\,\nabla c\cdot\boldsymbol{\xi} \\ &+\frac{1}{\mathbb{M}}\frac{1}{\rho_1}\rho p\nabla c\cdot\boldsymbol{\xi} - \frac{1}{\mathbb{M}}N_1\theta\rho\ln p\nabla c\cdot\boldsymbol{\xi} - \frac{1}{\mathbb{M}}K\rho\nabla c\cdot\boldsymbol{\xi} + \frac{\mathbb{C}}{2\mathbb{M}}\rho\nabla(|\mathbf{q}|^2)\cdot\boldsymbol{\xi} \\ &+\frac{1}{\mathbb{M}}\rho\mu_0(c)\nabla c\cdot\boldsymbol{\xi}\Big)\,dx - \frac{2}{\mathbb{R}e}\mathcal{B}(c,\mathbf{u},\boldsymbol{\xi}) + \int_{\mathcal{E}} F_2(c,\mathbf{u},p,\mu,\mathbf{q},\boldsymbol{\xi})\,ds, \end{aligned} \tag{5.2.2}$$

$$0 = \sum_{T\in\mathscr{T}_h}\int_T \left((\partial_t\rho)\,Z + \mathrm{div}(\rho\mathbf{u})Z\right)\,dx + \int_{\mathcal{E}} F_3(c,\mathbf{u},p,\mu,\mathbf{q},Z)\,ds, \tag{5.2.3}$$

$$\begin{aligned} 0 = \sum_{T\in\mathscr{T}_h}\int_T &\left(\rho\mu\psi - \rho\mu_0(c)\psi - \frac{p}{\rho_1}\rho\psi + N_1\theta\rho\ln p\psi + \mathbb{C}\,\mathrm{div}(\,\rho\,\mathbf{q}\,)\psi + K\rho\psi\right)\,dx \\ &+\int_{\mathcal{E}} F_4(c,\mathbf{u},p,\mu,\mathbf{q},\psi)\,ds, \end{aligned} \tag{5.2.4}$$

$$0 = \sum_{T\in\mathscr{T}_h}\int_T \left(\mathbf{q}\cdot\mathbf{T} - \nabla c\cdot\mathbf{T}\right)\,dx + \int_{\mathcal{E}} F_5(c,\mathbf{u},p,\mu,\mathbf{q},\mathbf{T})\,ds, \tag{5.2.5}$$

$$\forall\,(X,\boldsymbol{\xi},Z,\psi,\mathbf{T}) \in H^1(\mathscr{T}_h)\times\left(H_0^1(\mathscr{T}_h)\right)^2\times H^1(\mathscr{T}_h)\times H^1(\mathscr{T}_h)\times H^1_{\mathbf{n}}(\mathscr{T}_h),$$

in which

$$\begin{aligned} \mathcal{A}(\mu,X) &:= -\sum_{T\in\mathscr{T}_h}\int_T \nabla\mu\cdot\nabla X\,dx + \int_{\mathcal{E}}\{\!\{\nabla X\}\!\}\cdot[\![\mu]\!]\,ds \\ &\quad +\int_{\mathcal{E}}[\![X]\!]\cdot\{\!\{\nabla\mu\}\!\}\,ds - \int_{\mathcal{E}}\frac{\sigma}{h}[\![\mu]\!]\cdot[\![X]\!]\,ds, \end{aligned} \tag{5.2.6}$$

$$\begin{aligned} \mathcal{B}(c,\mathbf{u},\boldsymbol{\xi}) &:= -\sum_{T\in\mathscr{T}_h}\int_T (c\,\epsilon(\mathbf{u}):\epsilon(\boldsymbol{\xi}))\,dx + \int_{\mathcal{E}\cup\partial\Omega}\left(\{\!\{c\,\epsilon(\boldsymbol{\xi})\}\!\}:[\![\mathbf{u}]\!]_{\otimes}\right)\,ds \\ &\quad +\int_{\mathcal{E}\cup\partial\Omega}\left(\{\!\{c\,\epsilon(\mathbf{u})\}\!\}:[\![\boldsymbol{\xi}]\!]_{\otimes}\right)\,ds - \int_{\mathcal{E}\cup\partial\Omega}\frac{\gamma}{h}\left([\![\mathbf{u}]\!]_{\otimes}:[\![\boldsymbol{\xi}]\!]_{\otimes}\right)\,ds \end{aligned} \tag{5.2.7}$$

are the symmetric interior penalty discretisation of the laplacian of the chemical potential μ (see [1], [48]) and the DG formulation of the viscous terms (see [29] and [64]), where σ and γ are sufficiently large parameters and $\epsilon(\mathbf{u}) := 1/2(\nabla\mathbf{u} + (\nabla\mathbf{u})^T)$.
The elementwise numerical fluxes F_i, for $i = 1,...,5$, will be chosen in the next sections according to the properties of mass conservation, energy decrease and consistency of the spatially discrete mixed formulation, as for the LT system.

5.2.2 Spatially discrete mixed formulation.

Let us give a spatially discrete DG mixed formulation of (5.2.1)-(5.2.5): find

$$\begin{aligned} (c_h,\mathbf{u}_h,p_h,\mu_h,\mathbf{q}_h) \quad \in \quad & L^2(0,T;\mathbb{V})\times L^2(0,T;\mathbb{V}_0^2)\times L^2(0,T;\mathbb{V})\times \\ & L^2(0,T;\mathbb{V})\times L^2(0,T;\mathbb{V}_{\mathbf{n}}) \end{aligned}$$

such that

$$0 = \sum_{T\in\mathscr{T}_h}\int_T \left(\rho_h\left(\partial_t c_h\right)X + \rho_h(\mathbf{u}_h\cdot\nabla)c_h X\right)\,dx - \frac{1}{\mathbb{P}e}\mathcal{A}(\mu_h, X) + \int_{\mathcal{E}} F_1(c_h,\mathbf{u}_h,p_h,\mu_h,\mathbf{q}_h,X)\,ds, \tag{5.2.8}$$

$$\begin{aligned} 0 = \sum_{T\in\mathscr{T}_h}\int_T \Bigg(&\sqrt{\rho_h}\,\partial_t\left(\sqrt{\rho_h}\mathbf{u}_h\right)\cdot\boldsymbol{\xi} + \rho_h(\mathbf{u}_h\cdot\nabla)\mathbf{u}_h\cdot\boldsymbol{\xi} + \frac{1}{2}\,\mathrm{div}(\rho_h\mathbf{u}_h)\mathbf{u}_h\cdot\boldsymbol{\xi} + \frac{1}{\mathbb{M}}\nabla p_h\cdot\boldsymbol{\xi} \\ &-\frac{1}{\mathbb{M}}\rho_h\mu_h\,\nabla c_h\cdot\boldsymbol{\xi} + \frac{1}{\mathbb{M}}\frac{1}{\rho_1}\rho_h p_h\nabla c_h\cdot\boldsymbol{\xi} - \frac{1}{\mathbb{M}}N_1\theta\rho_h\ln p_h\nabla c_h\cdot\boldsymbol{\xi} - \frac{1}{\mathbb{M}}K\rho_h\nabla c_h\cdot\boldsymbol{\xi} \\ &+\frac{\mathbb{C}}{2\mathbb{M}}\rho_h\nabla(|\mathbf{q}_h|^2)\cdot\boldsymbol{\xi} + \frac{1}{\mathbb{M}}\rho_h\mu_0(c_h)\nabla c_h\cdot\boldsymbol{\xi}\Bigg)\,dx - \frac{2}{\mathbb{R}e}\mathcal{B}(c_h,\mathbf{u}_h,\boldsymbol{\xi}) \\ &+\int_{\mathcal{E}} F_2(c_h,\mathbf{u}_h,p_h,\mu_h,\mathbf{q}_h,\boldsymbol{\xi})\,ds, \end{aligned} \tag{5.2.9}$$

$$0 = \sum_{T\in\mathscr{T}_h}\int_T \left(\left(\partial_t\rho_h\right)Z + \mathrm{div}(\rho_h\mathbf{u}_h)Z\right)\,dx + \int_{\mathcal{E}} F_3(c_h,\mathbf{u}_h,p_h,\mu_h,\mathbf{q}_h,Z)\,ds, \tag{5.2.10}$$

$$\begin{aligned} 0 = \sum_{T\in\mathscr{T}_h}\int_T \Bigg(&\rho_h\mu_h\psi - \rho_h\mu_0(c_h)\psi - \frac{p_h}{\rho_1}\rho_h\psi + N_1\theta\rho_h\ln p_h\psi \\ &+\mathbb{C}\,\mathrm{div}(\,\rho_h\,\mathbf{q}_h\,)\psi + K\rho_h\psi\Bigg)\,dx + \int_{\mathcal{E}} F_4(c_h,\mathbf{u}_h,p_h,\mu_h,\mathbf{q}_h,\psi)\,ds, \end{aligned} \tag{5.2.11}$$

$$0 = \sum_{T\in\mathscr{T}_h}\int_T \left(\mathbf{q}_h\cdot\mathbf{T} - \nabla c_h\cdot\mathbf{T}\right)\,dx + \int_{\mathcal{E}} F_5(c_h,\mathbf{u}_h,p_h,\mu_h,\mathbf{q}_h,\mathbf{T})\,ds, \tag{5.2.12}$$

$$\forall\,(X,\boldsymbol{\xi},Z,\psi,\mathbf{T})\in\mathbb{V}\times\mathbb{V}_0^2\times\mathbb{V}\times\mathbb{V}\times\mathbb{V}_{\mathbf{n}}.$$

In the DG formulation (5.2.8)-(5.2.12) we have used, for simplicity, $\rho_h := \rho(c_h, p_h)$.

5.2.3 Spatially discrete mass conservation.

The conditions on the numerical fluxes $F_i, i = 1, ..., 5$, in order to ensure that a mass conservation relation holds for the spatial discretisation (5.2.8)-(5.2.12) will be the same as for the LT system according to the following result (the proof is the same as the one produced for Theorem 4.3.2).

Theorem 5.2.1 (Spatially discrete conservation of mass). *If $(c_h, \mathbf{u}_h, p_h, \mu_h, \mathbf{q}_h)$ is a solution of the spatially discrete system (5.2.8)-(5.2.12) then*

$$\frac{d}{dt}\left(\sum_{T\in\mathscr{T}_h}\int_T \rho_h\,dx\right) = 0 \tag{5.2.13}$$

if and only if

$$\int_{\mathcal{E}} F_3(c_h,\mathbf{u}_h,p_h,\mu_h,\mathbf{q}_h,1)\,ds = -\int_{\mathcal{E}}[\![\rho_h\mathbf{u}_h]\!]\,ds. \tag{5.2.14}$$

5.2.4 Spatially discrete energy dissipation law.

Let us define the spatially discrete total energy of the system (5.2.8)-(5.2.12) as

$$E_h := \sum_{T\in\mathscr{T}_h}\int_T\left(\frac{\rho_h}{2}\,|\mathbf{u}_h|^2 + \frac{1}{\mathbb{M}}\rho_h g(p_h,c_h,\mathbf{q}_h) - \frac{1}{\mathbb{M}}p_h\right)\,dx, \tag{5.2.15}$$

that is the spatially discrete version of the continuous total energy (5.1.22). The next theorem will set conditions on the numerical fluxes F_i, $i = 1, \dots, 5$, under which the spatially discrete system (5.2.8)-(5.2.12) preserves a spatially discrete formulation of the energy dissipation law (5.1.27).

Theorem 5.2.2 (Spatially discrete energy dissipation law)**.** *If $(c_h, \mathbf{u}_h, p_h, \mu_h, \mathbf{q}_h)$ is a solution of the spatially discrete system (5.2.8)-(5.2.12) then*

$$\begin{aligned} \frac{dE_h}{dt} &= \frac{d}{dt}\left(\sum_{T\in\mathscr{T}_h}\int_T\left(\frac{\rho_h}{2}|\mathbf{u}_h|^2+\frac{1}{\mathbb{M}}\rho_h g(p_h,c_h,\mathbf{q}_h)-\frac{1}{\mathbb{M}}p_h\right)dx\right) \\ &= \frac{1}{\mathbb{P}e\mathbb{M}}\mathcal{A}(\mu_h,\mu_h)+\frac{2}{\mathbb{R}e}\mathcal{B}(c_h,\mathbf{u}_h,\mathbf{u}_h) \end{aligned} \tag{5.2.16}$$

if and only if the following conditions on the numerical fluxes F_i, for $i = 1, \dots, 5$, are satisfied:

a.

$$\begin{aligned} 0 &= \int_{\mathcal{E}}\Bigg(F_1\left(\frac{\mu_h}{\mathbb{M}}\right)+F_2\left(\mathbf{u}_h\right)+F_3\Bigg(\frac{1}{\mathbb{M}}g_1(c_h)+\frac{\mathbb{C}}{2\,\mathbb{M}}|\mathbf{q}_h|^2+\frac{1}{\mathbb{M}}K(1-c_h)+\frac{1}{\mathbb{M}}\frac{1}{\rho_1}c_h p_h \\ &+\frac{1}{\mathbb{M}}N_1\theta(1-c_h)\ln p_h\Bigg)+\frac{1}{2}\left[\!\left[\rho_h(\mathbf{u}_h\cdot\mathbf{u}_h)\mathbf{u}_h\right]\!\right]+\frac{1}{\mathbb{M}}\left[\!\left[\rho_h g_1(c_h)\mathbf{u}_h\right]\!\right] \\ &+\frac{\mathbb{C}}{2\,\mathbb{M}}\left[\!\left[\rho_h|\mathbf{q}_h|^2\mathbf{u}_h\right]\!\right]+\frac{1}{\mathbb{M}}\left[\!\left[K\rho_h(1-c_h)\mathbf{u}_h\right]\!\right] \\ &+\frac{1}{\mathbb{M}}\frac{1}{\rho_1}\left[\!\left[\rho_h p_h c_h\mathbf{u}_h\right]\!\right]+\frac{N_1\theta}{\mathbb{M}}\left[\!\left[\rho_h(1-c_h)\ln p_h\mathbf{u}_h\right]\!\right]\Bigg)\,ds, \end{aligned} \tag{5.2.17}$$

b.

$$0 = \int_{\mathcal{E}}\left(\partial_t F_5\left(\frac{\mathbb{C}}{\mathbb{M}}\rho_h\mathbf{q}_h\right)-\frac{\mathbb{C}}{\mathbb{M}}\left[\!\left[\rho_h\mathbf{q}_h(\partial_t c_h)\right]\!\right]-F_4\left(\frac{1}{\mathbb{M}}\partial_t c_h\right)\right)ds. \tag{5.2.18}$$

Remark. Notice that $\mathcal{A}$ and $\mathcal{B}$, by definition, are negative definite.

Proof. Let us test equation (5.2.8) with $\frac{\mu_h}{\mathbb{M}}$ and equation (5.2.9) with $\mathbf{u}_h$ and sum them together. If we use the fact that

$$\begin{aligned} &\sum_{T\in\mathscr{T}_h}\int_T\left(\rho_h\left(\mathbf{u}_h\cdot\nabla\right)\mathbf{u}_h\cdot\mathbf{u}_h+\frac{1}{2}\operatorname{div}(\rho_h\mathbf{u}_h)\mathbf{u}_h\cdot\mathbf{u}_h\right)dx \\ &= \int_{\mathcal{E}}\frac{1}{2}\left[\!\left[\rho_h(\mathbf{u}_h\cdot\mathbf{u}_h)\mathbf{u}_h\right]\!\right]ds, \end{aligned} \tag{5.2.19}$$

we obtain:

$$\begin{aligned} 0 &= \sum_{T\in\mathscr{T}_h}\int_T\Bigg(\frac{1}{\mathbb{M}}\rho_h\mu_h(\partial_t c_h)-\frac{1}{\mathbb{P}e\mathbb{M}}\mathcal{A}(\mu_h,\mu_h)+\sqrt{\rho_h}\,\partial_t\left(\sqrt{\rho_h}\mathbf{u}_h\right)\cdot\mathbf{u}_h+\frac{1}{\mathbb{M}}\nabla p_h\cdot\mathbf{u}_h \\ &+\frac{1}{\mathbb{M}}\frac{1}{\rho_1}\rho_h p_h\nabla c_h\cdot\mathbf{u}_h-\frac{1}{\mathbb{M}}N_1\theta\rho_h\ln p_h\nabla c_h\cdot\mathbf{u}_h-\frac{1}{\mathbb{M}}K\rho_h\nabla c_h\cdot\mathbf{u}_h \\ &+\frac{\mathbb{C}}{2\mathbb{M}}\rho_h\nabla(|\mathbf{q}_h|^2)\cdot\mathbf{u}_h+\frac{1}{\mathbb{M}}\rho_h\mu_0(c_h)\nabla c_h\cdot\mathbf{u}_h\Bigg)\,dx-\frac{2}{\mathbb{R}e}\mathcal{B}(c_h,\mathbf{u}_h,\mathbf{u}_h) \\ &+\int_{\mathcal{E}}\left(F_1\left(\frac{\mu_h}{\mathbb{M}}\right)+F_2(\mathbf{u}_h)+\frac{1}{2}\left[\!\left[\rho_h(\mathbf{u}_h\cdot\mathbf{u}_h)\mathbf{u}_h\right]\!\right]\right)ds. \end{aligned} \tag{5.2.20}$$

Using equation (5.2.11) for the first term of (5.2.20), we obtain:

$$\begin{aligned}
0 \;=\; & \sum_{T\in\mathscr{T}_h}\int_T \Big(\sqrt{\rho_h}\,\partial_t\left(\sqrt{\rho_h}\mathbf{u}_h\right)\cdot\mathbf{u}_h + \frac{1}{\mathbb{M}}\nabla p_h\cdot\mathbf{u}_h + \frac{1}{\mathbb{M}}\frac{1}{\rho_1}\rho_h p_h\nabla c_h\cdot\mathbf{u}_h \\
& - \frac{1}{\mathbb{M}}N_1\theta\rho_h\ln p_h\nabla c_h\cdot\mathbf{u}_h + \frac{1}{\mathbb{M}}\frac{1}{\rho_1}\rho_h p_h(\partial_t c_h) - \frac{1}{\mathbb{M}}N_1\theta\rho_h\ln p_h(\partial_t c_h) \\
& + \frac{1}{\mathbb{M}}\rho_h\mu_0(c_h)\nabla c_h\cdot\mathbf{u}_h + \frac{1}{\mathbb{M}}\rho_h\mu_0(c_h)(\partial_t c_h) + \frac{\mathbb{C}}{2\,\mathbb{M}}\rho_h\nabla(|\mathbf{q}_h|^2)\cdot\mathbf{u}_h \\
& - \frac{\mathbb{C}}{\mathbb{M}}\,\mathrm{div}(\rho_h\mathbf{q}_h)(\partial_t c_h) - \frac{1}{\mathbb{M}}K\rho_h\nabla c_h\cdot\mathbf{u}_h - \frac{1}{\mathbb{M}}K\rho_h(\partial_t c_h)\Big)\,dx \\
& + \int_{\mathcal{E}}\left(F_1\left(\frac{\mu_h}{\mathbb{M}}\right) + F_2(\mathbf{u}_h) + F_4\left(\frac{1}{\mathbb{M}}\partial_t c_h\right) + \frac{1}{2}\left[\!\left[\rho_h(\mathbf{u}_h\cdot\mathbf{u}_h)\mathbf{u}_h\right]\!\right]\right)ds \\
& - \frac{1}{\mathbb{P}e\mathbb{M}}\mathcal{A}(\mu_h,\mu_h) - \frac{2}{\mathbb{R}e}\mathcal{B}(c_h,\mathbf{u}_h,\mathbf{u}_h). \qquad (5.2.21)
\end{aligned}$$

We get the following relations:

(I) the first term in (5.1.30) is

$$\sum_{T\in\mathscr{T}_h}\int_T \sqrt{\rho_h}\,\partial_t(\sqrt{\rho_h}\mathbf{u}_h)\cdot\mathbf{u}_h\,dx = \sum_{T\in\mathscr{T}_h}\int_T \partial_t\left(\frac{\rho_h}{2}|\mathbf{u}_h|^2\right)dx, \qquad (5.2.22)$$

(II) integrating by parts and using mass conservation equation (5.2.10), the terms containing $\mu_0(c_h)$ are equal to

$$\begin{aligned}
& \sum_{T\in\mathscr{T}_h}\int_T\left(\frac{1}{\mathbb{M}}\rho_h\mu_0(c_h)\nabla c_h\cdot\mathbf{u}_h + \frac{1}{\mathbb{M}}\rho_h\mu_0(c_h)(\partial_t c_h)\right)dx \\
= & \sum_{T\in\mathscr{T}_h}\int_T\left(\frac{1}{\mathbb{M}}\nabla(g_1(c_h))\cdot(\rho_h\mathbf{u}_h) + \frac{1}{\mathbb{M}}\rho_h\mu_0(c_h)(\partial_t c_h)\right)dx \\
= & \sum_{T\in\mathscr{T}_h}\int_T\left(-\frac{1}{\mathbb{M}}g_1(c_h)\,\mathrm{div}(\rho_h\mathbf{u}_h) + \frac{1}{\mathbb{M}}\rho_h\partial_t(g_1(c_h))\right)dx \\
& + \int_{\mathcal{E}}\frac{1}{\mathbb{M}}\left[\!\left[\rho_h g_1(c_h)\mathbf{u}_h\right]\!\right]ds \\
= & \sum_{T\in\mathscr{T}_h}\int_T\left(\frac{1}{\mathbb{M}}g_1(c_h)(\partial_t\rho_h) + \frac{1}{\mathbb{M}}\rho_h\partial_t(g_1(c_h))\right)dx \\
& + \int_{\mathcal{E}}\left(F_3\left(\frac{1}{\mathbb{M}}g_1(c_h)\right) + \frac{1}{\mathbb{M}}\left[\!\left[\rho_h g_1(c_h)\mathbf{u}_h\right]\!\right]\right)ds \\
= & \sum_{T\in\mathscr{T}_h}\int_T\partial_t\left(\frac{1}{\mathbb{M}}\rho_h g_1(c_h)\right)dx, \\
& + \int_{\mathcal{E}}\left(F_3\left(\frac{1}{\mathbb{M}}g_1(c_h)\right) + \frac{1}{\mathbb{M}}\left[\!\left[\rho_h g_1(c_h)\mathbf{u}_h\right]\!\right]\right)ds, \qquad (5.2.23)
\end{aligned}$$

(III) integrating by parts and using the mass conservation equation (5.2.10), the terms

containing the variable $\mathbf{q}_h$ are equal to

$$\begin{aligned}
&\sum_{T\in\mathscr{T}_h}\int_T\left(\frac{\mathbb{C}}{2\,\mathbb{M}}\rho_h\nabla(|\mathbf{q}_h|^2)\cdot\mathbf{u}_h-\frac{\mathbb{C}}{\mathbb{M}}\,\mathrm{div}(\rho_h\mathbf{q}_h)(\partial_t c_h)\right)dx\\
=\;&\sum_{T\in\mathscr{T}_h}\int_T\left(-\frac{\mathbb{C}}{2\,\mathbb{M}}|\mathbf{q}_h|^2\,\mathrm{div}(\rho_h\mathbf{u}_h)+\frac{\mathbb{C}}{\mathbb{M}}\,\rho_h\mathbf{q}_h\cdot\nabla(\partial_t c_h)\right)dx\\
&+\int_{\mathcal{E}}\left(\frac{\mathbb{C}}{2\,\mathbb{M}}[\![\rho_h|\mathbf{q}_h|^2\mathbf{u}_h]\!]-\frac{\mathbb{C}}{\mathbb{M}}\,[\![\rho_h\mathbf{q}_h(\partial_t c_h)]\!]\right)ds\\
=\;&\sum_{T\in\mathscr{T}_h}\int_T\left(\frac{\mathbb{C}}{2\,\mathbb{M}}|\mathbf{q}_h|^2(\partial_t\rho_h)+\frac{\mathbb{C}}{\mathbb{M}}\,\rho_h\mathbf{q}_h\cdot(\partial_t\mathbf{q}_h)\right)dx\\
&+\int_{\mathcal{E}}\left(F_3\left(\frac{\mathbb{C}}{2\,\mathbb{M}}|\mathbf{q}_h|^2\right)+\partial_t F_5\left(\frac{\mathbb{C}}{\mathbb{M}}\,\rho_h\mathbf{q}_h\right)\right)ds\\
&+\int_{\mathcal{E}}\left(\frac{\mathbb{C}}{2\,\mathbb{M}}[\![\rho_h|\mathbf{q}_h|^2\mathbf{u}_h]\!]-\frac{\mathbb{C}}{\mathbb{M}}\,[\![\rho_h\mathbf{q}_h(\partial_t c_h)]\!]\right)ds\\
=\;&\sum_{T\in\mathscr{T}_h}\int_T\partial_t\left(\frac{1}{\mathbb{M}}\rho_h g_2(\mathbf{q}_h)\right)dx\\
&+\int_{\mathcal{E}}\left(F_3\left(\frac{\mathbb{C}}{2\,\mathbb{M}}|\mathbf{q}_h|^2\right)+\partial_t F_5\left(\frac{\mathbb{C}}{\mathbb{M}}\,\rho_h\mathbf{q}_h\right)\right)ds\\
&+\int_{\mathcal{E}}\left(\frac{\mathbb{C}}{2\,\mathbb{M}}[\![\rho_h|\mathbf{q}_h|^2\mathbf{u}_h]\!]-\frac{\mathbb{C}}{\mathbb{M}}\,[\![\rho_h\mathbf{q}_h(\partial_t c_h)]\!]\right)ds,
\end{aligned}\tag{5.2.24}$$

(IV) integrating by parts and using the mass conservation equation (5.2.10), the terms containing the constant K are equal to

$$\begin{aligned}
&\sum_{T\in\mathscr{T}_h}\int_T\left(-\frac{1}{\mathbb{M}}K\rho_h\nabla c_h\cdot\mathbf{u}_h-\frac{1}{\mathbb{M}}K\rho_h(\partial_t c_h)\right)dx\\
=\;&\sum_{T\in\mathscr{T}_h}\int_T\left(\frac{1}{\mathbb{M}}K\rho_h\nabla(1-c_h)\cdot\mathbf{u}_h+\frac{1}{\mathbb{M}}K\rho_h\partial_t(1-c_h)\right)dx\\
=\;&\sum_{T\in\mathscr{T}_h}\int_T\left(-\frac{1}{\mathbb{M}}K(1-c_h)\,\mathrm{div}(\rho_h\mathbf{u}_h)+\frac{1}{\mathbb{M}}K\rho_h\partial_t(1-c_h)\right)dx\\
&+\int_{\mathcal{E}}\frac{1}{\mathbb{M}}[\![K\rho_h(1-c_h)\mathbf{u}_h]\!]\,ds\\
=\;&\sum_{T\in\mathscr{T}_h}\int_T\left(\frac{1}{\mathbb{M}}K(1-c_h)(\partial_t\rho_h)+\frac{1}{\mathbb{M}}K\rho_h\partial_t(1-c_h)\right)dx\\
&+\int_{\mathcal{E}}\left(F_3\left(\frac{1}{\mathbb{M}}K(1-c_h)\right)+\frac{1}{\mathbb{M}}[\![K\rho_h(1-c_h)\mathbf{u}_h]\!]\right)ds\\
=\;&\sum_{T\in\mathscr{T}_h}\int_T\partial_t\left(\frac{1}{\mathbb{M}}\rho_h g_0(c_h)\right)dx\\
&+\int_{\mathcal{E}}\left(F_3\left(\frac{1}{\mathbb{M}}K(1-c_h)\right)+\frac{1}{\mathbb{M}}[\![K\rho_h(1-c_h)\mathbf{u}_h]\!]\right)ds.
\end{aligned}\tag{5.2.25}$$

Now, as in the continuous case, let us consider the pressure terms:

$$\begin{aligned}
\sum_{T\in\mathscr{T}_h}\int_T\Big(&\frac{1}{\mathbb{M}}\nabla p_h\cdot\mathbf{u}_h+\frac{1}{\mathbb{M}}\frac{1}{\rho_1}\rho_h p_h\nabla c_h\cdot\mathbf{u}_h-\frac{1}{\mathbb{M}}N_1\theta\rho_h\ln p_h\nabla c_h\cdot\mathbf{u}_h\\
&+\frac{1}{\mathbb{M}}\frac{1}{\rho_1}\rho_h p_h(\partial_t c_h)-\frac{1}{\mathbb{M}}N_1\theta\rho_h\ln p_h(\partial_t c_h)\Big)\,dx.
\end{aligned}\tag{5.2.26}$$

Notice that, integrating by parts and using mass conservation equation (5.2.10):

(a)

$$\begin{aligned}
&\sum_{T\in\mathscr{T}_h}\int_T\left(\frac{1}{\mathbb{M}}\frac{1}{\rho_1}\rho_h p_h\nabla c_h\cdot\mathbf{u}_h\right)dx\\
=\;&\sum_{T\in\mathscr{T}_h}\int_T\left(-\frac{1}{\mathbb{M}}\frac{1}{\rho_1}c_h p_h\,\mathrm{div}(\rho_h\mathbf{u}_h)-\frac{1}{\mathbb{M}}\frac{1}{\rho_1}c_h\rho_h\mathbf{u}_h\cdot\nabla p_h\right)dx\\
&+\int_{\mathcal{E}}\frac{1}{\mathbb{M}}\frac{1}{\rho_1}[\![\rho_h p_h c_h\mathbf{u}_h]\!]\,ds\\
=\;&\sum_{T\in\mathscr{T}_h}\int_T\left(\frac{1}{\mathbb{M}}\frac{1}{\rho_1}c_h p_h(\partial_t\rho_h)-\frac{1}{\mathbb{M}}\frac{1}{\rho_1}\rho_h c_h\mathbf{u}_h\cdot\nabla p_h\right)dx\\
&+\int_{\mathcal{E}}\left(F_3\left(\frac{1}{\mathbb{M}}\frac{1}{\rho_1}c_h p_h\right)+\frac{1}{\mathbb{M}}\frac{1}{\rho_1}[\![\rho_h p_h c_h\mathbf{u}_h]\!]\right)ds,
\end{aligned}\tag{5.2.27}$$

(b)

$$\begin{aligned}
&\sum_{T\in\mathscr{T}_h}\int_T\left(-\frac{1}{\mathbb{M}}N_1\theta\rho_h\ln p_h\nabla c_h\cdot\mathbf{u}_h\right)dx\\
=\;&\sum_{T\in\mathscr{T}_h}\int_T\left(\frac{1}{\mathbb{M}}N_1\theta\rho_h\ln p_h\nabla(1-c_h)\cdot\mathbf{u}_h\right)dx\\
=\;&\sum_{T\in\mathscr{T}_h}\int_T\left(-\frac{1}{\mathbb{M}}N_1\theta(1-c_h)\ln p_h\,\mathrm{div}(\rho_h\mathbf{u}_h)\right.\\
&\qquad\left.-\frac{1}{\mathbb{M}}N_1\theta\rho_h(1-c_h)\frac{\nabla p_h}{p_h}\cdot\mathbf{u}_h\right)dx\\
&+\int_{\mathcal{E}}\frac{1}{\mathbb{M}}[\![N_1\theta\rho_h(1-c_h)\ln p_h\mathbf{u}_h]\!]\,ds\\
=\;&\sum_{T\in\mathscr{T}_h}\int_T\left(\frac{1}{\mathbb{M}}N_1\theta(1-c_h)\ln p_h(\partial_t\rho_h)-\frac{1}{\mathbb{M}}N_1\theta\rho_h(1-c_h)\frac{\nabla p_h}{p_h}\cdot\mathbf{u}_h\right)dx\\
&+\int_{\mathcal{E}}\left(F_3\left(\frac{1}{\mathbb{M}}N_1\theta\ln p_h(1-c_h)\right)+\frac{1}{\mathbb{M}}[\![N_1\theta\rho_h(1-c_h)\ln p_h\mathbf{u}_h]\!]\right)ds.
\end{aligned}\tag{5.2.28}$$

Using (5.2.27) and (5.2.28) into (5.2.26) we obtain:

$$\begin{aligned}
&\sum_{T\in\mathscr{T}_h}\int_T\left(\frac{1}{\mathbb{M}}\nabla p_h\cdot\mathbf{u}_h-\frac{1}{\mathbb{M}}\frac{1}{\rho_1}\rho_h c_h\mathbf{u}_h\cdot\nabla p_h-\frac{1}{\mathbb{M}}N_1\theta\rho_h(1-c_h)\frac{\nabla p_h}{p_h}\cdot\mathbf{u}_h\right.\\
&\qquad+\frac{1}{\mathbb{M}}\frac{1}{\rho_1}c_h p_h(\partial_t\rho_h)+\frac{1}{\mathbb{M}}\frac{1}{\rho_1}\rho_h p_h(\partial_t c_h)\\
&\qquad\left.+\frac{1}{\mathbb{M}}N_1\theta(1-c_h)\ln p_h(\partial_t\rho_h)-\frac{1}{\mathbb{M}}N_1\theta\rho_h\ln p_h(\partial_t c_h)\right)dx\\
&+\int_{\mathcal{E}}F_3\left(\frac{1}{\mathbb{M}}\frac{1}{\rho_1}c_h p_h+\frac{1}{\mathbb{M}}N_1\theta(1-c_h)\ln p_h\right)ds\\
&+\int_{\mathcal{E}}\left(\frac{1}{\mathbb{M}}\frac{1}{\rho_1}[\![\rho_h p_h c_h\mathbf{u}_h]\!]+\frac{1}{\mathbb{M}}[\![N_1\theta\rho_h(1-c_h)\ln p_h\mathbf{u}_h]\!]\right)ds.
\end{aligned}\tag{5.2.29}$$

If we notice the fact that, remembering the definition of ρ_h,

$$\begin{aligned}
&\sum_{T\in\mathscr{T}_h}\int_T\left(\frac{1}{\mathbb{M}}\nabla p_h\cdot\mathbf{u}_h-\frac{1}{\mathbb{M}}\frac{1}{\rho_1}\rho_h c_h\mathbf{u}_h\cdot\nabla p_h-\frac{1}{\mathbb{M}}N_1\theta\rho_h(1-c_h)\frac{\nabla p_h}{p_h}\cdot\mathbf{u}_h\right)dx\\
=\;&\sum_{T\in\mathscr{T}_h}\int_T\left(\frac{1}{\mathbb{M}}\nabla p_h\cdot\mathbf{u}_h-\frac{1}{\mathbb{M}}\left(\frac{c_h}{\rho_1}+\frac{N_1\theta(1-c_h)}{p_h}\right)\rho_h\mathbf{u}_h\cdot\nabla p_h\right)dx=0,
\end{aligned}\tag{5.2.30}$$

then we can rewrite (5.2.29) as

$$\begin{aligned}
&\sum_{T\in\mathscr{T}_h}\int_T\left(\frac{1}{\mathbb{M}}\frac{1}{\rho_1}c_h p_h(\partial_t\rho_h)+\frac{1}{\mathbb{M}}\frac{1}{\rho_1}p_h\rho_h(\partial_t c_h)-\frac{1}{\mathbb{M}}N_1\theta\rho_h(1-c_h)\frac{\partial_t p_h}{p_h}\right.\\
&\qquad+\frac{1}{\mathbb{M}}N_1\theta\rho_h(1-c_h)\frac{\partial_t p_h}{p_h}+\frac{1}{\mathbb{M}}N_1\theta(1-c_h)\ln p_h(\partial_t\rho_h)\\
&\qquad\left.-\frac{1}{\mathbb{M}}N_1\theta\rho_h\ln p_h(\partial_t c_h)\right)dx\\
&+\int_{\mathcal{E}}F_3\left(\frac{1}{\mathbb{M}}\frac{1}{\rho_1}c_h p_h+\frac{1}{\mathbb{M}}N_1\theta(1-c_h)\ln p_h\right)ds\\
&+\int_{\mathcal{E}}\left(\frac{1}{\mathbb{M}}\frac{1}{\rho_1}[\![\rho_h p_h c_h\mathbf{u}_h]\!]+\frac{1}{\mathbb{M}}[\![N_1\theta\rho_h(1-c_h)\ln p_h\mathbf{u}_h]\!]\right)ds
\end{aligned}\tag{5.2.31}$$

in which we have added and subtracted the quantity $\frac{1}{\mathbb{M}}N_1\theta\rho_h(1-c_h)\frac{\partial_t p_h}{p_h}$. Using the fact that p_h can be written, in terms of ρ_h and c_h, as

$$p_h=\frac{N_1\theta\rho_1\rho_h(1-c_h)}{\rho_1-\rho_h c_h},\tag{5.2.32}$$

we obtain:

$$\sum_{T\in\mathscr{T}_h}\int_T\left(-\frac{1}{\mathbb{M}}N_1\theta\rho_h(1-c_h)\frac{\partial_t p_h}{p_h}\right)dx=\sum_{T\in\mathscr{T}_h}\int_T\left(-\frac{1}{\mathbb{M}}\partial_t p_h+\frac{1}{\mathbb{M}}\frac{1}{\rho_1}\rho_h c_h(\partial_t p_h)\right)dx.\tag{5.2.33}$$

Using (5.2.33) into (5.2.31), we obtain:

$$\begin{aligned}
&\sum_{T\in\mathscr{T}_h}\int_T\left(\frac{1}{\mathbb{M}}\frac{1}{\rho_1}c_h p_h(\partial_t\rho_h)+\frac{1}{\mathbb{M}}\frac{1}{\rho_1}\rho_h p_h(\partial_t c_h)+\frac{1}{\mathbb{M}}\frac{1}{\rho_1}\rho_h c_h(\partial_t p_h)\right.\\
&\qquad+\frac{1}{\mathbb{M}}N_1\theta(1-c_h)\ln p_h(\partial_t\rho_h)+\frac{1}{\mathbb{M}}N_1\theta\rho_h\ln p_h\partial_t(1-c_h)\\
&\qquad\left.+\frac{1}{\mathbb{M}}N_1\theta\rho_h(1-c_h)\frac{\partial_t p_h}{p_h}-\frac{1}{\mathbb{M}}\partial_t p_h\right)dx\\
&+\int_{\mathcal{E}}F_3\left(\frac{1}{\mathbb{M}}\frac{1}{\rho_1}c_h p_h+\frac{1}{\mathbb{M}}N_1\theta(1-c_h)\ln p_h\right)ds\\
&+\int_{\mathcal{E}}\left(\frac{1}{\mathbb{M}}\frac{1}{\rho_1}[\![\rho_h p_h c_h\mathbf{u}_h]\!]+\frac{1}{\mathbb{M}}[\![N_1\theta\rho_h(1-c_h)\ln p_h\mathbf{u}_h]\!]\right)ds\\
=\;&\sum_{T\in\mathscr{T}_h}\int_T\frac{1}{\mathbb{M}}\partial_t\left(\frac{c_h}{\rho_1}p_h\rho_h+N_1\theta\rho_h(1-c_h)\ln p_h-p_h\right)dx\\
&+\int_{\mathcal{E}}F_3\left(\frac{1}{\mathbb{M}}\frac{1}{\rho_1}c_h p_h+\frac{1}{\mathbb{M}}N_1\theta(1-c_h)\ln p_h\right)ds\\
&+\int_{\mathcal{E}}\left(\frac{1}{\mathbb{M}}\frac{1}{\rho_1}[\![\rho_h p_h c_h\mathbf{u}_h]\!]+\frac{1}{\mathbb{M}}[\![N_1\theta\rho_h(1-c_h)\ln p_h\mathbf{u}_h]\!]\right)ds.
\end{aligned}\tag{5.2.34}$$

Using (5.2.22)-(5.2.25) and (5.2.26)-(5.2.34) into (5.2.21), we obtain:

$$\begin{aligned}
0 \quad = \quad & \sum_{T\in\mathcal{T}_h}\int_T \partial_t\left(\frac{\rho_h}{2}|\mathbf{u}_h|^2+\frac{1}{\mathbb{M}}\rho_h g(p_h,c_h,\mathbf{q}_h)-\frac{1}{\mathbb{M}}p_h\right)dx \\
& +\int_{\mathcal{E}}\left(F_1\left(\frac{\mu_h}{\mathbb{M}}\right)+F_2\left(\mathbf{u}_h\right)+F_3\left(\frac{1}{\mathbb{M}}g_1(c_h)+\frac{\mathbb{C}}{2\,\mathbb{M}}|\mathbf{q}_h|^2+\frac{1}{\mathbb{M}}K(1-c_h)\right.\right. \\
& \left.+\frac{1}{\mathbb{M}}\frac{1}{\rho_1}c_h p_h+\frac{1}{\mathbb{M}}N_1\theta(1-c_h)\ln p_h\right)-F_4\left(\frac{1}{\mathbb{M}}\partial_t c_h\right)+\partial_t F_5\left(\frac{\mathbb{C}}{\mathbb{M}}\rho_h\mathbf{q}_h\right) \\
& +\frac{1}{2}[\![\rho_h(\mathbf{u}_h\cdot\mathbf{u}_h)\mathbf{u}_h]\!]+\frac{1}{\mathbb{M}}[\![\rho_h g_1(c_h)\mathbf{u}_h]\!] \\
& +\frac{\mathbb{C}}{2\,\mathbb{M}}[\![\rho_h|\mathbf{q}_h|^2\mathbf{u}_h]\!]-\frac{\mathbb{C}}{\mathbb{M}}[\![\rho_h\mathbf{q}_h(\partial_t c_h)]\!]+\frac{1}{\mathbb{M}}[\![K\rho_h(1-c_h)\mathbf{u}_h]\!] \\
& \left.+\frac{1}{\mathbb{M}}\frac{1}{\rho_1}[\![\rho_h p_h c_h\mathbf{u}_h]\!]+\frac{N_1\theta}{\mathbb{M}}[\![\rho_h(1-c_h)\ln p_h\mathbf{u}_h]\!]\right)ds \\
& -\frac{1}{\mathbb{P}e\mathbb{M}}\mathcal{A}(\mu_h,\mu_h)-\frac{2}{\mathbb{R}e}\mathcal{B}(c_h,\mathbf{u}_h,\mathbf{u}_h). \qquad (5.2.35)
\end{aligned}$$

The scheme (5.2.8)-(5.2.12) preserves the energy law at the spatially discrete level iff

$$\begin{aligned}
0 \quad = \quad & \int_{\mathcal{E}}\left(F_1\left(\frac{\mu_h}{\mathbb{M}}\right)+F_2\left(\mathbf{u}_h\right)+F_3\left(\frac{1}{\mathbb{M}}g_1(c_h)+\frac{\mathbb{C}}{2\,\mathbb{M}}|\mathbf{q}_h|^2+\frac{1}{\mathbb{M}}K(1-c_h)\right.\right. \\
& \left.+\frac{1}{\mathbb{M}}\frac{1}{\rho_1}c_h p_h+\frac{1}{\mathbb{M}}N_1\theta(1-c_h)\ln p_h\right)+\frac{1}{2}[\![\rho_h(\mathbf{u}_h\cdot\mathbf{u}_h)\mathbf{u}_h]\!]+\frac{1}{\mathbb{M}}[\![\rho_h g_1(c_h)\mathbf{u}_h]\!] \\
& +\frac{\mathbb{C}}{2\,\mathbb{M}}[\![\rho_h|\mathbf{q}_h|^2\mathbf{u}_h]\!]+\frac{1}{\mathbb{M}}[\![K\rho_h(1-c_h)\mathbf{u}_h]\!] \\
& \left.+\frac{1}{\mathbb{M}}\frac{1}{\rho_1}[\![\rho_h p_h c_h\mathbf{u}_h]\!]+\frac{N_1\theta}{\mathbb{M}}[\![\rho_h(1-c_h)\ln p_h\mathbf{u}_h]\!]\right)ds \\
& +\int_{\mathcal{E}}\left(\partial_t F_5\left(\frac{\mathbb{C}}{\mathbb{M}}\rho_h\mathbf{q}_h\right)-\frac{\mathbb{C}}{\mathbb{M}}[\![\rho_h\mathbf{q}_h(\partial_t c_h)]\!]-F_4\left(\frac{1}{\mathbb{M}}\partial_t c_h\right)\right)ds. \qquad (5.2.36)
\end{aligned}$$

As for the LT system, it is clear from (5.2.8)-(5.2.12) that $\partial_t c_h$ does not depend from the other variables; so conditions (a) and (b) of the thesis are satisfied. □

5.2.5 Choice of the numerical fluxes.

In a similar way as for the LT system, we have to choose the numerical fluxes $F_i, i=1,...,5$. As for the LT system, from the spatially discrete mass conservation theorem (Theorem 5.2.1), it follows that we have mass conservation for the spatially discrete scheme (5.2.8)-(5.2.12) iff

$$\int_{\mathcal{E}}F_3(c_h,\mathbf{u}_h,p_h,\mu_h,\mathbf{q}_h,1)\,ds=-\int_{\mathcal{E}}[\![\rho_h\mathbf{u}_h]\!]\,ds. \qquad (5.2.37)$$

So, we can choose:

$$F_3(c_h,\mathbf{u}_h,p_h,\mu_h,\mathbf{q}_h,Z)=-[\![\rho_h\mathbf{u}_h]\!]\{\!\{Z\}\!\}. \qquad (5.2.38)$$

From condition (b) in the spatially discrete energy law, as for the LT system, it follows that

$$\begin{aligned}
F_4(c_h,\mathbf{u}_h,p_h,\mu_h,\mathbf{q}_h,\psi) \quad &= \quad -\mathbb{C}[\![\rho_h\mathbf{q}_h]\!]\{\!\{\psi\}\!\}, \qquad (5.2.39)\\
F_5(c_h,\mathbf{u}_h,p_h,\mu_h,\mathbf{q}_h,\mathbf{T}) \quad &= \quad [\![c_h]\!]\cdot\{\!\{\mathbf{T}\}\!\}. \qquad (5.2.40)
\end{aligned}$$

If we notice that

$$\begin{aligned}
&\int_{\mathcal{E}} F_3 \left(\frac{1}{\mathbb{M}} g_1(c_h) + \frac{\mathbb{C}}{2\,\mathbb{M}} |\mathbf{q}_h|^2 + \frac{1}{\mathbb{M}} K(1-c_h) + \frac{1}{\mathbb{M}} \frac{1}{\rho_1} c_h p_h + \frac{1}{\mathbb{M}} N_1 \theta (1-c_h) \ln p_h \right) ds \\
= &\int_{\mathcal{E}} \left(-\frac{1}{\mathbb{M}} [\![\rho_h \mathbf{u}_h]\!] \{\!\{ g_1(c_h) \}\!\} - \frac{\mathbb{C}}{2\,\mathbb{M}} [\![\rho_h \mathbf{u}_h]\!] \{\!\{ |\mathbf{q}_h|^2 \}\!\} - \frac{1}{\mathbb{M}} [\![\rho_h \mathbf{u}_h]\!] \{\!\{ K(1-c_h) \}\!\} \right. \\
&\left. - \frac{1}{\mathbb{M}} \frac{1}{\rho_1} [\![\rho_h \mathbf{u}_h]\!] \{\!\{ c_h p_h \}\!\} - \frac{N_1 \theta}{\mathbb{M}} [\![\rho_h \mathbf{u}_h]\!] \{\!\{ (1-c_h) \ln p_h \}\!\} \right) ds, \qquad (5.2.41)
\end{aligned}$$

from condition (a) we deduce that

$$\begin{aligned}
&\int_{\mathcal{E}} \left(F_1 \left(\frac{\mu_h}{\mathbb{M}} \right) + F_2(\mathbf{u}_h) \right) ds \\
= &\int_{\mathcal{E}} \left(-\frac{1}{2} [\![\rho_h (\mathbf{u}_h \cdot \mathbf{u}_h) \mathbf{u}_h]\!] - \frac{1}{\mathbb{M}} [\![g_1(c_h)]\!] \cdot \{\!\{ \rho_h \mathbf{u}_h \}\!\} \right. \\
&- \frac{\mathbb{C}}{2\,\mathbb{M}} [\![|\mathbf{q}_h|^2]\!] \cdot \{\!\{ \rho_h \mathbf{u}_h \}\!\} - \frac{1}{\mathbb{M}} [\![K(1-c_h)]\!] \cdot \{\!\{ \rho_h \mathbf{u}_h \}\!\} \\
&\left. - \frac{1}{\mathbb{M}} \frac{1}{\rho_1} [\![c_h p_h]\!] \cdot \{\!\{ \rho_h \mathbf{u}_h \}\!\} - \frac{N_1 \theta}{\mathbb{M}} [\![(1-c_h) \ln p_h]\!] \cdot \{\!\{ \rho_h \mathbf{u}_h \}\!\} \right) ds. \qquad (5.2.42)
\end{aligned}$$

Using the fact that

$$\int_{\mathcal{E}} \left((\{\!\{ \mathbf{u}_h \}\!\} \otimes \{\!\{ \rho_h \mathbf{u}_h \}\!\}) : [\![\mathbf{u}_h]\!]_{\otimes} - \frac{1}{2} [\![|\mathbf{u}_h|^2]\!] \cdot \{\!\{ \rho_h \mathbf{u}_h \}\!\} \right) ds = 0, \qquad (5.2.43)$$

we obtain the following expression for the numerical fluxes:

$$F_1(X) = 0, \qquad (5.2.44)$$

$$\begin{aligned}
F_2(\boldsymbol{\xi}) = &-\frac{1}{2} [\![\rho_h \mathbf{u}_h]\!] \{\!\{ \mathbf{u}_h \cdot \boldsymbol{\xi} \}\!\} - (\{\!\{ \boldsymbol{\xi} \}\!\} \otimes \{\!\{ \rho_h \mathbf{u}_h \}\!\}) : [\![\mathbf{u}_h]\!]_{\otimes} \\
&- \frac{1}{\mathbb{M}} [\![g_1(c_h)]\!] \cdot \{\!\{ \rho_h \boldsymbol{\xi} \}\!\} - \frac{\mathbb{C}}{2\,\mathbb{M}} [\![|\mathbf{q}_h|^2]\!] \cdot \{\!\{ \rho_h \boldsymbol{\xi} \}\!\} \\
&- \frac{1}{\mathbb{M}} [\![K(1-c_h)]\!] \cdot \{\!\{ \rho_h \boldsymbol{\xi} \}\!\} - \frac{1}{\mathbb{M}} \frac{1}{\rho_1} [\![c_h p_h]\!] \cdot \{\!\{ \rho_h \boldsymbol{\xi} \}\!\} \\
&- \frac{N_1 \theta}{\mathbb{M}} [\![(1-c_h) \ln p_h]\!] \cdot \{\!\{ \rho_h \boldsymbol{\xi} \}\!\}. \qquad (5.2.45)
\end{aligned}$$

In view of the above discussion, the spatially mixed discrete scheme for the MF system can be rewritten as follows. Find

$$\begin{aligned}
(c_h, \mathbf{u}_h, p_h, \mu_h, \mathbf{q}_h) \in &\; L^2(0,T;\mathbb{V}) \times L^2(0,T;\mathbb{V}_0^2) \times L^2(0,T;\mathbb{V}) \times \\
&\; L^2(0,T;\mathbb{V}) \times L^2(0,T;\mathbb{V}_{\mathbf{n}})
\end{aligned}$$

such that

$$0 = \sum_{T \in \mathcal{T}_h} \int_T \left(\rho_h \left(\partial_t c_h \right) X + \rho_h (\mathbf{u}_h \cdot \nabla) c_h X \right) dx - \frac{1}{\mathbb{P}e} \mathcal{A}(\mu_h, X), \qquad (5.2.46)$$

$$
\begin{aligned}
0 = & \sum_{T\in\mathscr{T}_h}\int_T \Big(\sqrt{\rho_h}\,\partial_t\left(\sqrt{\rho_h}\mathbf{u}_h\right)\cdot\boldsymbol{\xi} + \rho_h(\mathbf{u}_h\cdot\nabla)\mathbf{u}_h\cdot\boldsymbol{\xi} + \frac{1}{2}\,\mathrm{div}(\rho_h\mathbf{u}_h)\mathbf{u}_h\cdot\boldsymbol{\xi} + \frac{1}{\mathbb{M}}\nabla p_h\cdot\boldsymbol{\xi} \\
& -\frac{1}{\mathbb{M}}\rho_h\mu_h\,\nabla c_h\cdot\boldsymbol{\xi} + \frac{1}{\mathbb{M}}\frac{1}{\rho_1}\rho_h p_h\nabla c_h\cdot\boldsymbol{\xi} - \frac{1}{\mathbb{M}}N_1\theta\rho_h\ln p_h\nabla c_h\cdot\boldsymbol{\xi} - \frac{1}{\mathbb{M}}K\rho_h\nabla c_h\cdot\boldsymbol{\xi} \\
& + \frac{\mathbb{C}}{2\mathbb{M}}\rho_h\nabla(|\mathbf{q}_h|^2)\cdot\boldsymbol{\xi} + \frac{1}{\mathbb{M}}\rho_h\mu_0(c_h)\nabla c_h\cdot\boldsymbol{\xi}\Big)\,dx - \frac{2}{\mathbb{R}e}\mathcal{B}(c_h,\mathbf{u}_h,\boldsymbol{\xi}) \\
& + \int_{\mathcal{E}}\Big(-\frac{1}{2}\left[\!\left[\rho_h\mathbf{u}_h\right]\!\right]\left\{\!\left\{\mathbf{u}_h\cdot\boldsymbol{\xi}\right\}\!\right\} - \left(\left\{\!\left\{\boldsymbol{\xi}\right\}\!\right\}\otimes\left\{\!\left\{\rho_h\mathbf{u}_h\right\}\!\right\}\right) : \left[\!\left[\mathbf{u}_h\right]\!\right]_{\otimes} \\
& \quad - \frac{1}{\mathbb{M}}\left[\!\left[g_1(c_h)\right]\!\right]\cdot\left\{\!\left\{\rho_h\boldsymbol{\xi}\right\}\!\right\} - \frac{\mathbb{C}}{2\,\mathbb{M}}\left[\!\left[|\mathbf{q}_h|^2\right]\!\right]\cdot\left\{\!\left\{\rho_h\boldsymbol{\xi}\right\}\!\right\} \\
& \quad - \frac{1}{\mathbb{M}}\left[\!\left[K(1-c_h)\right]\!\right]\cdot\left\{\!\left\{\rho_h\boldsymbol{\xi}\right\}\!\right\} - \frac{1}{\mathbb{M}}\frac{1}{\rho_1}\left[\!\left[c_h p_h\right]\!\right]\cdot\left\{\!\left\{\rho_h\boldsymbol{\xi}\right\}\!\right\} \\
& \quad - \frac{N_1\theta}{\mathbb{M}}\left[\!\left[(1-c_h)\ln p_h\right]\!\right]\cdot\left\{\!\left\{\rho_h\boldsymbol{\xi}\right\}\!\right\}\Big)\,ds, \qquad (5.2.47)
\end{aligned}
$$

$$
0 = \sum_{T\in\mathscr{T}_h}\int_T \left((\partial_t\rho_h)\,Z + \mathrm{div}(\rho_h\mathbf{u}_h)Z\right)\,dx + \int_{\mathcal{E}}\left(-\left[\!\left[\rho_h\mathbf{u}_h\right]\!\right]\left\{\!\left\{Z\right\}\!\right\}\right)\,ds, \qquad (5.2.48)
$$

$$
\begin{aligned}
0 = & \sum_{T\in\mathscr{T}_h}\int_T \Big(\rho_h\mu_h\psi - \rho_h\mu_0(c_h)\psi - \frac{p_h}{\rho_1}\rho_h\psi + N_1\theta\rho_h\ln p_h\psi \\
& + \mathbb{C}\,\mathrm{div}(\,\rho_h\,\mathbf{q}_h\,)\psi + K\rho_h\psi\Big)\,dx + \int_{\mathcal{E}}\left(-\mathbb{C}\left[\!\left[\rho_h\mathbf{q}_h\right]\!\right]\left\{\!\left\{\psi\right\}\!\right\}\right)\,ds, \qquad (5.2.49)
\end{aligned}
$$

$$
0 = \sum_{T\in\mathscr{T}_h}\int_T \left(\mathbf{q}_h\cdot\mathbf{T} - \nabla c_h\cdot\mathbf{T}\right)\,dx + \int_{\mathcal{E}}\left(\left[\!\left[c_h\right]\!\right]\cdot\left\{\!\left\{\mathbf{T}\right\}\!\right\}\right)\,ds, \qquad (5.2.50)
$$

$$
\forall\,(X,\boldsymbol{\xi},Z,\psi,\mathbf{T})\in\mathbb{V}\times\mathbb{V}_0^2\times\mathbb{V}\times\mathbb{V}\times\mathbb{V}_{\mathbf{n}}.
$$

Remark. The choice of the numerical fluxes for the MF system is consistent with the choice we made for the LT system, because another possible choice for the LT numerical fluxes F_1 and F_2 is the following one:

$$
\begin{aligned}
F_1(X) &= 0, \qquad (5.2.51)\\
F_2(\boldsymbol{\xi}) &= -\frac{1}{2}\left[\!\left[\rho_h\mathbf{u}_h\right]\!\right]\left\{\!\left\{\mathbf{u}_h\cdot\boldsymbol{\xi}\right\}\!\right\} - \left(\left\{\!\left\{\boldsymbol{\xi}\right\}\!\right\}\otimes\left\{\!\left\{\rho_h\mathbf{u}_h\right\}\!\right\}\right) : \left[\!\left[\mathbf{u}_h\right]\!\right]_{\otimes} \\
&\quad -\frac{1}{\mathbb{M}}\left[\!\left[c_h\mu_h\right]\!\right]\cdot\left\{\!\left\{\rho_h\boldsymbol{\xi}\right\}\!\right\} - \frac{1}{\mathbb{M}}\left[\!\left[\bar{p}_h\right]\!\right]\cdot\left\{\!\left\{\rho_h\boldsymbol{\xi}\right\}\!\right\} \\
&\quad +\frac{\rho_0\,y}{\mathbb{F}r^2}\left[\!\left[\frac{1}{\rho_h}\right]\!\right]\cdot\left\{\!\left\{\rho_h\boldsymbol{\xi}\right\}\!\right\}. \qquad (5.2.52)
\end{aligned}
$$

Notice that, for the MF system, we have performed different transformations on the momentum equation and no gravitational effects have been included.

5.3 Temporal discretisation.

In this section we propose a semi-discretisation in time for the MF mixed formulation (5.1.14)-(5.1.18). We extend to the MF system the modified-midpoint type scheme we proposed for the LT system in the previous chapter.

5.3.1 Temporally discrete mixed formulation.

The temporally discrete scheme for (5.1.14)-(5.1.18) is written as follows.
Given initial conditions $(c^0, \mathbf{u}^0, p^0, \mu^0, \mathbf{q}^0)$, for all $n = 0, 1, ..., N-1$, find

$$(c^{n+1}, \mathbf{u}^{n+1}, p^{n+1}, \mu^{n+1}, \mathbf{q}^{n+1}) \in H^1(\Omega) \times (H^2(\Omega) \cap H_0^1(\Omega))^2 \times H^1(\Omega) \times H^2(\Omega) \times H^1_{\mathbf{n}}(\Omega)$$

such that

$$0 = \rho^{n+\frac{1}{2}}\, c_{\bar{t}}^{n+1} + \rho^{n+\frac{1}{2}} (\sqrt{\rho}\mathbf{u})^{n+1} \cdot \nabla c^{n+\frac{1}{2}} - \frac{1}{\mathbb{P}e} \Delta \mu^{n+\frac{1}{2}}, \tag{5.3.1}$$

$$\begin{aligned} \mathbf{0} = {} & \sqrt{\rho}^{\,n+\frac{1}{2}} (\sqrt{\rho}\mathbf{u})_{\bar{t}}^{n+1} + \rho^{n+\frac{1}{2}} \left((\sqrt{\rho}\mathbf{u})^{n+1} \cdot \nabla \right) (\sqrt{\rho}\mathbf{u})^{n+1} \\ & + \frac{1}{2} \operatorname{div}(\rho^{n+\frac{1}{2}} (\sqrt{\rho}\mathbf{u})^{n+1}) (\sqrt{\rho}\mathbf{u})^{n+1} + \frac{1}{\mathbb{M}} \nabla p^{n+\frac{1}{2}} \\ & - \frac{1}{\mathbb{M}} \rho^{n+\frac{1}{2}} \mu^{n+\frac{1}{2}} \nabla c^{n+\frac{1}{2}} + \frac{1}{\mathbb{M}} \frac{1}{\rho_1} \rho^{n+\frac{1}{2},*} p^{n+\frac{1}{2}} \nabla c^{n+\frac{1}{2}} - \frac{1}{\mathbb{M}} N_1 \theta \rho^{n+\frac{1}{2},*} (\ln p)^{n+\frac{1}{2}} \nabla c^{n+\frac{1}{2}} \\ & - \frac{1}{\mathbb{M}} K \rho^{n+\frac{1}{2},*} \nabla c^{n+\frac{1}{2}} + \frac{\mathbb{C}}{4\mathbb{M}} \rho^{n+\frac{1}{2},*} \nabla \left(\mathbf{q}^{n+1} \cdot \mathbf{q}^{n+1} + \mathbf{q}^n \cdot \mathbf{q}^n \right) \\ & + \frac{1}{2\,\mathbb{M}} \rho^{n+\frac{1}{2},*} \nabla \left(g_1(c^{n+1}) + g_1(c^n) \right) - \frac{2}{\mathbb{R}e} \operatorname{div} \left(c^{n+\frac{1}{2}} \mathbf{D}^{n+1} \right), \end{aligned} \tag{5.3.2}$$

$$0 = \rho_{\bar{t}}^{n+1} + \operatorname{div} \left(\rho^{n+\frac{1}{2},*} (\sqrt{\rho}\mathbf{u})^{n+1} \right), \tag{5.3.3}$$

$$\begin{aligned} 0 = {} & \rho^{n+\frac{1}{2}} \mu^{n+\frac{1}{2}} - \rho^{n+\frac{1}{2}} \frac{g_1(c^{n+1}) - g_1(c^n)}{c^{n+1} - c^n} - \frac{p^{n+\frac{1}{2}}}{\rho_1} \rho^{n+\frac{1}{2}} + N_1 \theta \rho^{n+\frac{1}{2}} (\ln p)^{n+\frac{1}{2}} \\ & + \mathbb{C} \operatorname{div} \left(\rho^{n+\frac{1}{2}}\, \mathbf{q}^{n+\frac{1}{2}} \right) + K \rho^{n+\frac{1}{2}}, \end{aligned} \tag{5.3.4}$$

$$\mathbf{0} = \mathbf{q}^{n+\frac{1}{2}} - \nabla c^{n+\frac{1}{2}}. \tag{5.3.5}$$

In (5.3.1)-(5.3.5) we have considered the same notation as in Section 4.4. The differences are in the time approximation of the density terms

$$\rho^{n+\frac{1}{2}} := \frac{\rho^{n+1} + \rho^n}{2}, \qquad \rho^{n+\frac{1}{2},*} := \rho(c^{n+\frac{1}{2}}, p^{n+\frac{1}{2}}), \tag{5.3.6}$$

and of the logarithmic terms

$$(\ln p)^{n+\frac{1}{2}} := \ln p^{n+\frac{1}{2}}, \tag{5.3.7}$$

$$(\ln p)^{n+1} := \ln p^{n+\frac{1}{2}} + \frac{p^{n+1} - p^n}{2p^{n+1}}, \qquad (\ln p)^n := \ln p^{n+\frac{1}{2}} - \frac{p^{n+1} - p^n}{2p^n}. \tag{5.3.8}$$

In addition,

$$\mathbf{D}^{n+1} := \frac{\nabla(\sqrt{\rho}\mathbf{u})^{n+1} + (\nabla(\sqrt{\rho}\mathbf{u})^{n+1})^T}{2}. \tag{5.3.9}$$

Remark. The choice of the temporal approximation related to $(\ln p)^{n+1}$ can be justified in the following way. Let us consider the quantity

$$\ln \frac{p^{n+\frac{1}{2}}}{p^{n+1}} = \ln p^{n+\frac{1}{2}} - \ln p^{n+1}. \tag{5.3.10}$$

From the Taylor expansion of the left-hand side of (5.3.10), we obtain

$$\frac{p^n - p^{n+1}}{2p^{n+1}}. \tag{5.3.11}$$

In a similar way it is possible to justify the choice of the temporal approximation related to $(\ln p)^n$.

5.3.2 Temporally discrete mass conservation.

The temporally discrete scheme (5.3.1)-(5.3.5) satisfies the mass conservation property as stated by the following result. The proof follows the same steps of the proof in the LT case (Theorem 4.4.1).

Theorem 5.3.1 (Temporally discrete conservation of mass). *The temporally discrete scheme (5.3.1)-(5.3.5) is mass-conservative, i.e.*

$$\int_\Omega \rho^{n+1}\,dx = \int_\Omega \rho^n\,dx, \qquad \text{for all } n = 0, 1, ..., N-1. \tag{5.3.12}$$

5.3.3 Temporally discrete energy dissipation law.

Let

$$E^n := \int_\Omega \left(\frac{1}{2}\rho^n |\mathbf{u}^n|^2 + \frac{1}{\mathbb{M}}\rho^n g(p^n, c^n, \mathbf{q}^n) - \frac{1}{\mathbb{M}}p^n \right) dx \tag{5.3.13}$$

be the temporally discrete version of the total energy (5.1.22), for $n = 0, 1, ..., N$. The next theorem will prove that our temporal scheme (5.3.1)-(5.3.5) preserves a temporally discrete formulation of the continuous energy dissipation law (5.1.27).

Theorem 5.3.2 (Temporally discrete energy dissipation law). *If* $(c^{n+1}, \mathbf{u}^{n+1}, p^{n+1}, \mu^{n+1}, \mathbf{q}^{n+1})$ *is a solution of the temporally discrete system (5.3.1)-(5.3.5). Then*

$$E_{\bar{t}}^{n+1} = -\frac{1}{\mathbb{P}e\mathbb{M}}\int_\Omega \left(\nabla \mu^{n+\frac{1}{2}}\right)^2 dx - \frac{2}{\mathbb{R}e}\int_\Omega c^{n+\frac{1}{2}}\left(\mathbf{D}^{n+1} : \mathbf{D}^{n+1}\right)dx, \tag{5.3.14}$$

for all $n = 0, 1, ..., N-1$, *where*

$$E_{\bar{t}}^{n+1} := \frac{E^{n+1} - E^n}{\Delta t}.$$

Proof. Let us test equation (5.3.1) with $\dfrac{\mu^{n+\frac{1}{2}}}{\mathbb{M}}$ and equation (5.3.2) with $(\sqrt{\rho}\mathbf{u})^{n+1}$ and sum them together. If we use the following identity

$$\begin{aligned}\int_\Omega \Big(&\rho^{n+\frac{1}{2}} \left((\sqrt{\rho}\mathbf{u})^{n+1} \cdot \nabla \right) (\sqrt{\rho}\mathbf{u})^{n+1} \cdot (\sqrt{\rho}\mathbf{u})^{n+1} \\ &+ \frac{1}{2}\operatorname{div}(\rho^{n+\frac{1}{2}}(\sqrt{\rho}\mathbf{u})^{n+1})(\sqrt{\rho}\mathbf{u})^{n+1} \cdot (\sqrt{\rho}\mathbf{u})^{n+1} \Big)\, dx = 0,\end{aligned} \tag{5.3.15}$$

we obtain:

$$\begin{aligned} 0 \;=\; \int_\Omega \Bigg(&\frac{1}{\mathbb{M}}\rho^{n+\frac{1}{2}}\mu^{n+\frac{1}{2}}\frac{c^{n+1}-c^n}{\Delta t} - \frac{1}{\mathbb{P}e\mathbb{M}}\mu^{n+\frac{1}{2}}\Delta\mu^{n+\frac{1}{2}} \\ &+ \sqrt{\rho}^{\,n+\frac{1}{2}}\,(\sqrt{\rho}\mathbf{u})_{\bar{t}}^{n+1} \cdot (\sqrt{\rho}\mathbf{u})^{n+1} + \frac{1}{\mathbb{M}}\nabla p^{n+\frac{1}{2}} \cdot (\sqrt{\rho}\mathbf{u})^{n+1} \\ &+ \frac{1}{\mathbb{M}}\frac{1}{\rho_1}\rho^{\,n+\frac{1}{2},*} p^{n+\frac{1}{2}}\nabla c^{n+\frac{1}{2}} \cdot (\sqrt{\rho}\mathbf{u})^{n+1} \\ &- \frac{1}{\mathbb{M}}N_1\theta\rho^{\,n+\frac{1}{2},*}(\ln p)^{n+\frac{1}{2}}\nabla c^{n+\frac{1}{2}} \cdot (\sqrt{\rho}\mathbf{u})^{n+1} \\ &- \frac{1}{\mathbb{M}}K\rho^{\,n+\frac{1}{2},*}\nabla c^{n+\frac{1}{2}} \cdot (\sqrt{\rho}\mathbf{u})^{n+1} \\ &+ \frac{\mathbb{C}}{4\mathbb{M}}\rho^{\,n+\frac{1}{2},*}\nabla(\mathbf{q}^{n+1}\cdot\mathbf{q}^{n+1} + \mathbf{q}^n\cdot\mathbf{q}^n) \cdot (\sqrt{\rho}\mathbf{u})^{n+1} \\ &+ \frac{1}{\mathbb{M}}\rho^{\,n+\frac{1}{2},*}\frac{\nabla(g_1(c^{n+1}) + g_1(c^n))}{2} \cdot (\sqrt{\rho}\mathbf{u})^{n+1} \\ &- \frac{2}{\mathbb{R}e}\operatorname{div}(c^{n+\frac{1}{2}}\mathbf{D}^{n+1}) \cdot (\sqrt{\rho}\mathbf{u})^{n+1} \Bigg)\, dx. \end{aligned} \tag{5.3.16}$$

Using equation (5.3.4) for the first term of (5.3.16) and integrating by parts the viscous term and term containing $\Delta\mu^{n+\frac{1}{2}}$, we obtain:

$$\begin{aligned}
0 \;=\; \int_\Omega \Bigg(& \sqrt{\rho}^{\,n+\frac{1}{2}} (\sqrt{\rho}\mathbf{u})_t^{n+1} \cdot (\sqrt{\rho}\mathbf{u})^{n+1} + \frac{1}{\mathbb{M}} \nabla p^{n+\frac{1}{2}} \cdot (\sqrt{\rho}\mathbf{u})^{n+1} \\
& + \frac{1}{\mathbb{M}} \frac{1}{\rho_1} \rho^{\,n+\frac{1}{2},*} p^{n+\frac{1}{2}} \nabla c^{n+\frac{1}{2}} \cdot (\sqrt{\rho}\mathbf{u})^{n+1} \\
& - \frac{1}{\mathbb{M}} N_1 \theta \rho^{\,n+\frac{1}{2},*} (\ln p)^{n+\frac{1}{2}} \nabla c^{n+\frac{1}{2}} \cdot (\sqrt{\rho}\mathbf{u})^{n+1} \\
& + \frac{1}{\mathbb{M}} \frac{1}{\rho_1} \rho^{n+\frac{1}{2}} p^{n+\frac{1}{2}} \frac{c^{n+1}-c^n}{\Delta t} - \frac{1}{\mathbb{M}} N_1 \theta \rho^{n+\frac{1}{2}} (\ln p)^{n+\frac{1}{2}} \frac{c^{n+1}-c^n}{\Delta t} \\
& + \frac{1}{\mathbb{M}} \rho^{\,n+\frac{1}{2},*} \frac{\nabla(g_1(c^{n+1}) + g_1(c^n))}{2} \cdot (\sqrt{\rho}\mathbf{u})^{n+1} \\
& + \frac{1}{\mathbb{M}} \rho^{n+\frac{1}{2}} \frac{g_1(c^{n+1}) - g_1(c^n)}{c^{n+1}-c^n} \frac{c^{n+1}-c^n}{\Delta t} \\
& + \frac{\mathbb{C}}{4\mathbb{M}} \rho^{\,n+\frac{1}{2},*} \nabla(\mathbf{q}^{n+1} \cdot \mathbf{q}^{n+1} + \mathbf{q}^n \cdot \mathbf{q}^n) \cdot (\sqrt{\rho}\mathbf{u})^{n+1} \\
& - \frac{\mathbb{C}}{\mathbb{M}} \operatorname{div}(\rho^{n+\frac{1}{2}} \mathbf{q}^{n+\frac{1}{2}}) \frac{c^{n+1}-c^n}{\Delta t} \\
& - \frac{1}{\mathbb{M}} K \rho^{\,n+\frac{1}{2},*} \nabla c^{n+\frac{1}{2}} \cdot (\sqrt{\rho}\mathbf{u})^{n+1} - \frac{1}{\mathbb{M}} K \rho^{n+\frac{1}{2}} \frac{c^{n+1}-c^n}{\Delta t} \\
& + \frac{1}{\mathbb{P}e\mathbb{M}} |\nabla \mu^{n+\frac{1}{2}}|^2 + \frac{2}{\mathbb{R}e} c^{n+\frac{1}{2}} (\mathbf{D}^{n+1} : \mathbf{D}^{n+1}) \Bigg)\, dx. \qquad (5.3.17)
\end{aligned}$$

We get the following relations:

(I) the first term in (5.3.17) is

$$\int_\Omega \sqrt{\rho}^{\,n+\frac{1}{2}} (\sqrt{\rho}\mathbf{u})_t^{n+1} \cdot (\sqrt{\rho}\mathbf{u})^{n+1}\, dx = \int_\Omega \frac{1}{2\Delta t} \left(\rho^{n+1} (\mathbf{u}^{n+1})^2 - \rho^n (\mathbf{u}^n)^2 \right) dx, \qquad (5.3.18)$$

(II) integrating by parts, and using the mass conservation equation (5.3.3), the terms containing g_1 are equal to

$$\begin{aligned}
& \int_\Omega \Bigg(\frac{1}{2\mathbb{M}} \rho^{\,n+\frac{1}{2},*} \nabla(g_1(c^{n+1}) + g_1(c^n)) \cdot (\sqrt{\rho}\mathbf{u})^{n+1} \\
& \qquad + \frac{1}{\mathbb{M}\Delta t} \rho^{n+\frac{1}{2}} (g_1(c^{n+1}) - g_1(c^n)) \Bigg)\, dx \\
= \; & \int_\Omega \Bigg(-\frac{1}{2\mathbb{M}} (g_1(c^{n+1}) + g_1(c^n)) \operatorname{div}(\rho^{\,n+\frac{1}{2},*} (\sqrt{\rho}\mathbf{u})^{n+1}) \\
& \qquad + \frac{1}{\mathbb{M}\Delta t} \rho^{n+\frac{1}{2}} (g_1(c^{n+1}) - g_1(c^n)) \Bigg)\, dx \\
= \; & \int_\Omega \Bigg(\frac{1}{2\mathbb{M}\Delta t} (g_1(c^{n+1}) + g_1(c^n))(\rho^{n+1} - \rho^n) \\
& \qquad + \frac{1}{2\mathbb{M}\Delta t} (g_1(c^{n+1}) - g_1(c^n))(\rho^{n+1} + \rho^n) \Bigg)\, dx \\
= \; & \int_\Omega \frac{1}{\mathbb{M}\Delta t} \left(\rho^{n+1} g_1(c^{n+1}) - \rho^n g_1(c^n) \right) dx, \qquad (5.3.19)
\end{aligned}$$

(III) integrating by parts and using mass conservation equation (5.3.3), the terms con-

taining the variable $\mathbf{q}$ are equal to

$$\begin{aligned}
&\int_\Omega \left(\frac{\mathbb{C}}{4\mathbb{M}} \rho^{\,n+\frac{1}{2},*} \nabla(\mathbf{q}^{n+1}\cdot\mathbf{q}^{n+1} + \mathbf{q}^n\cdot\mathbf{q}^n)\cdot(\sqrt{\rho}\mathbf{u})^{n+1} \right.\\
&\qquad \left. - \frac{\mathbb{C}}{\mathbb{M}}\, \mathrm{div}(\rho^{n+\frac{1}{2}}\mathbf{q}^{n+\frac{1}{2}}) \frac{c^{n+1}-c^n}{\Delta t} \right) dx \\
= &\int_\Omega \left(-\frac{\mathbb{C}}{4\mathbb{M}} (\mathbf{q}^{n+1}\cdot\mathbf{q}^{n+1} + \mathbf{q}^n\cdot\mathbf{q}^n)\, \mathrm{div}(\rho^{\,n+\frac{1}{2},*}(\sqrt{\rho}\mathbf{u})^{n+1}) \right.\\
&\qquad \left. + \frac{\mathbb{C}}{\mathbb{M}} \rho^{n+\frac{1}{2}}\mathbf{q}^{n+\frac{1}{2}} \cdot \frac{\mathbf{q}^{n+1}-\mathbf{q}^n}{\Delta t} \right) dx \\
= &\int_\Omega \left(\frac{\mathbb{C}}{4\mathbb{M}\Delta t} (\mathbf{q}^{n+1}\cdot\mathbf{q}^{n+1} + \mathbf{q}^n\cdot\mathbf{q}^n)(\rho^{n+1}-\rho^n) \right.\\
&\qquad \left. + \frac{\mathbb{C}}{\mathbb{M}\Delta t} \rho^{n+\frac{1}{2}}\mathbf{q}^{n+\frac{1}{2}} \cdot (\mathbf{q}^{n+1}-\mathbf{q}^n) \right) dx \\
= &\int_\Omega \frac{1}{\mathbb{M}\Delta t} \left(\rho^{n+1} g_2(\mathbf{q}^{n+1}) - \rho^n g_2(\mathbf{q}^n) \right) dx, \qquad (5.3.20)
\end{aligned}$$

(IV) integrating by parts and using mass conservation equation (5.3.3), the terms containing the constant K are equal to

$$\begin{aligned}
&\int_\Omega \left(-\frac{1}{\mathbb{M}} K \rho^{\,n+\frac{1}{2},*} \nabla c^{n+\frac{1}{2}} \cdot (\sqrt{\rho}\mathbf{u})^{n+1} - \frac{1}{\mathbb{M}} K \rho^{n+\frac{1}{2}} \frac{c^{n+1}-c^n}{\Delta t} \right) dx \\
= &\int_\Omega \left(\frac{1}{\mathbb{M}} K \rho^{\,n+\frac{1}{2},*} \nabla(1-c^{n+\frac{1}{2}}) \cdot (\sqrt{\rho}\mathbf{u})^{n+1} - \frac{1}{\mathbb{M}} K \rho^{n+\frac{1}{2}} \frac{c^{n+1}-c^n}{\Delta t} \right) dx \\
= &\int_\Omega \left(-\frac{1}{\mathbb{M}} K (1-c^{n+\frac{1}{2}})\, \mathrm{div}(\rho^{\,n+\frac{1}{2},*}(\sqrt{\rho}\mathbf{u})^{n+1}) - \frac{1}{\mathbb{M}} K \rho^{n+\frac{1}{2}} \frac{c^{n+1}-c^n}{\Delta t} \right) dx \\
= &\int_\Omega \left(\frac{1}{\mathbb{M}} K (1-c^{n+\frac{1}{2}}) \frac{\rho^{n+1}-\rho^n}{\Delta t} - \frac{1}{\mathbb{M}} K \rho^{n+\frac{1}{2}} \frac{c^{n+1}-c^n}{\Delta t} \right) dx \\
= &\int_\Omega \frac{1}{\mathbb{M}\Delta t} \left(\rho^{n+1} g_0(c^{n+1}) - \rho^n g_0(c^n) \right) dx. \qquad (5.3.21)
\end{aligned}$$

Now, let us consider the pressure terms:

$$\begin{aligned}
&\int_\Omega \left(\frac{1}{\mathbb{M}} \nabla p^{n+\frac{1}{2}} \cdot (\sqrt{\rho}\mathbf{u})^{n+1} + \frac{1}{\mathbb{M}} \frac{1}{\rho_1} \rho^{\,n+\frac{1}{2},*} p^{n+\frac{1}{2}} \nabla c^{n+\frac{1}{2}} \cdot (\sqrt{\rho}\mathbf{u})^{n+1} \right.\\
&\quad - \frac{1}{\mathbb{M}} N_1 \theta \rho^{\,n+\frac{1}{2},*} (\ln p)^{n+\frac{1}{2}} \nabla c^{n+\frac{1}{2}} \cdot (\sqrt{\rho}\mathbf{u})^{n+1} \\
&\quad \left. + \frac{1}{\mathbb{M}} \frac{1}{\rho_1} \rho^{n+\frac{1}{2}} p^{n+\frac{1}{2}} \frac{c^{n+1}-c^n}{\Delta t} - \frac{1}{\mathbb{M}} N_1 \theta \rho^{n+\frac{1}{2}} (\ln p)^{n+\frac{1}{2}} \frac{c^{n+1}-c^n}{\Delta t} \right) dx. \qquad (5.3.22)
\end{aligned}$$

Notice that, integrating by parts and using mass conservation equation (5.3.3):

(a)

$$\begin{aligned}
&\int_\Omega \left(\frac{1}{\mathbb{M}} \frac{1}{\rho_1} \rho^{\,n+\frac{1}{2},*} p^{n+\frac{1}{2}} \nabla c^{n+\frac{1}{2}} \cdot (\sqrt{\rho}\mathbf{u})^{n+1} \right) dx \\
= &\int_\Omega \left(-\frac{1}{\mathbb{M}} \frac{1}{\rho_1} c^{n+\frac{1}{2}} p^{n+\frac{1}{2}}\, \mathrm{div}(\rho^{\,n+\frac{1}{2},*}(\sqrt{\rho}\mathbf{u})^{n+1}) \right.\\
&\qquad \left. - \frac{1}{\mathbb{M}} \frac{1}{\rho_1} c^{n+\frac{1}{2}} \rho^{\,n+\frac{1}{2},*} (\sqrt{\rho}\mathbf{u})^{n+1} \cdot \nabla p^{n+\frac{1}{2}} \right) dx \\
= &\int_\Omega \left(\frac{1}{\mathbb{M}} \frac{1}{\rho_1} c^{n+\frac{1}{2}} p^{n+\frac{1}{2}} \frac{\rho^{n+1}-\rho^n}{\Delta t} - \frac{1}{\mathbb{M}} \frac{1}{\rho_1} \rho^{\,n+\frac{1}{2},*} c^{n+\frac{1}{2}} (\sqrt{\rho}\mathbf{u})^{n+1} \cdot \nabla p^{n+\frac{1}{2}} \right) dx, \qquad (5.3.23)
\end{aligned}$$

(b)

$$\begin{aligned}
&\int_\Omega \left(-\frac{1}{\mathbb{M}} N_1 \theta \rho^{\,n+\frac{1}{2},*} (\ln p)^{n+\frac{1}{2}} \nabla c^{n+\frac{1}{2}} \cdot (\sqrt{\rho}\mathbf{u})^{n+1} \right) dx \\
= &\int_\Omega \left(\frac{1}{\mathbb{M}} N_1 \theta \rho^{\,n+\frac{1}{2},*} (\ln p)^{n+\frac{1}{2}} \nabla (1 - c^{n+\frac{1}{2}}) \cdot (\sqrt{\rho}\mathbf{u})^{n+1} \right) dx \\
= &\int_\Omega \left(-\frac{1}{\mathbb{M}} N_1 \theta (1 - c^{n+\frac{1}{2}}) (\ln p)^{n+\frac{1}{2}} \operatorname{div}(\rho^{\,n+\frac{1}{2},*} (\sqrt{\rho}\mathbf{u})^{n+1}) \right. \\
&\qquad \left. - \frac{1}{\mathbb{M}} N_1 \theta \rho^{\,n+\frac{1}{2},*} (1 - c^{n+\frac{1}{2}}) \frac{\nabla p^{n+\frac{1}{2}}}{p^{n+\frac{1}{2}}} \cdot (\sqrt{\rho}\mathbf{u})^{n+1} \right) dx \\
= &\int_\Omega \left(\frac{1}{\mathbb{M}} N_1 \theta (1 - c^{n+\frac{1}{2}}) (\ln p)^{n+\frac{1}{2}} \frac{\rho^{n+1} - \rho^n}{\Delta t} \right. \\
&\qquad \left. - \frac{1}{\mathbb{M}} N_1 \theta \rho^{\,n+\frac{1}{2},*} (1 - c^{n+\frac{1}{2}}) \frac{\nabla p^{n+\frac{1}{2}}}{p^{n+\frac{1}{2}}} \cdot (\sqrt{\rho}\mathbf{u})^{n+1} \right) dx. \quad (5.3.24)
\end{aligned}$$

Using (5.3.23) and (5.3.24) into (5.3.22) we obtain:

$$\begin{aligned}
&\int_\Omega \left(\frac{1}{\mathbb{M}} \nabla p^{n+\frac{1}{2}} \cdot (\sqrt{\rho}\mathbf{u})^{n+1} - \frac{1}{\mathbb{M}} \frac{1}{\rho_1} \rho^{\,n+\frac{1}{2},*} c^{n+\frac{1}{2}} (\sqrt{\rho}\mathbf{u})^{n+1} \cdot \nabla p^{n+\frac{1}{2}} \right. \\
&\quad - \frac{1}{\mathbb{M}} N_1 \theta \rho^{\,n+\frac{1}{2},*} (1 - c^{n+\frac{1}{2}}) \frac{\nabla p^{n+\frac{1}{2}}}{p^{n+\frac{1}{2}}} \cdot (\sqrt{\rho}\mathbf{u})^{n+1} \\
&\quad + \frac{1}{\mathbb{M}} \frac{1}{\rho_1} c^{n+\frac{1}{2}} p^{n+\frac{1}{2}} \frac{\rho^{n+1} - \rho^n}{\Delta t} + \frac{1}{\mathbb{M}} \frac{1}{\rho_1} \rho^{n+\frac{1}{2}} p^{n+\frac{1}{2}} \frac{c^{n+1} - c^n}{\Delta t} \\
&\quad \left. + \frac{1}{\mathbb{M}} N_1 \theta (1 - c^{n+\frac{1}{2}}) (\ln p)^{n+\frac{1}{2}} \frac{\rho^{n+1} - \rho^n}{\Delta t} - \frac{1}{\mathbb{M}} N_1 \theta \rho^{n+\frac{1}{2}} (\ln p)^{n+\frac{1}{2}} \frac{c^{n+1} - c^n}{\Delta t} \right) dx.
\end{aligned} \quad (5.3.25)$$

If we notice the fact that, remembering the definition of $\rho^{\,n+\frac{1}{2},*}$,

$$\begin{aligned}
&\int_\Omega \left(\frac{1}{\mathbb{M}} \nabla p^{n+\frac{1}{2}} \cdot (\sqrt{\rho}\mathbf{u})^{n+1} - \frac{1}{\mathbb{M}} \frac{1}{\rho_1} \rho^{\,n+\frac{1}{2},*} c^{n+\frac{1}{2}} (\sqrt{\rho}\mathbf{u})^{n+1} \cdot \nabla p^{n+\frac{1}{2}} \right. \\
&\qquad \left. - \frac{1}{\mathbb{M}} N_1 \theta \rho^{\,n+\frac{1}{2},*} (1 - c^{n+\frac{1}{2}}) \frac{\nabla p^{n+\frac{1}{2}}}{p^{n+\frac{1}{2}}} \cdot (\sqrt{\rho}\mathbf{u})^{n+1} \right) dx \\
= &\int_\Omega \left(\frac{1}{\mathbb{M}} \nabla p^{n+\frac{1}{2}} \cdot (\sqrt{\rho}\mathbf{u})^{n+1} \right. \\
&\qquad \left. - \frac{1}{\mathbb{M}} \left(\frac{c^{n+\frac{1}{2}}}{\rho_1} + \frac{N_1 \theta (1 - c^{n+\frac{1}{2}})}{p^{n+\frac{1}{2}}} \right) \rho^{\,n+\frac{1}{2},*} (\sqrt{\rho}\mathbf{u})^{n+1} \cdot \nabla p^{n+\frac{1}{2}} \right) dx = 0,
\end{aligned} \quad (5.3.26)$$

then (5.3.25) can be rewritten as

$$\begin{aligned}
&\int_\Omega \left(\frac{1}{\mathbb{M}} \frac{1}{\rho_1} c^{n+\frac{1}{2}} p^{n+\frac{1}{2}} \frac{\rho^{n+1} - \rho^n}{\Delta t} + \frac{1}{\mathbb{M}} \frac{1}{\rho_1} p^{n+\frac{1}{2}} \rho^{n+\frac{1}{2}} \frac{c^{n+1} - c^n}{\Delta t} \right. \\
&\quad - \frac{N_1 \theta}{\mathbb{M}} \frac{p^{n+1} - p^n}{\Delta t} \frac{1}{2} \left(\frac{\rho^{n+1}}{p^{n+1}} (1 - c^{n+1}) + \frac{\rho^n}{p^n} (1 - c^n) \right) \\
&\quad + \frac{N_1 \theta}{\mathbb{M}} \frac{p^{n+1} - p^n}{\Delta t} \frac{1}{2} \left(\frac{\rho^{n+1}}{p^{n+1}} (1 - c^{n+1}) + \frac{\rho^n}{p^n} (1 - c^n) \right) \\
&\quad \left. + \frac{N_1 \theta}{\mathbb{M}} (1 - c^{n+\frac{1}{2}}) (\ln p)^{n+\frac{1}{2}} \frac{\rho^{n+1} - \rho^n}{\Delta t} - \frac{N_1 \theta}{\mathbb{M}} \rho^{n+\frac{1}{2}} (\ln p)^{n+\frac{1}{2}} \frac{c^{n+1} - c^n}{\Delta t} \right) dx,
\end{aligned} \quad (5.3.27)$$

in which we have added and subtracted the quantity

$$\frac{N_1\theta}{\mathbb{M}}\frac{p^{n+1}-p^n}{\Delta t}\frac{1}{2}\left(\frac{\rho^{n+1}}{p^{n+1}}(1-c^{n+1})+\frac{\rho^n}{p^n}(1-c^n)\right).$$

Using the fact that

$$p^{n+1}=\frac{N_1\theta\rho_1\rho^{n+1}(1-c^{n+1})}{\rho_1-\rho^{n+1}c^{n+1}},\qquad p^n=\frac{N_1\theta\rho_1\rho^n(1-c^n)}{\rho_1-\rho^nc^n},\tag{5.3.28}$$

we obtain:

$$\begin{aligned}&\int_\Omega\left(-\frac{N_1\theta}{\mathbb{M}}\frac{p^{n+1}-p^n}{\Delta t}\frac{1}{2}\left(\frac{\rho^{n+1}}{p^{n+1}}(1-c^{n+1})+\frac{\rho^n}{p^n}(1-c^n)\right)\right)dx\\ =\;&\int_\Omega\left(-\frac{1}{\mathbb{M}}\frac{p^{n+1}-p^n}{\Delta t}+\frac{1}{\mathbb{M}}\frac{1}{2\rho_1}(\rho^{n+1}c^{n+1}+\rho^nc^n)\frac{p^{n+1}-p^n}{\Delta t}\right)dx.\end{aligned}\tag{5.3.29}$$

Using (5.3.29) into (5.3.27), we obtain

$$\begin{aligned}&\int_\Omega\Bigg(\frac{1}{\mathbb{M}}\frac{1}{\rho_1}c^{n+\frac12}p^{n+\frac12}\frac{\rho^{n+1}-\rho^n}{\Delta t}+\frac{1}{\mathbb{M}}\frac{1}{\rho_1}p^{n+\frac12}\rho^{n+\frac12}\frac{c^{n+1}-c^n}{\Delta t}\\ &\quad+\frac{1}{\mathbb{M}}\frac{1}{2\rho_1}(\rho^{n+1}c^{n+1}+\rho^nc^n)\frac{p^{n+1}-p^n}{\Delta t}\\ &\quad+\frac{N_1\theta}{\mathbb{M}}(1-c^{n+\frac12})(\ln p)^{n+\frac12}\frac{\rho^{n+1}-\rho^n}{\Delta t}\\ &\quad+\frac{N_1\theta}{\mathbb{M}}\rho^{n+\frac12}(\ln p)^{n+\frac12}\frac{c^n-c^{n+1}}{\Delta t}\\ &\quad+\frac{N_1\theta}{\mathbb{M}}\frac{p^{n+1}-p^n}{\Delta t}\frac{1}{2}\left(\frac{\rho^{n+1}}{p^{n+1}}(1-c^{n+1})+\frac{\rho^n}{p^n}(1-c^n)\right)-\frac{1}{\mathbb{M}}\frac{p^{n+1}-p^n}{\Delta t}\Bigg)dx.\end{aligned}\tag{5.3.30}$$

If we notice that

$$\begin{aligned}&\int_\Omega\left(\frac{1}{\mathbb{M}}\frac{1}{\rho_1}c^{n+\frac12}p^{n+\frac12}\frac{\rho^{n+1}-\rho^n}{\Delta t}+\frac{1}{\mathbb{M}}\frac{1}{\rho_1}p^{n+\frac12}\rho^{n+\frac12}\frac{c^{n+1}-c^n}{\Delta t}\right.\\ &\qquad\left.+\frac{1}{\mathbb{M}}\frac{1}{2\rho_1}(\rho^{n+1}c^{n+1}+\rho^nc^n)\frac{p^{n+1}-p^n}{\Delta t}\right)dx\\ =\;&\int_\Omega\left(\frac{1}{\mathbb{M}\Delta t}\frac{1}{2\rho_1}(p^{n+1}+p^n)(c^{n+1}\rho^{n+1}-c^n\rho^n)\right.\\ &\qquad\left.+\frac{1}{\mathbb{M}\Delta t}\frac{1}{2\rho_1}(p^{n+1}-p^n)(c^{n+1}\rho^{n+1}+c^n\rho^n)\right)dx\\ =\;&\int_\Omega\frac{1}{\mathbb{M}\Delta t}\frac{1}{\rho_1}(p^{n+1}c^{n+1}\rho^{n+1}-p^nc^n\rho^n)\,dx,\end{aligned}\tag{5.3.31}$$

and

$$\begin{aligned}
&\int_\Omega \left(\frac{N_1\theta}{\mathbb{M}}(1-c^{n+\frac{1}{2}})(\ln p)^{n+\frac{1}{2}} \frac{\rho^{n+1}-\rho^n}{\Delta t} \right. \\
&\quad + \frac{N_1\theta}{\mathbb{M}} \rho^{n+\frac{1}{2}} (\ln p)^{n+\frac{1}{2}} \frac{c^n - c^{n+1}}{\Delta t} \\
&\quad \left. + \frac{N_1\theta}{\mathbb{M}} \frac{p^{n+1}-p^n}{\Delta t} \frac{1}{2} \left(\frac{\rho^{n+1}}{p^{n+1}}(1-c^{n+1}) + \frac{\rho^n}{p^n}(1-c^n) \right) \right) dx \\
= &\int_\Omega \left(\frac{N_1\theta}{\mathbb{M}} (\ln p)^{n+\frac{1}{2}} (\rho^{n+1}(1-c^{n+1}) - \rho^n(1-c^n)) \right. \\
&\quad \left. + \frac{N_1\theta}{\mathbb{M}} \frac{p^{n+1}-p^n}{\Delta t} \frac{1}{2} \left(\frac{\rho^{n+1}}{p^{n+1}}(1-c^{n+1}) + \frac{\rho^n}{p^n}(1-c^n) \right) \right) dx \\
= &\int_\Omega \frac{1}{\mathbb{M}\Delta t} N_1\theta ((\ln p)^{n+1}\rho^{n+1}(1-c^{n+1}) - (\ln p)^n \rho^n (1-c^n))\, dx,
\end{aligned} \tag{5.3.32}$$

we can rewrite (5.3.30) as

$$\begin{aligned}
&\int_\Omega \left(\frac{1}{\mathbb{M}\Delta t} \frac{1}{\rho_1} (p^{n+1}c^{n+1}\rho^{n+1} - p^n c^n \rho^n) - \frac{1}{\mathbb{M}\Delta t}(p^{n+1}-p^n) \right. \\
&\quad \left. + \frac{1}{\mathbb{M}\Delta t} N_1\theta ((\ln p)^{n+1}\rho^{n+1}(1-c^{n+1}) - (\ln p)^n \rho^n (1-c^n)) \right) dx.
\end{aligned} \tag{5.3.33}$$

Using (5.3.18)-(5.3.21) and (5.3.22)-(5.3.33) into (5.3.17), we obtain

$$\begin{aligned}
&\int_\Omega \left(\frac{1}{\Delta t} \left(\frac{\rho^{n+1}}{2} (\mathbf{u}^{n+1})^2 - \frac{\rho^n}{2} (\mathbf{u}^n)^2 \right) \right. \\
&\left. + \frac{1}{\Delta t} \left(\frac{1}{\mathbb{M}} \rho^{n+1} g(p^{n+1}, c^{n+1}, \mathbf{q}^{n+1}) - \frac{1}{\mathbb{M}} \rho^n g(p^n, c^n, \mathbf{q}^n) \right) - \frac{1}{\mathbb{M}} \frac{p^{n+1}-p^n}{\Delta t} \right) dx \\
= &-\frac{1}{\mathbb{P}e\mathbb{M}} \int_\Omega |\nabla \mu^{n+\frac{1}{2}}|^2\, dx - \frac{2}{\mathbb{R}e} \int_\Omega c^{n+\frac{1}{2}} \left(\mathbf{D}^{n+1} : \mathbf{D}^{n+1} \right) dx,
\end{aligned} \tag{5.3.34}$$

that is equivalent to the thesis (5.3.14). □

5.4 Fully discrete energy consistent DG numerical method.

In this section we propose a fully discretisation of the mixed system (5.1.14)-(5.1.18) based on the results of the previous sections for the semi-discretisations in space and time.

5.4.1 Fully discrete mixed formulation.

The fully discrete mixed formulation of (5.1.14)-(5.1.18) can be written as follows: given initial conditions $(c_h^0, \mathbf{u}_h^0, p_h^0, \mu_h^0, \mathbf{q}_h^0)$, for all $n = 0, 1, ..., N-1$, find

$$(c_h^{n+1}, \mathbf{u}_h^{n+1}, p_h^{n+1}, \mu_h^{n+1}, \mathbf{q}_h^{n+1}) \in \mathbb{V} \times \mathbb{V}_0^2 \times \mathbb{V} \times \mathbb{V} \times \mathbb{V}_\mathbf{n}$$

such that

$$
\begin{aligned}
0 = & \sum_{T\in\mathscr{T}_h}\int_T \left(\rho_h^{n+\frac{1}{2}}\,(c_h)_{\bar{t}}^{n+1}X+\rho_h^{n+\frac{1}{2}}((\sqrt{\rho_h}\mathbf{u}_h)^{n+1})\cdot\nabla c_h^{n+\frac{1}{2}}X\right)dx \\
& -\frac{1}{\mathbb{P}e}\mathcal{A}(\mu_h^{n+\frac{1}{2}},X)+\int_{\mathcal{E}}F_1(X)\,ds, \qquad (5.4.1)\\
0 = & \sum_{T\in\mathscr{T}_h}\int_T \Big(\sqrt{\rho_h}^{\,n+\frac{1}{2}}\,(\sqrt{\rho_h}\mathbf{u}_h)_{\bar{t}}^{n+1}\cdot\boldsymbol{\xi} \\
& \qquad +\rho_h^{n+\frac{1}{2}}\left((\sqrt{\rho_h}\mathbf{u}_h)^{n+1}\cdot\nabla\right)(\sqrt{\rho_h}\mathbf{u}_h)^{n+1}\cdot\boldsymbol{\xi} \\
& \qquad +\frac{1}{2}\,\mathrm{div}(\rho_h^{n+\frac{1}{2}}(\sqrt{\rho_h}\mathbf{u}_h)^{n+1})(\sqrt{\rho_h}\mathbf{u}_h)^{n+1}\cdot\boldsymbol{\xi}+\frac{1}{\mathbb{M}}\nabla p_h^{n+\frac{1}{2}}\cdot\boldsymbol{\xi} \\
& \qquad -\frac{1}{\mathbb{M}}\rho_h^{n+\frac{1}{2}}\mu_h^{n+\frac{1}{2}}\,\nabla c_h^{n+\frac{1}{2}}\cdot\boldsymbol{\xi}+\frac{1}{\mathbb{M}}\frac{1}{\rho_1}\rho_h^{n+\frac{1}{2},*}p_h^{n+\frac{1}{2}}\nabla c_h^{n+\frac{1}{2}}\cdot\boldsymbol{\xi} \\
& \qquad -\frac{1}{\mathbb{M}}N_1\theta\rho_h^{n+\frac{1}{2},*}\,(\ln p_h)^{n+\frac{1}{2}}\,\nabla c_h^{n+\frac{1}{2}}\cdot\boldsymbol{\xi}-\frac{1}{\mathbb{M}}K\rho_h^{n+\frac{1}{2},*}\nabla c_h^{n+\frac{1}{2}}\cdot\boldsymbol{\xi} \\
& \qquad +\frac{\mathbb{C}}{4\mathbb{M}}\rho_h^{n+\frac{1}{2},*}\nabla\left(\mathbf{q}_h^{n+1}\cdot\mathbf{q}_h^{n+1}+\mathbf{q}_h^{n}\cdot\mathbf{q}_h^{n}\right)\cdot\boldsymbol{\xi} \\
& \qquad +\frac{1}{2\,\mathbb{M}}\rho_h^{n+\frac{1}{2},*}\nabla\left(g_1(c_h^{n+1})+g_1(c_h^{n})\right)\cdot\boldsymbol{\xi}\Big)\,dx \\
& -\frac{2}{\mathbb{R}e}\mathcal{B}(c_h^{n+\frac{1}{2}},(\sqrt{\rho_h}\mathbf{u}_h)^{n+1},\boldsymbol{\xi})+\int_{\mathcal{E}}F_2(\boldsymbol{\xi})\,ds, \qquad (5.4.2)\\
0 = & \sum_{T\in\mathscr{T}_h}\int_T\left((\rho_h)_{\bar{t}}^{n+1}Z+\mathrm{div}\left(\rho_h^{n+\frac{1}{2},*}(\sqrt{\rho_h}\mathbf{u}_h)^{n+1}\right)Z\right)dx+\int_{\mathcal{E}}F_3(Z)\,ds, \qquad (5.4.3)\\
0 = & \sum_{T\in\mathscr{T}_h}\int_T\Bigg(\rho_h^{n+\frac{1}{2}}\mu_h^{n+\frac{1}{2}}\psi-\rho_h^{n+\frac{1}{2}}\frac{g_1(c_h^{n+1})-g_1(c_h^{n})}{c_h^{n+1}-c_h^{n}}\psi-\frac{p_h^{n+\frac{1}{2}}}{\rho_1}\rho_h^{n+\frac{1}{2}}\psi \\
& \qquad +N_1\theta\rho_h^{n+\frac{1}{2}}\,(\ln p_h)^{n+\frac{1}{2}}\,\psi+\mathbb{C}\,\mathrm{div}\left(\rho_h^{n+\frac{1}{2}}\,\mathbf{q}_h^{n+\frac{1}{2}}\right)\psi+K\rho_h^{n+\frac{1}{2}}\psi\Bigg)\,dx \\
& +\int_{\mathcal{E}}F_4(\psi)\,ds, \qquad (5.4.4)\\
0 = & \sum_{T\in\mathscr{T}_h}\int_T\left(\mathbf{q}_h^{n+\frac{1}{2}}\cdot\mathbf{T}-\nabla c_h^{n+\frac{1}{2}}\cdot\mathbf{T}\right)dx+\int_{\mathcal{E}}F_5(\mathbf{T})\,ds, \qquad (5.4.5)
\end{aligned}
$$

$$\forall\,(X,\boldsymbol{\xi},Z,\psi,\mathbf{T})\in\mathbb{V}\times\mathbb{V}_0^2\times\mathbb{V}\times\mathbb{V}\times\mathbb{V}_{\mathbf{n}},$$

and

$$
\begin{aligned}
F_1(X) &= 0, && (5.4.6)\\
F_2(\boldsymbol{\xi}) &= -\frac{1}{2}\left[\!\left[\rho_h^{n+\frac{1}{2}} (\sqrt{\rho_h}\mathbf{u}_h)^{n+1} \right]\!\right] \left\{\!\left\{ (\sqrt{\rho_h}\mathbf{u}_h)^{n+1} \cdot \boldsymbol{\xi} \right\}\!\right\} \\
&\quad - \left(\left\{\!\left\{ \boldsymbol{\xi} \right\}\!\right\} \otimes \left\{\!\left\{ \rho_h^{n+\frac{1}{2}} (\sqrt{\rho_h}\mathbf{u}_h)^{n+1} \right\}\!\right\} \right) : \left[\!\left[(\sqrt{\rho_h}\mathbf{u}_h)^{n+1} \right]\!\right]_{\otimes} \\
&\quad - \frac{1}{2\mathbb{M}} \left[\!\left[g_1(c_h^{n+1}) + g_1(c_h^n) \right]\!\right] \cdot \left\{\!\left\{ \rho_h^{n+\frac{1}{2},*} \boldsymbol{\xi} \right\}\!\right\} \\
&\quad - \frac{\mathbb{C}}{4\mathbb{M}} \left[\!\left[\mathbf{q}_h^{n+1} \cdot \mathbf{q}_h^{n+1} + \mathbf{q}_h^n \cdot \mathbf{q}_h^n \right]\!\right] \cdot \left\{\!\left\{ \rho_h^{n+\frac{1}{2},*} \boldsymbol{\xi} \right\}\!\right\} \\
&\quad - \frac{1}{\mathbb{M}} \left[\!\left[K(1 - c_h^{n+\frac{1}{2}}) \right]\!\right] \cdot \left\{\!\left\{ \rho_h^{n+\frac{1}{2},*} \boldsymbol{\xi} \right\}\!\right\} \\
&\quad - \frac{1}{\mathbb{M}} \frac{1}{\rho_1} \left[\!\left[c_h^{n+\frac{1}{2}} p_h^{n+\frac{1}{2}} \right]\!\right] \cdot \left\{\!\left\{ \rho_h^{n+\frac{1}{2},*} \boldsymbol{\xi} \right\}\!\right\} \\
&\quad - \frac{N_1\theta}{\mathbb{M}} \left[\!\left[(1 - c_h^{n+\frac{1}{2}})(\ln p_h)^{n+\frac{1}{2}} \right]\!\right] \cdot \left\{\!\left\{ \rho_h^{n+\frac{1}{2},*} \boldsymbol{\xi} \right\}\!\right\}, && (5.4.7)\\
F_3(Z) &= -\left[\!\left[\rho_h^{n+\frac{1}{2},*} (\sqrt{\rho_h}\mathbf{u}_h)^{n+1} \right]\!\right] \left\{\!\left\{ Z \right\}\!\right\}, && (5.4.8)\\
F_4(\psi) &= -\mathbb{C} \left[\!\left[\rho_h^{n+\frac{1}{2}} \mathbf{q}_h^{n+\frac{1}{2}} \right]\!\right] \left\{\!\left\{ \psi \right\}\!\right\}, && (5.4.9)\\
F_5(\mathbf{T}) &= \left[\!\left[c_h^{n+\frac{1}{2}} \right]\!\right] \cdot \left\{\!\left\{ \mathbf{T} \right\}\!\right\}. && (5.4.10)
\end{aligned}
$$

5.4.2 Fully discrete mass conservation and energy law.

We can state mass conservation property and energy dissipation law for the fully discrete scheme for MF system. The proofs of these results follow from the combination of the corresponding propositions in the spatial (Theorems 5.2.1, 5.2.2) and temporal (Theorems 5.3.1, 5.3.2) approximation.

Theorem 5.4.1 (Fully discrete conservation of mass). *The fully discrete scheme (5.4.1)-(5.4.5) is mass-conservative, i.e.*

$$
\sum_{T\in\mathscr{T}_h} \int_T \rho_h^{n+1}\, dx = \sum_{T\in\mathscr{T}_h} \int_T \rho_h^n\, dx, \qquad \text{for all } n = 0, 1, ..., N-1. \tag{5.4.11}
$$

Proof. The proof follows from the results proposed by Theorems 5.2.1 and 5.3.1 which provide a spatial and a temporal semidiscrete mass conservation result, respectively. □

Theorem 5.4.2 (Fully discrete energy dissipation law). *Let*

$$
E_h^n := \sum_{T\in\mathscr{T}_h} \int_T \left(\frac{\rho_h^n}{2} |\mathbf{u}_h^n|^2 + \frac{1}{\mathbb{M}} \rho_h^n g(p_h^n, c_h^n, \mathbf{q}_h^n) - \frac{1}{\mathbb{M}} p_h^n \right) dx \tag{5.4.12}
$$

be the fully discrete version of the total energy (5.1.22), for $n = 0, 1, ..., N$. If $(c_h^{n+1}, \mathbf{u}_h^{n+1}, p_h^{n+1}, \mu_h^{n+1}, \mathbf{q}_h^{n+1})$ is a solution of the fully discrete system (5.4.1)-(5.4.5), then

$$
(E_h)_{\bar{t}}^{n+1} = \frac{1}{\mathbb{P}e\mathbb{M}} \mathcal{A}(\mu_h^{n+\frac{1}{2}}, \mu_h^{n+\frac{1}{2}}) + \frac{2}{\mathbb{R}e} \mathcal{B}(c_h^{n+\frac{1}{2}}, (\sqrt{\rho_h}\mathbf{u}_h)^{n+1}, (\sqrt{\rho_h}\mathbf{u}_h)^{n+1}), \tag{5.4.13}
$$

for all $n = 0, 1, ..., N-1$, where

$$
(E_h)_{\bar{t}}^{n+1} := \frac{E_h^{n+1} - E_h^n}{\Delta t}
$$

and $\mathcal{A}, \mathcal{B}$ are negative definite, by definition.

Proof. The proof consists in the application of the results proposed by Theorems 5.2.2 and 5.3.2 which provide a spatial and a temporal semidiscrete energy dissipation law, respectively. □

Conclusions and Perspectives.

In this thesis, we have proposed a mathematical modeling for studying the expansion stage of metal foam production within the so-called "powder metallurgical route".

In Chapter 1 we have described the main properties and the different production routes of metal foams. We noticed as the lack of control of the processing routes causes difficulties in the industrial diffusion of this kind of materials and influences the quality of metal foam materials.

In Chapter 2 we have studied the expansion stage of the foam within the powder-route. From the outcome of the experiments we have performed together with MUSP researchers, we concluded that it was possible to consider a mathematical modeling of metal foam expansion under the two simplifying hypotheses of constant temperature and molten metal matrix.

In Chapter 3 we have proposed a thermodynamically consistent phase-field model for the description of the expansion stage of a foam inside a hollow mold under the hypotheses stated in the previous chapter. Future developments should concern the inclusion of the effects of the temperature in the mathematical derivation of the model.

In Chapter 4 we have derived an energy-based numerical approximation of the Lowengrub-Truskinovsky quasi-incompressible system of equations. We have shown first results of numerical experiments using conforming finite elements. Future developments should concern numerical experiments on the DG scheme we have proposed in the previous analysis.

In Chapter 5 we have derived an energy-based numerical approximation of the metal foam model. Numerical experiments on the metal foam model will be performed in the future.

Acknowledgements.

I am grateful to MUSP laboratory for having supported my research activity and to the MUSP researchers for the useful discussions on the mathematical modeling of metal foams presented in Chapter 3 and for providing me with the outputs of the experiments presented in Chapter 2.

Bibliography

[1] D. N. Arnold, F. Brezzi, B. Cockburn, and L. D. Marini. Unified Analysis of Discontinuous Galerkin Methods for Elliptic Problems. *SIAM J. Numer. Anal.*, 39(5):1749–1779, 2001.

[2] N. Babcsan and J. Banhart. Metal foams: Towards high-temperature colloid chemistry. In *Colloidal Particles at Liquid Interfaces*, pages 445–500. Cambridge University Press, 2006.

[3] N. Babcsan, J. Banhart, and D. Leitlmeier. Metal Foams-Manufacture and Physics of Foaming. In *International Conference "Advanced Metallic Materials"*, 2003.

[4] J. Banhart. Metallic foams. *Europhysics News*, 30:17–20, 1999.

[5] J. Banhart. Manufacturing routes for metallic foams. *JOM*, 52(12):22–27, 2000.

[6] J. Banhart. Manufacture, characterization and application of cellular metals and metal foams. *Progress in Materials Science*, 46:559–632, 2001.

[7] J. Banhart. Metal foams: production and stability. *Adv. Eng. Mater.*, 8:781–794, 2006.

[8] J. Banhart. Light-Metal Foams-History of Innovation and Technological Challenges. *Adv. Eng. Mater.*, 15:82–111, 2013.

[9] J. Barrett, J.F. Blowey, and Garcke H. Finite element approximation of the Cahn-Hilliard equation with degenerate mobility. *SIAM J. Numer. Anal.*, 37(1):286–318, 1999.

[10] G. Bertuzzi. *Caratterizzazione, fabbricazione e applicazione di manufatti in schiuma metallica*. PhD thesis, Università degli Studi di Bologna, 2011.

[11] F. Boyer. A theoretical and numerical model for the study of incompressible mixture flows. *Computers and Fluids*, 31(1):41–68, 2002.

[12] H. Brezis. *Functional Analysis, Sobolev Spaces and Partial Differential Equations*. Springer, 2011.

[13] J. Bruchon. *Étude de la formation d'une structure de mousse par simulation directe de l'expansion de bulles dans une matrice liquide polymère*. PhD thesis, École Nationale Supérieure des Mines de Paris, 2004.

[14] J. W. Cahn and J. E. Hilliard. Free energy of a nonuniform system. I. Interfacial free energy. *J. Chem. Phys.*, 28:258–267, 1958.

[15] M. I. M. Copetti and C. M. Elliott. Numerical analysis of the Cahn-Hilliard equation with a logarithmic free energy. *Numer. Math.*, 63(1):39–65, 1992.

[16] D.A. Drew and S.L. Passman. *Theory of Multicomponent Fluids*. Number 135 in Applied Mathematical Sciences. Springer, New York, 1999.

[17] I. Duarte and J. Banhart. A study of aluminium foam formation–kinetics and microstructure. *Acta Materialia*, 48(9):2349 – 2362, 2000.

[18] M. Durand and H. A. Stone. Relaxation Time of the Topological T1 Process in a Two-Dimensional Foam. *Phys. Rev. Lett.*, 97, Nov 2006.

[19] C.M. Elliott. The Cahn-Hilliard Model for the Kinetics of Phase Separation. In J.F. Rodrigues, editor, *Mathematical Models for Phase Change Problems*, volume 88 of *International Series of Numerical Mathematics*. Birkhäuser Basel, 1989.

[20] M. Fabrizio, C. Giorgi, and A. Morro. A thermodynamic approach to non-isothermal phase-field evolution in continuum physics. *Physica D*, 214:144 – 156, 2006.

[21] X. Feng. Fully Discrete Finite Element Approximations of the Navier-Stokes-Cahn-Hilliard Diffuse Interface Model for Two-Phase Fluid Flows. *SIAM J. Numer. Anal.*, 44(3), 2006.

[22] V. Gergely and T.W. Clyne. Drainage in standing liquid metal foams: modeling and experimental observations. *Acta Materialia*, 52:3047–3058, 2004.

[23] J.W. Gibbs. On the equilibrium of heterogeneous substances. In *The Collected Papers of J. Willard Gibbs*, volume I, pages 55–353. London: Yale University Press, 1957.

[24] J. Giesselmann, C. Makridakis, and T. Pryer. Energy consistent DG methods for the Navier-Stokes-Korteweg system. *Math. Comp.*, 83:2071–2099, 2014.

[25] J. Giesselmann and T. Pryer. Energy consistent discontinuous Galerkin methods for a quasi-incompressible diffuse two phase flow model. *Accepted for publication in Mathematical Modeling and Numerical Analysis M2AN*, 2014. http://arxiv.org/abs/1307.8248.

[26] S. Gross and A. Reusken. *Numerical Methods for Two-phase Incompressible Flows*. Springer, 2011.

[27] Z. Guo, P. Lin, and J.S. Lowengrub. A numerical method for the quasi-incompressible Cahn-Hilliard-Navier-Stokes equations for variable density flows with a discrete energy law. *Journal of Computational Physics*, 276(0):486 – 507, 2014.

[28] F. Hecht. New development in FreeFem++. *J. Numer. Math.*, 20(3-4):251–265, 2012.

[29] P. Houston, C. Schwab, and E. Süli. Discontinuous hp-Finite Element Methods for Advection-Diffusion-Reaction Problems. *SIAM J. Numer. Anal*, 39(6):2133–2163, 2002.

[30] D. D. Joseph. Fluid dynamics of two miscible liquids with diffusion and gradient stresses. *Eur. J. Mech. B/Fluids*, 9(6), 1990.

[31] D. Kay, V. Styles, and R. Welford. Finite element approximation of a Cahn-Hilliard-Navier-Stokes system. *Interfaces and Free Boundaries*, 10(1):15–43, 2008.

[32] M. Kelager and K. Erleben. *A Nonlinear Vertex-Based Model for Animation of Two-Dimensional Dry Foam*, pages 296–303. INSTICC Press, 2010.

[33] C. Körner. Foam formation mechanisms in particle suspensions applied to metal foam foams. *Materials Science and Engineering A*, 495:227–235, 2008.

[34] C. Körner. *Integral Foam Molding of Light Metals*. Springer-Verlag- Berlin Heidelberg, 2008.

[35] C. Körner, M. Arnold, and R. F. Singer. Metal foam stabilization by oxide network particles. *Materials Science and Engineering A*, 396:28 – 40, 2005.

[36] Labview. http://www.ni.com/labview/i/.

[37] L.P. Lefebvre, J. Banhart, and D.C. Dunand. Porous metals and metallic foams: current status and recent developments. *Adv. Eng. Mater.*, 10(9):775–787, 2008.

[38] J. Lowengrub and L. Truskinovsky. Quasi-incompressible Cahn-Hilliard fluids and topological transitions. *Proc. R. Soc. Lond. A*, 454:2617–2654, 1998.

[39] J. Marchalot, J. Lambert, I. Cantat, P. Tabeling, and M.C. Jullien. 2D foam coarsening in a microfluidic system. *EPL (Europhysics Letters)*, 83(6), 2008.

[40] B. Matijasevic. *Characterization and Optimization of Blowing Agent for Making Improved Metal Foams*. PhD thesis, Technische Universität Berlin, 2006.

[41] M. Monno and V. Mussi. Impiego di schiume metalliche nelle strutture delle macchine utensili. Macchine Utensili, 2007.

[42] A. Morro. Phase-field models for fluid mixtures. *Mathematical and Computer Modelling*, 45:1042–1052, 2007.

[43] A. Morro. A phase-field approach to non-isothermal transitions. *Mathematical and Computer Modelling*, 48:621–633, 2008.

[44] A. Naber, C. Liu, and J.J. Feng. The nucleation and growth of gas bubbles in a Newtonian fluid: an energetic variational phase field approach. *Contemporary Mathematics*, 466:95–120, 2008.

[45] A. Quarteroni and A. Valli. *Numerical Approximation of Partial Differential Equations*. Springer, 2008.

[46] W.S. Rasband. Imagej. U. S. National Institutes of Health, Bethesda, Maryland, USA, 1997-2005.

[47] L. E. Reichl. *A Modern Course in Statistical Mechanics*. University of Texas Press, Austin, 1980.

[48] B. Riviere. *Discontinuous Galerkin Methods for Solving Elliptic and Parabolic Equations: Theory and Implementation*. SIAM, 2008.

[49] J. S. Rowlinson. Translation of J. D. van der Waals' "The thermodynamic theory of capillarity under the hypothesis of a continuous variation of density. *J. Stat. Phys.*, 20:197–244, 1979.

[50] J.S. Rowlinson and B. Widom. *Molecular Theory of Capllarity*. Dover, Mineola, New York, 2002.

[51] J. Shen and X. Yang. Energy stable schemes for Cahn-Hilliard phase-field model of two-phase incompressible flows. *Chinese Annals of Mathematics, Series B*, 31(5):743–758, 2010.

[52] Y. Sun and C. Beckermann. Diffuse interface modeling of two-phase flows based on averaging: mass and momentum equations. *Physica D*, 198, 2004.

[53] Y. Sun and C. Beckermann. A two-phase diffuse-interface model for Hele-Shaw flows with large property contrasts. *Physica D*, 237:3089–3098, 2008.

[54] Y. Sun and C. Beckermann. Phase-Field Modeling of Bubble Growth and Flow in a Hele-Shaw Cell. *Int. J. Mass Transfer*, 53:2969–2978, 2010.

[55] M. Thies. *Lattice Boltzmann modeling with free surface applied to in-situ gas generated foam formation*. PhD thesis, University of Erlangen-Nürnberg, 2005.

[56] G. Tierra Chica and F. Guillén-González. Numerical methods for solving the Cahn-Hilliard equation and its applicability to related Energy-based models. *Archives of Computational Methods in Engineering*, pages 1–21, 2014.

[57] C. A. Truesdell. Sulle basi della termomeccanica. Nota I. *Atti Acc. Lincei- Rend. Sc. fis. mat e nat.*, 22:33–38, 1957.

[58] C. A. Truesdell. Sulle basi della termomeccanica. Nota II. *Atti Acc. Lincei- Rend. Sc. fis. mat e nat.*, 22:158–166, 1957.

[59] C. A. Truesdell. *Rational Thermodynamics*. Springer, New York, 2nd edition, 1984.

[60] C. A. Truesdell and R. G. Muncaster. *Fundamentals of Maxwell's Kinetic Theory of a Simple Monatomic gas. Treated as a Branch of Rational Mechanics*. Academic Press, New York, 1980.

[61] F. von Zeppelin, M. Hirscher, H. Stanzick, and J. Banhart. Desorption of hydrogen from blowing agents used for foaming metals. *Composites Science and Technology*, 63:2293–2300, 2003.

[62] D. Weaire, M. F. Vaz, P. I. C. Teixeira, and M. A. Fortes. Instabilities in liquid foams. *Soft Matter*, 3:47–57, 2007.

[63] D. Wearie and S. Hutzler. *The Physics of Foams*. Oxford University Press Inc., New York, 1999.

[64] T. P. Wihler. Locking-free adaptive discontinuous Galerkin FEM for linear elasticity problems. *Math. Comp.*, 75(255):1087–1102, 2006.

Ringraziamenti.

Ringrazio il Dott. Marco Verani per aver "scommesso" su di me e avermi sempre incoraggiata e consigliata durante tutto il percorso di dottorato.

Ringrazio il Prof. Riccardo Rosso per il prezioso aiuto nella costruzione del modello matematico.

Ringrazio i professori, i ricercatori e i dottorandi del Dipartimento di Matematica del Politecnico di Milano, in particolare del laboratorio MOX, per aver contribuito, ciascuno secondo le proprie competenze, alla mia crescita personale e per le amicizie che sono nate durante questi anni.

Ringrazio il laboratorio MUSP di Piacenza per avermi dato la possibilità di svolgere questa attività di ricerca.

Ringrazio la mia famiglia e il mio fidanzato Matteo per avermi "sopportato e supportato" con pazienza in questo percorso.